Transition Metal Cyaphides: Synthesis, Reactivity, and Electrochemistry

by

Matthew Christopher Leech

Submitted for the degree of Doctor of Philosophy

University of Sussex

September 2018

Declaration

I hereby declare that this thesis has not been and will not be, submitted in whole or in part to another university for the award of any other degree.

Signature: .....

Matthew Christopher Leech

Acknowledgements

Undertaking a PhD is a lot like riding a rollercoaster: there are ups, downs, moments when you feel like you're going backwards, and times when you're just going around and around in circles. Of course, no person rides alone, and I'd like to take this opportunity to thank those who've ridden with me over the past four years, because I certainly couldn't have done it without you.

Starting with members of faculty, thanks to: Ian for your supervision; Iain, Ali, and Mark, for not getting fed up with me wanting to "pick your brain" what surely felt like every five minutes; Shane and George for your advice and guidance over the years; and John Turner, for our chats outside of the lab, and your words of encouragement.

Secondly, to the teaching lab team over the years, but specifically to Mick & Verity for allowing me to "acquire" extra glassware over the years and giving me free roam over the teaching lab and instruments. It was much appreciated, and I swear that I've given back everything I stole…I mean, borrowed! Likewise, to Alex, Paul, and Barry, the technical services who have, quite literally in some instances, held the lab together and stopped everything from falling down around me (although that last flood was a bit of a close one).

To my brothers in arms Matt Molloy and James Mattock. We've made it! We survived (even if Matt nearly burnt the building down by accident a couple of times along the way)! To Nikki and Amy, for helping me start in the lab, and to Nikos, for adding to their teachings with your own wisdom over the years.

To my MChem students Luke, Leanne, and Peter, who made the first year of my PhD a completely unforgettable experience (and not just from Pete's passionate renditions of "Let it Go"!), and to the students that, though I may not have had the pleasure to supervise, still got to enjoy the company of all the same, Steph, Rachel G, Joe, and Josh.

To Tom and Giac, who welcomed me as an honorary member of the Nano group & Phys Chem team, showed me some of the best places to eat in Brighton, and provided me with some of the best stories that the department had to offer. To Dan Commandeur, the current Nano group torch-bearer whose friendship, unwavering support, and quite impressive ability to listen to me ranting, was greatly appreciated, and I couldn't have made it through the final stretch without you.

To Daniel Fuller, the best flatmate and friend that a guy could ask for, however, if you hadn't introduced me to Reddit, this thesis would've been finished a whole lot sooner! To Rachel (AKA Penguin) for your wisdom, guidance, and the best gluten-free chocolate fudge cake that I have ever eaten! To Vicki, for the best company, support, and proof-reading skills over the years, even after you'd left Sussex. Who could forget our late nights in lab, singing along to Disney music, followed by a trip to the Elm Grove fish 'n' chip shop? Or when we were the classiest people on campus, eating microwave pizza in the office while proof-reading Ian's grant proposal at 9 o'clock in the evening (with, you guessed it, more Disney music)?

Lastly, and perhaps most importantly, to my family. Come rain or shine, you've helped me, encouraged me, and supported me through all of my trials. I know that it's not been easy, but I am truly grateful for everything that you've all done, and it will not be forgotten.

Now that that's all out of the way, let the journey begin! My name is Matt, I'll be your guide for this rollercoaster adventure through my research project. Please be sure to keep your hands, feet, arms, and legs inside the vehicle at all times and keep your seatbelts on, and I hope that you enjoy the ride!

Summary

This thesis describes the synthesis, characterisation, and electrochemical behaviour of a series of transition metal cyaphide complexes, with the aim of understanding how the introduction of low-coordinate phosphorus fragments into through-conjugated organometallic systems affects their electronic structure.

Formation of mono-metallic ruthenium cyaphide complexes, *trans*-[Ru(C≡P)(C≡CR)(dppe)$_2$], *via* the corresponding η^1-coordinated phosphaalkyne complexes, was achieved alongside the synthesis of the analogous carbocentric mixed acetylide complexes *trans*-[Ru(C≡CH)(C≡CR)(dppe)$_2$]. This allowed the first direct comparison of ligated cyaphide and acetylide, revealing contrasting effects on the electrochemical behaviour when compared to their parent chloride complexes. This was supplemented by the synthesis of the systems *trans*-[RuH(C≡E)(dppe)$_2$] (E = P, CH, N), facilitating the exploration of the isolobal analogy between carbon and phosphorus, alongside the relationship between multiply-bonded pnictogens.

Multimetallic cyaphide complexes were also prepared, featuring either one or two cyaphide fragments. The electronic structure of these hetero- and homo-bimetallic complexes was explored using both computational and experimental investigations, with the latter achieved using UV-Vis spectroscopy and cyclic voltammetry. It was found that introduction of cyaphide greatly reduced the stability of the mixed-valence state resulting from mono-oxidation, however, complete destabilisation of this species was not observed. Furthermore, DFT calculations revealed that the HOMOs still exhibited the expected out-of-phase mixing of the ligand and metal π-orbitals.

The synthesis of transition metal cyaphide complexes featuring less sterically-encumbering ancillary ligand sets was also pursued. This resulted in the successful synthesis of the complexes

$[MCp^{R'}(dppe)(\eta^1\text{-}P{\equiv}CSiMe_3)]^+$ (M = Ru, Fe; R' = H, Me), with variable temperature NMR, and X-ray diffraction studies used to ascertain the coordination mode of the phosphaalkyne. Attempts to convert to the corresponding cyaphide complexes were undertaken using a variety of desilylating reagents, however, the identity of the final product appeared to be dependent on the base used.

Attempts to oxidise the phosphorus centre of the ligated cyaphide from P(III) to P(V) using different chalcogen sources were undertaken, however, only sources of oxygen or sulfur were observed to undergo reactivity. Lastly, reactions with BR''_3, X_2 (X = Br, I), and $PhICl_2$ have shown some evidence that reactivity of the C≡P moiety *via* either the lone pair or C≡P π-system is possible, opening up new avenues for further cyaphide chemistry.

Contents

List of Abbreviations

°	Degrees
°C	Degrees Celsius
Å	Angstrom
Ad	Adamantyl
An	Anisole
Ar	Arene
***ca*.**	Circa
cm^{-1}	Wavenumber
Cp	Cyclopentadienyl
Cp*	Pentamethylcyclopentadienyl
Cp^R	R-Substituted Cyclopentadienyl
Cy	Cyclohexyl
DABCO	1,4-diazabicyclo[2.2.2]octane
DBU	1,8-Diazabicyclo[5.4.0]undec-7-ene
DCM	Dichloromethane
DFT	Density Functional Theory
DIPA	Diisopropylamine
DIPEA	Diisopropylethylamine
DIPP	Diisopropylphenyl
DME	Dimethoxyethane
DMP	2,6-dimesitylphenyl
dmpe	1,2-bis(dimethylphosphino)ethane
DMSO	Dimethylsulfoxide

dppe	1,2-bis(diphenylphosphino)ethane
dppeS_2	1,2-bis(diphenylphosphino)ethane disulfide
dppeSe_2	1,2-bis(diphenylphosphino)ethane diselenide
Dppm	Bis-(diphenylphosphino)methane
***E*-**	*E*- Isomer
ESI-MS	Electron-Spray Ionisation Mass Spectrometry
Et	Ethyl
eV	Electronvolt
Fc	Ferrocenyl
FVP	Flash Vacuum Pyrolysis
HMDS	Hexamethyldisilazide
HOMO	Highest Occupied Molecular Orbital
ILCT	Intra-Ligand Charge Transfer
^{i}Pr	Isopropyl
IR	Infrared
K_c	Comproportionation Constant
L	Ligand
LLCT	Ligand to Ligand Charge Transfer
LUMO	Lowest Unoccupied Molecular Orbital
M	Molar
***m*-**	*Meta*-
m/z	Mass/Charge Ratio
MCPT	Methylcyclopentane
MCY	Methylcyclohexane
Me	Methyl

Mes*	2,4,6-Tri-*tert*-butyl phenyl
MLCT	Metal to Ligand Charge Transfer
mmHg	Millimetres of Mercury
NBO	Natural Bond Orbital
^{n}Bu	*n*-Butyl
Np	Neopentyl
NRT	Natural Resonance Theory
o-	ortho
OFET	Organic Field Effect Transistor
OLED	Organic Light Emitting Diode
OTf	Triflate
p	*Para-*
Ph	Phenyl
PPE	poly(phenyleneethynylene)
PPV	poly(*p*-phenylene vinylene)
pz	Pyrazine
TBAF	Tetrabutylammonium fluoride
TBAT	Tetrabutylammonium difluorotriphenylsilicate
^{t}Bu	*Tert*-butyl
TD-DFT	Time Dependent Density Functional Theory
THF	Tetrahydrofuran
TIP	2,4,6-triisopropylphenyl
^{t}Pent	Tert-pentyl, 1,1-dimethylpropyl
Z-	*Z*- isomer
λ	Valency

σ	Coordination Number

NMR Abbreviations

{^{1}H}	Proton Decoupled
br	Broad
d	Doublet
dquint	Doublet of Quintets
dt	Doublet of Triplets
HMBC	Heteronuclear Multiple Bond Correlation
HSQC	Heteronuclear Single-Quantum Coherence
Hz	Hertz
K	Kelvin
m	Multiplet
NMR	Nuclear Magnetic Resonance
ppm	Parts Per Million
q	Quartet
quint	Quintet
s	Singlet
t	Triplet
VT	Variable Temperature
^{x}*J*	Coupling Constant Over *x* Bonds
δ	Chemical Shift
$\nu_{½}$	Half-Height Linewidth

Electrochemistry Abbreviations

$[FeCp_2]^{0/+}$	Ferrocene/Ferrocenium Reference Potential
ΔE	Difference in Half-Wave Potentials
CV	Cyclic Voltammetry
$E_{½}$	Half-Wave Potential
E_{pa}	Oxidation Peak Potential
E_{pc}	Reduction Peak Potential

List of Figures

List of Schemes

List of Tables

List of Compounds

2.1 *Trans*-[RuCl(C≡CPh)(dppe)$_2$]

2.2 *Trans*-[RuCl(C≡C-*p*-An)(dppe)$_2$]

2.3 *Trans*-[RuCl(C≡CC_6H_3-*3,5*-CF_3)(dppe)$_2$]

2.4 *Trans*-[Ru(η^1-P≡C$SiMe_3$)(C≡CPh)(dppe)$_2$]PF_6

2.5 *Trans*-[Ru(η^1-P≡C$SiMe_3$)(C≡C-*p*-An)(dppe)$_2$]PF_6

2.6 *Trans*-[Ru(η^1-P≡C$SiMe_3$)(C≡CC_6H_3-*3,5*-CF_3)(dppe)$_2$]PF_6

2.7 *Trans*-[Ru(C≡P)(C≡CPh)(dppe)$_2$]

2.8 *Trans*-[Ru(C≡P)(C≡C-*p*-An)(dppe)$_2$]

2.9 *Trans*-[Ru(C≡P)(C≡CC_6H_3-*3,5*-CF_3)(dppe)$_2$]

2.10 *Trans*-[Ru(C≡CH)(C≡CPh)(dppe)$_2$]

2.11 *Trans*-[Ru(C≡CH)(C≡CC_6H_3-*3,5*-CF_3)(dppe)$_2$]

2.12 *Trans*-[Ru(C≡CH)(C≡C-*p*-An)(dppe)$_2$]

2.13 *Trans*-[RuH(C≡N)(dppe)$_2$]

2.14 *Trans*-[RuH(C≡P)(dppe)$_2$]

2.15 *Trans*-[RuH(C≡CH)(dppe)$_2$]

2.16 *Trans*-[RuH(C≡CH_2Cl)(dppe)$_2$]

2.17 *Trans*-[FeH(η^1-P≡C$SiMe_3$)(dppe)$_2$]OTf

2.18 *Trans*-[FeH(C≡P)(dppe)$_2$]

2.19 *Trans*-[RuH(η^1-P≡C$SiMe_3$)(dppe)$_2$]PF_6

2.20 *Trans*-[FeH{P(O)=C$HSiMe_3$}{dppe}$_2$]

3.1 *Trans*-[RuCl(C≡CFc)(dppe)$_2$]

3.2 *Trans*-[Ru(η^1-P≡C$SiMe_3$)(C≡CFc)(dppe)$_2$]OTf

3.3 *Trans*-[Ru(C≡P)(C≡CFc)(dppe)$_2$]

3.4 [{Ru(dppe)$_2$}$_2${μ-(C≡C-C≡C)}Cl$_2$]

3.5 *Trans*-[RuCl(=C=CH$_2$)(dppe)$_2$]PF$_6$

3.6 *Trans*-[RuCl(C≡CH)(dppe)$_2$]PF$_6$

3.7 *Trans*-[RuH(C≡CC≡CH)(dppe)$_2$]

3.8 [{Ru(dppe)$_2$}$_2${μ-(C≡C)$_2$C$_6$H$_4$-*p*}Cl$_2$]

3.9 [{Ru(dppe)$_2$}$_2${μ-(C≡C)$_2$C$_6$H$_4$-*p*}(η^1-P≡CSiMe$_3$)$_2$].2OTf

3.10 [{Ru(dppe)$_2$}$_2${μ-(C≡C)$_2$C$_6$H$_4$-*p*}(C≡P)$_2$]

3.11 [{Ru(dppe)$_2$}$_2${μ-(C≡C)$_2$C$_6$H$_4$-*p*}(η^1-P≡CSiMe$_3$)(C≡P)]OTf

3.12 [{Ru(dppe)$_2$}$_2${μ-(C≡C)$_2$C$_6$F$_4$-*p*}Cl$_2$]

3.13 [{Ru(dppe)$_2$}$_2${μ-(C≡C)$_2$C$_6$F$_4$-*p*}(η^1-P≡CSiMe$_3$)$_2$].2OTf

3.14 [{Ru(dppe)$_2$}$_2${μ-(C≡C)$_2$C$_6$F$_4$-*p*}(C≡P)$_2$]

4.1 *Trans*-[RuH(η^1-P≡CSiMe$_3$)(dppm)$_2$]OTf

4.2 *Trans*-[Ru(C≡CPh)(η^1-P≡CSiMe$_3$)(dppm)$_2$]OTf

4.3 *Trans*-[RuH{P(OH)$_2$CHSiMe$_3$}{dppm}$_2$]

4.4 *Trans*-[RuH(C≡P)(dppm)$_2$]

4.5 *Trans*-[RuH{P(O^{t}Bu)CHSiMe$_3$}{dppm}$_2$]

4.6 [FeCp*(dppe)(η^1-P≡CSiMe$_3$)]BPh$_4$

4.7 [FeCp(dppe)(η^1-P≡CSiMe$_3$)]BPh$_4$

4.8 [RuCp*(dppe)(η^1-P≡CSiMe$_3$)]OTf

4.9 [RuCp(dppe)(η^1-P≡CSiMe$_3$)]OTf

4.10 Product of prolonged heating of **4.9**

4.11 Product of the Reaction Between **4.7** and KO^{t}Bu

4.12 Product of the Reaction Between **4.7** and NaOPh

4.13 Product of the Reaction Between **4.7** and LiN(SiMe$_3$)$_2$

5.1 *Trans*-[Ru(C≡P-BPh$_3$)(C≡CPh)(dppe)$_2$]

5.2 *Trans*-[Ru{C≡P-B(C_6F_5)$_3$}{C≡CPh}{dppe}$_2$]

5.3 *Trans*-[Ru(C≡P=S)(C≡C-*p*-An)(dppe)$_2$]

5.4 *Trans*-[Ru(C≡P=Se)(C≡C-*p*-An)(dppe)$_2$]

5.5 *Trans*-[Ru(C≡P=O)(C≡CPh)(dppe)$_2$]

5.6 *Trans*-[Ru(Cl_3)(C≡C-*p*-An)(dppe)$_2$]

5.7 *Trans*-[Ru(Cl_3)(C≡CPh)(dppe)$_2$]

5.7a *Trans*-[Ru{C(I)=P(I)}{C≡CPh}{dppe}$_2$]

5.7b *Trans*-[Ru(Cl_2PI_2)(C≡CPh)(dppe)$_2$]

“However ordinary each of us may seem, we are all in some way special, and can do things that are extraordinary, perhaps until then…even thought impossible.”

- ***Roger Bannister***

Chapter 1 – Introduction

1.1 Low-Coordinate Phosphorus

1.1.1 Organophosphorus Chemistry

Phosphorus possesses an extensive and diverse chemistry that transcends the boundaries of both organic and inorganic chemistry, with its best known applications being in coordination chemistry, catalysis, and biological systems.[1] This is primarily due to the ability of phosphorus to access a variety of coordination numbers (σ) and valences (λ) (Figure 1.1),[2] which afford it versatility in both its chemistry and coordinative behaviour.

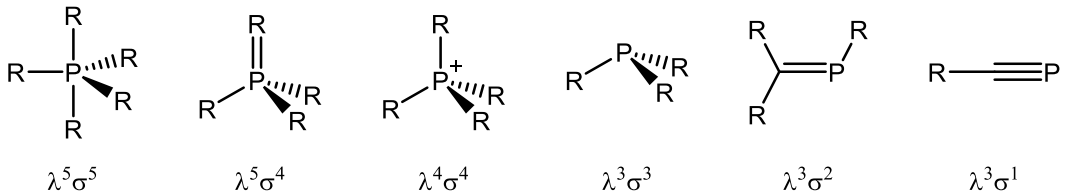

Figure 1.1: *Common organophosphorus compounds*

It could be envisaged that organophosphorus compounds should behave akin to their nitrogen counterparts as ligands in organometallic systems (e.g. PR_3 vs NR_3). However, due to the presence of additional low-lying, unoccupied orbitals, in conjunction with its inherently larger atomic radius, the chemistry of phosphorus is much more diverse than its first row counterpart. Furthermore, due to the greater ease with which the donor properties of organophosphorus fragments can be tuned, their use as ligands in homogenous catalysis is almost unrivalled, with the exception of recent developments in carbene chemistry.

A distinct sub-class of organophosphorus compounds are the phosphacarbons, the chemistry of which tends to mimic that of their carbocentric analogues. This is due to the isolobal

relationship between phosphorus and the CH fragment, which has led to the development of numerous examples of phosphacarbons which contain low-coordinate phosphorus fragments.

The isolobal analogy was first described by Roald Hoffmann in 1976, who drew equivalences between organic and inorganic compounds.[3] The archetypal example of this principle is the relationship between a CH_3 fragment and a d^7-ML_5 metal centre, such as $Mn(CO)_5$. While not isoelectronic or isostructural, both possess similar frontier orbitals, exhibit very similar radical-based chemistry, and are prone to dimerisation.[3]

Fragments are deemed to be isolobal if their frontier molecular orbitals are of comparable energy, symmetry, and electron occupancy (*e.g.* a "CH_3" fragment is isolobal with $Mn(CO)_5$, or $Fe(CO)_5^+$ fragments; Figure 1.2)[3]. This relationship is particularly useful for rationalising observed mechanisms and reactivity traits in inorganic chemistry by drawing parallels to their organic counterparts.

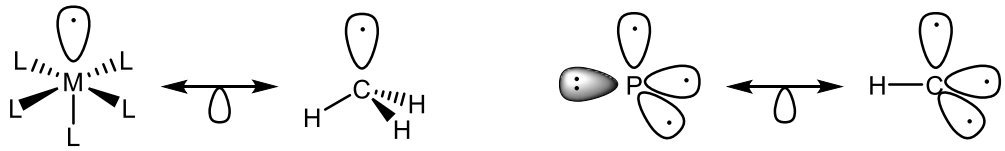

Figure 1.2: *Examples of the isolobal relationship*

In addition to being isolobal, phosphorus and the "CH" fragment are isoelectronic and of similar electronegativity (C = 2.5, P = 2.2). Consequently, it is possible to replace a CH fragment within a molecule with phosphorus, forming a new compound which should exhibit similar bonding, provided that the resulting compound is either kinetically or thermodynamically stable. Indeed, the isolobal relationship between phosphorus and the CH fragment is so much more apparent than that with nitrogen, its pnictogen counterpart, that it has resulted in the notion that phosphorus behaves as a "carbon copy".[4]

This has been extensively exploited in the area of low-coordinate phosphorus chemistry, where phosphorus possesses a coordination number of less than three. Key examples include phosphaalkenes, phosphaalkynes, and phosphinidines (**A–C**), which are based upon the carbocentric alkenes, alkynes, and carbenes respectively (**D–F**; Figure 1.3).[1] The field of low-coordinate phosphorus chemistry is diverse, however, due to the nature of the work described herein, only phosphaalkynes will be discussed, including their synthesis, coordination chemistry, and reactivity.

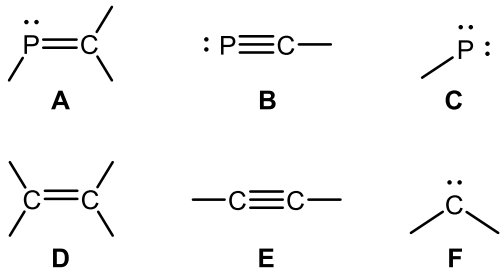

Figure 1.3: *Common low-coordinate carbon compounds and their isolobal phosphorus counterparts*

1.2 Phosphaalkynes

1.2.1 Synthesis of Phosphaalkynes

The first phosphaalkyne, methinophosphide (HC≡P),[5] was reported by Gier in 1961 which, alongside its arsenic analogue, had previously been believed to be inherently unstable and therefore not possible to synthesise, due to poor *p*π-*p*π overlap.[6] Formed by passing PH_3 gas through a rotating arc struck between graphite electrodes at low pressure, the phosphaalkyne could be condensed at −196 °C alongside other volatile matter in a 1:4 ratio, and separated using gas-chromatography (Scheme 1.1).

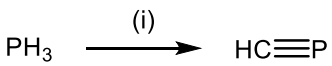

Scheme 1.1: *Synthesis of methinophosphide.[5] Reagents and conditions: (i) rotating arc (50-100 A, 25 V), graphite electrodes, 40 mmHg, flow rate 20 g* h^{-1}

The resulting colourless pyrophoric gas was highly reactive, with polymerisation occurring at temperatures above −130 °C. Elemental analyses and mass spectrometry studies of the resulting polymer supported the empirical formula of the monomer, with the latter showing an intense signal at *m/z* = 44, consistent with the molecular ion. Furthermore, the presence of a C≡P stretching mode at 1265 cm^{-1} in the infrared spectrum, alongside the absence of any H-P stretching modes, was deemed consistent with the formulation of H-C≡P.

Later work from Tyler utilised microwave spectroscopy to confirm the connectivity of methinophosphide and, through comparison of HC≡P and its deuterated counterpart, a C-P bond distance of 1.54 Å was determined.[7]

Building upon this, Kroto and Nixon proposed that the elimination of hydrogen halides from saturated precursors using flash vacuum pyrolysis (FVP) would be a suitable method to synthesise phosphaalkynes (Scheme 1.2).[8–13] It should be noted that the formation of FC≡P actually proceeds more effectively at room temperature in the presence of a dehydrofluorinating agent, such as KOH.

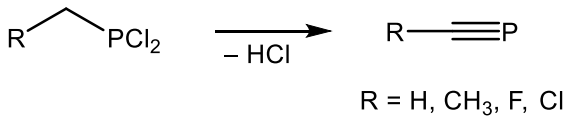

Scheme 1.2: *Phosphaalkyne synthesis using flash vacuum pyrolysis*

An alternative method was proposed by Appel and co-workers, utilising FVP to effect elimination of chlorotrimethylsilane.[14] This was demonstrated though the synthesis of phenylphosphaalkyne from an unsaturated precursor, with the resulting product condensed at −196 °C (Scheme 1.3).[14]

In contrast to HC≡P, Ph-C≡P possesses some stability due to the steric bulk of the phenyl substituent, with a half-life of seven minutes at 0 °C. A resonance in the $^{31}P\{^{1}H\}$ NMR spectrum

at −32 ppm, in conjunction with a doublet resonance in the $^{13}C\{^{1}H\}$ spectrum at 164.9 ppm ($^{1}J_{CP}$ = 48 Hz), supported the formation of a C≡P bond. Moreover, addition of HCl to a sample of the proposed phosphaalkyne resulted in the formation of $PhCH_2PCl_2$ (Scheme 1.3), suggesting addition across a reactive C≡P bond. Later investigations by Märkl increased the phosphaalkyne stability through the introduction of *tert*-butyl groups in the *ortho* positions of the phenyl ring, resulting in the formation of a phosphaalkyne that is stable under ambient conditions.[14]

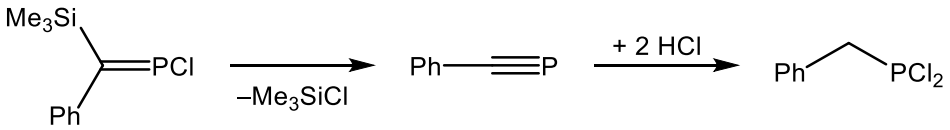

Scheme 1.3: *Synthesis of phenyl phosphaalkyne, and subsequent addition of HCl across the C≡P triple bond*

The first kinetically stabilised phosphaalkyne, *tert*-butylphosphaacetylene (^{t}BuC≡P) was synthesised by Becker in 1981,[15] and represented the major synthetic breakthrough in phosphaalkyne chemistry, with the versatility of this procedure promoting facile derivatisation. Initial reaction of *tert*-butylacetyl chloride with $P(SiMe_3)_3$, followed by subsequent rearrangement, resulted in the formation of the corresponding phosphaalkene. Upon treatment with base, rapid elimination of hexamethyldisiloxane afforded the desired phosphaalkyne (Scheme 1.4).

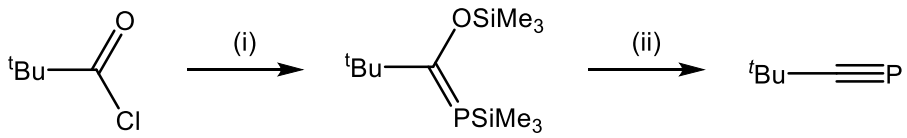

Scheme 1.4: *Synthesis of tert-butylphosphaacetylene via base-induced elimination of hexamethyldisiloxane. Reagents and conditions: (i) $P(SiMe_3)_3$; (ii) NaOH, diglyme, 20 °C, 12 h.*

Alongside its adamantyl analogue, ^{t}BuC≡P is the most widely studied and utilised phosphaalkyne due to the stability arising from the steric bulk of the *tert*-butyl substituent. X-ray diffraction

studies showed a C-P bond length of 1.548(1) Å,[16,17] similar to that reported in HC≡P.[7] Furthermore, electron density calculations predicted that the lone pair is more tightly-bound to the phosphorus centre than in the corresponding phosphaalkene precursor, which was attributed to the *sp*, as opposed to sp^2, character of the phosphorus atom.[17] Moreover, the first and second electron ionisation energies (9.61 eV for π_{CP} and 11.44 eV for the phosphorus lone pair) are much lower than those observed in the corresponding nitrile, and the HOMO is based on the C≡P bond.[18] As a result, phosphaalkynes possess similar chemistry to that of alkynes, as opposed to nitriles, exemplified by the polarisation of the C≡P unit ($C^{\delta-}$–$P^{\delta+}$).[19]

1.2.2 Phosphaalkyne Reactivity

Similar to nitriles, phosphaalkynes readily react with nucleophiles, allowing facile access to both phosphaalkenes and 1,3-diphosphabutadienes, as reported by Cowley and co-workers.[20] Reaction of ArC≡P (Ar = *2,4,6*-$^tBu_3C_6H_2$) with one equivalent of methyllithium in THF, followed by addition of water, resulted in the formation of the corresponding phosphaalkene (Scheme 1.5), as indicated by a shift in the $^{31}P\{^1H\}$ NMR resonance to higher frequency (*ca.* 33 ppm[21] to 260 ppm), and the presence of coupling between the phosphorus centre and the methyl protons ($^2J_{PH}$ = 34 Hz).

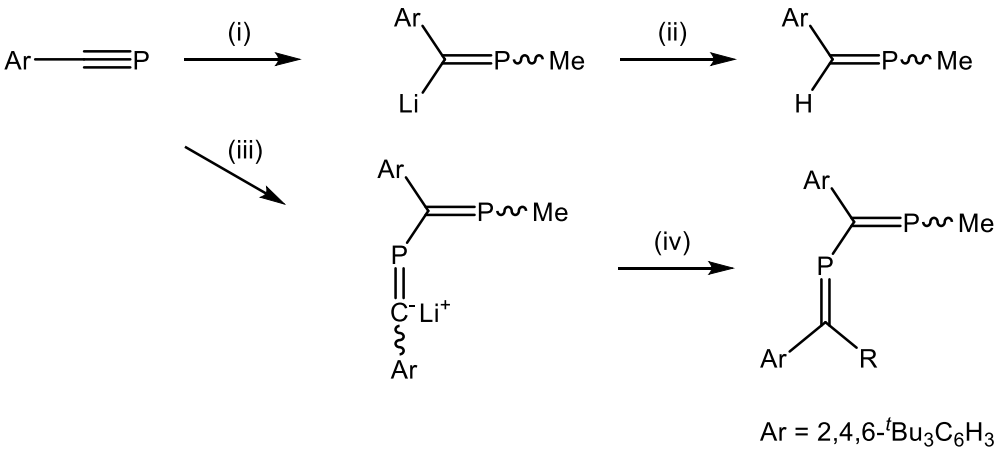

Scheme 1.5: *Reaction of a phosphaalkyne with MeLi. Reagents and conditions: (i) MeLi, THF, −78 °C;(ii) H_2O, hexane, −78 °C;(iii) 0.5 eq. MeLi, THF, −78 °C;(iv) RCl, hexane, −78 °C*

Interestingly, when a two-fold excess of phosphaalkyne was reacted with methyllithium, the formation of a 1,3-diphosphabutadienyl anion was achieved, apparent from the higher frequency $^{31}P\{^{1}H\}$ NMR shifts at 290 and 31 ppm, in conjunction with mass spectrometry data consistent with the formation of $[M\text{-}H]^+$. While treatment with water resulted in cleavage of one of the P-C bonds, the addition of an alkyl chloride afforded the corresponding 1,3-diphosphabutadiene, characterised by two resonances in the $^{31}P\{^{1}H\}$ NMR spectrum at 337.9 and 55.3 ppm, with a mutual coupling of 87 Hz. However, it is important to note that the assignment of the chemical shifts was based on the generalisation that the attachment of substituents with lone pairs to the carbon atom of a phosphaalkene results in a lower frequency chemical shift.[20]

It has also been demonstrated by Regitz and co-workers that cyclooligomerisation reactions of phosphaalkynes can occur within the coordination sphere of a transition metal, the most notable of which utilised a *tert*-butylimido-vanadium(V) complex to form trisubstituted triphosphabenzene rings (Scheme 1.6).[22] This method offers significant advantages over previous reports based on hafnium,[23] including the accessibility of the cyclooligomerisation reagent, and moderate to good yields depending on the phosphaalkyne used (36 – 68%).

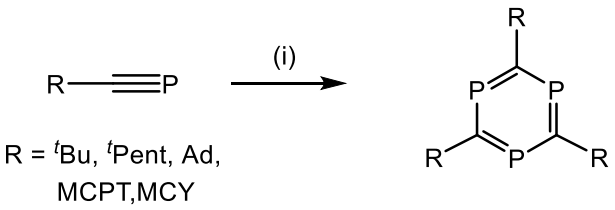

Scheme 1.6: *Synthesis of triphosphabenzenes. Reagents and conditions: (i) ^{t}BuN=VCl$_3$, toluene, −78 °C*

However, it has also been demonstrated that phosphaalkynes will readily undergo thermally-induced oligomerisation in the absence of a transition metal centre.[24] When samples of ^{t}BuC≡P were heated for prolonged periods of time and then distilled, an air-stable crystalline solid was formed. Elemental analysis and mass spectrometry data supported the formation of a tetrameric compound (Scheme 1.7).

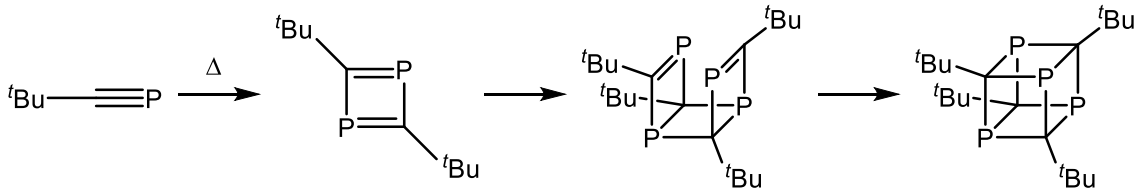

Scheme 1.7: *Thermally induced oligomerisation of a phosphaalkyne.*

The ^{13}C{^{1}H} NMR spectrum of the tetramer displayed three multiplets at −29.0, 21.6, and 30.6 ppm consistent with an AX$_3$Y spin system, alongside a high frequency shift of the ^{31}P{^{1}H} NMR resonance at 257.4 ppm. This was postulated to be due to a shift of electron density from the phosphorus atoms to carbon. The structure was elucidated by means of X-ray diffraction experiments, which revealed that the tetraphosphacubane exhibits a distorted-cube structure, with internal C-P-C angles of *ca*. 85 °, leading to an increase in the exocyclic P-C-C angles to *ca*. 94 °.

1.2.3 Phosphaalkyne Coordination Chemistry

Due to the presence of both the C≡P π-system and the phosphorus lone pair, a variety of coordination modes of a phosphaalkyne to a transition metal centre can be achieved (Figure 1.4).[4] Typically, η^2-coordination (**G**) is the most common mode observed, however, should the ancillary ligand set around the metal centre be sufficiently bulky, only η^1-coodination (**H**) is possible. While coordination modes **I–K** are also possible, there are significantly fewer examples than **G** and **H**.

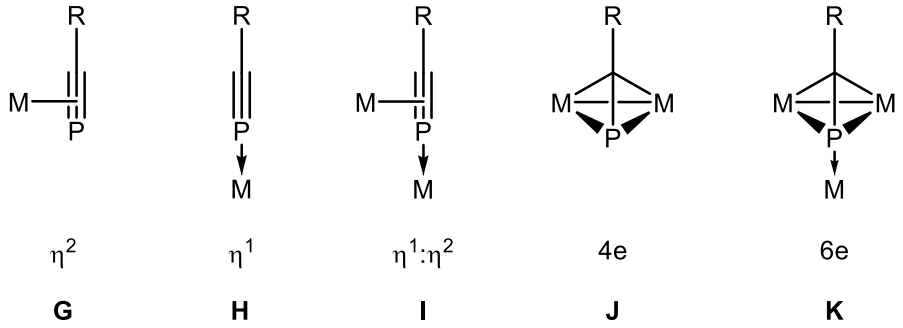

Figure 1.4: *Possible coordination modes of a phosphaalkyne to a metal centre*

The first instance of a phosphaalkyne ligated to a transition metal centre was reported by Nixon in 1981 (Scheme 1.8).[25] Single crystal X-ray diffraction studies revealed that, upon coordination, a significant lengthening of the C≡P bond was observed (1.672(17) Å *vs* 1.548(1) Å),[16,17] alongside a substantial bending of the *t*-butyl group (132(2) °), consistent with back-bonding from the platinum centre.

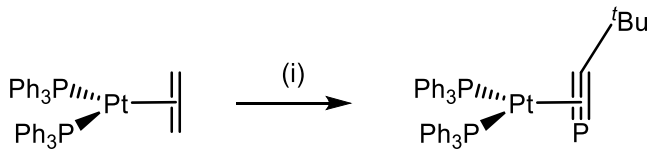

Scheme 1.8: *Formation of an η^2-phosphaalkyne platinum complex. Reagents and conditions: (i) 1 eq. ^{t}BuC≡P, C_6H_6*

Later, the synthesis of the first μ^3-η^2 phosphaalkyne complex was reported, achieved through the reaction of ^{t}BuC≡P with Pt(dppe)$_2$, followed by subsequent reaction with [Fe$_2$(CO)$_9$] or [Fe$_3$(CO)$_{12}$] to give the corresponding trimetallic complexes (Scheme 1.9).[26]

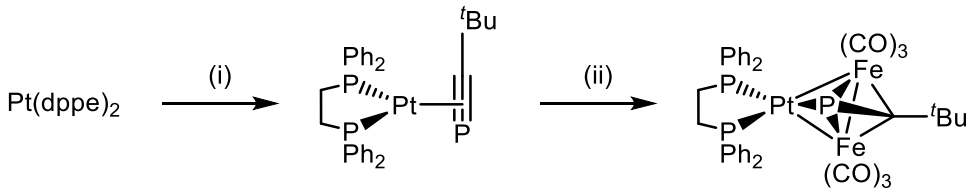

Scheme 1.9: *Synthesis of the first μ^3-η^2 phosphaalkyne complex. Reagents and conditions: (i) 1 eq. ^{t}BuC≡P; (ii) Fe$_2$(CO)$_9$ or Fe$_3$(CO)$_{12}$, toluene*

The parent phosphaalkyne complex exhibited an ABX pattern in the ^{31}P{^{1}H} NMR spectrum, with two dppe resonances at 47.4 and -53.1 ppm, and the phosphaalkyne resonance at 87.7 ppm, which exhibited a relatively low P-Pt coupling of 166 Hz, supporting the notion of η^2-coordination.[26]

Treatment with either [Fe$_2$(CO)$_9$] or [Fe$_3$(CO)$_{12}$] resulted in an AX$_2$ splitting pattern in the ^{31}P{^{1}H} NMR spectrum, with resonances at −51.8 and 61.1 ppm corresponding to the now-equivalent dppe centres and the phosphaalkyne respectively. Crystallographic studies showed transverse bridging of the phosphaalkyne over the Fe-Fe bond, with an associated lengthening of the C-P bond to 1.703(6) Å, which is more akin to a double, as opposed to triple, bond.[27]

Nixon also reported that the displacement of ligated stilbene from a transition metal centre could be utilised to form complexes featuring an η^2-coordinated phosphaalkyne (Scheme 1.10).[28] The resulting complex exhibited two singlet resonances in the ^{31}P{^{1}H} NMR spectrum at 467.8 and 157.3 ppm, corresponding to the phosphaalkyne and bidentate diphosphite respectively. Addition of further equivalents of phosphaalkyne resulted in the formation of a 1,3-diphosphabutadiene complex, formed *via* a cycloaddition between the free and ligated phosphaalkyne. It was speculated that the bound phosphaalkyne switched from a four-electron

binding mode to a two-electron mode to accommodate the second equivalent of phosphaalkyne.

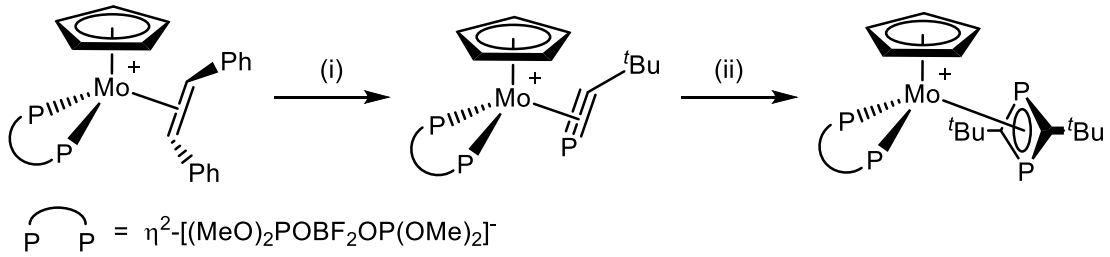

Scheme 1.10: *Coordination and subsequent cycloaddition of ^{t}BuC≡P at a molybdenum Centre. Reagents and conditions: (i) ^{t}BuC≡P, THF, −78 °C; (ii) ^{t}BuC≡P, toluene, 25 °C, 3 days.*

More recently, Russell and co-workers reported the formation of the first cationic, gold(I) phosphaalkyne complex.[29] Previous reports have shown that gold cations readily interact with the π-system of alkenes and alkynes,[30] with bonding achieved through a combination of substrate to metal sigma donation and metal to substrate backdonation. This results in interesting coordination behaviour, most notably slippage of the metal centre from a favoured symmetrical η^2 position.

Reaction of an excess of either AdC≡P or ^{t}BuC≡P with a cationic gold complex resulted in rapid formation of the corresponding η^2-phosphaalkyne complex (less than five minutes; Scheme 1.11), evidenced by very broad resonances in the $^{31}P\{^{1}H\}$ NMR spectrum at 72 and −22 ppm, corresponding to the ligand scaffold and coordinated phosphaalkyne respectively. The large line widths of these signals were evidence of a dynamic process in solution, which the authors considered likely to be rapid exchange of free and coordinated phosphaalkyne on the NMR timescale, which was supported by low temperature NMR studies, with each resonance resolving into a doublet at −40 °C, with a mutual coupling of *ca.* 32 Hz.

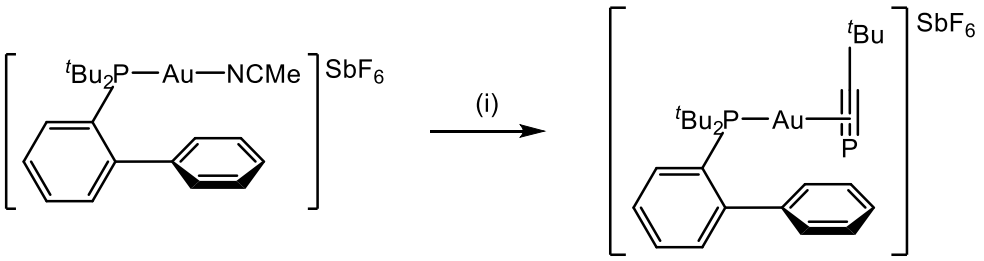

Scheme 1.11: *Formation of a gold phosphaalkyne complex. Reagents and conditions: (i) 3 eq. ^{t}BuC≡P, DCM*

In the solid state, a slight deviation from linearity of the P-Au-phosphaalkyne unit (*ca.* 169 °) was observed, and η^2-coordination of the phosphaalkyne was confirmed, with a C≡P bond length that was statistically indistinguishable from that of the free substrate.[16,17] Additionally, comparison of the P-C-C angle in the gold complex (163.5(8) °) to that in Nixon's [Pt(PPh_3)$_2$(η^2-P≡C^{t}Bu)] (132(2) °)[25] revealed diminished backbonding between the gold centre and the C≡P triple bond, thus C≡P character was maintained. Similar to gold acetylide complexes,[30] the phosphaalkyne complex also displayed slippage of the gold centre, with distances comparable to the covalent triple bond radii of carbon (0.6 Å) and phosphorus (0.95 Å).

The first example of a phosphaalkyne coordinated in an η^1-fashion to a transition metal centre was reported by Nixon in 1987.[31] Since the phosphorus lone pair is of significantly lower energy than the C≡P π-system (*ca.* 1.8 eV),[18] the use of a sufficiently bulky ancillary ligand set was required to preclude η^2-coordination of the phosphaalkyne. This was achieved through displacement of ligated dinitrogen from tungsten and molybdenum complexes of the type *trans*-[M(PP)$_2$(N_2)$_2$] (PP = chelating diphosphane) (Scheme 1.12).

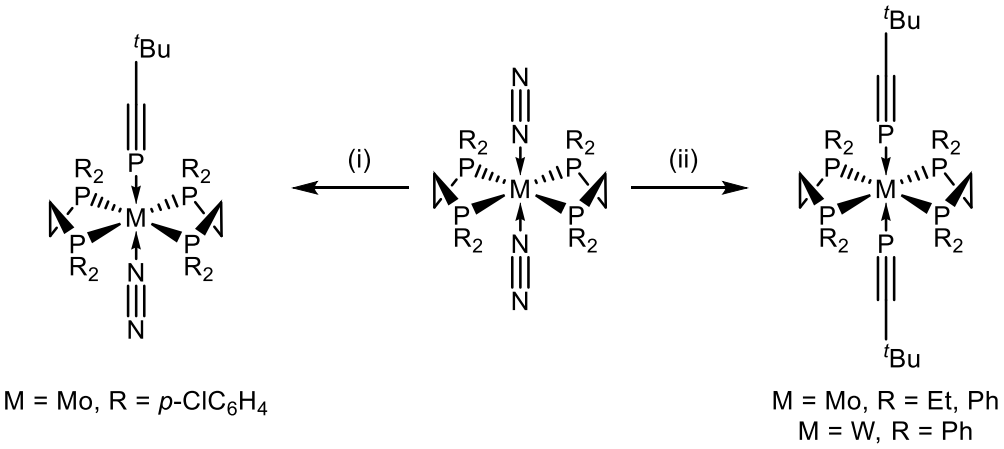

Scheme 1.12: *Formation of the first examples of η[1]-phosphaalkyne coordination. Reagents and conditions: (i) 1 eq. [t]BuC≡P; (ii) 2 eq. [t]BuC≡P*

The syntheses were supported by solution-phase $^{31}P\{^{1}H\}$ NMR spectroscopic data, with splitting patterns consistent with either an AA'BB'X or A_4X_2 spin system for the mono- and diphosphaalkyne complexes respectively. The mutual coupling between the phosphaalkyne and diphosphane centres in the diphosphaalkyne complexes was reported to be consistent with η^1-coordination ($^2J_{PP}$ = *ca.* 40 Hz), as much smaller coupling constants would be expected for an η^2-coordinated phosphaalkyne. Crystallographic studies on a sample of *trans*-[Mo(dppe)$_2$(P≡CAd)$_2$] showed a linear C-C-P-Mo-P-C-C unit, with P-C-C and C-P-Mo angles of 176.3(5) ^{o} and 177.9(8) ^{o} respectively, and a relatively short C-P bond length of 1.520(12) Å. This confirmed that the chelating diphosphanes did indeed possess enough steric bulk to preclude side-on coordination of the phosphaalkyne, thus only allowing axial coordination to the metal centre *via* the phosphorus lone pair.

Further work reported by Nixon extended this concept to group VIII metal complexes, with the abstraction of chloride from *trans*-FeHCl(dppe)$_2$, followed by η^1-coordination of a phosphaalkyne (Scheme 1.13).[32,33] The resulting complex exhibited a splitting pattern consistent with an AX_4 spin system in the $^{31}P\{^{1}H\}$ NMR spectrum, with two resonances at 13.0 ppm and 78.7 ppm, assigned to the phosphaalkyne and dppe respectively, with a mutual coupling of 36 Hz. In

the solid state, the expected octahedral geometry around the iron centre was observed, with the phosphaalkyne coordinated *trans* to the hydride ligand. Most notably, a significant shortening of the C-P bond to 1.512(5) Å was observed, directly contrasting to the lengthening seen in complexes featuring η^2-coordinated phosphaalkynes.

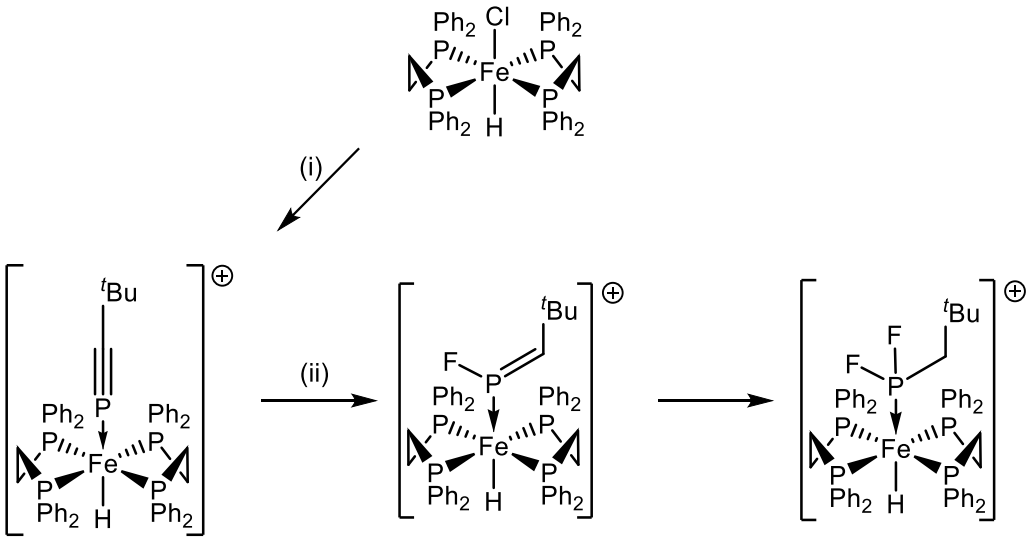

Scheme 1.13: *Formation and subsequent reactivity of an iron phosphaalkyne complex. Reagents and conditions: (i)* ^{t}*BuC≡P, TlBF*$_4$*, [NH*$_4$*][BF*$_4$*], THF, 24 h.; (ii) [Et*$_2$*OH][BF*$_4$*], DCM, 24 h.*

It had previously been reported that this complex serendipitously reacted with its BF_4 counterion to give the corresponding fluorophosphaalkene complex, which could be reproduced reliably upon addition of either HBF_4 or $[Et_2OH][BF_4]$ to a DCM solution of *trans*-$[FeH(P{\equiv}C^tBu)(dppe)_2]BF_4$. The resulting product exhibited a doublet of quintets in the $^{31}P\{^1H\}$ NMR spectrum at 318.6 ppm ($^1J_{PF}$ = 985 Hz, $^2J_{PP}$ = 38 Hz), alongside a doublet at 79.3 ppm ($^2J_{PP}$ = 38 Hz), corresponding to the phosphaalkenyl and ancillary ligand set respectively. In the solid state, the phosphaalkene moiety displayed a shorter than expected C-P bond length of 1.66(4) Å when compared to free phosphaalkenes,[34] in direct contrast to the anticipated elongation arising from metal to ligand backdonation into the $\pi^*_{C=P}$ orbital.

This reaction also proceeded further to give the corresponding difluorophosphane complex, as determined by $^{31}P\{^{1}H\}$ NMR spectroscopy, with the $PF_2CH_2{}^tBu$ fragment appearing as a triplet of quintets at 278.5 ppm, and a doublet resonance in the ^{19}F spectrum at −39.3 ppm. The determined $^{1}J_{PF}$ value of 1067 Hz was significantly higher than that observed in similar group VIII fluorophosphane complexes (*cf.* 844 Hz),[35,36] though this was believed to arise from the presence of two, as opposed to one, electronegative fluorine atoms.

Similar reactivity of a ligated phosphaalkyne was observed at a rhenium(I) centre with an identical ancillary ligand set, which formed a rare example of a P-bonded phosphinidene oxide, synthesised by displacement of dinitrogen from $[ReCl(dppe)_2(N_2)]$ by $^{t}BuC{\equiv}P$, followed by subsequent addition of H_2O across the activated C≡P triple bond (Scheme 1.14).[37] The phosphinidine oxide complex displayed a quintet and doublet resonance at 340.1 and 24.9 ppm in the $^{31}P\{^{1}H\}$ NMR spectrum, with an associated $^{2}J_{PP}$ value of 25.6 Hz, alongside characteristic resonances in the ^{1}H NMR spectrum at 0.21 and −0.24 ppm, corresponding to the *tert*-butyl and methylene protons respectively.

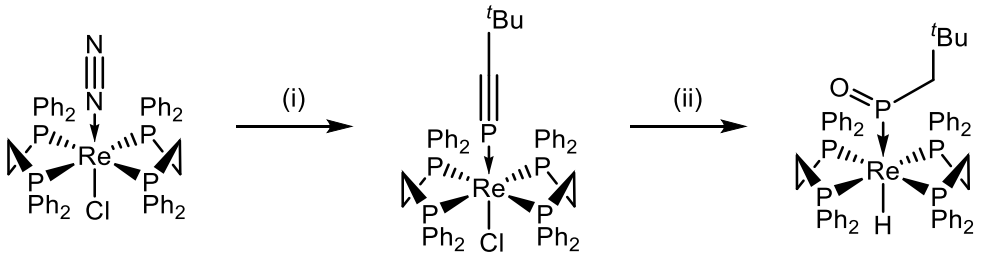

Scheme 1.14: *Formation of a phosphinidene oxide of rhenium(I). Reagents and conditions: (i) $^{t}BuC{\equiv}P$, THF; (ii) H_2O, THF*

In the solid state, the coordination of the phosphinidine oxide was confirmed to be *via* the phosphorus lone pair and displayed the expected trigonal planar geometry around phosphorus. A Re-P distance of 2.203(1) Å was reported to be considerably shorter than the average $Re\text{-}P_{dppe}$ distances (2.433(1) Å), which was attributed to the smaller radius of the sp^2 hybridised

phosphorus of the phosphinidine oxide ligand. It should be noted that this type of reactivity is in direct contrast to that observed for related C- or N-unsaturated ligands (*cf.* vinylidenes, isonitriles) which, when ligated to the same rhenium(I) centre, are activated towards β-protonation as opposed to nucleophilic attack.

1.2.4 Diphosphaalkynes

Currently, there are only three unequivocal examples of diphosphaalkynes reported in the chemical literature.[38–40] The first, 1,4-diphosphabutadiyne, was reported in 2000 by Schumann and co-workers,[38] after theoretical studies suggested that the compound would be thermodynamically stable.[41,42] Electron ionisation of $Cl_2P\text{-}C{\equiv}C\text{-}PCl_2$ or $Cl_2PCH_2P(Cl)CH_3$ in a mass spectrometer formed a species with a *m/z* = 86, attributed to the radical cation $[P{\equiv}C\text{-}C{\equiv}P]^{+\bullet}$. Subsequent neutralisation-reionisation experiments led to the formation of the neutral diphosphaalkyne P≡C-C≡P.

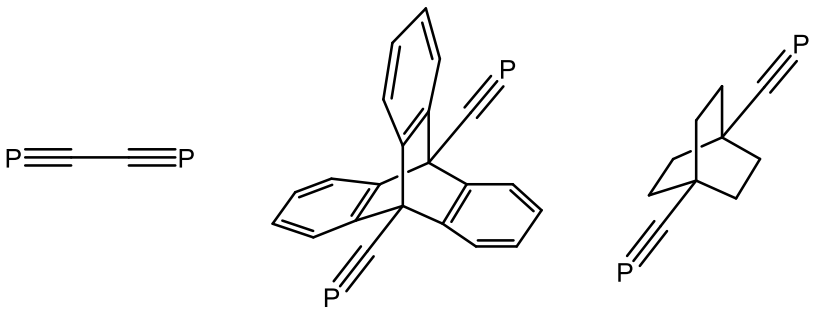

Scheme 1.15: *Currently reported examples of diphosphaalkynes*

The first unequivocal and isolable diphosphaalkyne was prepared by Jones and co-workers in 2003 by reacting 9,10-triptycenedicarbonyl chloride with two equivalents of $[LiP(SiMe_3)_2(DME)]$, forming the corresponding diphosphaalkene which, upon treatment with a catalytic amount of potassium hydroxide, afforded the desired diphosphaalkyne (Scheme 1.16).[39]

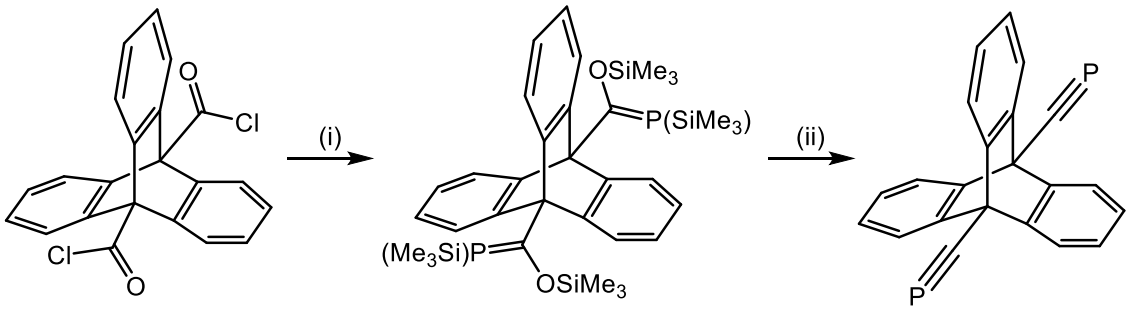

Scheme 1.16: *Synthesis of a diphosphaalkyne featuring a triptycene spacer. Reagents and conditions: (i) $LiP(SiMe_3)_2(DME)$, cyclohexane; (ii) $LiN(SiMe_3)_2$, DME*

This air and moisture stable phosphaalkyne displayed a singlet in the $^{31}P\{^1H\}$ NMR spectrum at −15.7 ppm, which is in the typical region for alkyl phosphaalkynes (*ca.* −70 – 35 ppm),[4,43] as well as a doublet in the $^{13}C\{^1H\}$ spectrum at 164.0 ppm ($^1J_{CP}$ = 47 Hz). Furthermore, in the solid state, the phosphaalkyne was monomeric, exhibited no intermolecular close contacts, and the C≡P bond length (1.531(2) Å) was comparable to other phosphaalkynes in the literature.[4]

Later work by Jones and co-workers sought to reduce the steric bulk around the C≡P units by replacing the triptocenyl spacer with a much less bulky bicyclo[2.2.2]octanediyl spacer, so as to enhance the C≡P unit's reactivity.[40] Reaction of the corresponding dicarbonylchloride with $[LiP(SiMe_3)_2(DME)]$ resulted in the formation of the expected phosphaalkene as a mixture of the *E* and *Z* isomers which, upon treatment with $LiN(SiMe_3)_2$, resulted in elimination of hexamethyldisiloxane to afford the desired diphosphaalkyne (Scheme 1.17).

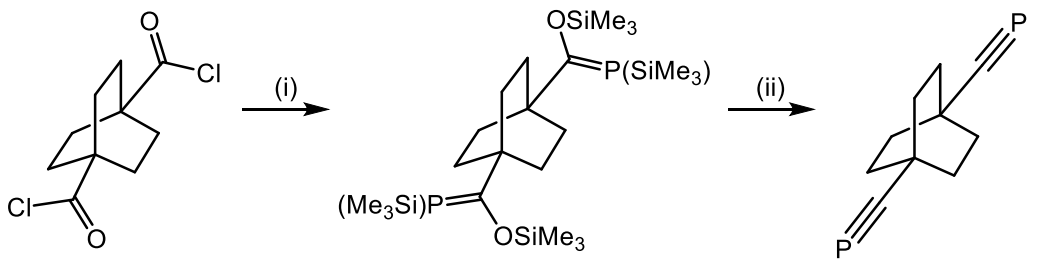

Scheme 1.17: *Synthesis of a diphosphaalkyne featuring a bicyclo[2.2.2]octanediyl spacer. Reagents and conditions: (i) $LiP(SiMe_3)_2(DME)$, cyclohexane; (ii) $LiN(SiMe_3)_2$, DME*

The phosphaalkyne displayed a singlet resonance in the $^{31}P\{^{1}H\}$ NMR spectrum at −60.8 ppm, which was consistent with previously described phosphaalkynes,[4] and has been shown to react with both CyMgCl and methyllithium to give the corresponding diphosphavinyl metallates. However, due to thermal instability these could only be observed in the $^{31}P\{^{1}H\}$ NMR spectrum at −30 °C (singlets at 322 and 264 ppm respectively) and have not yet been isolated as discrete species.

1.2.5 The 2-Phosphaethynolate Anion

The 2-phosphaethynolate anion, [P≡CO$^-$] (the phosphorus analogue of the cyanate anion [N≡CO$^-$]) has received a significant amount of interest in the current decade.[44] Isoelectronic with FC≡P, O=C=S, and S=C=N$^-$, this anion was first synthesised by Becker and co-workers in 1992, *via* the reaction of dimethylcarbonate with lithium bis(trimethylsilyl)phosphanide,[45] with later work seeking to synthesise other group I and II salts of the anion (Scheme 1.18).[46]

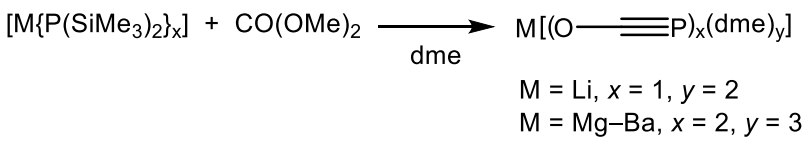

Scheme 1.18: *Synthesis of group I & II 2-phosphaethynolate salts*

In 2011 Grützmacher and co-workers reported the facile synthesis of sodium phosphaethynolate from sodium phosphide and carbon monoxide under high pressure (Scheme 1.19).[47] X-ray diffraction studies revealed an average bond length of 1.589(3) Å, similar to that reported for HC≡P.[7] Unlike previous reports, this salt demonstrated significant thermal stability, showing no signs of decomposition when heated to 110 °C in either THF or DME.

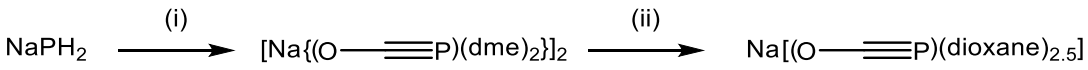

Scheme 1.19: *Synthesis of the 2-phosphaethynolate anion from $NaPH_2$ and CO. Reagents and conditions: (i) CO, 110 bar, 80 °C, DME; (ii) dioxane*

Alternative synthetic methods were devised, using $[NaPH_2{\cdot}(NaO^tBu)_x]$ and $[Fe(CO)_5]$. [47,48] *In situ* NMR studies of the reaction mixtures in THF showed only one phosphorus-containing species in the $^{31}P\{^1H\}$ NMR spectrum, with a chemical shift consistent with the THF adduct of sodium phosphaethynolate (Scheme 1.20). Furthermore, reactions of $[NaPH_2{\cdot}(NaO^tBu)_x]$ with ethylene carbonate afforded NaOC≡P upon workup, this reaction being preferable due to its ability to be conducted at room temperature without the need for specialised equipment.

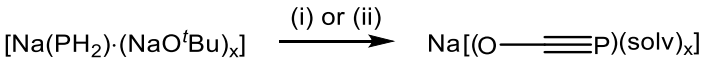

Scheme 1.20: *Alternative synthesis of the 2-phosphaethynolate anion. Reagents and conditions: (i) $Fe(CO)_5$, THF; (ii) ethylene carbonate, DME*

Cummins and co-workers reported the synthesis of sodium phosphaethynolate using organometallic chemistry, *via* multiple bond metathesis between an anionic niobium phosphide complex and carbon dioxide (Scheme 1.21).[49]

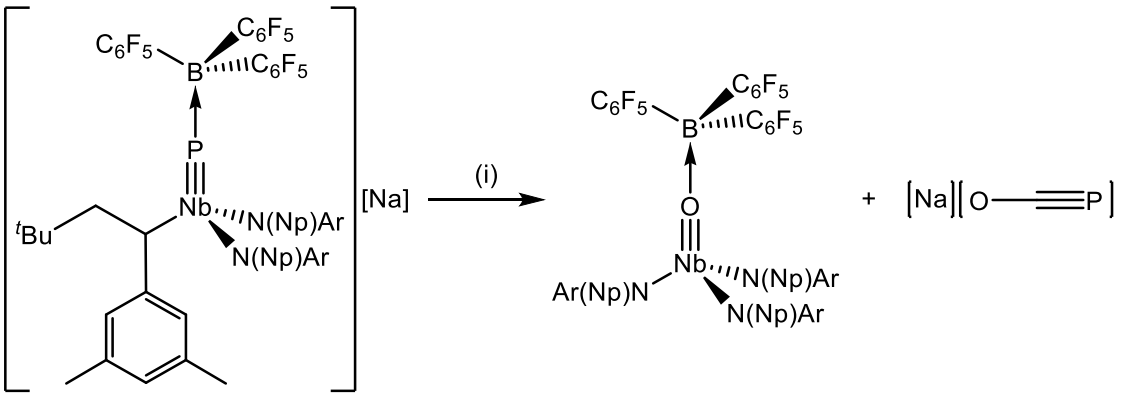

Scheme 1.21: *Synthesis of sodium phosphaethynolate via a niobium phosphide complex. Reagents and conditions: (i) 1 eq. CO_2, Et_2O, 25 °C*

Initial $^{31}P\{^1H\}$ NMR studies of the crude reaction mixture revealed a low frequency resonance at −393 ppm, similar to that reported by Becker for lithium phosphaethynolate.[45] After workup, the sodium salt could be isolated in up to 70% yield, with $^{13}C\{^1H\}$ NMR and infrared spectroscopic data supporting the formation of the phosphaethynolate anion (δ_C: 169, ν_{CP}: 1773 cm^{-1}), alongside X-ray structural analysis.

Later work by Goicoechea established the synthesis of the potassium salt [K(18-C-6)][OC≡P] from a substituent-free polyphosphide and carbon monoxide in moderate yields (*ca.* 38%; Scheme 1.22).[50] It was postulated by the authors that the salt was formed *via* the formal transfer of a phosphide anion to the carbon monoxide.

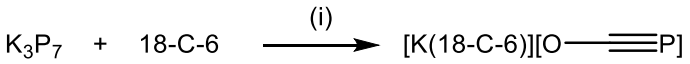

Scheme 1.22: *Synthesis of [K(18-C-6)][OC≡P]. Reagents and conditions: (i) 1 atm. CO, 150 °C, DMF, 24 h.*

The $^{31}P\{^1H\}$ and $^{13}C\{^1H\}$ NMR spectra exhibited singlet and doublet resonances at −396.8 and 170.3 ppm respectively, while the solid-state IR spectrum revealed a band at 1730 cm^{-1}, which were consistent with previous literature reports. The solid-state structure showed a single

"O−C≡P" unit demonstrating close electrostatic contact with the complexed potassium cation (d_{K-P} = 3.383(1) Å). The C-P and O-C bond data were consistent with a formal C≡P triple bond.

The chemistry of this anion was then explored, demonstrating behaviour akin to that of phosphaalkynes, first exemplified through the [2+2] cycloaddition with diphenylketene (Scheme 1.23).[50] The reaction resulted in formal addition of the C≡P triple bond across the C=C double bond of the ketene, with the final product exhibiting one singlet resonance in the $^{31}P\{^{1}H\}$ NMR spectrum at −165.7 ppm. An analogous reaction using bis(2,6-diisopropylphenyl)carbodiimide was shown to form the analogous four-membered ring, though later studies showed that this reaction was highly sensitive to the nature of the substituents on the carbodiimide, with no reaction observed when using bis(cyclohexyl)carbodiimide.

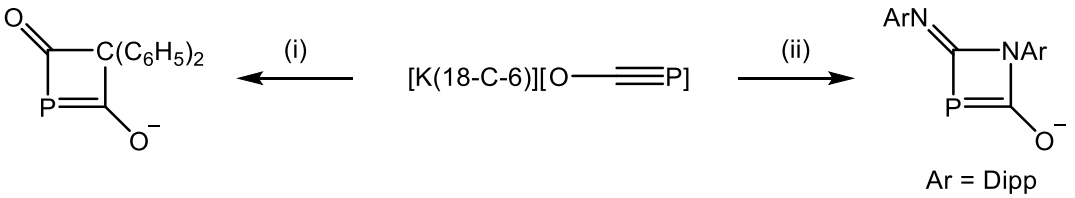

Scheme 1.23: *Cycloaddition chemistry of 2-phosphaethynolate. Reagents and conditions: (i) diphenylketene, pyridine; (ii) C(NDipp)$_2$, pyridine-d$_5$*

Later, it was reported that the 2-phosphaethynolate anion could be utilised as a phosphide transfer reagent.[51] Addition to a sample of a cyclotrisilene resulted in cleavage of the C≡P triple bond, and addition of CO and P across the Si=Si double bond (Scheme 1.24), with the structure elucidated through NMR spectroscopic and X-ray diffraction studies. Subsequent photolysis resulted in a shift to higher frequency of the phosphorus resonance in the $^{31}P\{^{1}H\}$ NMR spectrum from −323.0 to −93.9 ppm, alongside loss of the characteristic carbonyl resonance in the $^{13}C\{^{1}H\}$ NMR spectrum, which suggested decarbonylation. This was supported by X-ray diffraction studies, where loss of the carbonyl group was observed, alongside the direct incorporation of phosphide into the unsaturated ring system.

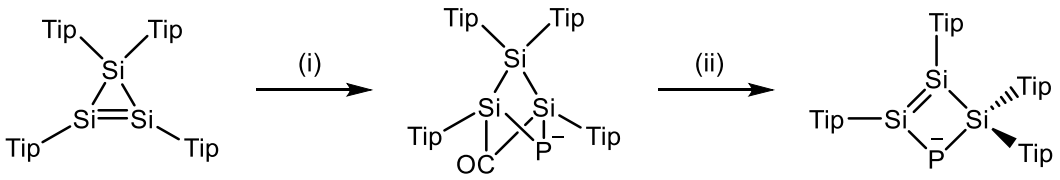

Scheme 1.24: *Use of 2-phosphaethynolate as a phosphide transfer reagent. Reagents and conditions: (i) [K(18−crown−6)][PCO]; (ii) hv*

Similar to phosphaalkynes,[4] the 2-phosphaethynolate anion readily undergoes dimerisation reactions, as reported by Stephan and Grützmacher.[52] Addition of borane resulted in the formation of borane-stabilised isomeric dimers, with the isomer formed dependent on the borane used (Scheme 1.25). The BPh_3 system rapidly dissociated in solution at room temperature to give free $^{-}$[PCO], thus precluding spectroscopic characterisation; however, the structure was confirmed by X-ray diffraction experiments, which revealed the anion comprises of a dimeric $[(PCO)_2]^{2-}$ core, stabilised by BPh_3 moieties bound to each of the phosphorus atoms.

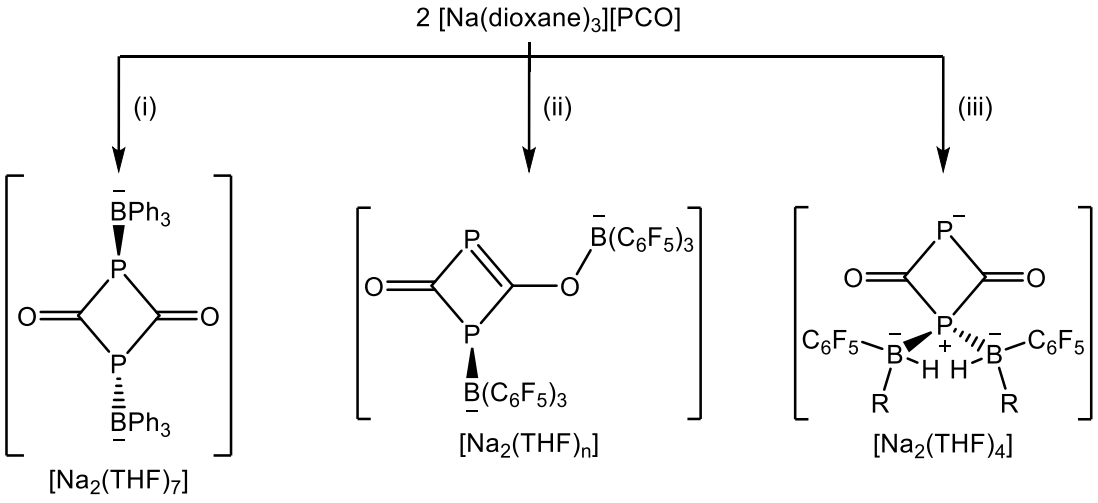

Scheme 1.25: *Reaction of 2-phosphaethynolate with boranes to form isomeric dimers. Reagents and conditions: (i) BPh_3, THF; (ii) $B(C_6F_5)_3$, THF; (iii) $HB(R)(C_6F_5)$, THF, R = H, C_6F_5*

Interestingly, the reaction of $B(C_6F_5)_3$ with [Na(dioxane)$_3$][PCO] in THF was monitored by NMR spectroscopy, with the $^{31}P\{^1H\}$ spectrum initially displaying four resonances, with those at −309.8

(singlet) and −288.2 (septet, $^{4}J_{PF}$ = 47 Hz) believed to correspond to the formation of $[P{\equiv}C{-}O{-}B(C_6F_5)_3]^-$ and $[O{=}C{=}P{-}B(C_6F_5)_3]^-$ respectively. After 24 hours under ambient conditions, the remaining broad singlet and doublet resonances in the $^{31}P\{^{1}H\}$ NMR spectrum at 269.1 and 124.7 ppm respectively were observed, alongside $^{11}B\{^{1}H\}$ NMR resonances at −2.4 and −4.6 ppm, suggesting formation of an asymmetric dimer of reduced symmetry when compared to the BPh_3 system. The observation of the transient monomeric borate-oxyphosphaalkyne and boryl-phosphaketene suggested that these products arise from [2+2] cycloaddition reactions.

Further, unexpected results were obtained upon reaction with $HB(C_6F_5)_2$, which has previously demonstrated the ability to hydroborate C≡P multiple bonds, as reported by Russell and co-workers.[53] The reaction proceeded rapidly (< 30 minutes), with the $^{11}B\{^{1}H\}$ NMR spectrum displaying a broad resonance at −25.6 ppm, alongside two resonances, a doublet and a broad singlet, in the $^{31}P\{^{1}H\}$ spectrum at 278.8 and 125.8 ppm respectively. The $^{13}C\{^{1}H\}$ spectrum showed a doublet of doublets at 232.2 ppm, which was indicative of a deshielded carbon atom neighboured by two chemically inequivalent phosphorus atoms. Low temperature NMR studies revealed the formation of $[(C_6F_5)_2HBPCO]^-$, thus supporting the belief that these dimers are formed by a [2+2] cycloaddition, followed by borane migration.

Similarly, Grützmacher reported the use of a transition metal centre to facilitate end-on dimerisation of the 2-phosphaethynolate anion (Scheme 1.26),[54] with scandium chosen due to being typically redox-inactive and oxophilic, thus reducing the chance of decarbonylation, which had been observed previously.[55,56] Reaction of sodium phosphaethynolate with the scandium complex resulted in the formation of a single product, as determined by $^{31}P\{^{1}H\}$ NMR studies. A single resonance at −343.5 ppm, which is at a slightly lower frequency than the starting material and known *O*-bound actinide complexes, was observed.[57–59] Later X-ray studies confirmed *O*-coordination of the OCP fragment to the metal centre, which had remained intact rather than undergoing any decarbonylation.

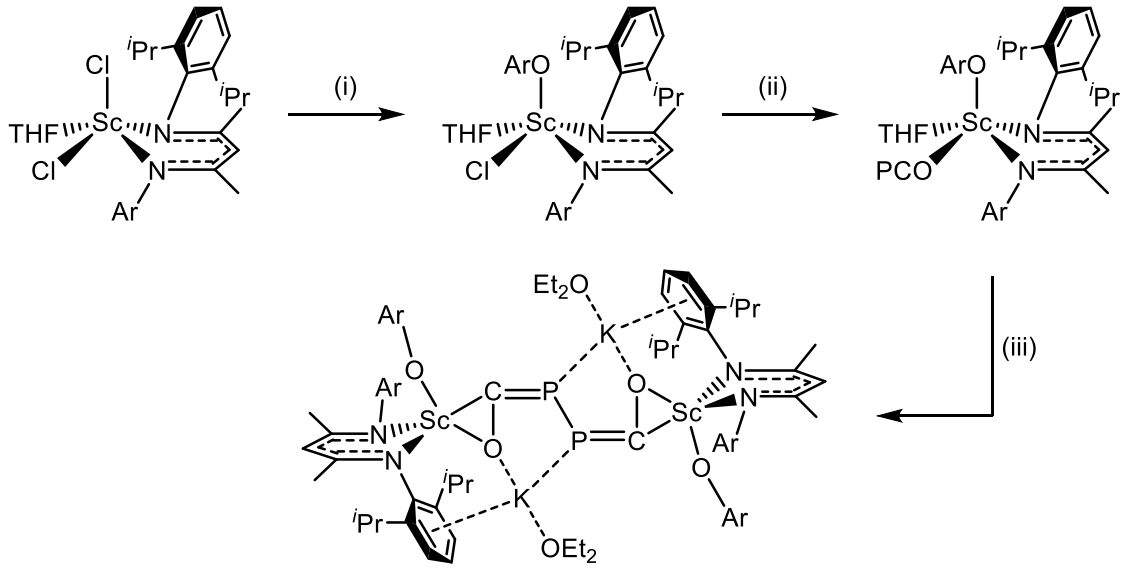

Scheme 1.26: *Synthesis and dimerisation of a scandium phosphaethynolate complex. Reagents and conditions: (i) NaOAr, THF; (ii) NaOCP(dioxane)$_{2.5}$, THF; (iii) KC_8, Et_2O. Ar = 2,6-^{i}Pr$_2$C$_6$H$_3$*

Subsequent reaction with KC_8 afforded a thermally unstable and highly insoluble orange solid, with ^{1}H NMR spectroscopic data suggesting a complex of similar symmetry to its precursors, and ^{31}P{^{1}H} NMR spectroscopic data suggesting altered electronics of the "OCP" moiety, owing to a higher frequency resonance at 69.7 ppm. X-ray diffraction experiments revealed the formation of a dinuclear-ate complex, formed by reductive coupling without the extrusion of CO to form a diisophosphaethynolate ligand, where each CO unit of the OCPPCO core is bound in an η^2-fashion to the scandium centres.

Additionally, the coordination chemistry of the 2-phosphaethynolate anion has been explored, in particular the contrasting behaviour when compared to cyanate.[60] Cyclic voltammetry studies of Na(OCP) showed irreversible oxidation at low anodic potentials (E = −0.06 V *vs* $[FeCp_2]^{0/+}$ in DMSO, −0.3 V in THF), with no corresponding reductive event observed, which the authors attributed to high stability of the oxidised species. The authors postulated that since rhenium is typically a low-spin d^6 metal centre, coordination of OCP could be achieved, as its complexes would be stable against reduction by Na(OCP) (Scheme 1.27).

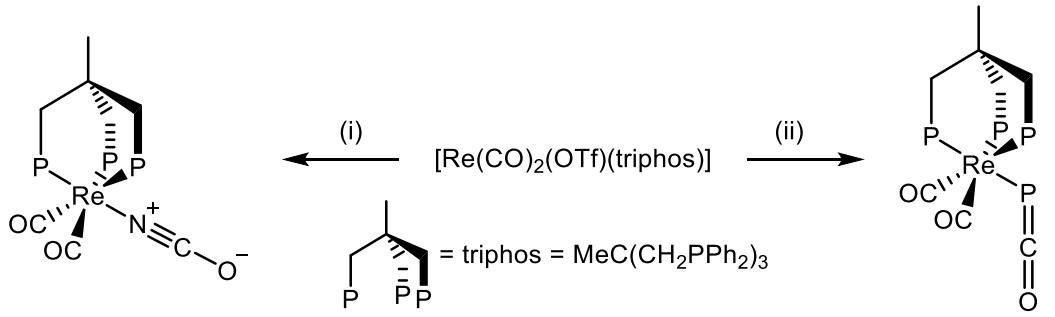

Scheme 1.27: *Syntheses of terminal isocyanate and phosphaethynolate rhenium complexes. Reagents and conditions: (i) K(OCN), THF/H_2O; (ii) Na(OCP), THF.*

In the solid state, both the phosphaethynolate and cyanate complexes exhibited distorted octahedral geometries at the metal centre, with binding occurring *via* the pnictogen atom. Unfortunately, no bond parameters could be reported due to significant crystallographic disorder, however, further investigations were undertaken using DFT, based upon the observed solid-state geometries. The most significant difference observed was the coordination mode of phosphaethynolate *vs* cyanate, with the former exhibiting a bent coordination mode, with a calculated Re-P-C angle of 97.7 °. This, in conjunction with NRT and NBO calculations, suggested that the OCN fragment should be considered as an O-C≡N moiety, whereas the phosphaethynolate behaves more akin to an allene-like P=C=O resonance form. This agreed with previous reports, which stated that the stability of $^{-}$O-C≡P arises from the existence of the P=C=O resonance form.[50]

1.3 Cyaphide

1.3.1 The Cyaphide Anion

The cyaphide anion, $^{-}$C≡P, is the phosphorus analogue of the cyanide anion, $^{-}$C≡N, and acetylide fragment, [$^{-}$C≡CH]. Unlike its carbon and nitrogen counterparts, it has yet to be isolated in the

form of a discrete salt, thus eluding experimental characterisation. As a result, computational studies have been undertaken to assess both the structure and reactivity of this fragment.

Initial investigations by Pascoli, Lavendy, and Poliart predicted C-P bond distances in the region of 1.604–1.609 Å,[61,62] which are more consistent with a strong C=P double bond, and are slightly longer than the experimentally derived distance observed in ^{t}BuC≡P. Furthermore, Mulliken charge analysis determined that the negative charge is largely localised on carbon (65%) as opposed to phosphorus, which accounts for the higher gas-phase basicity of $^{-}$C≡P than $^{-}$C≡N.[61]

1.3.2 Cyaphide Complexes

The first reported example of a transition metal cyaphide complex was reported by Angelici in 1992, and was obtained *via* the reaction of *trans*-[PtCl(PEt$_3$)$_2${C(Cl)=PR}] (R = Mes*) with [Pd(PEt$_3$)$_4$].[63] Subsequent trapping with [Pt(PEt$_3$)$_4$] afforded an η^2-bridging cyaphide complex (Scheme 1.28), the structure of which was confirmed using solid state X-ray diffraction studies.

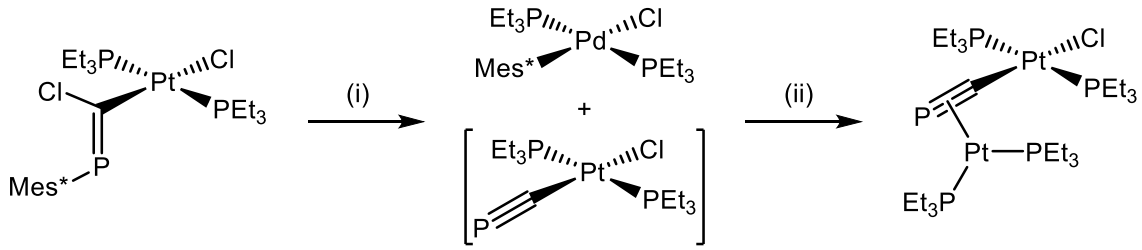

Scheme 1.28: *Formation and trapping of a terminal cyaphide ligand. Reagents and conditions: (i) Pd(PEt$_3$)$_4$, benzene; (ii) Pt(PEt$_3$)$_4$, benzene*

The solution state ^{31}P{^{1}H} NMR spectrum of the intermediary mixture exhibited doublet and triplet resonances at 7.3 and 68.0 ppm respectively, with a mutual coupling of 9.2 Hz. The observed $J_{P\text{-}Pt}$ value of 2871 Hz suggested a mutual *trans* geometry of the two phosphane ligands, suggesting that the triplet resonance arises from the terminal cyaphide ligand.

Formation of the cyaphide complex was believed to occur through insertion of the palladium centre into the C-Cl bond of the phosphaalkene, followed by subsequent transfer of the Mes* group from phosphorus to palladium and elimination of the palladium complex.

The first unequivocal example of a terminal transition metal cyaphide complex was reported by Grützmacher in 2006, *via* desilylative rearrangement of an η^1-coordinated phosphaalkyne precursor.[64] Reaction of the phosphaalkyne $Ph_3SiC{\equiv}P$ with $[RuH(dppe)_2]^+$ resulted in η^1-coordination to the metal centre (Scheme 1.29); subsequent addition of NaOPh resulted in desilylative rearrangement over a period of 14 hours to afford the corresponding cyaphide complex.

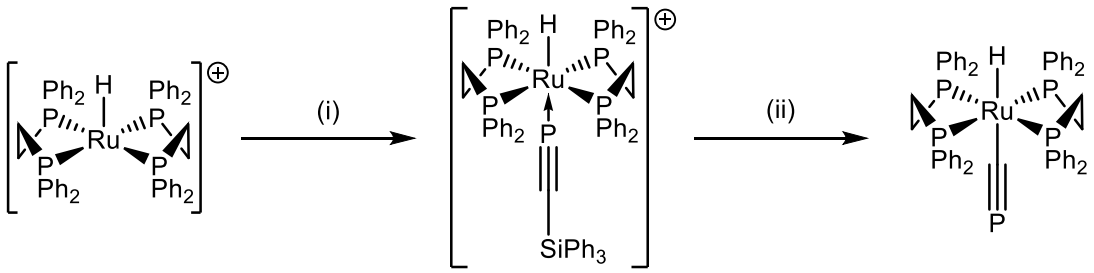

Scheme 1.29: *Synthesis of trans-$[RuH(dppe)_2(C{\equiv}P)]$. Reagents and conditions: (i) $Ph_3SiC{\equiv}P$, DCM/tol.; (ii) NaOPh, THF*

The $^{31}P\{^1H\}$ NMR spectrum of *trans*-$[RuH(dppe)_2(\eta^1\text{-}P{\equiv}CSiPh_3)]^+$ displayed a characteristic AX_4 splitting pattern, with a quintet and doublet at 143.8 and 60.1 ppm, corresponding to the phosphaalkyne and dppe ligand set respectively, with a mutual coupling of 28.7 Hz. Coordination of the phosphaalkyne was further supported by the ^1H NMR spectrum, which displayed a doublet of quintets at -8.13 ppm, resulting from coupling to both the ancillary ligand set and the η^1 phosphaalkyne to the metal hydride.

Crystallographic studies on the η^1-phosphaalkyne complex showed a C-P bond distance of 1.530(3) Å, which was statistically indistinguishable from that observed for $Ph_3CC{\equiv}P$ (1.538(2) Å) and therefore consistent with a triple bond.[65] Moreover, the complex exhibited a slightly bent

P≡C-Si unit, with an associated bond angle of 165.5(2) °, which was attributed to steric interactions arising from the ancillary ligand set.[64]

Upon treatment with base, the resonances in the $^{31}P\{^{1}H\}$ NMR spectrum shifted to higher frequencies, 165 and 65.2 ppm for the cyaphide and dppe ligand set respectively, and a reduction in the J_{PP} value was observed. In the ^{1}H NMR spectrum, the hydride resonance shifted to −11.22 ppm, with an associated *trans*-P-H coupling of approximately 20 Hz (*vs* 122 Hz for the parent phosphaalkyne complex). In the crystal structure, *trans*-[RuH(dppe)$_2$(C≡P)] exhibited a near-linear Ru-C≡P unit, with an associated bond angle of 177.9 ° and a C≡P bond length of 1.573(2) Å, which was significantly longer than that observed in ^{t}BuC≡P (1.548(1) Å).[66]

The desilylation step had been envisaged to proceed *via* nucleophilic attack at the silicon centre, forming an isocyaphide intermediate.[67] This could then undergo rearrangement to the terminal cyaphide ligand *via* an η^2-coordinated intermediate (Scheme 1.30). A secondary product was observed *in situ* in the $^{31}P\{^{1}H\}$ NMR spectrum, with a chemical shift of 310 ppm, which was believed to arise from reversible attack at phosphorus by phenoxide but was not part of the mechanism of cyaphide formation, as determined by computational investigations.

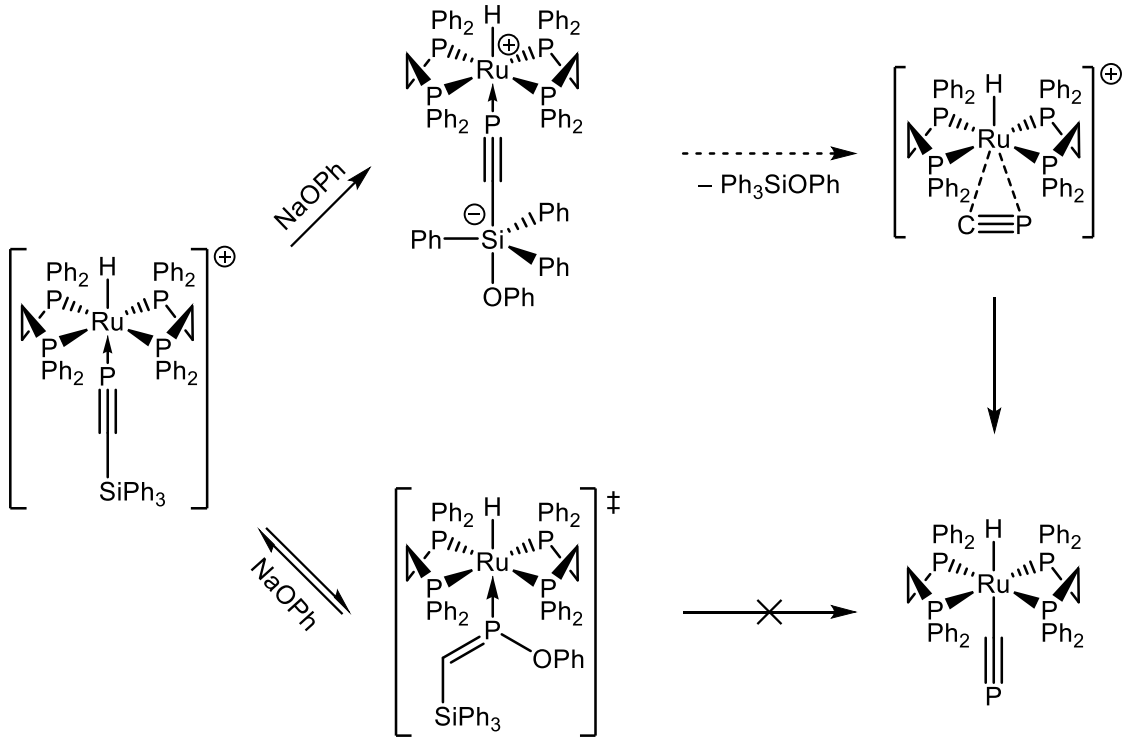

Scheme 1.30: *Proposed reaction pathway for desilylative rearrangement*

In 2012, Russell and co-workers reported the coordination chemistry and reactivity of the phosphaalkyne $Me_3SiC{\equiv}P$, notably, its η^1-coordination to a molybdenum centre in an analogous fashion to previous reports with ^{t}BuC≡P (Scheme 1.31).[68,69]

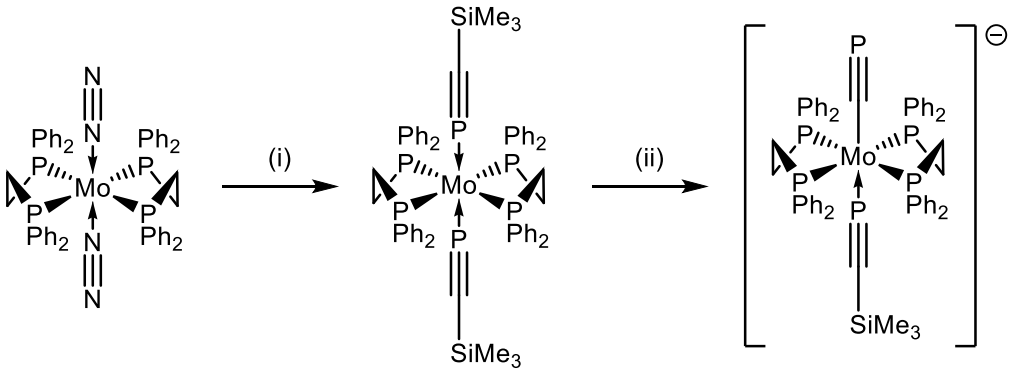

Scheme 1.31: *Synthesis and reaction of trans-[Mo(η^1-P≡CSiMe$_3$)$_2$(dppe)$_2$]. Reagents and conditions: (i) 2 eq. Me$_3$SiC≡P, tol.; (ii) TBAT, THF*

The $^{31}P\{^{1}H\}$ NMR spectrum of *trans*-[Mo(η^1-P≡CSiMe$_3$)$_2$(dppe)$_2$] displayed mutually coupling quintet and triplet resonances at 171.7 and 62.8 ppm ($^2J_{PP}$ = 39 Hz) in a 2:4 ratio, corresponding to the phosphaalkynes and ancillary ligand set respectively. In the solid state, the two phosphaalkynes were identical, with a C-P distance of 1.540(2) Å, considerably shorter than that observed in the analogous *trans*-[Mo(η^1-P≡CAd)$_2$(dppe)$_2$].[69]

Attempts to induce desilylative rearrangement with NaOPh were unsuccessful, and the thermal instability of the complex impeded further attempts. However, treatment with TBAT (TBAT = [^{N}Bu$_4$][Ph$_3$SiF$_2$]) resulted in the loss of both resonances in the $^{31}P\{^{1}H\}$ NMR spectrum, and their replacement by a doublet of doublets and two complex multiplets at 65.5, 197.8 and 183.0 ppm respectively.[68] In the ^{19}F NMR spectrum, the presence of Ph$_3$SiF from the TBAT and Me$_3$SiF, in conjunction with the $^{31}P\{^{1}H\}$ NMR spectroscopic data, supported the removal of one Me$_3$Si group, suggesting a mixed cyaphide-phosphaalkyne complex, however, no conclusive evidence has been reported.

Later, Crossley and co-workers reported the use of Me$_3$SiC≡P to introduce cyaphide functionality into organometallic systems, resulting in the synthesis of the first conjugated cyaphide-alkynyl systems (Scheme 1.32).[70] Building upon Grützmacher's seminal work,[64] a more facile synthesis was established, allowing access to several terminal cyaphide complexes of the type *trans*-[Ru(C≡P)(C≡CR)(dppe)$_2$] *via* the isolable intermediates *trans*-[Ru(η^1-P≡CSiMe$_3$)(C≡CR)(dppe)$_2$] (R = CO$_2$Me, *p*-An).[71]

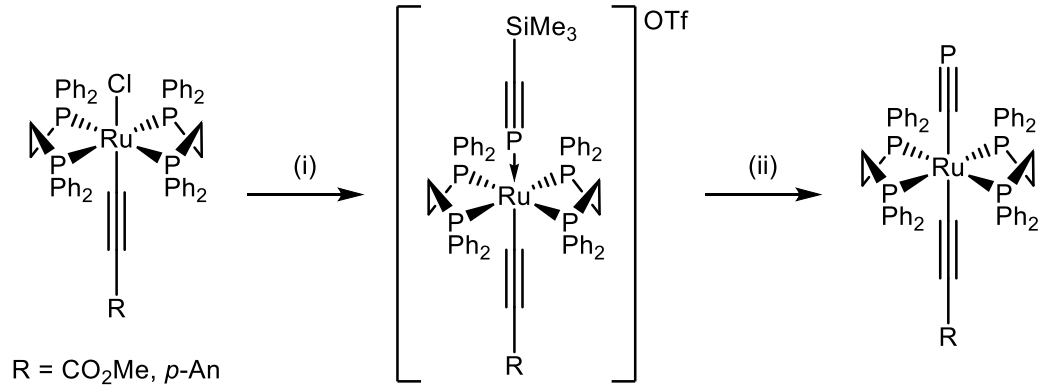

Scheme 1.32: *Synthesis of conjugated cyaphide complexes. Reagents and conditions: (i) AgOTf, $Me_3SiC{\equiv}P$, DCM/tol.; (ii) KO^{t}Bu, THF*

In the $^{31}P\{^1H\}$ NMR spectra, the η^1-phosphaalkyne complexes displayed mutually coupled doublet and quintet resonances at *ca.* 42 and 110 ppm in a 4:1 ratio ($^2J_{PP}$ = 34 Hz), corresponding to the ancillary ligand set and phosphaalkyne fragment respectively. The solid-state structure of *trans*-[Ru(η^1-P≡CSiMe$_3$)(C≡CCO$_2$Me)(dppe)$_2$]OTf exhibited a near-linear Ru-P-C unit (175.7(4) °), and a C-P distance which is comparable to that reported by Grützmacher in *trans*-[RuH(η^1-P≡CSiPh$_3$)(dppe)$_2$]BF$_4$ (1.528(11) *vs* 1.530(3) Å respectively).

Addition of KO^{t}Bu to a THF solution of *trans*-[Ru(η^1-P≡CSiMe$_3$)(C≡CR)(dppe)$_2$] resulted in rapid desilylative rearrangement (*ca.* 1 h) to the corresponding cyaphide complexes (Scheme 1.32). Resonances in the $^{31}P\{^1H\}$ NMR spectrum were of a higher frequency than those of the parent phosphaalkyne complexes at *ca.* 51 and 160 ppm, alongside a diminished coupling constant (*ca.* 3 Hz).

Crystallographic studies of *trans*-[Ru(C≡P)(C≡C-*p*-An)(dppe)$_2$] showed a slight deviation from linearity, with Ru-C-P and Ru-C-C angles of 172.(2) and 174.4(3) ° respectively, consistent with other ruthenium-alkynyl complexes,[64] however, the C≡P bond length of 1.544(4) Å is significantly shorter than that reported by Grützmacher as a result of the *trans* influence of the alkynyl fragment (*cf*. hydride).

More recently, the synthesis of ligated cyaphide from the 2-phosphaethynolate anion at a uranium centre was reported by Grützmacher and Meyer.[72] Addition of [Na(OCP)(dioxane)$_{2.5}$] and 2.2.2-cryptand to a solution of [{(^{Ad,Me}ArO)$_3$N}U^{III}{DME}] resulted C-O bond cleavage, and the formation of the corresponding dinuclear cyaphide complex in 80% yield (Scheme 1.33). It was postulated that [Na(OCP)(dioxane)$_{2.5}$] undergoes C-O, as opposed to C-P, bond cleavage due to both the oxophilicity and highly reducing nature of uranium(III).[73]

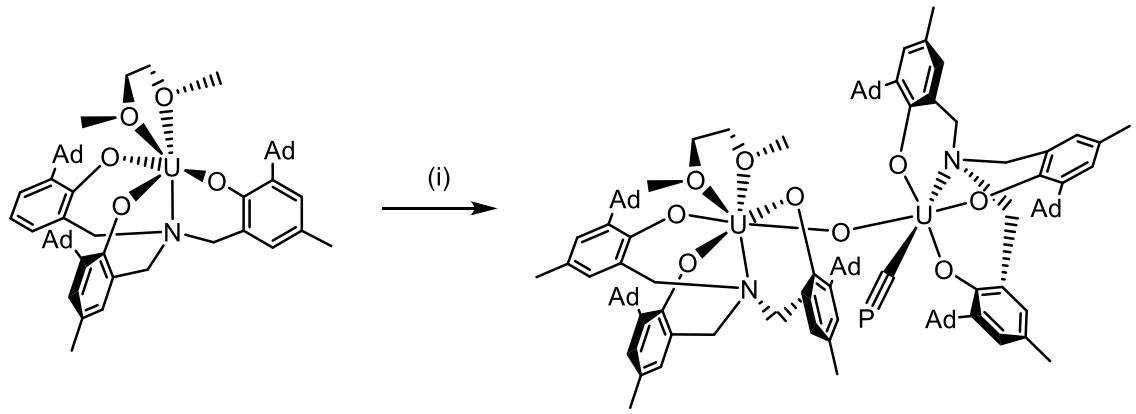

Scheme 1.33: *Synthesis of the First Uranium Cyaphide Complex. Reagents and conditions: (i) [Na(OCP)(dioxane)$_{2.5}$], 2.2.2-cryptand, DME*

The ^{31}P{^{1}H} NMR spectrum of the resulting complex exhibited one resonance at 265.8 ppm, corresponding to the bound cyaphide anion, a significantly higher frequency shift when compared to reported ruthenium-based systems (*ca.* 160 – 165 ppm),[64,70] attributed to the paramagnetic nature of uranium(IV).

While no C≡P stretching mode was observed in the IR spectrum, owing to broad and intense absorptions arising from the ancillary ligand set, the identity of this complex was determined using X-ray diffraction studies. The reported C-P bond distance of 1.523(8) Å was comparable to those observed in the ruthenium systems, and a near-linear U-C-P unit was apparent, with an associated angle of 177.5(4) °.

1.4 Molecular Electronics

Conjugated organic systems are of interest due to their potential uses in photovoltaics (OPVs), field-effect transistors (OFETs), and light emitting diodes (OLEDs),[1,74–76] due to the ease with which their properties can be modified. Since Friend's report in 1990,[77] significant efforts have been focused on the use of poly(phenylvinylene)s (PPVs) in such devices (Figure 1.5),[74,76,78–82] owing to a band gap that lies within the 1.5 to 3.0 eV photon energy range of the visible spectrum (band gap ≈ 2.4 eV).[83] This field has been largely dominated by carbocentric systems, while systematic investigation of compounds featuring low-coordinate phosphorus atoms have not yet been undertaken.

Owing to the isolobal nature of the CH fragment and phosphorus,[4] it could be envisaged that the synthesis of highly conjugated phosphacarbons is achievable, alongside those featuring low-coordinate phosphorus fragments, such as phospha-PPVs or phospha-poly(phenyleneethynylene)s (phospha-PPEs) (Figure 1.5).

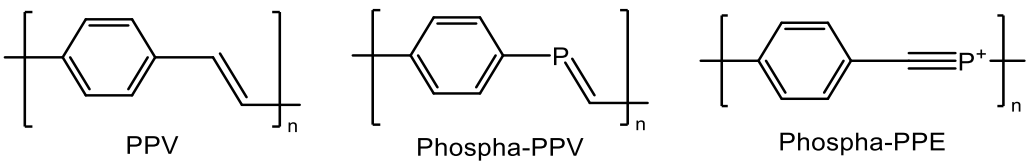

Figure 1.5: *Phosphorus containing derivatives of poly(phenylvinylene)*

1.4.1 Conjugated Phosphacarbons

The most studied phosphacarbons in this context are those derived from phospholes. Due to the pyramidal phosphorus centre, a reduced interaction between the phosphorus lone pair and the π-system is typically observed, allowing the ring to act as an effective diene.[84] Furthermore, they also possess a reduced HOMO-LUMO gap, resulting from σ*-π* interactions between the phosphorus centre and the conjugated backbone, which is an ideal facilitator for electron transport.[85,86] The most seminal example, an α-linked quaterphosphole, was reported by

Mathey and co-workers in 1994 (Scheme 1.34), however, $^{31}P\{^{1}H\}$ NMR studies showed a complex mixture of diastereoisomers had formed, thus further studies were precluded.[87]

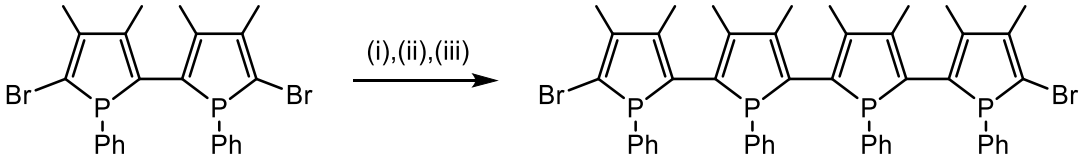

Scheme 1.34: *Synthesis of a quaterphosphole. Reagents and conditions: (i) ^{n}BuLi, THF, –90 °C; (ii) $CuCl_2$, – 90°C, 1 h.; (iii) 25 °C, 2 h.*

As mentioned previously, polyphosphaalkenes would be an ideal target for organic electronics, which was exemplified by Wright and Gates in 2002 (Scheme 1.35).[88] Formed *via* a Becker condensation reaction, poly(*p*-phenylenephosphaalkene) exhibited overlapping resonances in the $^{31}P\{^{1}H\}$ NMR spectrum, corresponding to a mixture of the *E* and *Z* isomers, with mass spectrometry showing a degree of polymerisation between *n* = 5 and *n* = 21. Solution-state UV-Vis studies showed a red shift of smaller magnitude than that for *trans*-PPV when compared to *trans*-stilbene (*ca.* 426 nm vs 294/307 nm),[88] which was believed to arise from conformational non-planarity of the main chain resulting from the steric bulk of the C_6Me_4 groups. Furthermore, broader absorbances in the UV-Vis spectrum were observed when compared to samples of pure *cis*- or *trans*-stilbene, which was believed to be due to both the polydispersity of the material, and the non-integer *Z/E* ratio of *ca*. 1.1:1; however, the observed data still supported the presence of extended π-conjugation.

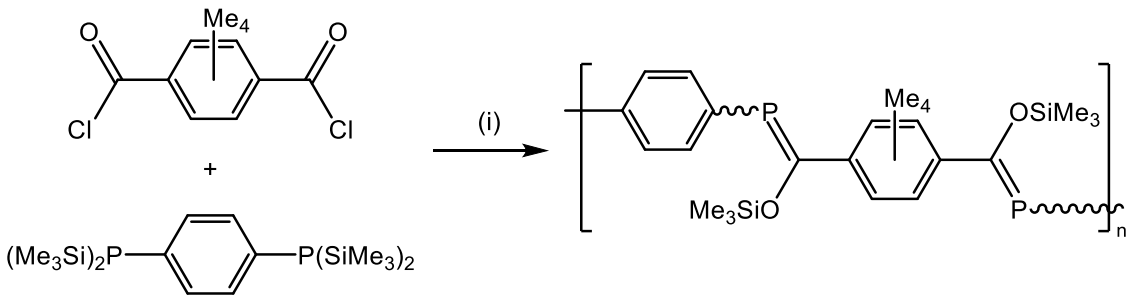

Scheme 1.35: *Synthesis of poly(p-phenylenephosphaalkene). Reagents and conditions: (i) 85 °C, 24 h.*

Similarly, Protasiewicz and co-workers reported the synthesis of a compound featuring a conjugated π-system which incorporated phosphaalkene functionalities *via* an extension of their established "Phospha-Wittig" methodology.[89,90] Addition of zinc and trialkylphosphane to a solution of bis-dichlorophosphane, and subsequent treatment with an aldehyde resulted in the formation of the corresponding diphosphaalkene (Scheme 1.36).

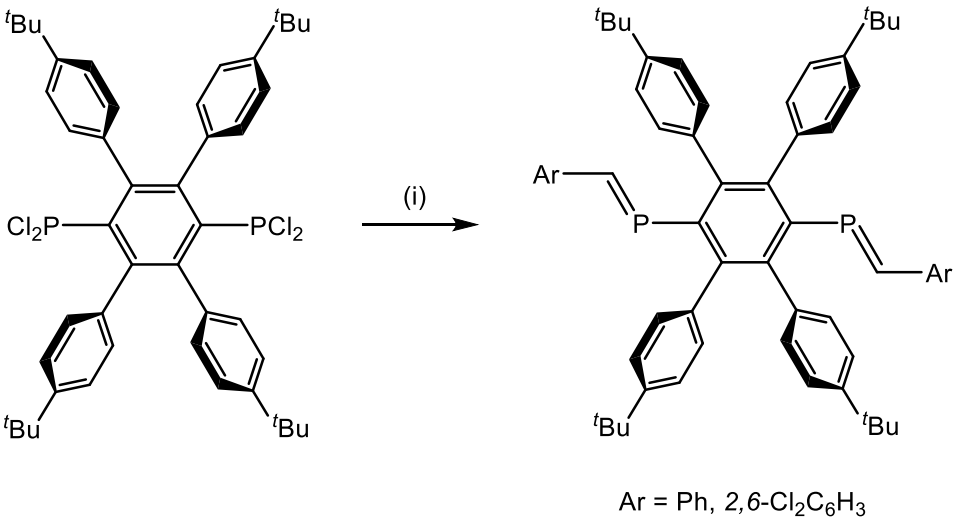

Scheme 1.36: *Synthesis of a diphosphaalkene featuring an extended π-system. Reagents and conditions: (i) Zn, PMe_3, ArC(H)O, THF, 2 h. (Ar = Ph, 2,6-$Cl_2C_6H_3$)*

A bis(phosphanylidene-σ^4-phosphorane) intermediate was postulated but not isolated. The $^{31}P\{^1H\}$ NMR spectra showed a single isomer of each phosphaalkene (δ_P: *ca.* 250 and 290 for Ar = Ph and *2,6*-$Cl_2C_6H_3$ respectively), believed to be the *E* conformation based on a $^2J_{PH}$ coupling constant of *ca.* 25 Hz,[91] which was later confirmed by X-ray diffraction studies. When compared to the monofunctionalised analogue DmpP=C(H)Ph,[89] the diphosphaalkenes exhibited a red shift of 15 nm in the UV-Vis spectrum (λ_{max} = 349 nm vs 334 nm),[90] similar to those reported for other comparative studies between mono- and diphosphaalkenes.[89] Further, it was postulated that in solution the steric bulk of the bridging arene unit was not sufficient to isolate the C=P units, thus resulting in electronic communication between the two moieties.

1.4.2 Conjugated Organometallic Systems

Polymetallic systems incorporating unsaturated hydrocarbon chains with σ-bonded metal centres have attracted considerable interest in recent years. [92] Most commonly, these systems are referred to as "carbon σ-bonded molecular wires",[92] with their one-dimensional, semi-rigid structure, allowing communication between the two redox active metal centres upon electrochemical- or photo-induction (Figure 1.6).[93,94] Consequently, these complexes have shown promise in molecular-scale devices.[94,95]

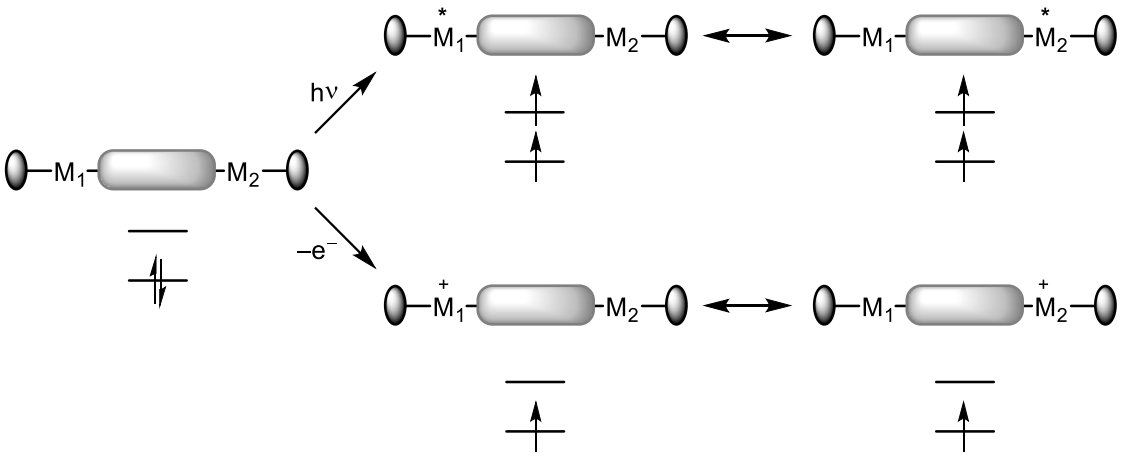

Figure 1.6: *Communication between redox-active metal centres upon electrochemical- or photo-induction*

By far the most intensively studied systems are those incorporating conjugated linear chains comprising solely of carbon atoms, such as alkenes and alkynes, due to their ability to facilitate long range metal-metal interactions.[94] However, unlike purely organic molecular wires, the reduced stability of these systems has hindered their synthesis and development, resulting in bridging ligands of much shorter length than their organic counterparts.[96,97] Despite this, growth of the field has been prolific, and has been enhanced through the use of cyclic voltammetry to study the potential electronic interactions between the two metal centres.

1.4.2.1 sp-hybridised Systems

The most common examples of bimetallic complexes featuring *sp*-hybridised bridging units of the type $L_nM{-}(C{\equiv}C)_x{-}ML_n$ have been those where $x = 1$,[98–101] however, there have been reports of higher homologues up to and including $x = 28$,[102–106] with these systems representing the most fundamental category of carbon σ-bonded molecular wires. Furthermore, systems incorporating chains with an even number of carbon atoms are more common due to the ease with which they can be synthesised when compared to their odd number counterparts.[94] Additionally, depending on the *d*-electron count of the metal centres, the bridging units can assume either their reduced (polyynic) or oxidised (cumulenic) structures (Figure 1.7), the properties of which have been investigated extensively using DFT calculations.[102,107]

Figure 1.7: *Possible even-numbered chain structures*

The most extensively investigated of these systems are those of the type $Cp^R(PP)M{-}(C{\equiv}C)_x{-}M(PP)Cp^R$ (M = Fe, Ru, Os; R = H, Me; PP = PPh_3, dppe, dppm; Figure 1.8), which have been shown to exhibit a variety of redox processes depending on the ligand system used. Most significantly, electrochemical studies have shown that the presence of strong electron-donating ligands results in a decrease in the oxidative potentials observed, and that efficient electronic communication occurs between the two metal centres *via* the unsaturated carbon bridge.[108]

Investigations of these systems (Figure 1.8) by Bruce and co-workers using cyclic voltammetry showed a large peak-to-peak separation of the two redox events (Δ*E*), suggestive of an interaction between the two metal centres and an appreciable stability of the transient mixed-

valence species, with only slight variation in the oxidative potential between the Cp/Cp and Cp/Cp* systems (E = −0.61 V *vs* $[FeCp_2]^{0/+}$ *vs* −0.60 V when *n* = 1).[109,110]

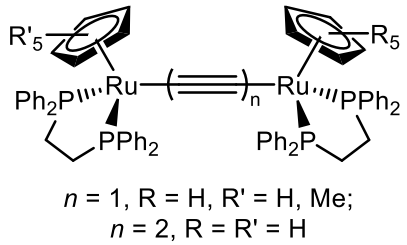

Figure 1.8: *Systems investigated by Bruce and co-workers. For n = 1, R = H, R' = H, Me; n = 2, R = R' = H*

Theoretical studies showed a gradual change in bonding character of the bridging unit from ethynediyl (M-C≡C-M) to cumulenic upon oxidation, which was supported by the observation of a shortening of the M−C bonds and a lengthening of the C-C distances in the solid state, which is indicative of charge delocalisation across the two metal centres and the carbon chain. Furthermore, the complexes became more difficult to oxidise as the length of the bridging chain was increased (E_{pa} = −0.24 V *vs* $[FeCp_2]^{0/+}$). This was believed to be due to a reduction in the coupling between the metal centres, resulting in a decrease in metal-metal interactions.[110]

1.4.2.2 sp/sp²-Hybridised Systems

Similar to polyynediyl complexes, there are numerous examples of mixed *sp*/*sp²*-bridged molecular wires in the literature,[111,112] with a significant proportion of reports focussed upon systems with aromatic rings incorporated into the bridging unit.[95,113–115] Field and Rigaut reported the synthesis and investigation of complexes that feature phenyl rings as effective ethenyl fragments within the conjugated bridge (Figure 1.9),[95,114,115] and demonstrated through electrochemical studies that these systems also exhibit electronic interactions between the two metal centres. However, it was also shown that the degree of electronic communication

decreases proportionally with the number of ethenyl fragments, as reflected by a decrease in the comproportionation constant for the mixed valence complexes.

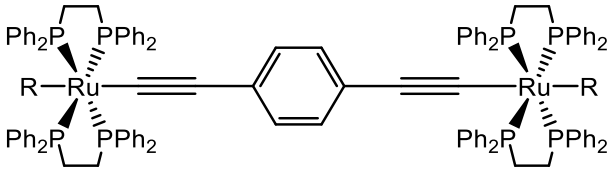

Figure 1.9: *Use of bridging phenyl rings as effective ethenyl fragments*

This was further exemplified by Klein and coworkers,[116] who showed that the insulating nature of the linker between the two metal centres could be increased through the addition of multiple phenyl rings (Figure 1.10). While the system incorporating two phenyl rings displayed two reversible, one-electron oxidation steps in the cyclic voltammogram, the second system featuring three rings only displayed one reversible oxidation wave, which was reported to correspond to a 1.9-electron process. It was suggested that this process should be interpreted as two coinciding one-electron waves, due to non-coupling of the two individual redox processes at each metal centre, thus showing that there was no connection between the two metal centres, and that they were in fact both oxidised at the same potential independently.[116]

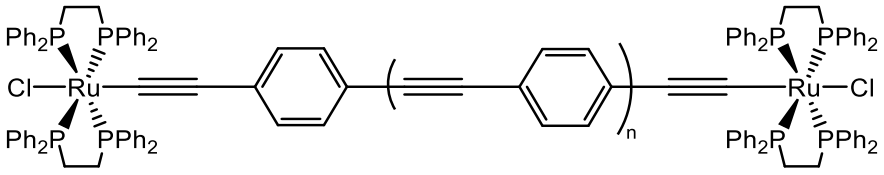

Figure 1.10: *Homobimetallic systems incorporating multiple phenyl rings in the bridging unit*

This work was further complimented by studies into the metal-metal interactions observed in systems featuring mixed acetylide/arene bridges capped by "$FeCp^{R}$(dppe)" fragments (Figure 1.11).[117–123] These systems typically exhibited two, one-electron oxidations, with associated Δ*E*

values within the range of 220—360 mV, which is consistent with electronic communication *via* the bridging unit and indicative of appreciable stability of the mixed valence state.

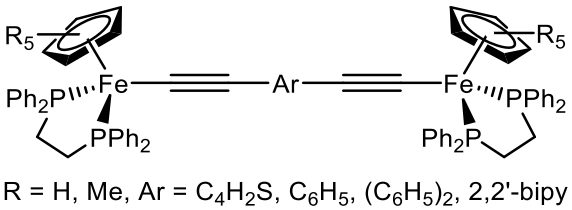

Figure 1.11: *Conjugated acetylide-arene bridges capped by $FeCp^R(dppe)$ fragments*

However, it was also noted that introduction of a biphenyldiyl fragment significantly reduced the degree of electronic communication to such a degree that the mono-oxidised mixed-valence species was no longer stable. These observations were consistent with those previously reported by Lapinte and Paul,[93,121,124] however, some influence of the electron-donating effect of Cp* vs Cp on the thermodynamic stability of the mixed-valence species was apparent.

1.4.3 Linearly Conjugated Phosphaorganometallics

Despite the significant advances in both π-conjugated organophosphorus and organometallic molecular scale conductors, [74–76,85,92,93] there have been no reports on the combination of the two, namely conjugated phosphaorganometallics (Figure 1.12). The incorporation of low-coordinate phosphorus(III) fragments into linearly conjugated organometallic systems, particularly phosphaalkyne moieties, is of considerable interest, since these fragments typically possess strong π-acceptor properties and low lying π* orbitals. [84]

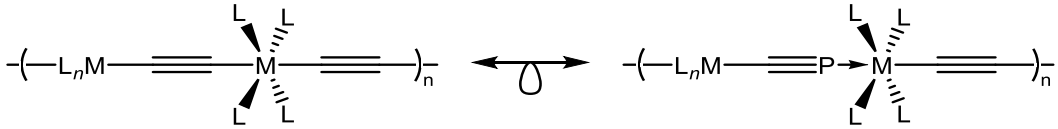

Figure 1.12: *Possible linearly conjugated organometallic phosphacarbons arising from the isolobal relationship between the "CH" fragment and phosphorus*

Introduction of cyaphide, the simplest phosphaalkyne, into pre-established systems could facilitate the development of this area of chemistry. Indeed, recent efforts have shown that incorporation of cyaphide into conjugated organometallic systems is possible,[70] thus beginning to address the dichotomy between acetylide and phosphaalkyne-based molecular wires.

Herein, the incorporation of cyaphide into conjugated mono- and bimetallic systems is explored, focussing on the synthesis of novel complexes, alongside investigations into their electrochemical behaviour compared to their acetylide analogues. Furthermore, efforts to introduce phosphaalkyne functionality into a variety of half-sandwich complexes are undertaken, alongside the first forays into reactivity studies of ligated cyaphide.

Chapter 2 – Investigating the Effects of Isolobal Fragment Exchange

2.1 Introduction

Carbon rich organometallics, particularly those incorporating σ-alkynyl metal fragments have exhibited a wide variety of uses in recent years,[92,93,103,114,125,126] including carbon σ-bonded molecular wires and non-linear optics.[94,103,104,114,127] This is due to the ease with which different functionalities can be introduced, which facilitates fine-tuning of their electronic properties, alongside their well-defined one-dimensional, semi-rigid structures.[92]

Perhaps the most intensively studied systems are those based on the "$Ru(dppe)_2$" architecture, which were initially synthesised *via* the substitution of metal halides by alkynyl derivatives of lithium, magnesium, or copper.[128,129] Alternative routes were established, though these typically necessitated the use of toxic alkynyltin reagents in the presence of a palladium catalyst.[130,131]

Later, Touchard and Dixneuf reported the synthesis of a variety of vinylidene ruthenium complexes from *cis*-$[RuCl_2(dppe)_2]$ and terminal alkynes in the presence of a sodium-based halide abstractor (Scheme 2.1).[132,133] The facile deprotonation of these complexes afforded the desired ruthenium(II) acetylide complexes, which could be functionalised further to give both symmetrical and unsymmetrical bis(acetylide) complexes.[132]

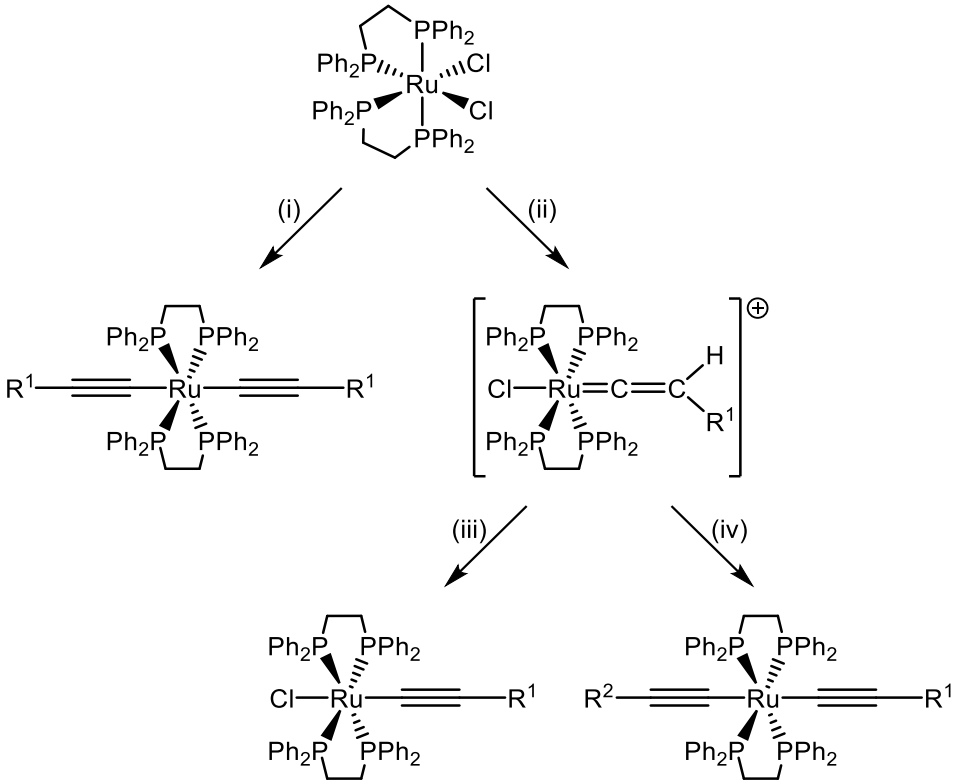

Scheme 2.1: *The synthesis of vinylidene-, alkynyl-, and trans-bis(alkynyl) ruthenium complexes. Reagents and conditions: (i) HC≡CR¹, $NaPF_6$, NEt_3, DCM; (ii) HC≡CR¹, $NaPF_6$, DCM; (iii) DBU, CH_2Cl_2; (iv) HC≡CR², $NaPF_6$, NEt_3, DCM*

More recently, reports have focused on the use of isolated $[RuCl(dppe)_2]^+$ salts as an entry point to acetylide complexes of the type *trans*-$[RuCl(C{\equiv}CR)(dppe)_2]$ and their functionalised derivatives.[71,92,94,114] Such systems have been intensively studied both spectroscopically and electrochemically, to assess the ability to fine-tune their electrochemical response *via* modification of the acetylide fragment.[71,114,133]

The *n*-type dopant properties of phosphorus are well established, and the introduction of phosphorus fragments into conjugated systems has profound effects on their electronic properties,[4,76,82,84,87,88] however, there are currently no examples of linearly conjugated phosphaorganometallic systems in the literature. Due to the isolobal relationship between phosphorus and the CH fragment, it could be envisaged that introduction of cyaphide into conjugated organometallic systems would be an ideal starting point. However, examples of

transition metal cyaphide complexes are rare, with the first unequivocal example only reported in 2006.[64] Nevertheless, attempts to incorporate cyaphide into extended π-systems have been undertaken, as reported by Crossley and co-workers in 2014,[70] though the effects of the introduction of this functionality on the electronic behaviours of these systems have not, as of yet, been investigated. This work seeks to examine the relationship between cyaphide, cyanide, and acetylide, as well as investigate how the exchange of these fragments within a complex (C≡P *vs* C≡N *vs* C≡CH) affects their electronic structure.

2.2 Syntheses of *Trans*-[Ru(C≡P)(C≡CAr)(dppe)$_2$]

2.2.1 Synthesis and Characterisation

Complexes of the type *trans*-[RuCl(C≡CAr)(dppe)$_2$] (**2.1**–**2.3**) were combined with $AgPF_6$, followed by subsequent coordination of the phosphaalkyne (Scheme 2.2) to give the novel η^1-phosphaalkyne complex cations *trans*-[Ru(η^1-P≡CSiMe$_3$)(C≡CAr)(dppe)$_2$]$^+$ (**2.4**–**2.6**), in an analogous fashion to that reported in 2014.[70]

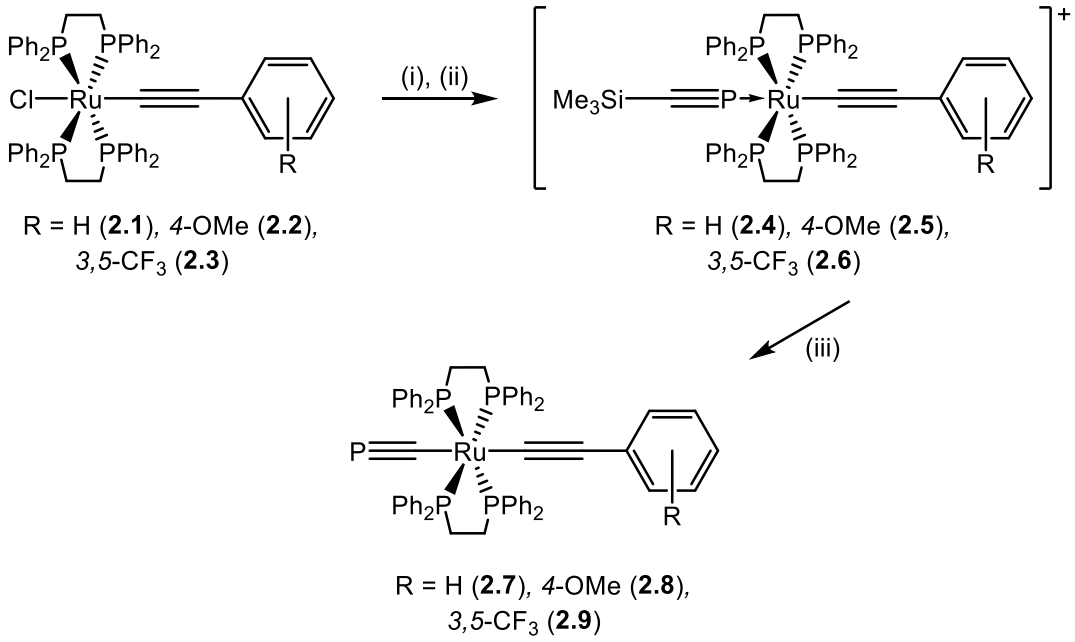

Scheme 2.2: *Synthesis of **2.4–2.6** and subsequent conversion to cyaphide complexes **2.7–2.9.** Reagents and conditions: (i) 1 eq. $AgPF_6$, DCM, 10 min.; (ii) 1 eq. $P{\equiv}CSiMe_3$ in toluene, 1 h.; (iii) 1 eq. KO^tBu, THF, 1 h.*

All three phosphaalkyne complexes (**2.4–2.6**) exhibit a characteristic AX_4 pattern in the $^{31}P\{^1H\}$ NMR spectrum (δ_P: ~110, C≡P; 42, dppe), with a mutual coupling of approximately 33 Hz, consistent with coordination of the phosphaalkyne moiety in an η^1 binding mode. The observation of a resonance for the PF_6 counterion in the $^{31}P\{^1H\}$ NMR spectra support the formation of cationic complexes, while the presence of an $SiMe_3$ resonance in both the ^1H and ^1H-^{29}Si HMBC NMR spectra (δ_{Si}: *ca*. −13) support phosphaalkyne retention. The $^{13}C\{^1H\}$ NMR spectra display a doublet resonance at *ca*. 190 ppm ($^1J_{CP} \approx 88$ Hz), with correlation observed to the $SiMe_3$ proton resonance in the ^1H-^{13}C HMBC spectrum, attributable to the quaternary centre of the phosphaalkyne. IR spectroscopic data were also consistent with the presence of a C≡P unit ($\nu_{C\equiv P}$: 1244-1276 cm^{-1}), alongside an unsaturated C≡C bond ($\nu_{C\equiv C}$: 2085-2102 cm^{-1}). A summary of the spectroscopic data obtained is presented in Table 2.1.

Treatment of **2.4–2.6** with stoichiometric amounts of KO^tBu resulted in rapid desilylation of the phosphaalkyne and afforded the corresponding cyaphide complexes **2.7–2.9**, with the reaction

complete within one hour. This was primarily determined by $^{31}P\{^{1}H\}$ NMR spectroscopy, where a shift to higher frequency was observed for resonances associated with both the C≡P moiety (δ_P: 160–170) and the ancillary ligand set (δ_P: *ca.* 51), alongside a 10-fold reduction in spin-spin coupling, which was consistent with literature reports.[64,70] Additionally, a significant shift of the phosphaalkyne carbon centre to higher frequency by *ca*. 50 ppm was observed, akin to that reported by Grützmacher and Crossley,[64,70] alongside loss of the $SiMe_3$ proton resonance in the ^{1}H NMR spectrum. All three complexes also displayed a strong band in their IR spectrum consistent with the presence of a C≡P bond ($\nu_{C\equiv P}$: 1242-1275 cm^{-1}), alongside a weaker band associated with an unsaturated alkynyl unit ($\nu_{C\equiv C}$: 2032-2067 cm^{-1}).

Table 2.1: *Selected $^{31}P\{^{1}H\}$, $^{13}C\{^{1}H\}$, $^{29}Si\{^{1}H\}$, and ^{1}H NMR shifts (ppm), and IR stretches (cm^{-1}) for complexes of the type trans-[Ru(η^1-P≡CSiMe$_3$)(C≡CAr)(dppe)$_2$]$^+$ and trans−[Ru(C≡P)(C≡CAr)(dppe)$_2$]*

		δ_P		δ_C				δ_{Si}	δ_H	ν	
Arene Substituent	**Compound Number**	**$Ph_2PC_2H_4PPh_2$ ($^2J_{PP}$, Hz)**	**C≡P ($^2J_{PP}$, Hz)**	**C≡P ($^1J_{CP}$, Hz)**	**C_α≡C**	**C≡C_β**	**$Si(CH_3)_3$**	**$Si(CH_3)_3$**	**$Si(CH_3)_3$**	**C≡P**	**C≡C**
H	**2.4**	42.3 (33.8)	111.9 (33.8)	190.0 (88)	108.6	116.2	−13.1	0.5		1245	2096
***4*-OMe**	**2.5**	42.2 (32.9)	112.7 (32.9)	188.4 (87)	–	115.9	−13.3	0.5		1244	2102
***3,5*-CF_3**	**2.6**	41.6 (32.2)	108.8 (32.2)	191.2 (89)	105.5	112.3	−12.5	−0.05		1276	2085
H	**2.7**	50.8 (3.5)	160.4	281.5	123.9	119.8	–	–		1242	2067
***4*-OMe**	**2.8**	50.8 (3.4)	159.5	281.9	123.6	119.0	–	–		1261	2032
***3,5*-CF_3**	**2.9**	50.9 (br, $\nu_{½}$: 23 Hz)	172.9	280.1	123.1	–	–	–		1275	2055

* Values marked with "−" could not be assigned, or were not applicable

2.2.2 Molecular Structure Analysis

Crystals of **2.4** suitable for X-ray diffraction studies were obtained from a saturated DCM solution of the complex, which had been layered with pentane and stored at −20 °C. In the solid state, **2.4** exhibited the anticipated η^1-coordination mode of the phosphaalkyne *trans* to the phenylacetylene fragment (Figure 2.1). The geometry around the metal centre (∠ P-M-C) exhibits a similar distortion to that observed in *trans*-[Ru(η^1-P≡CSiMe$_3$)(C≡CCO$_2$Me)(dppe)$_2$]OTf (176.57(8) *vs* 177.0(3) °),[70] which is considerably smaller than those reported for Grützmacher's system and Jones' *trans*-[RuH(η^1-P≡CMe)(dppe)$_2$]OTf.[64,134] Furthermore, the C-P distance of the phosphaalkyne fragment fell within the expected range (1.53—1.55 Å)[64,68,70,134] and was statistically indistinguishable from both Grützmacher's and Crossley's reports.[64,70] Moreover, when compared to **2.1**, complex **2.4** exhibits a statistically indistinguishable C≡C distance (1.159(4) Å vs 1.198(7) Å).[130] These observations have been summarised in Table 2.2.

Table 2.2 *Selected experimental bond lengths (Å) and angles (°) for* ***2.4*** *and related complexes* *trans*−*[RuR(η^1−P≡CSiMe$_3$)(dppe)$_2$]$^+$*

	2.4	**R = C≡CCO$_2$Me**[70]	**R = H**[64]
Ru$_1$−P$_{dppe\ average}$	2.403	2.423	2.370
Ru$_1$−P$_1$	2.2638(8)	2.274(3)	2.2486(8)
Ru$_1$−C$_2$	2.82(3)	2.08(1)	−
C$_2$−C$_3$	1.159(4)	1.15(1)	−
P$_1$−C$_1$	1.534(4)	1.53(1)	1.530(3)
Si$_1$−C$_1$	1.836(4)	1.86(1)	1.824(3)
P$_1$−C$_1$−Si$_1$	174.9(3)	178.3(7)	165.5(2)
C$_2$−Ru$_1$−P$_1$	176.57(8)	177.0(3)	−
C$_3$−C$_2$−Ru$_1$	179.7(3)	178.1(9)	−
Ru$_1$−P$_1$−C$_1$	176.5(2)	175.7(4)	174.9(1)

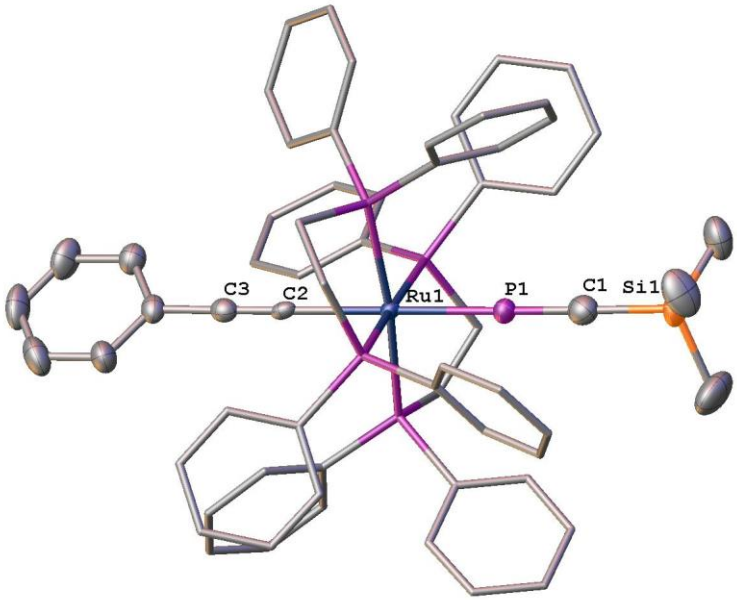

Figure 2.1: *Molecular structure of* ***2.4****; 50% thermal ellipsoids, hydrogen atoms and counter-ion omitted, and ancillary ligand set reduced for clarity.*

X-ray diffraction studies on a single crystal of the analogous cyaphide complex (**2.7**), obtained through slow evaporation of a saturated solution in DCM, facilitated comparison with other known transition metal cyaphide complexes, alongside the optimised gas-phase geometry (Figure 2.2; Table 2.3). The C-P distance of 1.463(7) Å was considerably shorter than reports for *trans*-[RuH(C≡P)(dppe)$_2$] and **2.8** (1.573(2) and 1.544(4) Å respectively),[64,70] however, the C≡C distance in **2.7** was statistically indistinguishable from that reported for **2.8** (1.222(7) vs 1.205(5) Å respectively). Furthermore, a diminished deviation from linearity was observed in **2.7** than **2.8** (174.4(2) *vs* 171.9(1) °),[70] though this likely arises from crystal packing forces in the solid state.

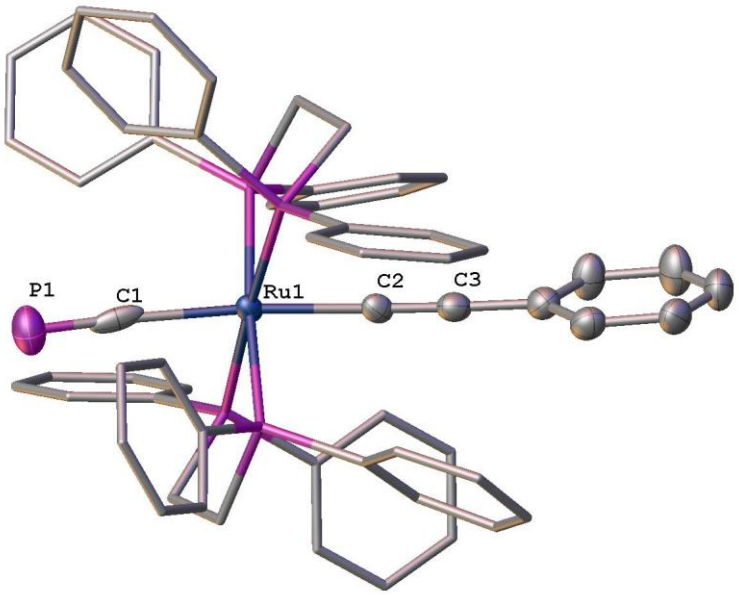

Figure 2.2: *Molecular structure of **2.7**; 50% thermal ellipsoids, hydrogen atoms omitted, and ancillary ligand set reduced for clarity.*

The gas-phase optimised geometry of **2.7** (B3LYP/6-31G** for all non-metal atoms; LANL2DZ for Ru) revealed a slightly greater degree of linearity around the metal centre (∠ C-Ru-C; 177.4 vs 174.4(2) °), alongside elongated C≡P and C≡C linkages, consistent with the presence of crystal packing forces in the solid state, and the absence of intermolecular interactions in the gas phase. Due to the good agreement between the experimental and calculated bond metrics, it can be concluded that these systems have been well-modelled using using this functional and basis set.

Comparison of the optimised geometries of **2.7-2.9** revealed a minor contraction of the C≡P distance in the electron-poor system (**2.9**),[70] with the opposite observed in the electron rich system (**2.8**). Similarly, it appeared that the Ru-$C_{C\equiv P}$ distance became elongated upon the introduction of an electron rich arene, suggesting a reduction in the competitive back bonding to the *trans*-alkynyl ligand. These observations have been summarised in Table 2.3.

Table 2.3: *Selected experimental and calculated bond lengths (Å) and angles (°) for* ***2.7–2.9***

	2.7	**2.8**[70]	**2.7$_{calc}$**	**2.8$_{calc}$**[70]	**2.9$_{calc}$**
Ru$_1$–P$_{dppe\ average}$	2.362	2.362	2.448	2.448	2.451
Ru$_1$–C$_1$	2.142(7)	2.065(4)	2.044	2.046	2.047
Ru$_1$–C$_2$	2.057(5)	2.084(4)	2.109	2.111	2.095
C$_2$–C$_3$	1.222(7)	1.205(5)	1.235	1.234	1.235
C$_1$–P$_1$	1.463(7)	1.544(4)	1.586	1.587	1.585
Ru$_1$–C$_1$–P$_1$	175.2(3)	172.3(2)	178.2	178.1	178.2
C$_2$–Ru$_1$–C$_1$	174.4(2)	171.9(1)	177.4	177.3	177.7
C$_3$–C$_2$–Ru$_1$	176.5(4)	174.4(3)	177.3	176.9	178.6

The frontier molecular orbitals of **2.7**–**2.9** are like those observed in monometallic alkynyl,[71,132] bis(alkynyl), and cyaphide complexes,[70] with the HOMO comprising of out of phase mixing of the $\pi_{C\equiv C}$, $\pi_{C\equiv P}$, and ruthenium *d*-orbitals, while the LUMO is primarily based on the ancillary ligand set and metal centre (Figure 2.3). As electron richness of the terminal arene increased, the percentage contribution from both the metal centre and $\pi_{C\equiv P}$ decreased from 36 and 40% to 30 and 24% respectively. The converse was observed for the contributions from the $\pi_{C\equiv C}$ and arene, with an increase from 13 and 7% to 24 and 17% apparent upon exchange of the *3,5*-trifluoromethyl groups for *4*-methoxy. Interestingly, it appeared that the nature of the *trans*-alkynyl has very little influence on the relative energies of the phosphorus lone pair (HOMO−7) and $\pi^*_{C\equiv P}$ orbital, and the HOMO-LUMO gap of each system (3.53 eV for **2.7**, 3.61 eV for **2.9**) was comparable (Figure 2.3).

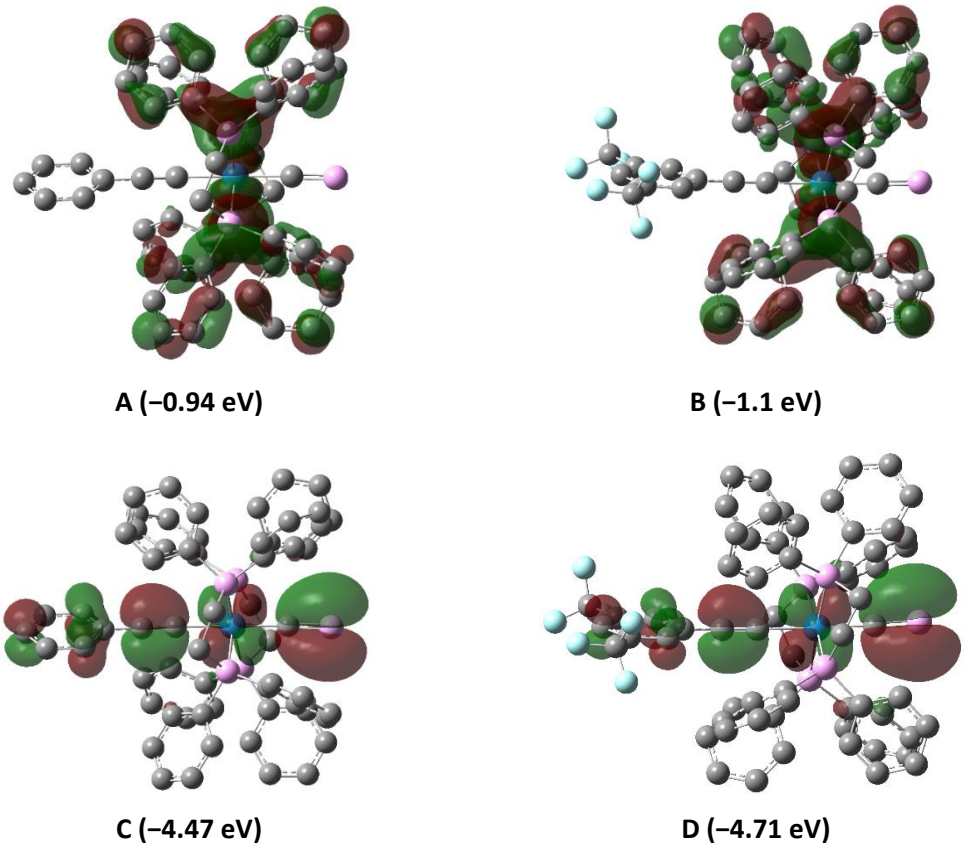

Figure 2.3: *Calculated frontier molecular orbitals of* ***2.7*** *(Left) and* ***2.9*** *(Right). LUMO (A & B) and HOMO (C & D)*

2.2.3 Electrochemical and UV-Vis Investigations

2.2.3.1 Cyclic Voltammetry

The electrochemical behaviours of these cyaphide complexes were probed using cyclic voltammetry. Unlike the parent chloride complexes, **2.7–2.9** exhibited irreversible oxidative behaviour, with large peak to peak separation values (Δ*E*) values indicative of this (Table 2.4).[71] A minor shift of the oxidative events to more negative potentials by *ca*. 50 mV was observed upon exchange of chloride for cyaphide. The small magnitude of this shift suggests that the electron withdrawing capacity of cyaphide is similar to that of chloride, with the shifts of the anodic processes to more negative potentials likely attributable to the lower σ-withdrawing capacity of cyaphide when compared to chloride.

Table 2.4: *Cyclic voltammetry data of ruthenium(II) complexes* ***2.1–2.3*** *and their cyaphide analogues* ***2.7–2.9***

Arene Substituent	Compound Number	E_{pa}	E_{pc}	ΔE	$E_{½}$
H	**2.1**[71]	–	–	0.07	+0.01
***4*-OMe**	**2.2**[71]	–	–	–	−0.10
***3,5*-CF_3**	**2.3**	0.21	0.12	0.09	+0.17
H	**2.7**	−0.01	−0.67	0.66	–
***4*-OMe**	**2.8**	−0.06	−0.7	0.64	–
***3,5*-CF_3**	**2.9**	0.16	−0.65	0.81	–

Notably, a shift to more positive potential of the anodic process in **2.9** was observed when compared to **2.7** (+0.17 V), in direct correlation to a decrease in the electron density at the metal centre, facilitated by the introduction of electron-withdrawing trifluoromethyl groups (Figure 2.4). The reverse trend was observed upon introduction of the electron rich *para*-anisole fragment, however, the observed shift of −0.02 V was considerably less.

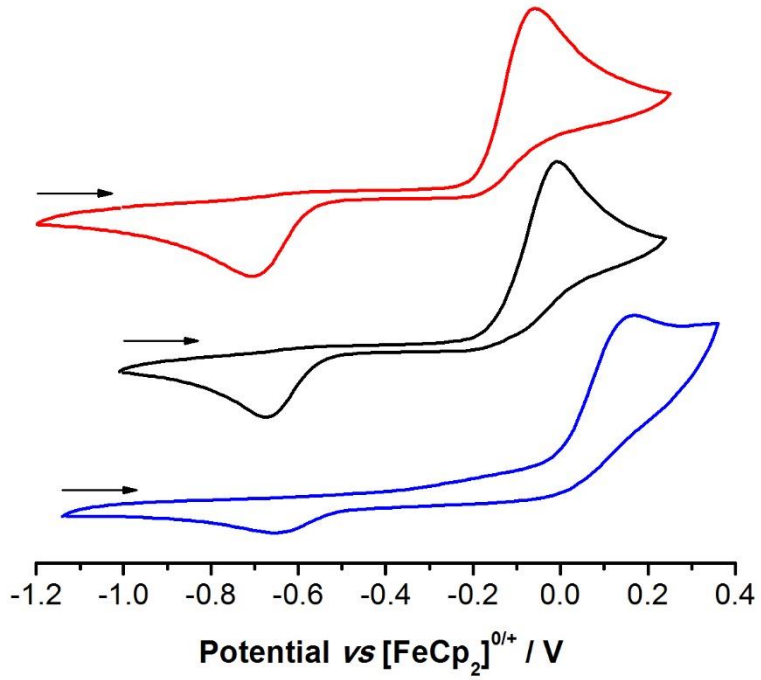

Figure 2.4: *Normalised voltammograms of* ***2.7*** *(black),* ***2.8*** *(red), and* ***2.9*** *(blue) as a solution in DCM (1 mM) with* $[^nBu_4N][PF_6]$ *supporting electrolyte (0.1 M), 0.1 V* s^{-1} *scan rate.*

Furthermore, as the electron density at the metal centre was decreased, the peak to peak separation of the anodic and cathodic processes increased from 0.66 (**2.7**) to 0.81 V (**2.9**). As a result, it can be deduced that the oxidation product becomes increasingly stabilised towards reduction in the electron poor systems, resulting in the need for a greater overpotential to regenerate the original Ru(II) complex. Consequently, similar electron-deficient systems would be ideal targets for in-depth studies into the nature of the transient Ru(III) species, due to their high stability towards reduction, facilitated either by bulk electrolysis or chemical oxidation.

By analogy, it could be envisaged that by sufficiently increasing the electron density at the metal centre, these systems would tend towards either quasi- or full-reversibility. However, due to the electron-withdrawing nature of cyaphide, significant work would be required to design systems with the required electron-donating capacity.

2.2.3.2 UV-Vis Spectroscopy

In their UV-Vis spectra, both **2.7** and **2.9** exhibit high energy features akin to those reported for **2.8**,[70] with two distinct features in the former, and three in the latter (Figure 2.5). The assignment of these features was assisted by TD-DFT calculations, with the first 100 excited states computed in the absence of a solvent model (B3LYP/3-21G* for all non-metal atoms; LANL2DZ for Ru). Complex **2.7** exhibits a strong feature at 250 nm, which is dominated by LLCT from the C≡C, C≡P, and arene π-systems to the ancillary ligand set, alongside some smaller contributions from MLCT. A further feature at 310 nm was also dominated by the same LLCT, however, some ILCT was apparent between the $\pi_{C\equiv P}$ (HOMO) and $\pi^*_{C\equiv P}$ orbitals (LUMO+19).

Similarly, **2.9** exhibited high energy, albeit weaker, features at *ca*. 250 nm consistent with the same LLCT observed in **2.7** and **2.8**, alongside another feature at 335 nm which was also dominated by LLCT and MLCT. A further feature at 275 nm displayed some ILCT between the $\pi_{C\equiv P}$ (HOMO and HOMO-1) and $\pi^*_{C\equiv P}$ orbitals (LUMO+18, +20), however, the contributions from

these (*ca*. 3%) are significantly smaller than those arising from LLCT from the conjugated π-systems to the dppe.

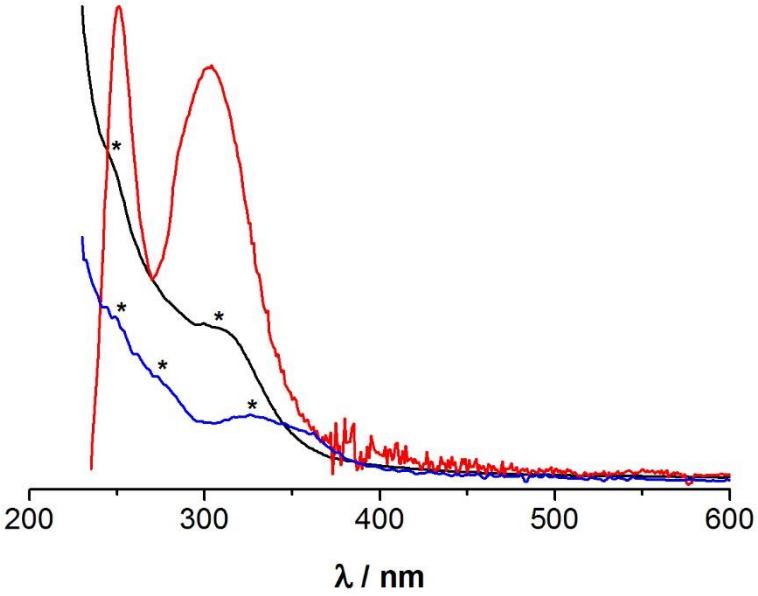

Figure 2.5: *Normalised UV-Vis spectra of **2.7** (Black), **2.8** (Red), and **2.9** (Blue). Ca. 1.0 × 10^{-5} mol dm^{-3} in DCM, 1 cm path Length. Weak features have been marked with an asterix (*)*

2.3 Syntheses of *Trans*-[Ru(C≡CH)(C≡CAr)(dppe)$_2$]

2.3.1 Synthesis and Characterisation

Complexes **2.10** and **2.11** were prepared in a similar fashion to **2.7–2.9**. The parent chloride complexes were treated with stoichiometric quantities of silver triflate, followed by addition of trimethylsilylacetylene to give the corresponding mixed acetylide-vinylidene complexes. Deprotonation with base afforded the desired mixed acetylide complexes (Scheme 2.3).

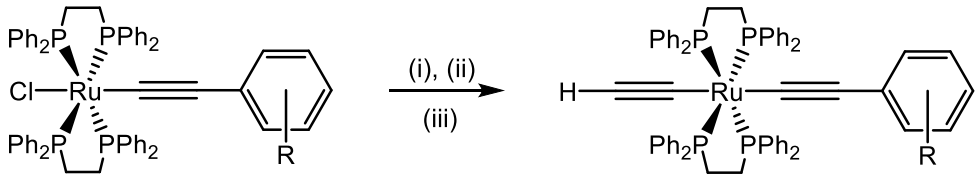

R = H (**2.1**), *3,5*-CF_3 (**2.3**) R = H (**2.10**), *3,5*-CF_3 (**2.11**)

Scheme 2.3: *Synthesis of **2.10** and **2.11**. Reagents and conditions: (i) 1 eq. AgOTf, DCM, 10 min.; (ii) 1 eq. $HC{\equiv}CSiMe_3$, DCM 1 h.; (iii) 1 eq. DBU, DCM, 1 h.*

Complexes **2.10** and **2.11** each displayed a single resonance in their $^{31}P\{^1H\}$ NMR spectrum, with a minor shift to higher frequency (*ca*. 2 ppm) observed, associated with the exchange of chloride for acetylide.[71] Further, the ^1H NMR spectra of **2.10** and **2.11** displayed a characteristic resonance for the acetylenic proton at 1.63 and 1.92 ppm respectively, in a 1:8 ratio when integrated with respect to the dppe backbone. The higher shift in **2.11** is attributable to the electron-deficiency of the metal centre, resulting in a deshielding of the proton environment. Perhaps the most distinctive features were observed in the $^{13}C\{^1H\}$ NMR spectra, as summarised in Table 2.5. In both complexes, distinctive resonances were observed for both acetylide fragments, with minimal overlapping, and were assigned with the support of HMBC and HSQC experiments.

Table 2.5: *Selected $^{31}P\{^1H\}$, $^{13}C\{^1H\}$, $^{29}Si\{^1H\}$, and ^1H NMR shifts (ppm), and IR stretches (cm^{-1}) for complexes of the type trans-[Ru(C≡CH)(C≡CAr)(dppe)$_2$]*

		δ_P	δ_C				δ_H	ν
Arene Substituent	**Compound Number**	**$Ph_2PC_2H_4PPh_2$**	**$C_\alpha{\equiv}CH$**	**$C{\equiv}C_\beta H$**	**$C_\alpha{\equiv}C$**	**$C{\equiv}C_\beta$**	**C≡CH**	**C≡CH**
H	**2.10**	52.9	116.1	121.5	116.1	123.3	1.63	1925
***3,5*-CF_3**	**2.11**	53.2	112.9	120.0	105.9	115.6	1.92	1923
***4*-OMe**	**2.12**	53.0	103.7	121.7	124.3	115.1	1.62	1923

Attempts to synthesise *trans*-[Ru(C≡CH)(C≡C-*p*-An)(dppe)$_2$] (**2.12**) were initially unsuccessful, forming either an intractable mixture of products, or the symmetrical bis-acetylide complex *trans*-[Ru(C≡C-*p*-An)$_2$(dppe)$_2$], as identified by $^{31}P\{^1H\}$ NMR spectroscopy. The synthesis of **2.12** was later achieved *via* a modified procedure, commencing from *trans*-[RuCl(C≡CH)(dppe)$_2$] and installing the *4*-ethynylanisole fragment as the final step (Scheme 2.4).

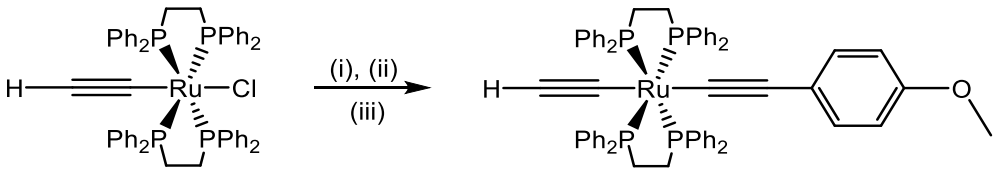

(**2.12**)

Scheme 2.4: *Synthesis of* ***2.12****. Reagents and conditions: (i) 1 eq. AgOTf, DCM, 10 min.; (ii) 1 eq. HC≡CC$_6$H$_4$–4-OMe, 1 h.; (iii) 1 eq. DBU, DCM, 1 h.*

Complex **2.12** displayed similar spectroscopic data when compared to **2.10** and **2.11** (Table 2.5), with a minor shift in the $^{31}P\{^1H\}$ NMR spectrum upon addition of the *4*-ethynylanisole fragment (from 49.8 to 53.0 ppm), alongside the expected acetylide proton at 1.63 ppm in the ^1H NMR spectrum. The small difference in shift of the acetylide proton compared to that of complex **2.10** suggests that the degree of electron donation is much smaller than the electron-withdrawing effect observed in **2.11**, where the change in shift is much greater (0.29 ppm *vs* 0.01 ppm). Two distinctive C≡C stretching modes were observed in the IR spectra of **2.10–2.12**, with DFT calculations suggesting that the lower frequency modes (1923 and 1925 cm^{-1}) correspond to the terminal acetylide fragment.

2.3.2 Molecular Structure Analysis

X-ray crystallographic studies confirmed the formation of **2.10**-**2.12** and allowed the comparison of bond lengths and angles, however, the data collected for **2.12** were of insufficient quality to determine accurate bond metrics and thus serves only to demonstrate connectivity (Figure 2.6).

All three complexes exhibited the expected *trans*-geometry of the two alkynyl ligands, which adopt a virtually linear geometry around the metal centre. A slight contraction of the Ru-C distances for both alkynes was observed upon the reduction of electron density at the metal centre, with C≡C distances consistent with previously described ruthenium(II) acetylide and bis(acetylide) complexes (Table 2.6).[70]

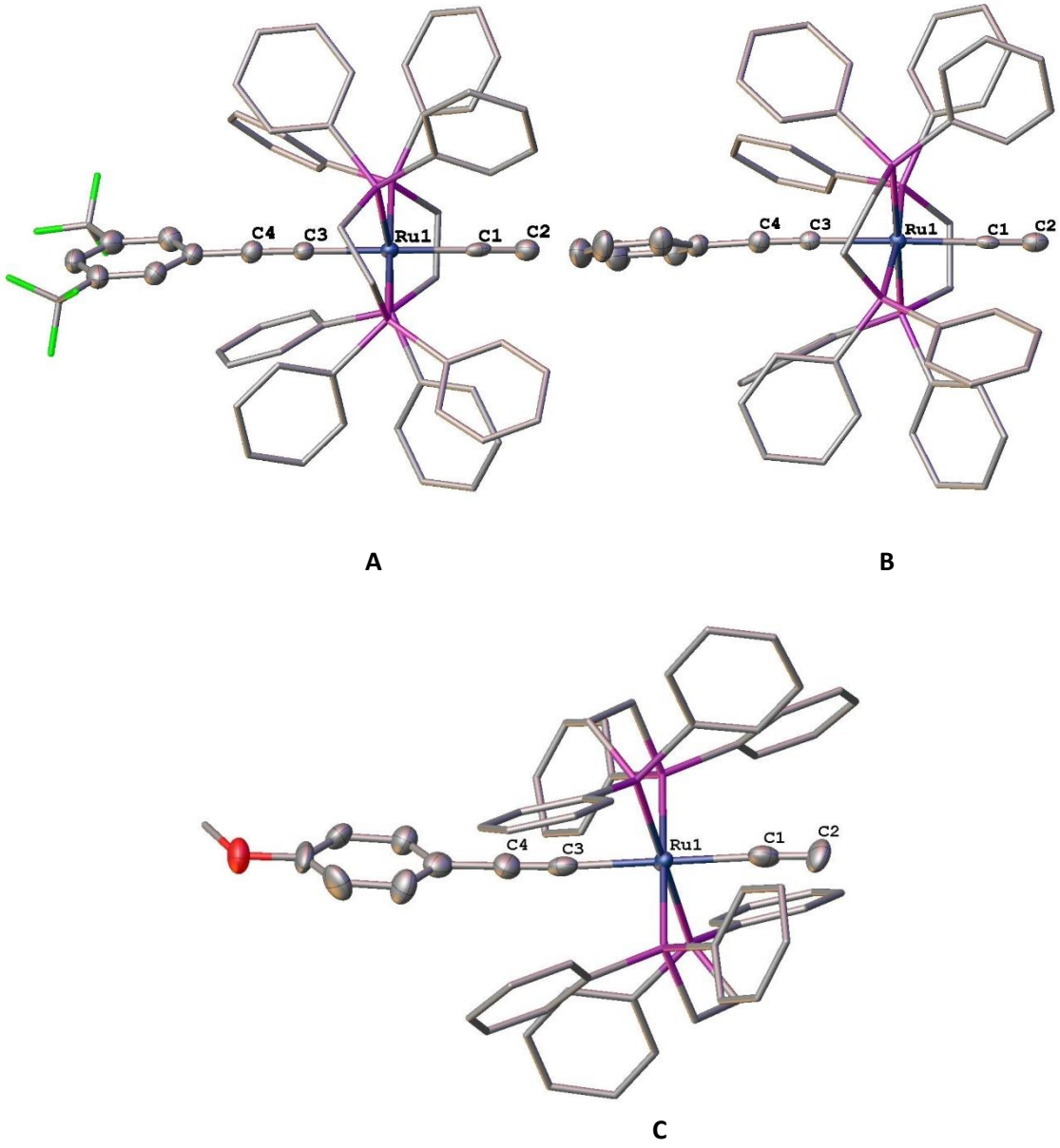

Figure 2.6: *Molecular structure of* ***2.10–2.12****; 50% thermal ellipsoids, hydrogen atoms omitted, and ancillary ligand set and arene substituents reduced for clarity*

In the absence of a complete data set for **2.12**, DFT calculations were utilised to compare the optimised gas-phase geometries of **2.10**-**2.12** (B3LYP/6-31G** for all non-metal atoms; LANL2DZ for Ru), as summarised in Table 2.6. A greater degree of linearity about the metal centre (∠ C-Ru-C) was observed in all three complexes when compared to the experimental structures of **2.10** and **2.11**, alongside elongated C≡C distances, consistent with a lack of crystal packing effects in the gas-phase. Furthermore, very little change was observed in the $C_1{\equiv}C_2$, $C_3{\equiv}C_4$, and Ru-C bond lengths upon exchange of *3,5*-trifluoromethylphenyl for phenyl or *para*-anisole, which suggested limited influence of the *trans*-alkynyl.

Table 2.6: *Selected experimental and calculated bond lengths (Å) and angles (°) for* ***2.10–2.12***

	2.10	**2.11**	**2.10$_{calc}$**	**2.11$_{calc}$**	**2.12$_{calc}$**
Ru_1–$P_{dppe\ average}$	2.348	2.356	2.434	2.432	2.434
Ru_1–C_1	2.125(3)	2.113(4)	2.090	2.089	2.090
Ru_1–C_3	2.060(3)	2.031(4)	2.094	2.078	2.094
C_1–C_2	1.121(4)	1.164(2)	1.229	1.228	1.229
C_3–C_4	1.189(4)	1.228(6)	1.235	1.237	1.235
Ru_1–C_1–C_2	174.8(3)	174.6(4)	177.2	179.0	177.2
C_3–Ru_1–C_1	176.0(1)	175.1(1)	178.4	176.8	178.4
C_4–C_3–Ru_1	177.9(3)	178.1(3)	177.8	176.6	177.8

In each system, the frontier molecular orbitals were similar to those observed for the cyaphide complexes **2.7**-**2.9**, with the HOMOs exhibiting out of phase mixing of the ruthenium *d*-orbitals with the $\pi_{C\equiv C}$ orbitals, and the LUMO being primarily based on the ancillary ligand set (Figure 2.7). A decrease in the percentage contribution from the metal centre and the terminal acetylide fragment was observed on moving to more electron donating ligands (43 to 32% and 23 to 11% respectively). It is notable that the percentage contributions from acetylide are considerably smaller than those from cyaphide in **2.7**–**2.9** (11–23% *vs* 24–40%). Furthermore, an increase in the contributions to the HOMO from the arene and $\pi_{C\equiv C}$ orbitals was observed

upon increasing the electron richness of the arene (11 to 25% and 19 to 28% respectively), which is similar to the trend observed for the cyaphide complexes **2.7**–**2.9**.

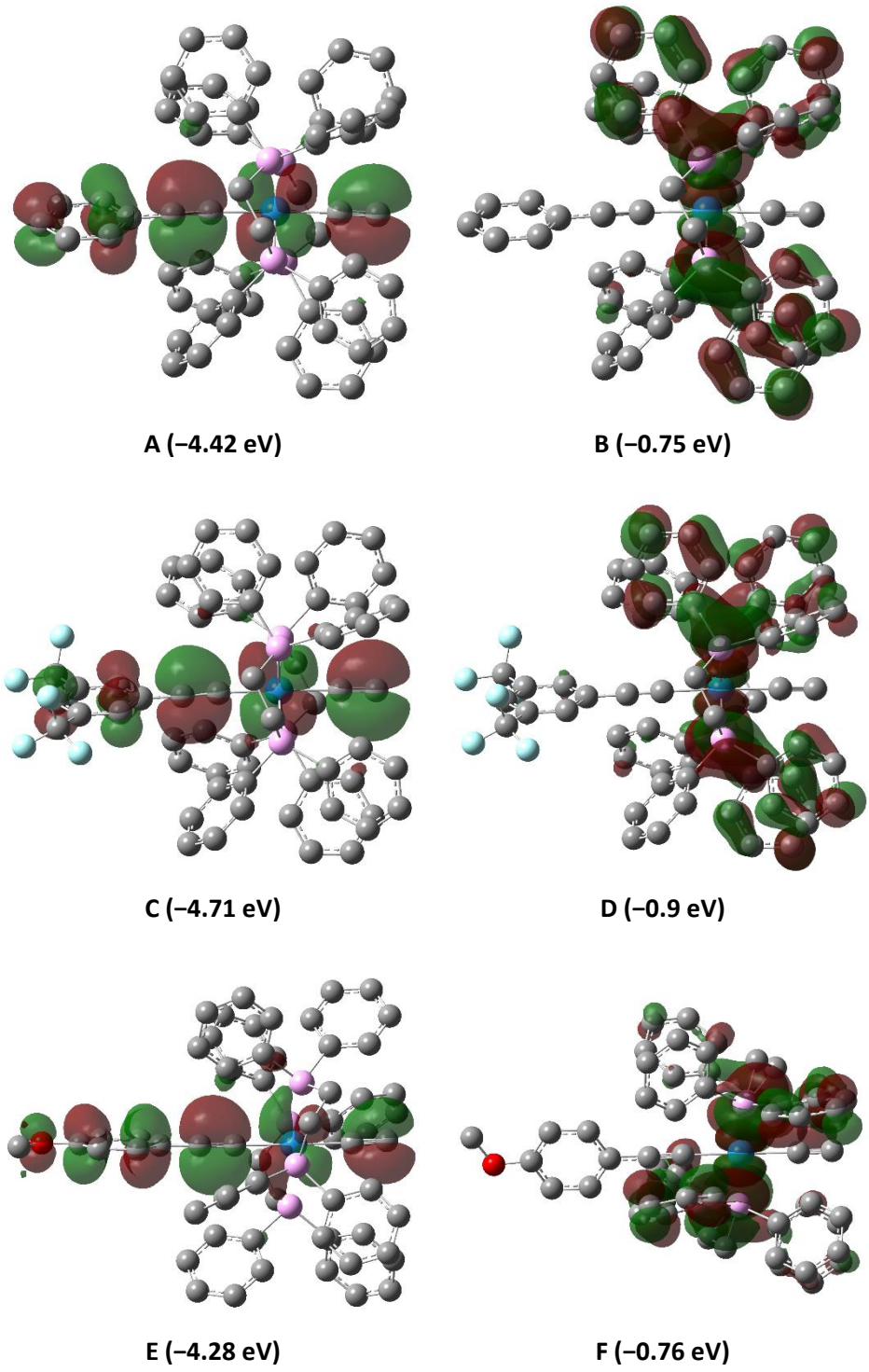

Figure 2.7: *Calculated frontier molecular orbitals of* ***2.10*** *(top),* ***2.11*** *(middle), and* ***2.12*** *(bottom). HOMO (A, C, & E), LUMO (B, D, & F)*

2.3.3 Electrochemical and UV-Vis Investigations

2.3.3.1 Cyclic Voltammetry

The cyclic voltammograms of **2.10–2.12** are shown in Figure 2.8. When compared to their parent chloride complexes ($E_{½}$ = −0.1 – 0.2 V; Table 2.7), a shift of the anodic process to more negative potentials was observed. The extent of this shift was lesser than observed for the cyaphide complexes **2.7–2.9** (*ca*. 25 mV *vs ca*. 50 mV) with the exception of **2.11**, which exhibits a much greater shift towards negative potentials than its cyaphidic counterpart (~110 mV). These potential shifts suggest that the σ-acceptor capacity of acetylide is between that of cyaphide and chloride (C≡P < C≡CH < Cl).

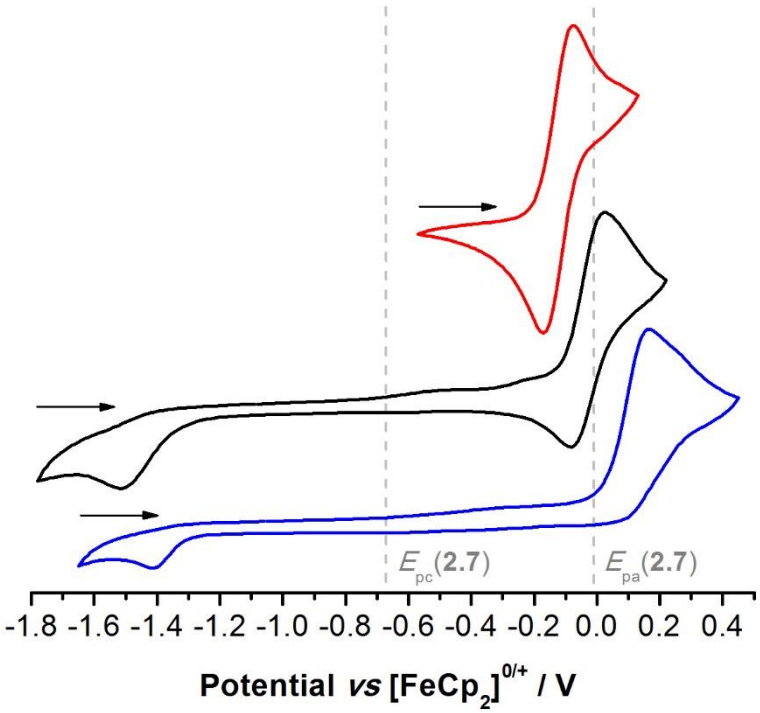

Figure 2.8: *Normalised voltammograms of* ***2.10*** *(black),* ***2.11*** *(blue), and* ***2.12*** *(red) as a solution in DCM (1 mM) with* $[^nBu_4N][PF_6]$ *supporting electrolyte (0.1 M), 0.1 V* s^{-1} *scan rate.* E_{pa} *and* E_{pc} *Values for* ***2.7*** *have been plotted for comparison.*

Unlike **2.7–2.9**, the electrochemical behaviour of the mixed acetylide complexes **2.10–2.12** appeared to be much more influenced by the electronic nature of the *trans* alkynyl ligand. The

degree of reversibility of the Ru^{II}/Ru^{III} redox couple increased with the electron density at the metal centre, with **2.11** exhibiting one irreversible oxidation at 0.09 V followed by a corresponding reductive event at −1.49 V (Figure 2.8). In contrast, **2.12** exhibited one quasi-reversible oxidative process at $E_{½}$ = −0.12 V, whereas **2.10** exhibited a single quasi-reversible oxidation at $E_{½}$ = −0.03 V followed by a further related reductive event at −1.51 V, which resulted in complete reduction of any remaining Ru(III) species back to Ru(II). These data have been summarised in Table 2.7.

Table 2.7: *Cyclic voltammetry data of ruthenium(II) complexes* ***2.1–2.3*** *and their cyaphide and mixed acetylide analogues* ***2.7–2.12***

Arene Substituent	Compound Number	E_{pa}	E_{pc}	ΔE	$E_{½}$
H	**2.1**[71]	–	–	0.07	+0.01
***4*-OMe**	**2.2**[71]	–	–	–	−0.10
***3,5*-CF_3**	**2.3**	0.21	0.12	0.09	+0.17
H	**2.7**	−0.01	−0.67	0.66	–
***4*-OMe**	**2.8**	−0.06	−0.7	0.64	–
***3,5*-CF_3**	**2.9**	0.16	−0.65	0.81	–
H	**2.10**	0.02	−0.07	0.09	−0.03
			−1.51	–	–
***3,5*-CF_3**	**2.11**	0.09	−1.49	1.58	–
***4*-OMe**	**2.12**	−0.08	−0.16	0.08	−0.12

2.3.3.2 UV-Vis Spectroscopy

All three complexes exhibited a relatively strong feature at *ca*. 250 nm in their UV-Vis spectra (Figure 2.9), which TD-DFT calculations revealed is primarily composed of MLCT to the ancillary ligand set, with some minor contributions arising from LLCT from the C≡C and C≡CH π-systems to the dppe. Complex **2.10** also exhibited a second feature at 325 nm, which was calculated to

be the result of LLCT from the C≡C, C≡CH, and arene π-systems (HOMO) to the ancillary ligand set (LUMO), alongside some additional contributions from MLCT.

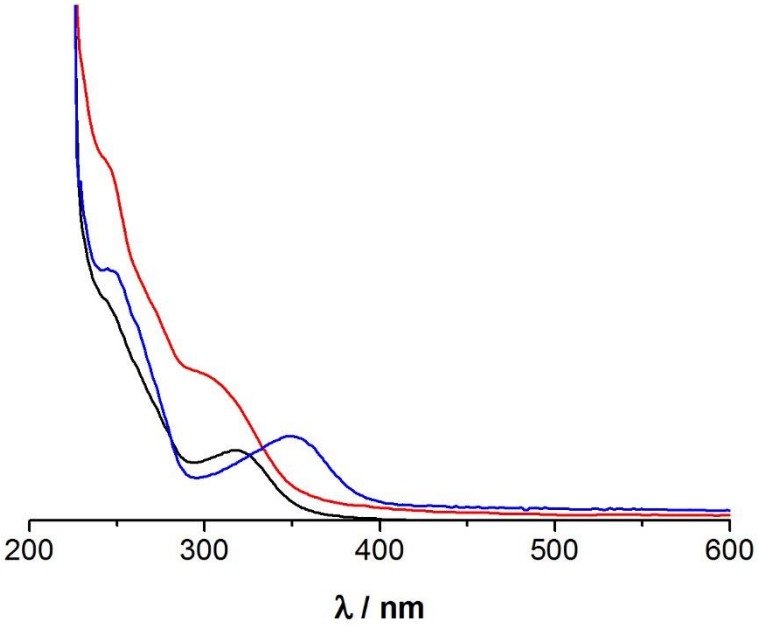

Figure 2.9: *Normalised UV-Vis spectra of* ***2.10*** *(Black),* ***2.12*** *(Red), and* ***2.11*** *(Blue). Ca. 1.0 ×* $\mathbf{10^{-5}}$ *mol dm*$^{-3}$ *in DCM, 1 cm Path Length*

Complex **2.11** exhibited a bathochromic shift of this feature to 345 nm, likely arising from increased contributions from the C≡CH moiety to the HOMO (23 *vs* 16% in **2.10**), as determined by DFT calculations. In contrast, the terminal acetylide fragment contributes less to the HOMO in **2.12** (11%), resulted in diminished through conjugation and thus a hypsochromic shift of the same feature to 310 nm.

2.4 Attempted Synthesis of *Trans*-[Ru(C≡CAr)(C≡N)(dppe)$_2$]

2.4.1 Attempted Synthesis

In order to develop further understanding of ligated cyaphide, the synthesis of complexes of the type *trans*-[Ru(C≡CAr)(C≡N)(dppe)$_2$] was attempted, thus facilitating direct comparison of

ligated cyaphide with both acetylide and cyanide. However, there are currently no examples of *trans* cyanide-acetylide complexes bearing a dppe scaffold in the literature. Consequently, the salt metathesis of sodium cyanide with *trans*-[RuCl(C≡CPh)(dppe)$_2$] was attempted, following the procedure reported by Morris and Rigo for hydridic systems, and afforded a pale yellow solid (Scheme 2.5).[135,136]

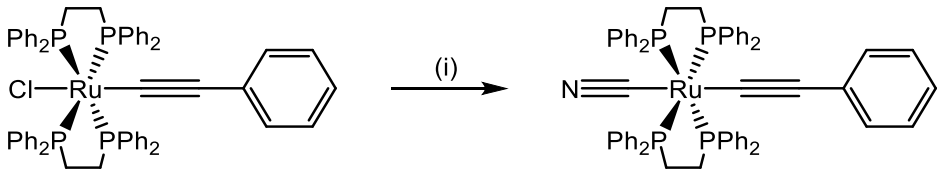

Scheme 2.5: *Attempted synthesis of trans-[Ru(C≡N)(C≡CPh)(dppe)$_2$]. Reagents and conditions: (i) excess NaC≡N, MeOH, 16 h.*

Spectroscopic characterisation by $^{31}P\{^1H\}$ and ^1H NMR spectroscopy revealed a mixture of two complexes in solution, one of which was unreacted starting material. The product displayed a singlet resonance in the $^{31}P\{^1H\}$ NMR spectrum at *ca*. 53 ppm which, in conjunction with the ^1H NMR spectroscopic data and literature comparisons, was assigned as the undesired symmetrical bis-acetylide complex *trans*-[Ru(C≡CPh)$_2$(dppe)$_2$].[132] Variation of the reagents and reaction durations did not result in the formation of the desired complex.

Recently, Wang and co-workers have reported the synthesis of *trans*-[RuCl(C≡N)(dppe)$_2$], achieved through the reaction of *trans*-[RuCl$_2$(dppe)$_2$] with aqueous potassium cyanide.[137] This is a potential starting point for the synthesis of ruthenium(II) cyanide-alkynyl complexes, if formation of the intermediate vinylidene complex is possible, though this has not been investigated.

2.5 Synthesis of *Trans*-[MH(C≡E)(dppe)$_2$]

2.5.1 Synthesis and Characterisation of Trans-[RuH(C≡E)(dppe)$_2$]

The synthesis of both *trans*-[RuH(C≡N)(dppe)$_2$] (**2.13**) and *trans*-[RuH(C≡P)(dppe)$_2$] (**2.14**) was achieved through use of literature procedures,[64,135,136] with the latter formed using $Me_3SiC{\equiv}P$, as opposed to $Ph_3SiC{\equiv}P$. Interestingly, no literature precedent had been established for the synthesis of their acetylide counterpart, *trans*-[RuH(C≡CH)(dppe)$_2$] (**2.15**).

Previous observations have shown that addition of base to samples of *trans*-[RuCl(C≡CR)(dppe)$_2$] in protic solvents led to exchange of the chloride ligand for hydride, resulting in the formation of the complexes *trans*-[RuH(C≡CR)(dppe)$_2$].[138,139] Accordingly, samples of *trans*-[RuCl(C≡CH)(dppe)$_2$] were treated with one equivalent KO^{t}Bu in DCM/MeOH (Scheme 2.6), with subsequent filtration affording a pale yellow solid after one hour.

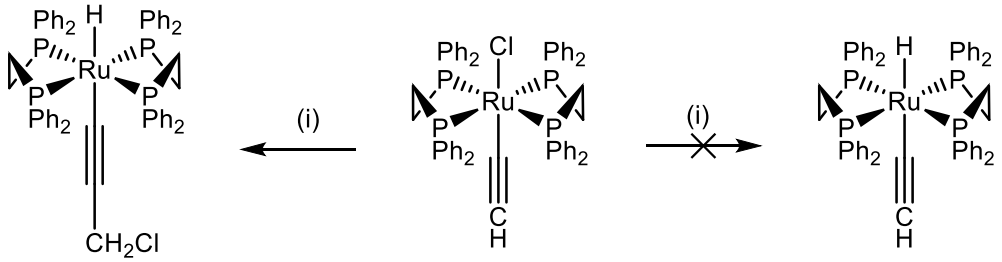

Scheme 2.6: *Attempted synthesis of **2.15**, resulting in the formation of **2.16**. Reagents and conditions: (i) 1 eq. KO^{t}Bu, DCM/MeOH, 1 h.*

NMR studies indicated the formation of one product, which was apparent in the $^{31}P\{^1H\}$ NMR spectrum as a singlet at 63.4 ppm. In the ^1H NMR spectrum, a hydride resonance at −10.46 ppm was observed (quintet, J_{HP} = 19.5 Hz), alongside a resonance at 4.14 ppm, which was shown by HSQC to be a CH_2 group and correlated with a carbon resonance at 55.2 ppm. Two acetylenic resonances were observed in the $^{13}C\{^1H\}$ spectrum at 123.0 and 112.8 ppm, alongside a C≡C stretching mode in the IR spectrum ($\nu_{C\equiv C}$: 2072 cm^{-1}). It is believed that reaction with the

chlorinated solvent gave rise to the formation of complex **2.16**, instead of the desired **2.15** (Scheme 2.5).

Consequently, a different synthetic approach was undertaken. Similar to the formation of **2.13**, *trans*-[RuHCl(dppe)$_2$] was reacted with an excess of sodium acetylide as a suspension in methanol over a period of 4 weeks (Scheme 2.6), with the reaction's progress monitored by $^{31}P\{^1H\}$ NMR studies of periodically taken aliquots. Upon completion, filtration and washing with methanol afforded a pale-yellow solid.

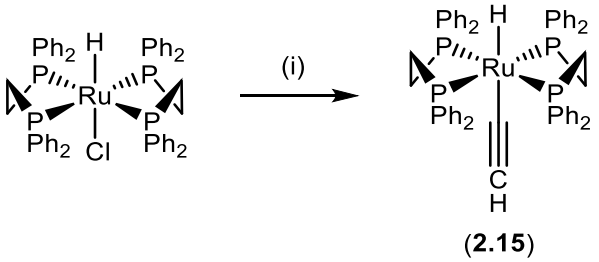

(**2.15**)

Scheme 2.7: *Synthesis of* ***2.15****. Reagents and conditions: (i) 10 eq. NaC≡CH, MeOH, 4 weeks.*

Complex **2.15** displayed a broad doublet in the $^{31}P\{^1H\}$ NMR spectrum at 69.4 ppm ($^2J_{PH}$ = 3.0 Hz) which is in line with the shifts of both **2.13** and **2.14** (65.2 and 68.9 ppm respectively). The ^1H NMR spectrum revealed the retention of the metal hydride, with a quintet displayed at −10.77 ppm (J_{HP} = 19.8 Hz), alongside a characteristic acetylenic proton resonance at 1.75 ppm. In the $^{13}C\{^1H\}$ NMR spectrum both the C_α and C_β of the acetylene moiety were observed at 101.4 and 122.9 ppm respectively, alongside a C≡C stretching mode in the IR spectrum ($\nu_{C\equiv C}$: 2070 cm^{-1}).

2.5.2 Electrochemical and UV-Vis Investigations

2.5.2.1 Cyclic Voltammetry

The effects of isolobal and isoelectronic fragment exchange on the electronic structure of "RuH(dppe)$_2$" scaffolded systems were investigated using cyclic voltammetry (Table 2.8; Figure

2.10). Complex **2.14** exhibited one irreversible oxidation at −0.11 V, consistent with the Ru^{II}/Ru^{III} redox couple, with no increase in current observed up to a potential of −1.5 V in the inverse cathodic scan (Figure 2.10).

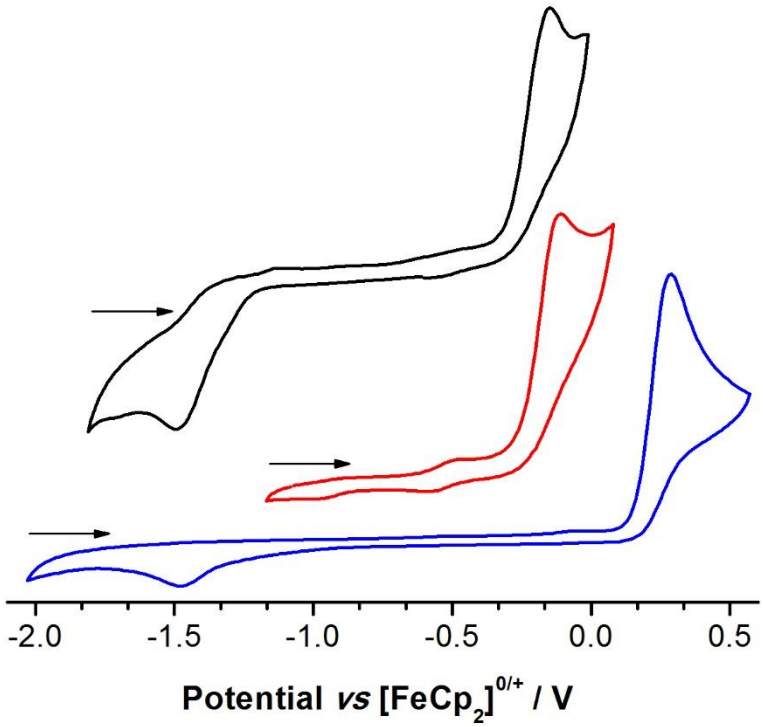

Figure 2.10: *Normalised voltammograms of* ***2.13*** *(blue),* ***2.14*** *(red), and* ***2.15*** *(black) as a solution in DCM (1 mM) with* $[^{n}Bu_4N][PF_6]$ *supporting electrolyte (0.1 M), 0.1 V* s^{-1} *scan rate*

Similarly, complex **2.15** exhibits a single oxidative event at −0.16 V, consistent with a one-electron oxidation from Ru(II) to Ru(III), alongside a single reductive event at −1.48 V. The large peak-to-peak separation (1.32 V) was indicative of irreversible oxidative behaviour, with a significant overpotential required to reduce the highly stable oxidation product. The small discrepancy between the oxidative potential of the cyaphidic and acetylenic systems suggests that cyaphide possesses similar electronic characteristics to acetylide.

Complex **2.13** exhibits two irreversible redox processes. The first at 0.28 V corresponded to the oxidation of Ru^{II} to Ru^{III}, with the second at −1.47 V signifying the reverse reductive event, with a peak to peak separation greater than that observed in the acetylenic system (Table 2.8).

Interestingly, the shift to positive potential when compared to **2.14** (E_{pa} = −0.11 V) suggested greater electron withdrawing capacity of cyanide compared to cyaphide and acetylide. This is perhaps unsurprising, given the greater electronegativity of nitrogen compared to phosphorus and carbon (3.0 *vs* 2.2 and 2.5 respectively).

Table 2.8: *Selected cyclic voltammetry data for complexes* ***2.13–2.15***

E	Compound Number	E_{pa}	E_{pc}	ΔE
N	**2.13**	0.28	−1.47	1.75
P	**2.14**	−0.11	–	–
CH	**2.15**	−0.16	−1.48	1.32

To explain the observed difference in electrochemical behaviour, DFT was used to calculate the percentage contributions of the metal centre and the C≡E (E = P, CH, N) fragment to the HOMO of each complex (Figure 2.11). While the HOMO of each complex appeared similar, the percentage contributions reflected the behaviour observed by cyclic voltammetry. While **2.15** and **2.14** had similar contributions from the C≡E π-system and the metal centre, with a slightly larger contribution from ruthenium, the HOMO of **2.13** appeared to be predominantly metal-based, with a 72% contribution *vs ca*. 55%. It could therefore be rationalised that the redox behaviour is much more metal-based in the cyanide system than in the other two complexes, resulting in a much more positive oxidative potential. However, the influence of the higher electronegativity of nitrogen compared to phosphorus and carbon (3.0 *vs* 2.2 and 2.5 respectively) could also lead to the same outcome.

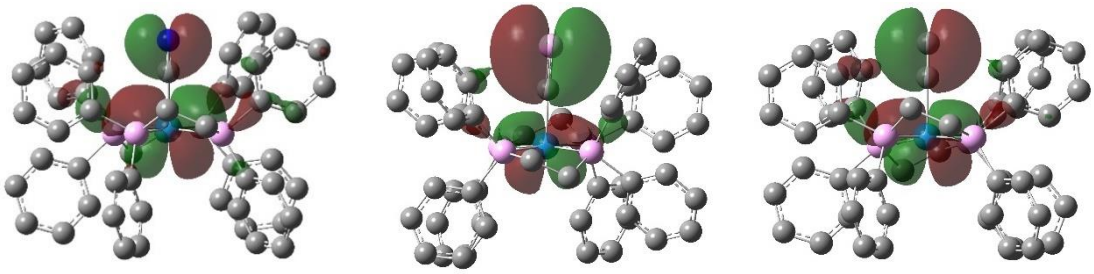

72% Ru, 16% C≡N | 55% Ru, 37% C≡P | 54% Ru, 35% C≡CH

Figure 2.11: *Calculated HOMOs of* ***2.13–2.15*** *and percentage orbital contributions*

2.5.2.2 UV-Vis Spectroscopy

The electronic spectra of **2.13**-**2.15** were recorded (Figure 2.12), and the transitions assigned with the assistance of TD-DFT calculations. Complex **2.13** exhibited two weak features in the UV-Vis spectrum at 250 and 340 nm, with excited state calculations suggesting that they were primarily composed of LLCT from the $\pi_{C\equiv N}$ orbitals to the ancillary ligand set, alongside some smaller contributions from MLCT. No ILCT between the $\pi_{C\equiv N}$ and $\pi^*_{C\equiv N}$ orbitals was observed, due to the high energy of the anti-bonding orbital (LUMO+22), which lies *ca*. 7.1 eV higher in energy relative to the HOMO.

Complex **2.14** and **2.15** exhibited similar spectroscopic behaviour to **2.13**, each displaying a strong feature at *ca*. 240 nm, which is comprised of the same LLCT and MLCT observed for **2.13**. Lower energy features at 360 and 420 nm for **2.14** and 340 and 456 nm in complex **2.15** were also dominated by LLCT from the C≡P and C≡CH π-systems to the ancillary ligand set. The $\pi^*_{C\equiv P}$ and $\pi^*_{C\equiv CH}$ orbitals lie 5.15 and 7.47 eV higher in energy than their respected HOMOs in the LUMO+16 and LUMO+30 respectively, resulting in little ILCT based on the C≡P and C≡CH moieties. Furthermore, the energy difference between the $\pi_{C\equiv P}$ and $\pi^*_{C\equiv P}$ orbitals in **2.14** is similar to that of the previously described cyaphide alkynyl complexes (*ca*. 5 eV) and is significantly lower than its nitrogen- and carbon-based counterparts.

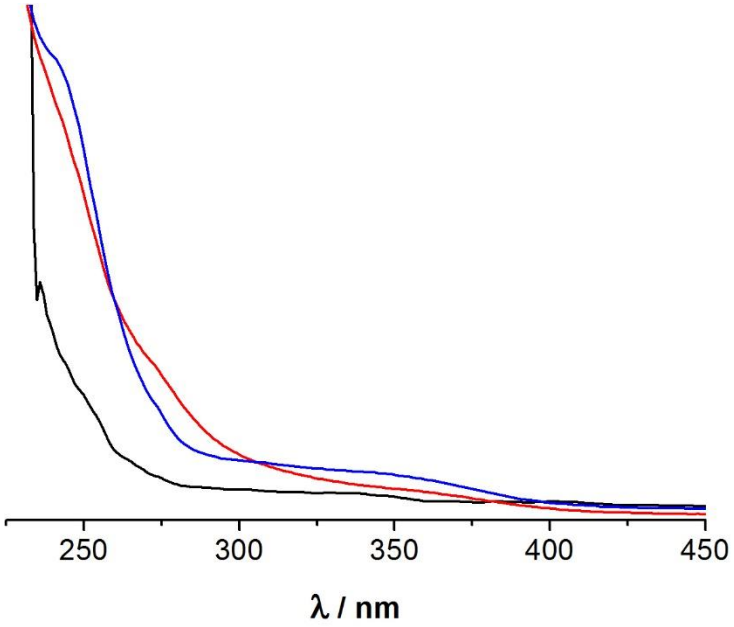

Figure 2.12: *Normalised UV-Vis spectra of* ***2.13*** *(Black),* ***2.14*** *(Red), and* ***2.15*** *(Blue). Ca. 1.0* $\times$ $\mathbf{10^{-5}}$ *mol dm^{-3} in DCM, 1 cm path length*

2.5.3 Synthesis and Characterisation of Trans-[FeH(C≡P)(dppe)$_2$]

As mentioned previously (see Chapter 1), it has been shown that coordination of phosphaalkynes in an η^1-binding mode can be achieved at an iron(II) centre, if there is enough steric protection provided by the ancillary ligand set.[33] With this in mind, the synthesis of the first example of a first-row transition metal cyaphide complex was attempted.

Initial attempts to synthesise *trans*-[FeH(η^1-P≡CSiMe$_3$)(dppe)$_2$] (**2.17$^+$**) following established procedures were made,[70] which resulted in the formation of a brick-red solid upon workup. However, ^{31}P{^{1}H} and ^{1}H NMR studies revealed no resonances, which was inconsistent with previous reports of similar phosphaalkyne complexes of iron.[33] This was attributed to the formation of a paramagnetic iron(III) species, resulting from chemical oxidation by the silver(I) salts. Consequently, later attempts utilised either KOTf or TlOTf to abstract the halide instead of AgOTf,[65] which successfully afforded **2.17** (Scheme 2.8).

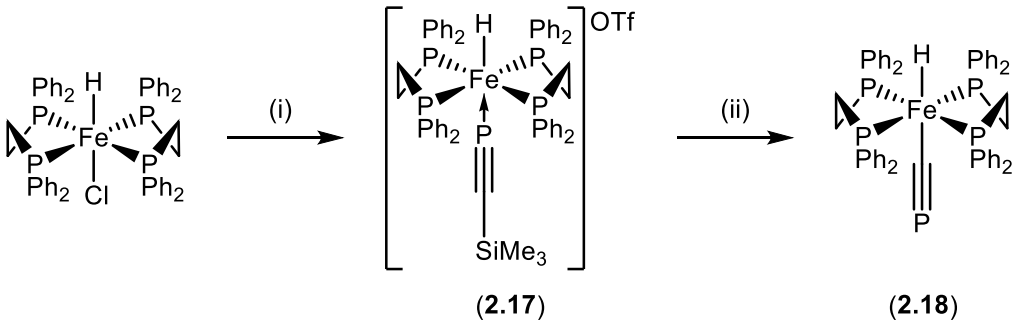

Scheme 2.8: *Synthesis of* ***2.17*** *and conversion to cyaphide complex* ***2.18****. Reagents and conditions: (i) 1 eq. KOTf, DCM, 10 min.; (ii) 2 eq. P≡CSiMe$_3$ in toluene, 16 h.; (iii) 1 eq. NaOPh, THF, 16 h.*

Upon workup, **2.17** was afforded as a yellow-orange solid, and exhibited the expected AX_4 splitting pattern in the $^{31}P\{^1H\}$ NMR spectrum, with quintet and doublet resonances at 159.7 and 80.0 ppm respectively, consistent with previously described iron and ruthenium hydride η^1-phosphaalkyne complexes.[32,33,64,65] In the ^1H NMR spectrum, the presence of a quintet at −10.45 ppm supported retention of the iron hydride, while a singlet at 0.10, integrating as nine with respect to the hydridic resonance, supported retention of the $SiMe_3$ group of the phosphaalkyne. The $^{13}C\{^1H\}$ NMR spectrum displayed a doublet resonance at 189.9 ppm, with a $^2J_{CP}$ value of 80 Hz, consistent with retention of the C≡P triple bond. While slightly higher in frequency than Grützmacher's report for *trans*-[RuH(η^1-P≡CSiPh$_3$)(dppe)$_2$]OTf, it is similar to the previously described alkynyl-phosphaalkyne complexes.[70] The increase in frequency of the phosphaalkyne carbon resonance centre arises from the exchange of $SiPh_3$ for $SiMe_3$, as observed upon comparison of Grützmacher's complex with the analogous *trans*-[RuH(η^1-P≡CSiMe$_3$)(dppe)$_2$]PF_6 (**2.19**) (δ_C: 175.1 *vs* 188.5).[64] This was further supported by the presence of a C≡P stretching mode in the IR spectrum ($\nu_{C\equiv P}$: 1262 cm^{-1}). The structure of **2.17** was ultimately confirmed by X-ray diffraction studies on a single crystal grown from a saturated DCM solution that had been layered with pentane. Unfortunately, the data collected were of insufficient quality to determine accurate bond metrics and thus serves only to demonstrate

connectivity (Figure 2.13), although the placement of the metal hydride was possible using the difference map.

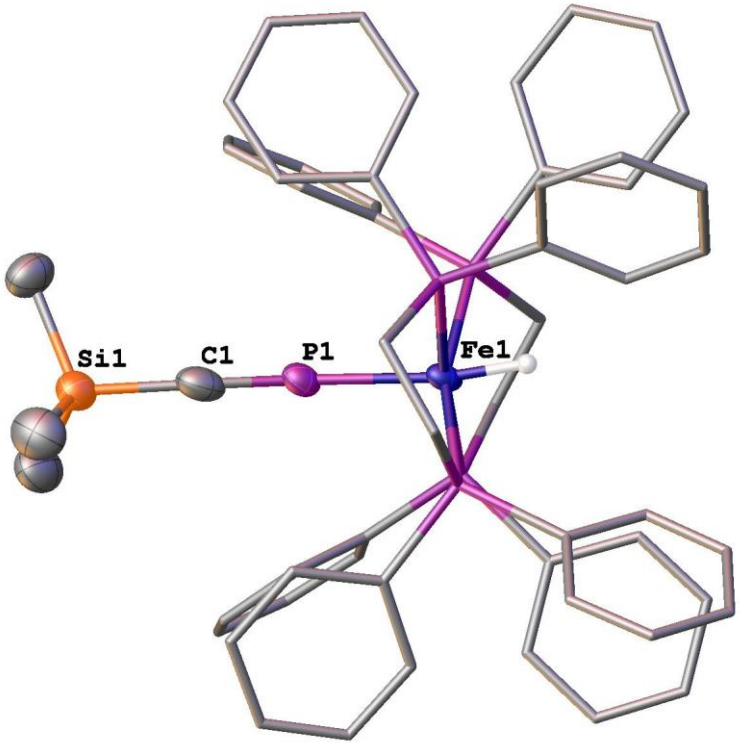

Figure 2.13: *Molecular structure of* ***2.17****; 50% thermal ellipsoids, selected hydrogen atoms and counterion omitted, and ancillary ligand set reduced for clarity*

While addition of KO^{t}Bu to a sample of **2.17** resulted in an intractable mixture of products, reaction with NaOPh over a period of 16 hours afforded a pale-yellow solid upon removal of solvent and subsequent washing with acetonitrile. Complex **2.18** displayed two broad resonances in the $^{31}P\{^1H\}$ NMR spectrum at 201.6 and 85.3 ppm in a 1:4 ratio, which are at a significantly higher frequency than reported for *trans*-[RuH(C≡P)(dppe)$_2$] (**2.14**). This was attributed to the reduced shielding effect of the iron(II) centre when compared to ruthenium(II), which is similarly exhibited upon comparison of *trans*-RuHCl(dppe)$_2$ (δ_P: 62.9) and *trans*-FeHCl(dppe)$_2$ (δ_P: 81.4). The diminished coupling interaction was consistent with reports by Grützmacher for the desilylation of the analogous ruthenium system.[64] The ^{1}H NMR spectrum

revealed loss of the $SiMe_3$ resonance and displayed several broad resonances for the ancillary ligand set, alongside a multiplet at −14.46, suggesting retention of the metal hydride. While no cyaphidic resonance was observed in the $^{13}C\{^1H\}$ spectrum, due to sample concentration limitations, the presence of a C≡P unit was supported by the observation of the corresponding stretching mode in the IR spectrum at 1246 cm^{-1}. The shift in the C≡P stretching mode to lower frequency by *ca*. 20 cm^{-1} is consistent with a change from and η^1-phosphaalkyne complex to a terminal cyaphide complex,[70] and thus supports the formation of **2.18**.

Interestingly, during the formation of **2.18** a second product was observed in the $^{31}P\{^1H\}$ NMR spectrum, with a distinctive resonance at 330 ppm, similar to reports by Grützmacher, who postulated an intermediate with an observed $^{31}P\{^1H\}$ NMR resonance at 309.5 ppm.[64,67] Hints to the identity of this complex were obtained serendipitously when the reaction of NaOPh with **2.17** was performed in wet THF. A new product was formed exclusively, with quintet and doublet resonances in the $^{31}P\{^1H\}$ NMR spectrum at 328.1 and 80.1 ppm respectively in a 1:4 ratio, and with a mutual coupling of 37 Hz. Retention of the hydride and $SiMe_3$ group was supported by the presence of the corresponding resonances in the ^1H NMR spectrum at −9.87 and −0.50 ppm respectively, with the latter functionality also observed in the $^{13}C\{^1H\}$ NMR spectrum at 1.0 ppm. No evidence of a cyaphidic carbon resonance was observed in the $^{13}C\{^1H\}$ NMR spectrum, however, a doublet at 120.8 ppm with a $^1J_{CP}$ coupling of 3 Hz was apparent. Furthermore, this resonance was seen to correlate to a broad doublet resonance in the ^1H NMR spectrum at 6.12 ppm, as observed in the ^1H-^{13}C HSQC spectrum. These data are consistent with the formation of a $\lambda^5\sigma^3$-phosphaketenyliron complex (**2.20**), in an analogous fashion to that described by Grützmacher (δ_C: 110.5, $^1J_{CP}$ = 5.3 Hz; Scheme 2.9).[67]

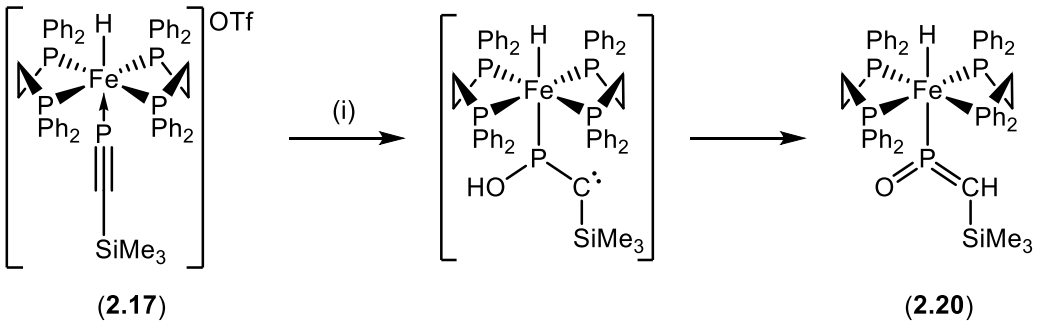

Scheme 2.9: *Serendipitous synthesis of* ***2.20****. Reagents and conditions: (i)* H_2O*, THF, 16 h.*

2.5.3.1 Electrochemical Investigations

At moderate scan rates (0.1 V s^{-1}), complex **2.18** exhibited a single irreversible redox event at 0.51 V consistent with the Fe^{II}/Fe^{III} redox couple, with no increase in current observed down to a potential of −1.0 V in the inverse cathodic scan, which suggested a high stability of the oxidation product against reduction (Figure 2.14). This irreversible oxidative behaviour was similar to that observed for *trans*-[RuH(C≡P)(dppe)$_2$] (**2.14**), however, the observed oxidative potential was much more positive for **2.18** than **2.14** (0.51 *vs* –0.11 V).

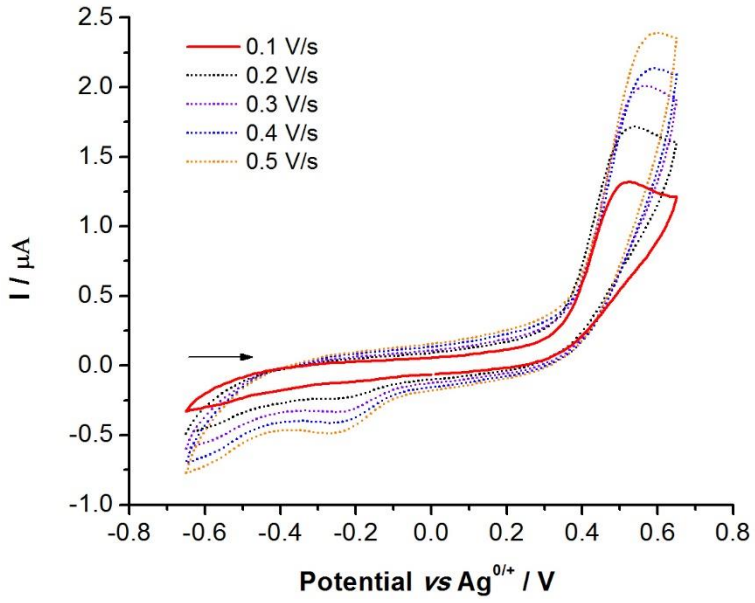

Figure 2.14: *Cyclic voltammograms of* ***2.18*** *at various scan rates as a solution in DCM (1 mM) with [*^{n}*Bu$_4$N][PF$_6$] supporting electrolyte (0.1 M)*

While **2.14** did not display any change in redox behaviour upon increase in scan rate, **2.18** could be reduced back to Fe(II) at higher scan rates, with a reductive event observed at −0.25 V. This could be attributable to the differing percentage contributions of the C≡P unit and metal centre to the HOMO (48% C≡P, 44% Fe vs 37% C≡P, 55% Ru; Figure 2.15), resulting in more ligand-based redox behaviour, however, further investigations are required.

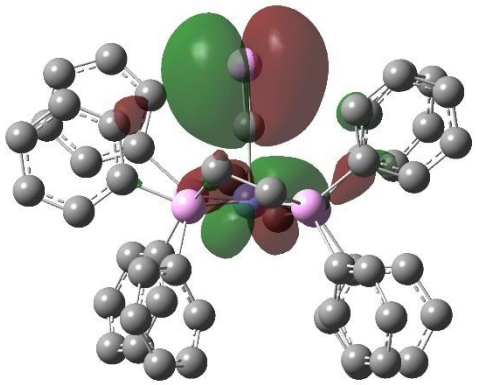

Figure 2.15: *Calculated HOMO of* ***2.18***

2.6 Concluding Remarks

The synthesis of the cyaphide complexes **2.7–2.9** has been achieved, and their electronic structure investigated using cyclic voltammetry and UV-Vis spectrometry. It was demonstrated that the introduction of cyaphide greatly alters the electrochemical behaviour of these complexes, with **2.7–2.9** all exhibiting irreversible oxidative behaviour, with minor shifts of the anodic process to higher or lower potential depending on the electron-withdrawing capacity of the *trans*-alkynyl ligand.

These were compared with the analogous unsymmetrical bis-acetylide complexes **2.10–2.12**, whose electrochemical behaviour demonstrated a much greater dependence on the nature of the *trans*-alkynyl, with **2.12** demonstrating quasi-reversible behaviour, **2.11** demonstrating irreversible oxidative behaviour, and **2.10** lying somewhere in-between.

The synthesis of hydridic systems **2.13–2.15** allowed the direct comparison of ligated cyanide, cyaphide and acetylide, the UV-Vis spectra of which demonstrated high energy transitions dominated by LLCT between the C≡E π-systems and the ancillary ligand set. Cyclic voltammetry showed that cyaphide behaves more acetylide than cyanide, and this was supported by DFT calculations.

Lastly, the synthesis of the first example of cyaphide ligated to a first-row transition metal has been reported, as inferred from NMR spectroscopic data in lieu of X-ray crystallography. The electrochemical behaviour of **2.18** was investigated and found to be similar to its second-row analogue, exhibiting one irreversible oxidative process with no corresponding reductive process observed at moderate scan rates.

Chapter 3 – Bimetallic Ruthenium Cyaphide Complexes

3.1 Introduction

Since its discovery,[140] the Creutz-Taube ion $[(H_3N)_5Ru(pz)Ru(NH_3)_5]^{5+}$ has been intensively studied and is considered by many to be the standard example of inner sphere electron transfer between two transition metal centres,[141,142] and the first definitive example of a mixed valence complex. From this, a wide variety of derivatives have been synthesised and studied both spectroscopically and electrochemically as well as, more recently, much more exotic and highly conjugated homobimetallic mixed valence species.[92,143–145]

Perhaps the most promising systems incorporating conjugated acetylide chains feature the "$Ru(dppe)_2$" fragment, which has been widely used in the development of carbon σ-bonded molecular wires, owing to the steric bulk which prevents acetylide oligomerisation.[92] Indeed, monometallic complexes based upon this fragment have been investigated for several uses including, but not limited to, non-linear optics[93,94,146] and molecular wires.[92–94,127] This has been furthered by the introduction of additional redox sites, either through direct incorporation or functionalisation of coordinating tectons (Figure 3.1).[147–152]

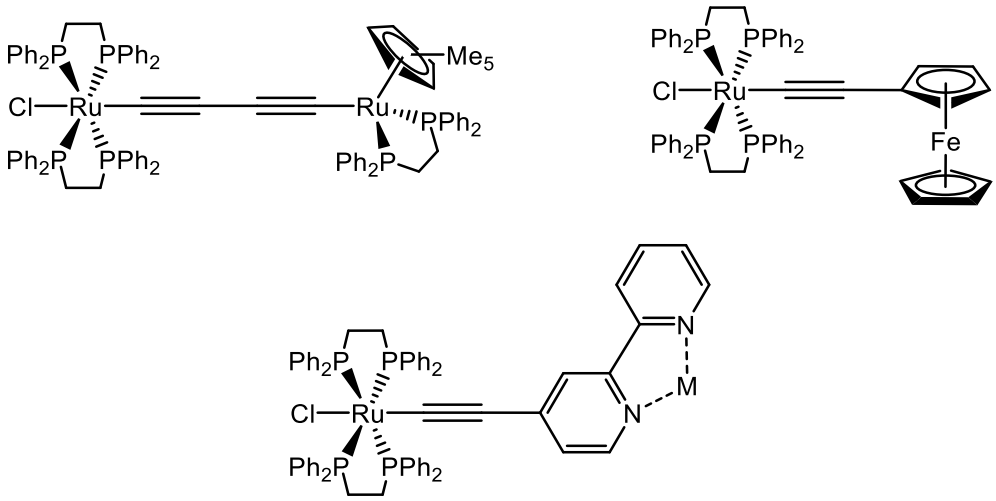

Figure 3.1: *Examples of multimetallic acetylide complexes, formed through either direct incorporation of redox active sites, or via functionalisation of coordinating tectons*

The theme of symmetrical homobimetallic mixed valence complexes has promoted various studies,[92] including systems incorporating all-carbon *sp*-bridges, sp^2-bridges, and mixed sp/sp^2-bridges, alongside others based solely upon aromatic rings as linkers between the metal centres.[92] Electronic communication in di-ruthenium complexes *via* the bridge containing ethenyl and ethynyl fragments has been investigated in detail by Chen,[153] Field,[115] and Rigaut (Figure 3.2),[95,114] with the latter two investigating systems which utilised a dppe scaffold. Later work by Klein and co-workers assisted in supplementing the understanding of the effects of the nature of the bridging fragment (Figure 3.2).[116]

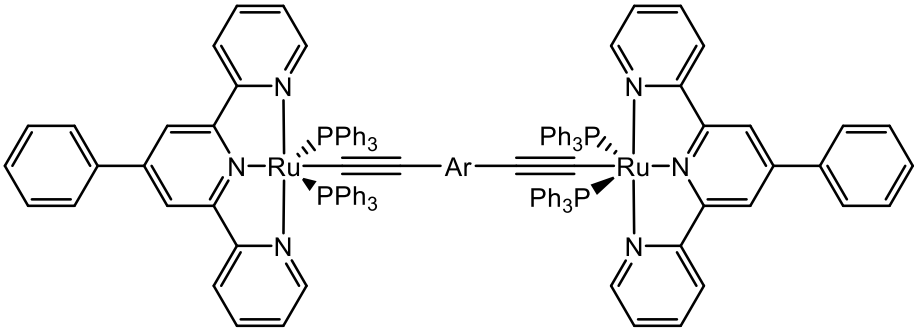

Ar = 2,5-(C_4H_2S), [2,5-(C_4H_2S)]$_2$, [2,5-(C_4H_2S)]$_3$, 1,4-C_6H_4, 1,4-(C_6H_4)$_2$

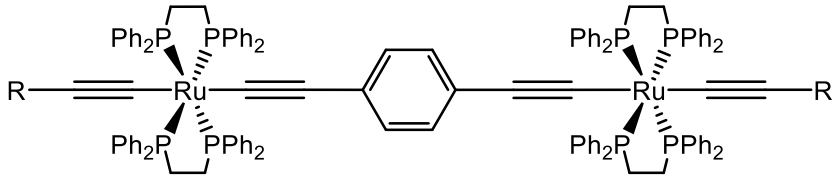

R = R' = 1,4-C_6H_4CN; R = Ph, R' = 1,4-C_6H_4CN

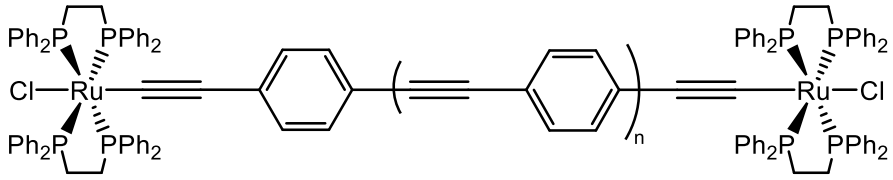

n = 0, 1, 2

Figure 3.2: *examples of bimetallic complexes featuring the bridging units comprising of ethenyl and ethynyl fragments*

Recent reports have shown that cyaphide can be incorporated into monometallic systems and exhibits through conjugation with *trans*-alkynyl ligands,[70] however, this has yet to be applied to systems featuring multiple metal centres or extended to multiple C≡P fragments. The synthesis of these complexes, and electrochemical investigations into their redox behaviour is described herein.

3.2 Heterobimetallic Systems

3.2.1 Synthesis of Trans-[Ru(C≡P)(dppe)$_2$(C≡CFc)]

In an analogous fashion to previously described monometallic complexes (See Chapter 2), treatment of a sample of *trans*-[RuCl(dppe)$_2$(C≡CFc)] (**3.1**) with successive stoichiometric amounts of AgOTf and P≡CSiMe$_3$ afforded the corresponding η^1-phosphaalkyne complex in moderate yields upon workup (*ca*. 50%; Scheme 3.1). Subsequent treatment with base in THF gave rise to the corresponding cyaphide complex as a free-flowing orange-yellow powder upon lyophilisation with benzene.

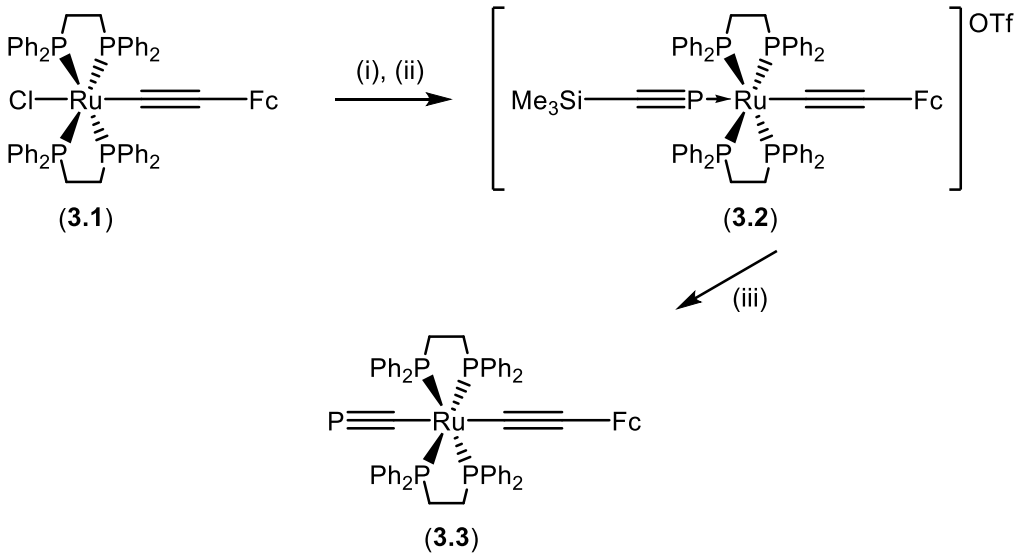

Scheme 3.1: *Synthesis of **3.2** and subsequent conversion to cyaphide complex **3.3**. Reagents and conditions: (i) 1 eq. AgOTf, DCM, 10 min.; (ii) 1 eq. P≡CSiMe$_3$ in toluene, 1 h.; (iii) 1 eq. KO^{t}Bu, THF, 1 h.*

The formation of **3.2** was convincingly established from NMR spectroscopic data, with a quintet and doublet resonance displayed in the $^{31}P\{^1H\}$ spectrum at 112.9 and 42.6 ppm respectively, with a mutual coupling of 34 Hz. Retention of the SiMe$_3$ group of the phosphaalkyne was supported by a singlet resonance in both the ^1H and $^{13}C\{^1H\}$ NMR spectra at −0.15 and 0.5 ppm, alongside a single cross-peak observed in the ^1H-^{29}Si HMBC spectrum (δ_{Si}: −13.3). The phosphaalkyne carbon resonance displayed as a doublet at 187.8 ppm (J_{CP} = 89 Hz), which is

consistent with literature reports,[70] and was supported by a characteristic C≡P stretching mode in the IR spectrum ($\nu_{C\equiv P}$: 1262 cm^{-1}). Retention of the ethynylferrocene unit was evidenced in the $^{13}C\{^1H\}$ spectrum, with distinctive resonances displayed for both C_α and C_β (119.7 and 113.3 ppm), characteristic cyclopentadienyl resonances for both the substituted and unsubstituted rings in the $^{13}C\{^1H\}$ and ^1H NMR spectra, and the presence of a C≡C stretching mode in the IR spectrum ($\nu_{C\equiv C}$: 1991 cm^{-1}).

Conversion of **3.2** to **3.3** was primarily indicated by a shift in both resonances in the $^{31}P\{^1H\}$ NMR spectrum to higher frequency (*ca*. 158 and 51 ppm), alongside a reduction in coupling (J_{PP} = 4 Hz) consistent with a change from a $^2J_{PP}$ to $^3J_{PP}$ interaction. This was further supported by a shift of the phosphaalkyne carbon resonance to 201.2 ppm, a reduction in the C≡P stretching frequency ($\nu_{C\equiv P}$: 1251 cm^{-1}), and loss of $SiMe_3$ resonances in the ^1H, $^{13}C\{^1H\}$, and ^1H-^{29}Si NMR spectra. Both the acetylide fragment and ancillary ligand set remained intact, as evidenced by ^1H and $^{13}C\{^1H\}$ NMR experiments and the retention of the C≡C stretching mode in the IR spectrum ($\nu_{C\equiv C}$: 2067).

3.2.2 Molecular Structure Analyses

The structures of both **3.2** and **3.3** were unequivocally confirmed using X-ray crystallographic characterisation and were compared to the optimised gas-phase geometries calculated using DFT (B3LYP/6-31G** for H, C, P, Si; LANL2DZ for Ru, Fe). Selected bond lengths and angles have been summarised in Table 3.1.

In the solid state, **3.2** exhibited the expected η^1-coordination mode of the phosphaalkyne moiety *trans* to the ethynylferrocene fragment (Figure 3.3). The geometry around the ruthenium centre (∠ $P_{C\equiv P}$-Ru-C) exhibited a minor distortion from linearity, though less-so than in *trans*-[Ru(η^1-P≡C$SiMe_3$)(C≡CCO_2Me)(dppe)$_2$]OTf (179.0(2) ° *vs* 177.0(3) °).[70] Further, the observed Ru-P distance of 2.246(2) Å is comparable to that observed in Grützmacher's *trans*-[RuH(η^1-

P≡CSiPh$_3$)(dppe)$_2$]BF$_4$ (2.249(1) Å),[64] however, this is considerably shorter than that reported by Crossley (*viz* 2.274(3) Å).[70] The C−C distance of the alkyne in **3.2** showed some lengthening when compared to free ethynylferrocene,[154] which is to be expected upon coordination to a transition metal centre. The C−P distance of the phosphaalkyne fragment fell within the expected range and was statistically indistinguishable from both Grützmacher's and Crossley's complexes. Overall, longer bond distances were observed in **3.2$_{calc}$** when compared to **3.2**, alongside a greater tendency towards overall linearity, however, this is most likely due to the absence of intermolecular interactions in the gas-phase calculations. Despite this, the good agreement between the experimental and calculated bond metrics suggests that these systems have been well-modelled using using this functional and basis set.

Table 3.1: *Selected experimental and calculated bond lengths (Å) and angles (°) for* ***3.2*** *and* ***3.3***

	3.2	**3.2$_{calc}$**	**3.3**	**3.3$_{calc}$**
Ru$_1$–P$_{dppe\ average}$	2.401	2.485	2.363	2.446
Ru$_1$–P$_1$	2.246(2)	2.352	–	–
Ru$_1$–C$_1$	–	–	2.032(6)	2.044
Ru$_1$–C$_2$	2.055(7)	2.043	2.111(6)	2.122
C$_2$–C$_3$	1.182(12)	1.230	1.218(8)	1.235
P$_1$–C$_1$	1.522(9)	1.548	1.553(6)	1.586
Si$_1$–C$_1$	1.846(9)	1.856	–	–
P$_1$–C$_1$–Si$_1$	171.0(7)	174.7	–	–
C$_2$–Ru$_1$–P$_1$	179.0(2)	173.9	–	–
C$_2$–Ru$_1$–C$_1$	–	–	173.9(2)	174.6
Ru$_1$–C$_2$–C$_3$	177.5(7)	170.7	170.4(5)	170.6
Ru$_1$–P$_1$–C$_1$	173.8(4)	178.3	–	–
Ru$_1$–C$_1$–P$_1$	–	–	177.8(4)	177.0

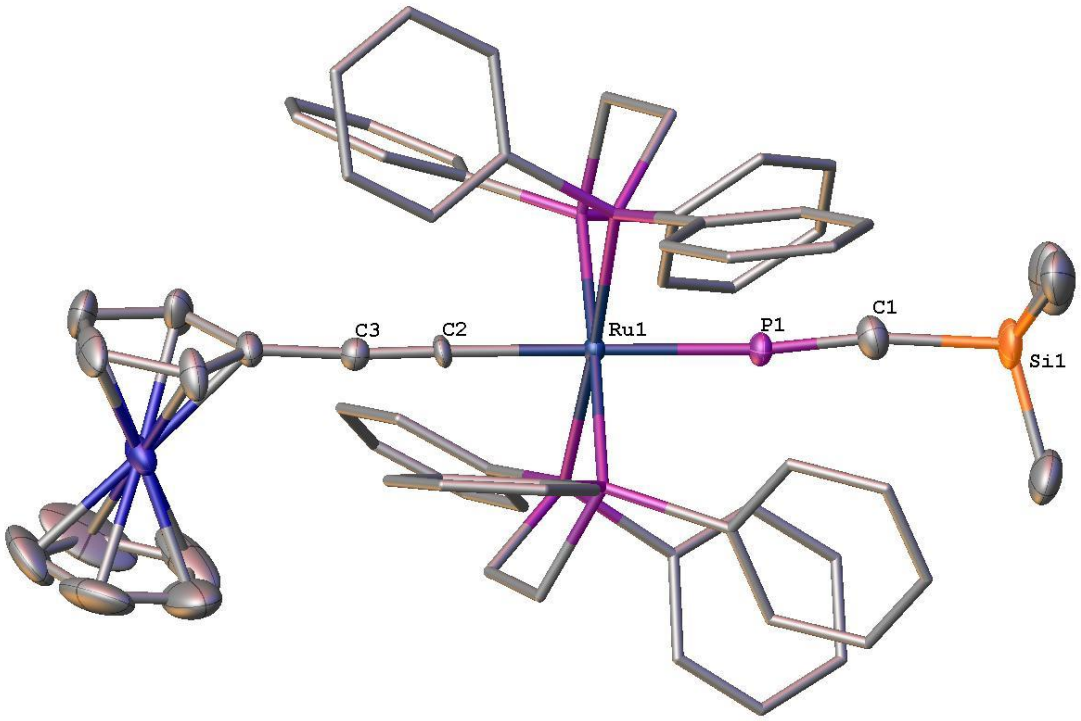

Figure 3.3: *Molecular structure of* ***3.2****; 50% thermal ellipsoids, hydrogen atoms and counter-ion omitted, and ancillary ligand set reduced for clarity.*

Comparison of the solid-state structure of **3.3** (Figure 3.4) with other known transition metal cyaphide complexes revealed a comparable C–P distance to those observed in *trans*-[Ru(C≡P)(C≡C-*p*-An)(dppe)$_2$] and Grützmacher's *trans*-[RuH(C≡P)(dppe)$_2$] (1.553(6) vs 1.544(4) and 1.573(2) Å respectively),[64,70] alongside statistically indistinguishable Ru–$C_{C\equiv P}$ distances (2.032(6) vs 2.065(4) and 2.057(2) Å respectively).[64,70] Furthermore, a diminished deviation from linearity around the metal centre (∠ C-Ru-C) was observed in **3.3**, alongside a lengthening of the acetylide C–C distance when compared to both **3.2** and the free ligand.[154]

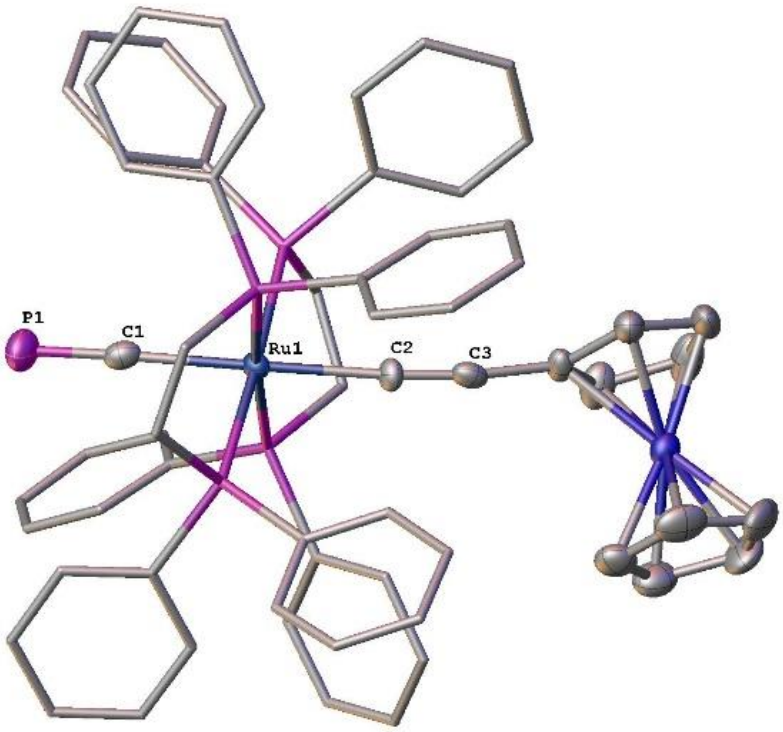

Figure 3.4: *Molecular structure of* ***3.3****; 50% thermal ellipsoids, hydrogen atoms omitted, and ancillary ligand set reduced for clarity.*

The frontier molecular orbitals of **3.3** (Figure 3.5) are similar to those seen in monometallic cyaphide, alkynyl, and bis(alkynyl) complexes,[70] with the HOMO comprising of classic out of phase mixing of the $\pi_{C\equiv C}$, $\pi_{C\equiv P}$, and ruthenium *d*-orbitals (21, 26, and 31% respectively), while only a slight contribution from the ferrocene moiety is observed (18%). The cyaphidic lone pair is appreciably stabilised, residing *ca.* 1.9 eV lower in energy in the HOMO-10. Additionally, NBO calculations suggest that it resides in an orbital of *ca*. 75% *s* and 25% *p* character, which is typical of both phosphaalkynes and monometallic cyaphide complexes. The LUMO is mostly dppe-based and lies 3.5 eV higher in energy than the HOMO. Contributions from the $\pi^*_{C\equiv P}$ orbitals are only observed from the LUMO+18 and higher, with the majority of the preceding molecular orbitals being almost exclusively dppe-based.

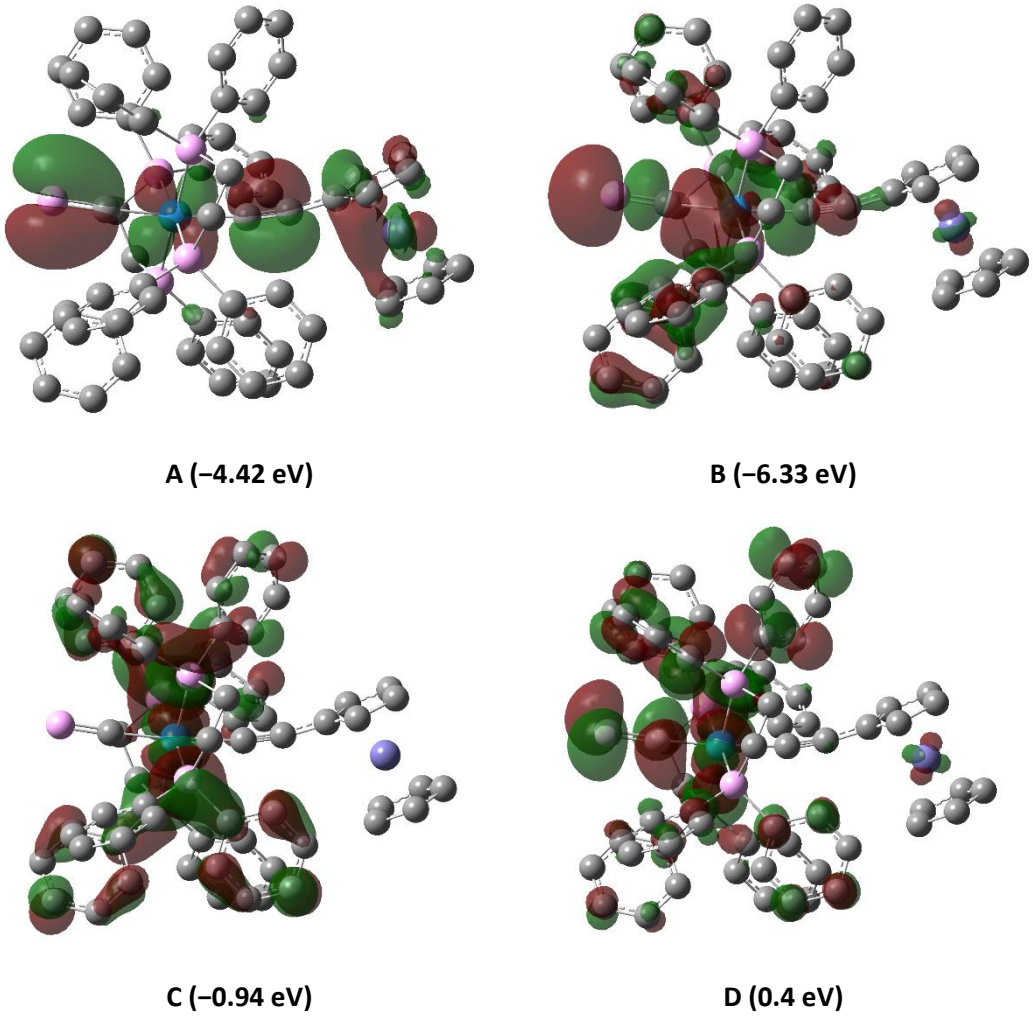

Figure 3.5: *Calculated frontier molecular orbitals of* ***3.3****. HOMO (A), HOMO−10 (B), LUMO (C), LUMO+18 (D)*

3.2.3 Electrochemical and UV-Vis Investigations

3.2.3.1 Cyclic Voltammetry

Akin to previous examples, **3.3** displayed an oxidative wave at −0.29 V, with the corresponding reductive event observed at a much more negative potential of −0.63 V, consistent with the Ru^{II}/Ru^{III} redox couple (Figure 3.6). Compared to the cyaphide complexes in Chapter 2, the peak to peak separation was much smaller for **3.3** (ΔE = 0.34 V), and the anodic process occurred at a more negative potential, a direct consequence of the strong electron-donating properties of the ethynylferrocene fragment. Similarly, a shift to more negative potential was observed when

compared to the parent chloride complex **3.1** (E_{pa} = 0.38 V), suggesting less electron withdrawing character of ligated cyaphide when compared to chloride.

Complex **3.3** also exhibited a secondary oxidation wave at 0.03 V, with the corresponding reductive wave observed at −0.05 V (ΔE = 80 mV), consistent with the Fe^{II}/Fe^{III} redox couple. However, a significant shift to a more positive potential was observed when compared to the parent chloride complex ($E_{½}$ = −0.34 V).[155,156] Unlike the redox processes observed for **3.1** or ferrocene,[155,156] this process appeared to be quasireversible, as evidenced by the I_{pa}:I_{pc} ratio (I_{pa}/I_{pc} = 1.21), and the strong dependence of the oxidative and reductive potentials on the experimental scan rate.

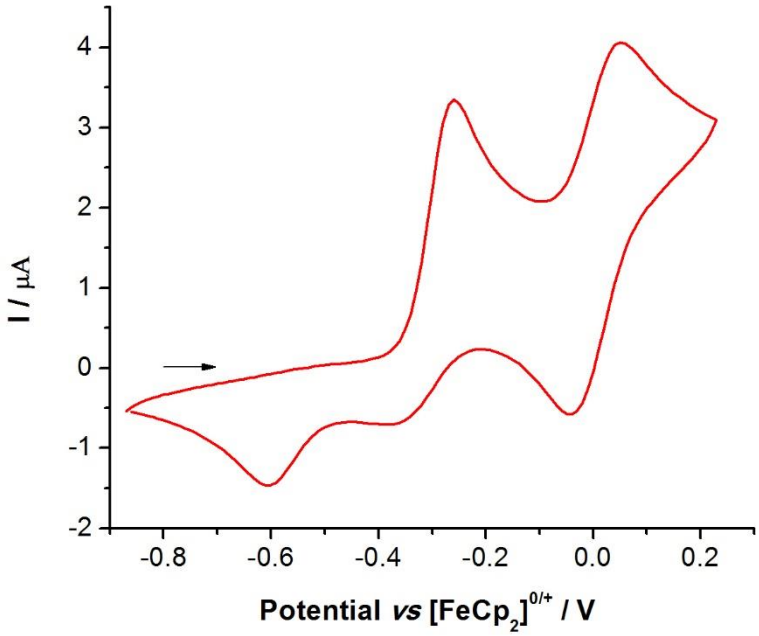

Figure 3.6: *Cyclic voltammogram of* ***3.3*** *as a solution in DCM (1 mM) with [$^{n}Bu_4N$][PF_6] supporting electrolyte (0.1 M), 0.1 V s^{-1} scan rate*

3.2.3.2 UV-Vis Spectroscopy

The UV-Vis spectrum of **3.3** (Figure 3.7) shows three distinct features at 248, 285, and 340 nm, which were assigned with the assistance of excited state TD-DFT calculations (B3LYP/3-21G* for C, H, P; LANL2DZ for Fe, Ru).

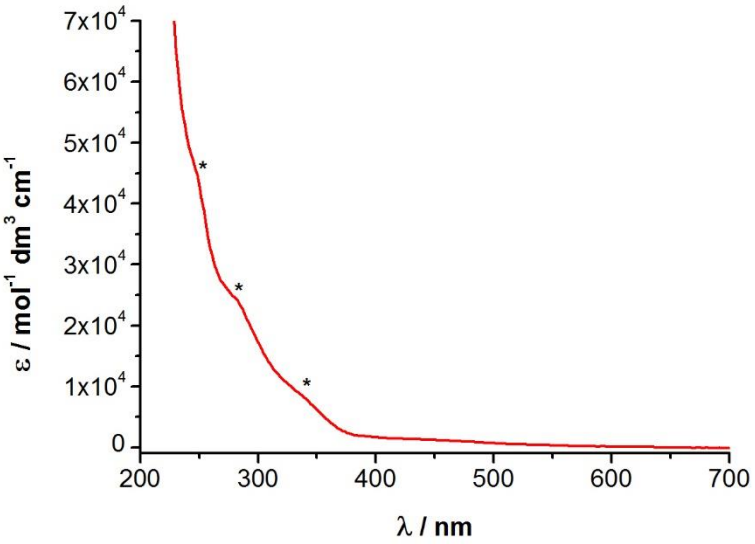

Figure 3.7: *Experimental UV-Vis spectrum of **3.3**. 1.35 × 10^{-5} mol dm^{-3} in DCM, 1 cm path length. Weak features have been marked with an asterix (*)*

Like previously described monometallic chloride and cyaphide complexes (See Chapter 2 and references therein), the high energy features (λ = 248, 285 nm) in the UV-Vis spectrum of **3.3** are consistent with ligand to ligand charge transfer (LLCT) from the C≡C and C≡P π-systems to the dppe antibonding orbitals. Further, some intraligand charge transfer (ILCT) between the $\pi_{C\equiv P}$ and $\pi^*_{C\equiv P}$ orbitals is apparent in the calculated UV-Vis spectrum, however, the contributions from this (11%) are considerably smaller.

The later feature at 340 nm exhibits similar LLCT from the C≡C and C≡P π-systems to the ancillary ligand set, however, it is primarily dominated by metal to ligand charge transfer (MLCT) from both the ruthenium and iron centres (HOMO = −4.42 eV, and HOMO−2 = −5.01 eV) to the dppe antibonding orbitals (LUMO = −0.94 eV and LUMO+5 = −0.35 eV). Despite this, some ILCT between the $\pi_{C\equiv P}$ (HOMO−6 = −5.98 eV) and $\pi^*_{C\equiv P}$ (LUMO+18 = 0.4 eV) orbitals is observed, with greater contributions than those in the higher energy features.

3.3 1,3-butadiyne Bridged Systems

3.3.1 Attempted Synthesis of [{Ru(dppe)$_2$}$_2${μ-(C≡C-C≡C)}Cl$_2$]

Due to the inherent instability of 1,3-butadiyne, the protected derivative 1,4-bis(trimethylsilyl)butadiyne was employed, using a one-pot procedure similar to that reported by Lapinte and co-workers for the synthesis of symmetric iron(II) and ruthenium(II) polyacetylide complexes.[157] The attempted synthesis of [{Ru(dppe)$_2$}$_2${μ-(C≡C-C≡C)}Cl$_2$] (**3.4**) was undertaken in methanol under reflux conditions, with desilylation of the protected alkyne effected using potassium fluoride to generate 1,3-butadiyne *in-situ*. It was anticipated that upon formation of the corresponding vinylidene complex, deprotonation with a suitable base would afford the desired bimetallic complex (Scheme 3.2).

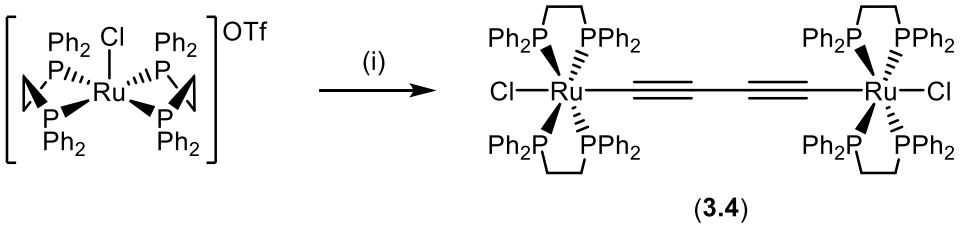

(**3.4**)

Scheme 3.2: *Attempted synthesis of* ***3.4****. Reagents and conditions: (i) 0.5 eq. Me$_3$Si-C≡C-C≡C-SiMe$_3$, 1 eq. KF, 1 eq. DIPA, methanol, reflux, 16 h*

The reaction in Scheme 3.2 afforded a single product, with the $^{31}P\{^1H\}$ NMR spectrum displaying a doublet resonance at 62.6 ppm (J = 18 Hz). In the ^1H NMR spectrum, a quintet at −19.14 ppm was observed which exhibited H-P coupling (J_{HP} = 18 Hz), which is consistent with the formation of *trans*-[RuHCl(dppe)$_2$]. It has been shown by the author that the reaction of [RuCl(dppe)$_2$]OTf with DIPA in protic solvents gives clean conversion to *trans*-[RuHCl(dppe)$_2$] (See Chapter 2), thus the reaction was re-attempted using Hünig's base (N^{i}Pr$_2$Et, DIPEA) as an alternative to DIPA, though the same product was afforded. Further attempts were undertaken in an aprotic solvent (THF) using DIPEA, alongside substitution of potassium fluoride for tetrabutylammonium

fluoride due to the solubility limitations of the former in THF, however, *trans*-[RuHCl(dppe)$_2$] was formed as the sole product in all cases.

An alternative synthetic method was devised, based on a similar procedure reported by Lapinte and Bruce for the synthesis of systems of the type [{M(dppe)}$_2${μ-(C≡C-C≡C)}] by chemical oxidation of a terminal acetylide complex with ferrocenium hexafluorophosphate.[158,159] NMR scale reactions using *trans*-[RuCl(dppe)$_2$(C≡CH)] and oxidising reagent that had been synthesised by the author (Scheme 3.3) led to the formation of a mixture of products in the $^{31}P\{^1H\}$ NMR spectrum, with the primary product displaying a singlet resonance at 41.0 ppm. This was observed to couple to a broad resonance at 2.47 ppm in the ^1H NMR spectrum, as shown in ^1H-^{31}P HMBC experiments, which integrated in a 1:4 ratio against the protons of the dppe backbone. These data were consistent with the formation of the parent vinylidene complex trans-[RuCl(=C=CH$_2$)(dppe)$_2$]PF$_6$ (**3.5**), believed to have formed through reaction with trace amounts of residual H_2SO_4 present in the ferrocenium hexafluorophosphate. Repeated attempts with acid-free oxidising agent (Scheme 3.3) resulted in a single product in the $^{31}P\{^1H\}$ NMR spectrum, with an associated chemical shift of 48.8 ppm, alongside a counterion resonance at −144.5 ppm. In the ^1H NMR spectrum, a broad singlet at 1.34 ppm was observed, consistent with an acetylenic proton. However, these data were consistent with the formation of the oxidised monometallic complex *trans*-[RuCl(dppe)$_2$(C≡CH)]PF$_6$ (**3.6**), as opposed to the desired complex **3.4**.

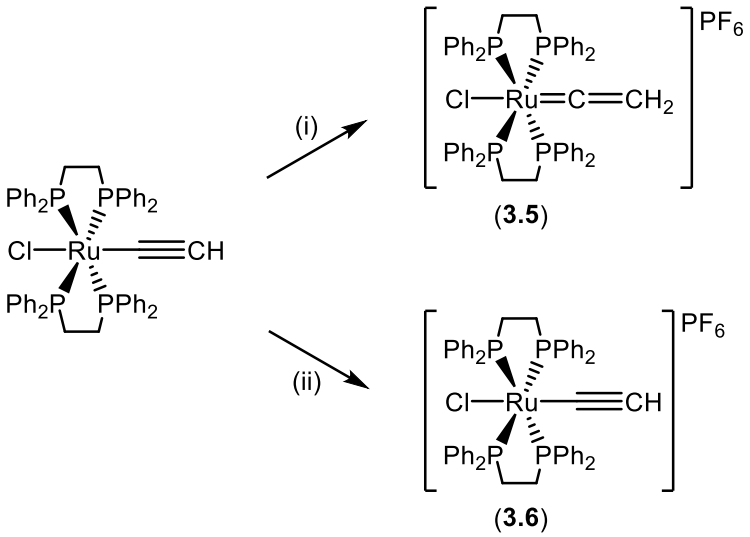

Scheme 3.3: *Formed products from chemical oxidation of trans-[RuCl(dppe)$_2$(C≡CH)]. Reagents and conditions: (i) 0.5 eq. FcPF$_6$, trace H_2SO_4, CD_2Cl_2; (ii) 0.5 eq. FcPF$_6$,DCM-d_2*

The difficulties encountered synthesising **3.4** were believed to arise from steric interactions and were investigated using DFT, through analysis of the similar monometallic complex *trans*-[RuH(dppe)$_2$(C≡C−C≡CH)] (**3.7**) at the B3LYP/6-31G**/LANL2DZ level of theory. Upon observation of the space-filled optimised structure (Figure 3.8) it was apparent that the ancillary ligand set was too large to accommodate a 1,4-butadiyne bridge between two metal centres, as the majority of the di-yne was shielded by the ligand framework.

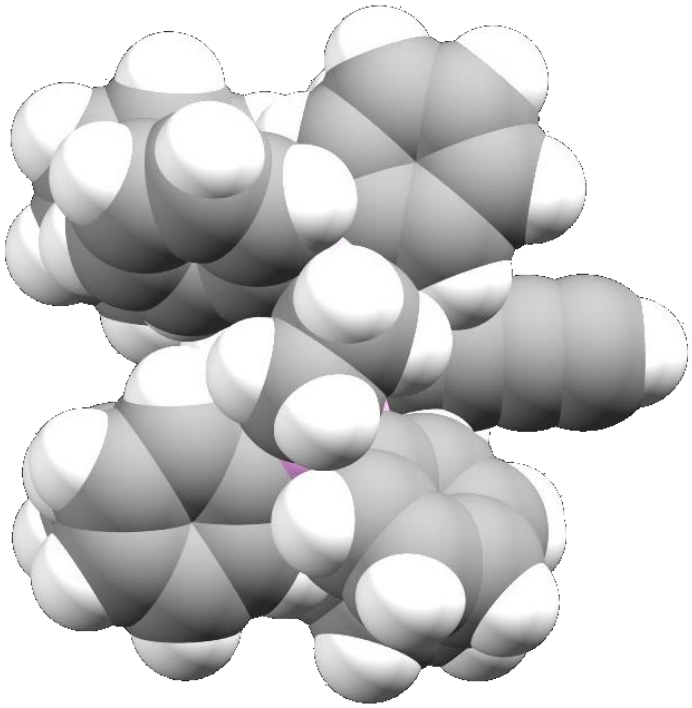

Figure 3.8: *Space filled optimised structure of* ***3.7****, 100% van der waal radii*

3.4 1,4-diethynylbenzene Bridged Systems

*3.4.1 Synthesis of [{Ru(dppe)$_2$}$_2${μ-(C≡C)$_2$C$_6$H$_4$-*p*}(η^1-P≡CSiMe$_3$)$_2$].2OTf*

As the synthesis of **3.4** was not feasible, the synthesis of bimetallic complexes featuring longer bridging units was undertaken, due to the ease with which the precursors could be synthesised and handled, alongside the precedent for electrochemical investigation of such species. To a mixture of [{Ru(dppe)$_2$}$_2${μ-(C≡C)$_2$C$_6$H$_4$-*p*}Cl$_2$] (**3.8**) and two equivalents of AgOTf, DCM was added, and the mixture stirred under ambient conditions for 10 minutes, followed by addition of two equivalents of P≡CSiMe$_3$ in toluene and further stirring for 2 h. After workup, the compound [{Ru(dppe)$_2$}$_2${μ-(C≡C)$_2$C$_6$H$_4$-*p*}(η^1-P≡CSiMe$_3$)$_2$].2OTf (**3.9**; Scheme 3.4) was afforded as a yellow solid in moderate yield (*ca.* 50%).

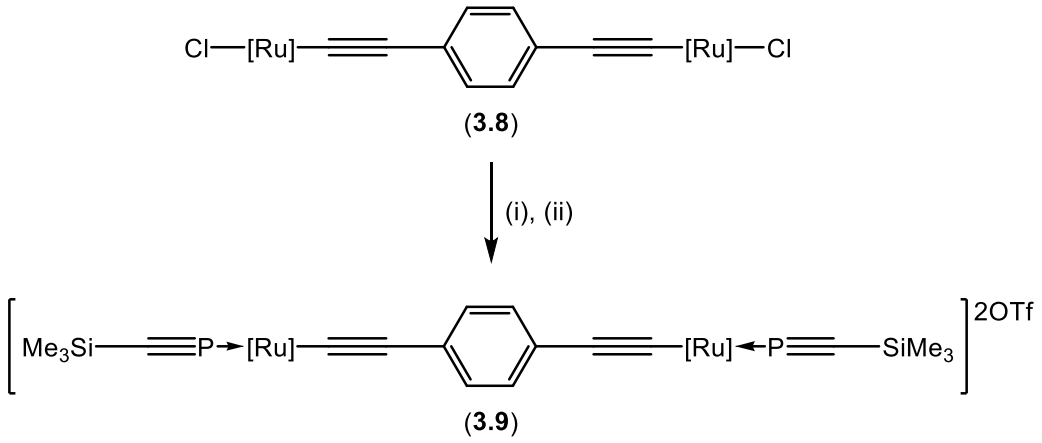

Scheme 3.4: *Synthesis of* ***3.9****. Reagents and conditions: (i) 2 eq. AgOTf, DCM, 10 minutes. [Ru] = Ru(dppe)₂*

In the $^{31}P\{^{1}H\}$ NMR spectrum, **3.9** displayed the expected AX_4 pattern consistent with η^1-coordination of the phosphaalkyne (δ_P: 114.4, $^2J_{PP}$ = 33 Hz) in proximity to the dppe scaffold (δ_P: 42.2, $^2J_{PP}$ = 33 Hz).[70] Retention of the $SiMe_3$ group of the phosphaalkyne was supported by the presence of a single $SiMe_3$ resonance in both the ^1H and ^1H-^{29}Si HMBC spectra (δ_H: −0.08, δ_{Si}: −12.9). Furthermore, the observation of the triflate counterion in the ^{19}F NMR spectrum (δ_F: −78.9), and IR spectroscopic data were consistent with previously described phosphaalkyne complexes ($\nu_{C\equiv P}$: 1262 cm^{-1}).[70] Retention of the 1,4-diethynylbenzene bridge was supported by ^1H NMR and IR spectroscopic data (δ_H: 6.73, $\nu_{C\equiv C}$: 2054 cm^{-1}), with further confirmation arising from ^1H-^{13}C HSQC and HMBC experimental data.

3.4.2 Molecular Structure Analysis

The connectivity of **3.9** was further supported by X-ray diffraction data, with crystals obtained from a saturated DCM solution layered with *n*-hexane at −20 °C, with no crystalline symmetry observed. The geometry around the ruthenium centres (∠ $P_{C\equiv P}$-Ru-C) exhibited minor deviation from linearity, while the overall deviation of the 1,4-diethynylbenzene unit was much more pronounced (Figure 3.9). These data are consistent with both known monometallic ruthenium

acetylide complexes and bimetallic complexes featuring similar bridging units such as Field's *trans,trans*-[(^{t}BuC≡C)Ru(dmpe)$_2$(μ-C≡CC$_6$H$_4$C≡C)Ru(dmpe)$_2$(C≡C^{t}Bu)].[71,160] The phosphaalkyne fragments exhibited C-P distances of 1.526(5) Å, which is consistent with those observed in the systems reported for Grützmacher's *trans*-[RuH(P≡CSiPh$_3$)(dppe)$_2$]BF$_4$ and Crossley's *trans*-[Ru(η^1-P≡CSiMe$_3$)(C≡CCO$_2$Me)(dppe)$_2$]OTf, alongside other similar systems (Table 3.2).[64,70] It should be noted that the two triflate counter ions were disorderd and could not be modelled. The associated electron density was therefore treated with SQUEEZE, however, their presence was supported by ^{19}F NMR spectroscopic data (δ_F: −78.9).

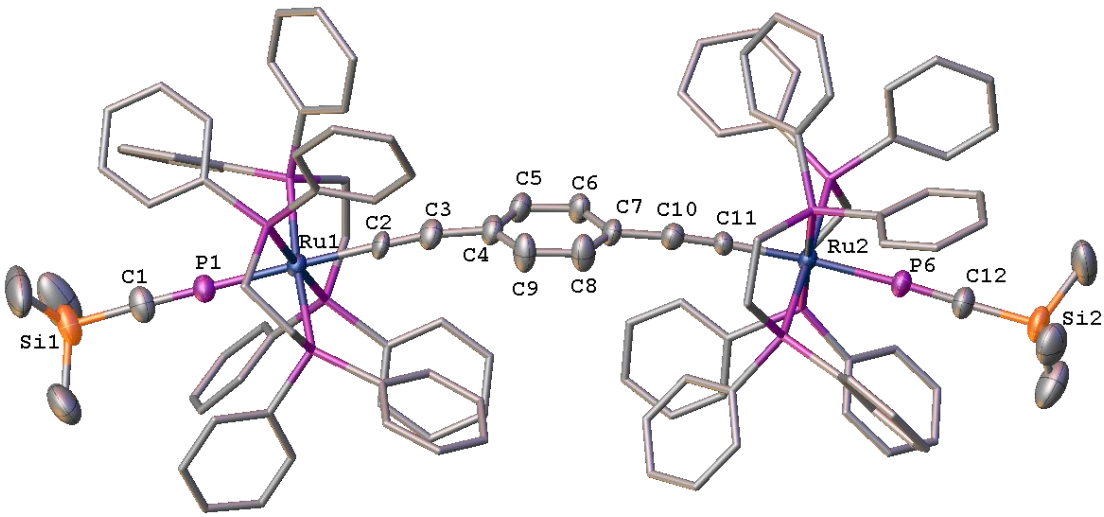

Figure 3.9: *Molecular structure of* ***3.9****; 50% thermal ellipsoids, hydrogen atoms and disorder omitted, and ancillary ligand set reduced for clarity.*

Table 3.2: *Selected bond lengths (Å) and angles (°) for* ***3.8****, comparable complexes, and complexes of the type trans-[RuR(η¹-P≡CSiMe₃)(dppe)₂]⁺*

	3.9	**R = C≡CFc (3.2)**	**Field**[160†]	**R = C≡CCO$_2$Me**[70]	**R = H**[64]	**Jones**[134‡]
M-P	2.264(1)	2.246(2)	–	2.274(3)	2.2486(8)	2.315(1)
C-P	1.526(5)	1.522(9)	–	1.53(1)	1.530(3)	1.535(6)
C-C	1.214(6)	1.182(12)	1.20(1)	1.15(1)	–	–
M-P-C	179.3(2)	173.8(4)	–	175.7(4)	174.9(1)	153.7(2)
R-M-R'	175.3(1)	179.0(2)	177.9(3)	177.0(3)	–	–

The optimised gas phase geometry of **3.9** (B3LYP/6-31G** for H, C, P, Si; LANL2DZ for Ru; Figure 3.10) exhibited a slightly greater degree of linearity (∠ $P_{C\equiv P}$-Ru-C) when compared to the solid state, alongside slightly elongated C-P linkages (1.58 Å vs 1.53 Å), consistent with the presence of crystal packing forces in the solid state, for which there is precedent in η^1-coordinated phosphaalkyne complexes.[33,65,69,70,161] The HOMO of **3.9** was composed primarily of the bridging π-system (76%), with some contribution from the two metal centres (14%). Most notably, the contributions from the two phosphaalkyne moieties were negligible in the HOMO (4%) but were much more pronounced in the more stabilised HOMO−3 and HOMO−4 (14 and 20% respectively; Figure 3.10).

† T*rans,trans*-[(^{t}BuC≡C)Ru(dmpe)$_2$(μ-C≡CC$_6$H$_4$C≡C)Ru(dmpe)$_2$(C≡C^{t}Bu)][160]

‡ *Trans*-[RuH(η^1-P≡CMe)(dppe)$_2$]OTf[134]

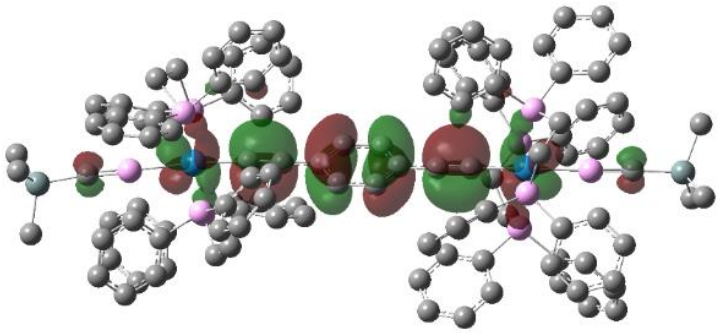

A (−8.09 eV)

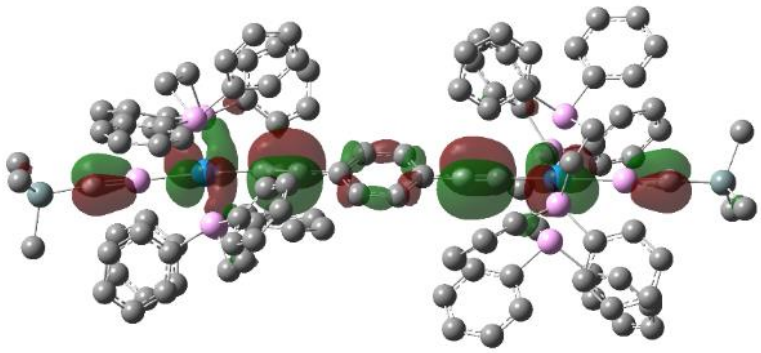

B (−8.84 eV)

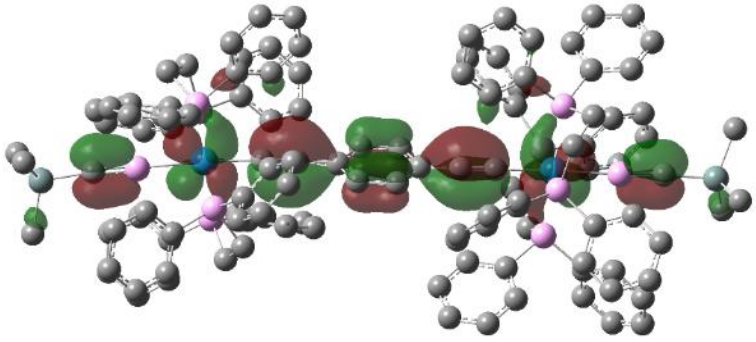

C (−9.06 eV)

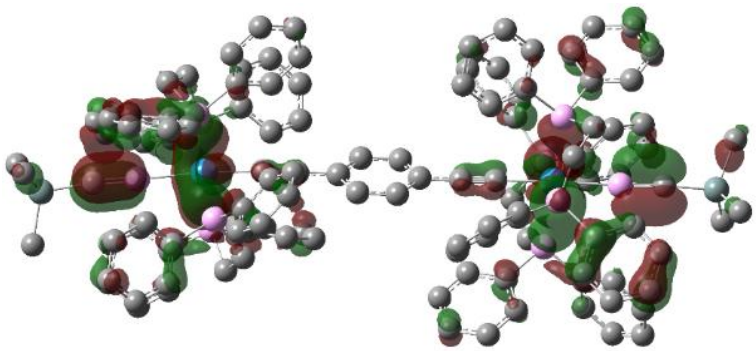

D (−9.47 eV)

Figure 3.10: *Calculated frontier molecular orbitals of* ***3.9****. HOMO (A), HOMO−1 (B), HOMO−3 (C), HOMO−4 (D)*

3.4.3 Electrochemical and UV-Vis Investigations

3.4.3.1 Cyclic Voltammetry

The electronic structure of **3.9** was further probed using cyclic voltammetry, displaying two distinct oxidative processes which are consistent with sequential oxidation of the two metal centres (*i.e.* $Ru^{II}/Ru^{II} \rightarrow Ru^{II}/Ru^{III} \rightarrow Ru^{III}/Ru^{III}$) (Figure 3.11). Compound **3.9** underwent an initial quasi-reversible oxidation at 0.71 V, which is significantly higher than the initial oxidation in the parent chloride complex (*ca.* −0.27 V), though this is likely due to the cationic nature of **3.9**. The second oxidative process at 1.00 V was irreversible, with a separation between the two processes (ΔE_{pa}) of 0.29 V. Comparison of the comproportionation constants[§] for **3.8** and **3.9** (K_c = 8.9×10^5 and 0.8×10^5 respectively) indicated comparable stability of the transient mixed-valence species **[3.9]**$^+$.

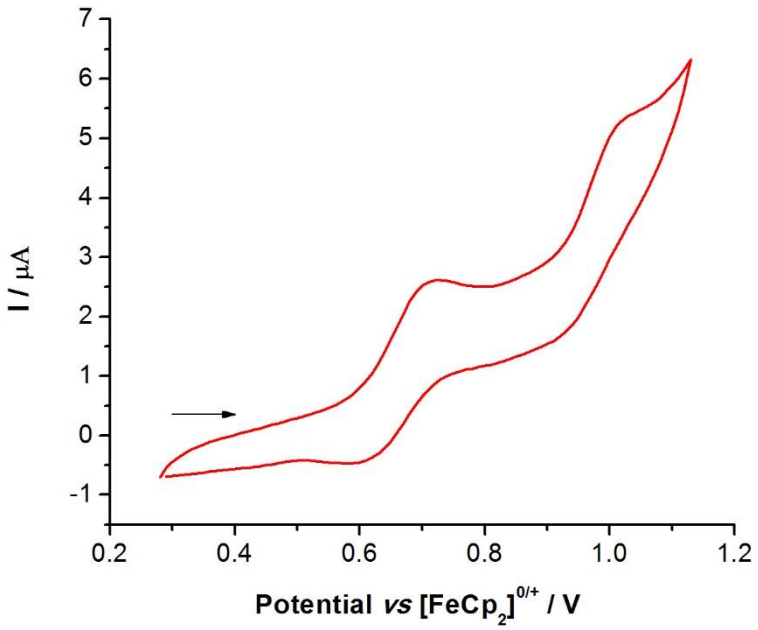

Figure 3.11: *Cyclic voltammogram of **3.9** as a solution in DCM (1 mM) with [^{n}Bu$_4$N][PF$_6$] supporting electrolyte (0.1 M), 0.1 V s^{-1} scan rate*

[§] $K_c = 10^{\Delta E/59\ mV}$ at 298 K[192]

3.4.3.2 UV-Vis Spectroscopy

The electronic spectrum of **3.9** (Figure 3.12) showed three features at 230, 250, and 360 nm, which were assigned with the assistance of TD-DFT calculations for the first 200 excited states (B3LYP/3-21G* for H, C, P, Si; LANL2DZ for Ru).

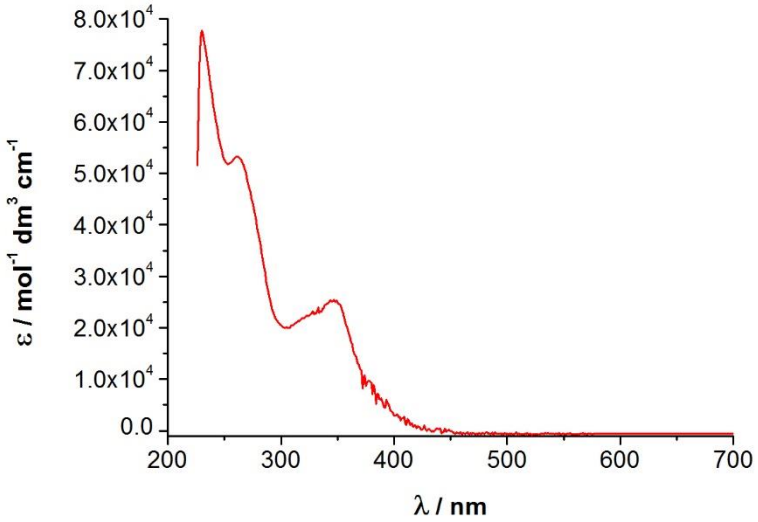

Figure 3.12: *Experimental UV-Vis spectrum of **3.9**, 2.0 × $\mathbf{10^{-5}}$ mol dm^{-3} in DCM, 1 cm path length*

The feature at 350 nm is primarily composed of MLCT and LLCT consistent with excitation from the HOMO to the low-lying dppe based orbitals, however, significant contributions from LLCT consistent with $\pi_{C\equiv C} \rightarrow \pi^*_{Ar}$ and $\pi_{C\equiv C} \rightarrow \pi^*_{C\equiv P}$ transitions are also present, alongside some intraligand charge transfer from the C≡C π-system to the corresponding antibonding orbital. The higher energy feature at 260 nm is primarily composed of ILCT within the ancillary ligand set, however, there are appreciable contributions from $\pi_{C\equiv P} \rightarrow \pi^*_{C\equiv P}$ and $\pi_{Ar} \rightarrow \pi^*_{C\equiv P}$ transitions.

3.4.4 Synthesis of [{Ru(dppe)$_2$}$_2${μ-(C≡C)$_2$C$_6$H$_4$-p}(C≡P)$_2$]

Treatment of **3.9** with 2 eq. of KO^{t}Bu resulted in rapid desilylation and rearrangement to the corresponding cyaphide complex **3.10** (Scheme 3.5). This was supported by characteristic

changes in the spectroscopic data, particularly in the $^{31}P\{^{1}H\}$ NMR spectrum, where a shift to higher frequency of both the C≡P and dppe resonances was observed (δ_P: 159.7 and 50.7 respectively) alongside diminished coupling consistent with a change from a $^{2}J_{PP}$ to $^{3}J_{PP}$ interaction. It should be noted that no coupling was observed in the $^{31}P\{^{1}H\}$ NMR spectrum between the two resonances which, while inconsistent with described monometallic cyaphide alkynyl complexes, remains consistent with observations reported by Grützmacher for *trans*-[RuH(C≡P)(dppe)$_2$].[64,67] This is likely due to the small magnitude of the coupling, and slight broadening of the signal ($\nu_{½}$ = 12 Hz).

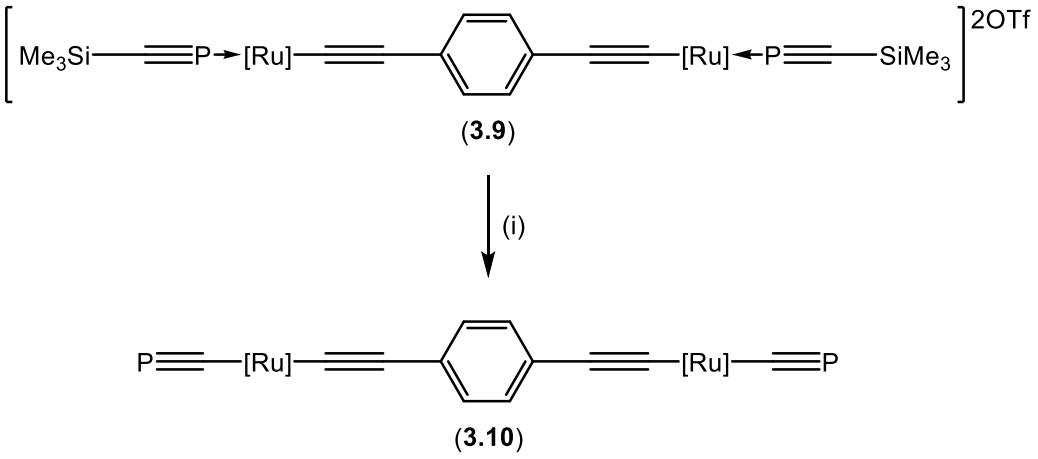

Scheme 3.5: *Synthesis of* ***3.10****. Reagents and conditions: (i) 2 eq. KO^{t}Bu, THF, 1 h. [Ru] = Ru(dppe)$_2$*

Loss of both the OTf and $SiMe_3$ resonances in their respective NMR spectra supported desilylation and conversion to a neutral complex, combined with an increased frequency of the cyaphidic resonance in the $^{13}C\{^{1}H\}$ spectrum (281.8 *vs* 189.8 ppm) and reduction in the C≡P stretching frequency (1247 vs 1262 cm^{-1}), which are consistent with the formation of an organometallic linkage (*cf.* M-C≡O, M-C≡N). These data are consistent with previous reports of cyaphide formation,[70] facilitating identification in the absence of crystallographic data, as crystals of **3.10** tended to undergo rapid desolvation and decomposition at both room and low temperature, which hindered solid-state studies.

Interestingly, addition of only 1 eq. of KO^{t}Bu to a sample of **3.9** resulted in the formation of a species with $^{31}P\{^1H\}$ NMR resonances consistent with both **3.9** and **3.10** (Figure 3.13). This was tentatively assigned as the asymmetric phosphaalkyne-cyaphide complex, **3.11**.

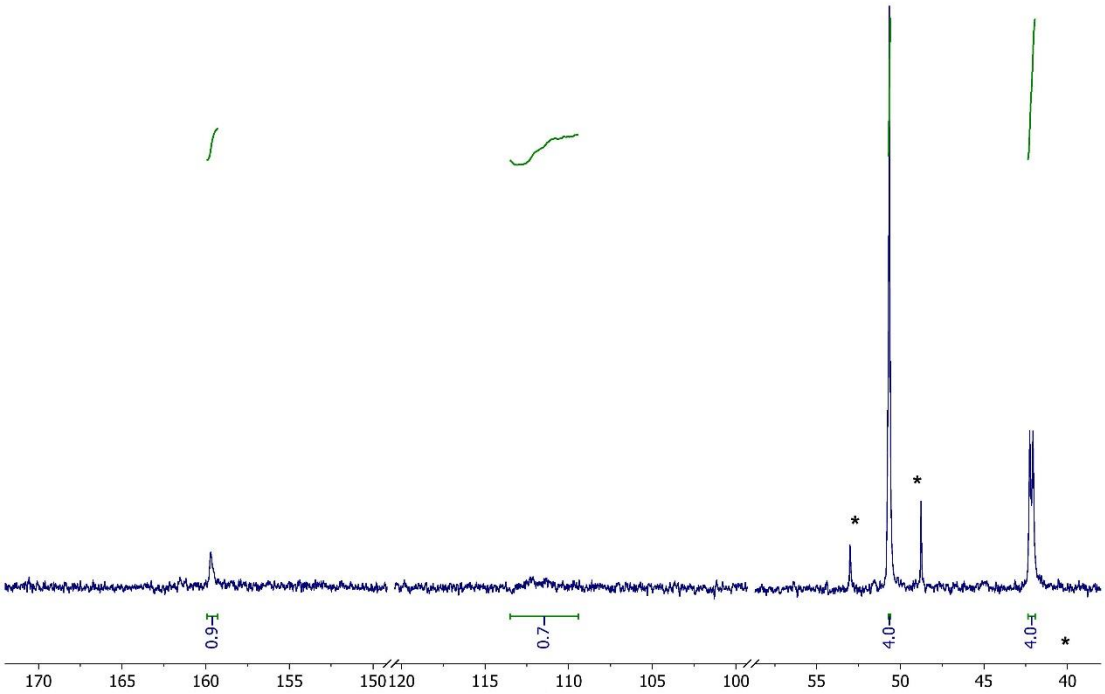

Figure 3.13: *$^{31}P\{^1H\}$ NMR spectrum of **3.11** (4.0 Hz line broadening). Resonances marked with an asterix (*) are unrelated, unidentified species*

However, in the absence of further conclusive spectroscopic data, the identity of **3.11** was investigated using NMR calculations (GIAO method, PBEPBE/6-31G** for C, H, P, Si; LANL2DZ for Ru), allowing comparison of the $^{31}P\{^1H\}$ NMR shifts of **3.9**, **3.10**, and **3.11** (Table 3.3). From the differences between the calculated shifts of the three complexes, it was possible to conclude that **3.11** was not the desired asymmetric system, but instead a statistical mixture of **3.9** and **3.10**, however, separation of these two complexes was not achieved.

Table 3.3: *Experimental and calculated $^{31}P\{^{1}H\}$ NMR shift values*

	δ_P (C≡P) experimental	δ_P (C≡P) calculated
3.9	111.4	118.4
3.10	159.7	166.4
3.11	111.5	122.5
	159.7	160.4

3.4.5 Electronic Structure, Electrochemical, and UV-Vis Investigations

3.4.5.1 Electronic Structure

While the reaction furnishing **3.10** has not yet yielded crystals stable enough for X-ray diffraction studies, DFT modelling has been utilised to provide insight into its structural properties. As expected, the calculated gas-phase structure of **3.10** exhibited greater linearity around the ruthenium atoms compared to the solid-state structure of **3.9** (177.2 ° *vs* 175.23(13) °), though this is most likely due to the absence of crystal packing forces and intermolecular interactions. Complex **3.10** also exhibited slightly longer C≡P distances of 1.587 Å when compared to previously described cyaphide complexes (Table 3.4),[64,67] alongside elongated C≡C distances when compared to the parent phosphaalkyne complex. However, it should be noted that elongated distances are typically observed in the calculated gas phase structures when compared to experimental solid-state data.[70]

Table 3.4: *Selected bond lengths (Å) and angles (°) for* ***3.10$_{calc}$, 3.9,*** *and the complexes trans-[RuR(C≡P)(dppe)$_2$]*

	3.10$_{Calc}$	**3.9**	**R = H**[64]	**R = C≡CCO$_2$Me**[70]
C-P	1.587	1.526(5)	1.573(2)	1.544(4)
C-C	1.235	1.214(6)	–	1.205(5)
Ru-C	2.044	–	2.057(2)	2.065(4)
Ru-C-P	178.168	–	177.9(1)	172.3(2)
C-Ru-R	177.195	175.23(13)	–	171.9(1)

The HOMO of **3.10** showed evidence of contributions from the π-system of the C≡P units (14%), which undergo classic out-of-phase mixing with the ruthenium *d*-orbitals (d_{xy} and d_{xz}) and 1,4-diethynylbenzene π-orbitals, consistent with through-conjugation. The contribution from the C≡P units increased in the lower energy states (specifically the HOMO−1 and HOMO−2), though the contribution from the bridging unit was negligible.

The cyaphidic lone pairs reside in the highly stabilised HOMO−14 and HOMO−15, with NBO calculations suggesting they reside in orbitals of 75% *s* and 25% *p* character, which is consistent with observations reported for monometallic cyaphide complexes,[70] and is typical for phosphaalkynes.[4]

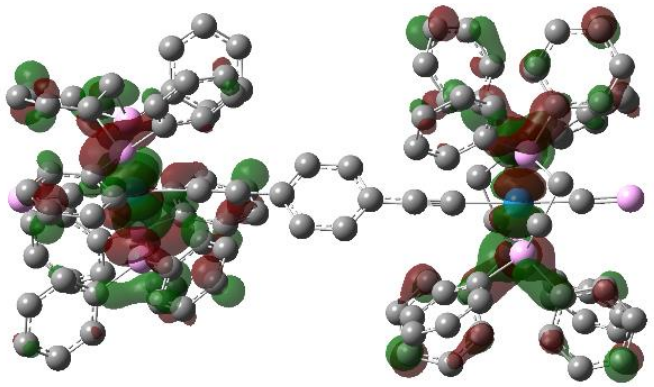

A (–0.93 eV)

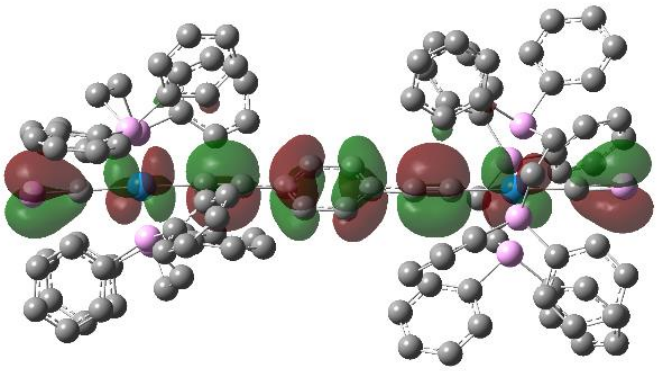

B (–4.17 eV)

Figure 3.14: *Calculated frontier molecular orbitals of* ***3.10****. LUMO (A) and HOMO (B)*

3.4.6 Cyclic Voltammetry

Complex **3.10** exhibited two irreversible oxidation waves at −0.21 and −0.02 V, with only the former exhibiting a well-defined corresponding reductive event at −0.78 V (Figure 3.15). A heavily diminished separation between the two oxidative events was indicative of reduced stability of the transient mono-oxidised species [**3.10**]$^{+}$, and this was reflected in the calculated comproportionation constant ($K_c = 1.7 \times 10^3$), which is a factor of 100 lower than that of **3.9** and **3.8**. However, the observed behaviour was still consistent with two, one-electron oxidations, as opposed to one, two-electron oxidation, implying that the electronic coupling behaviour of the [Ru_2{μ-(C≡C)C_6H_4-*p*}] scaffold is retained.

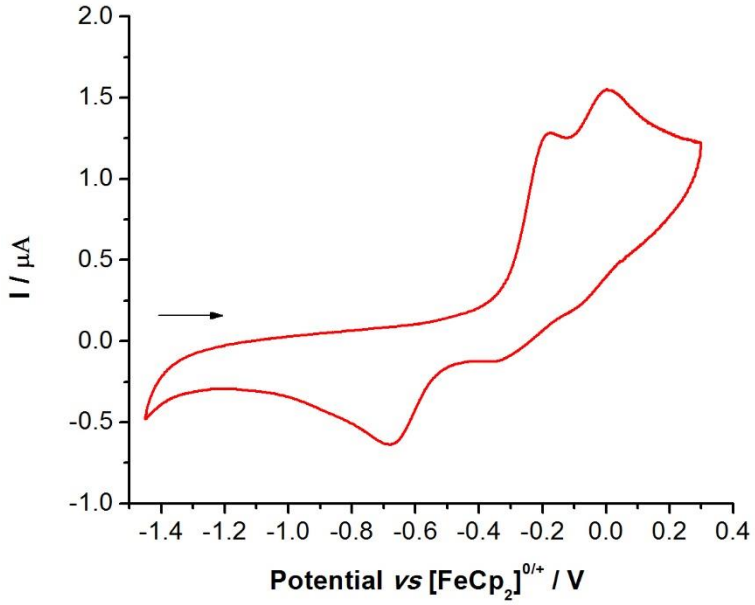

Figure 3.15: *Cyclic voltammogram of* ***3.10*** *as a solution in DCM (1 mM) with [^{n}Bu$_4$N][PF$_6$] supporting electrolyte (0.1 M), 0.1 V s^{-1} scan rate*

3.4.6.1 UV-Vis Spectroscopy

The electronic spectrum of **3.10** (Figure 3.16) exhibits three high-energy features at 230, 250, and 370 nm which are consistent with MLCT and LLCT to the ancillary ligand set, the assignments of which are supported by TD-DFT calculations. Contributions from ILCT within the bridging 1,4-

diethynylbenzene unit were also apparent, though are much smaller contributions in comparison. It is notable that the π* orbitals of the C≡P fragments are in fact of high energy, residing between the LUMO+36 and LUMO+39, with any contributions from them being negligible within the range of states calculated, in direct contrast to **3.9**.

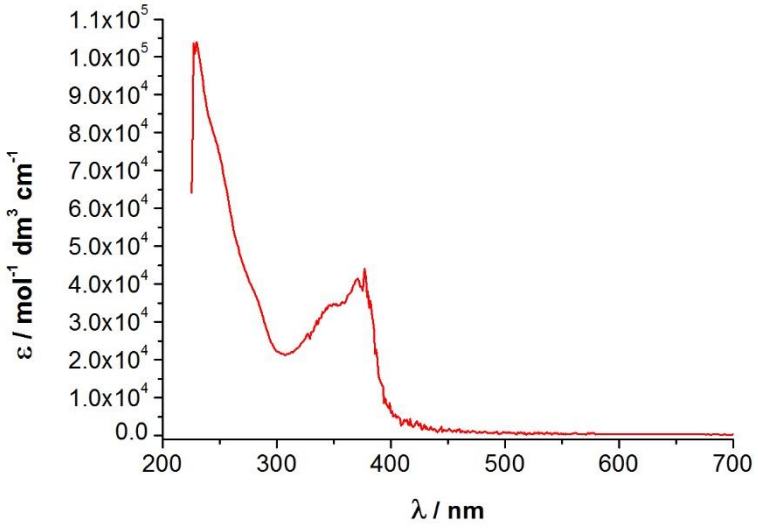

Figure 3.16: *Experimental UV-Vis spectrum of* ***3.10****, 1.0 ×* $\mathbf{10^{-5}}$ *mol dm^{-3} in DCM, 1 cm path length*

3.5 1,4-diethynyltetrafluorobenzene Bridged Systems

3.5.1 Synthesis and characterisation of [{Ru(dppe)$_2$}$_2${μ-(C≡C)$_2$C$_6$F$_4$-p}Cl$_2$]

Attempts to fine-tune the electrochemical response were undertaken through modification of the bridging arene, with initial studies utilising a perfluorinated bridging unit, which exploited the π-donor and σ-acceptor properties of fluorine. The synthesis of [{Ru(dppe)$_2$}$_2${μ−(C≡C)$_2$C$_6$F$_4$−*p*}Cl$_2$] (**3.12**) was achieved in an analogous fashion to **3.8**, from [RuCl(dppe)$_2$]OTf and 1,4-diethynyltetrafluorobenzene *via* the corresponding vinylidene complex, with bulk purity confirmed by elemental analysis. The spectroscopic data of **3.12** were largely unremarkable, displaying singlet resonances in the ^{31}P{^{1}H} and ^{19}F NMR spectra at 48.6 and −146.4 ppm respectively. Retention of the unsaturated bridging unit was supported by the

presence of an acetylenic stretching mode in the IR spectrum at 2025 cm^{-1}, alongside characteristic $^{13}C\{^1H\}$ NMR resonances for the centres directly bound to fluorine of the perfluorinated aromatic ring and the α-carbon of the C≡C units.

Complex **3.12** also exhibited similar electrochemical behaviour to that of **3.8**, with two reversible oxidation waves at −0.09 and 0.29 V (Figure 3.17). Further, a significant anodic shift of the two events was observed when compared to the non-fluorinated analogue, signifying a decrease in the electron density at the metal centres, alongside an increase in the comproportionation constant from 8.9×10^5 to 2.8×10^6, suggesting an increased stability of the mono-oxidised species, presumably due to a decrease in the insulating nature of the bridging unit.

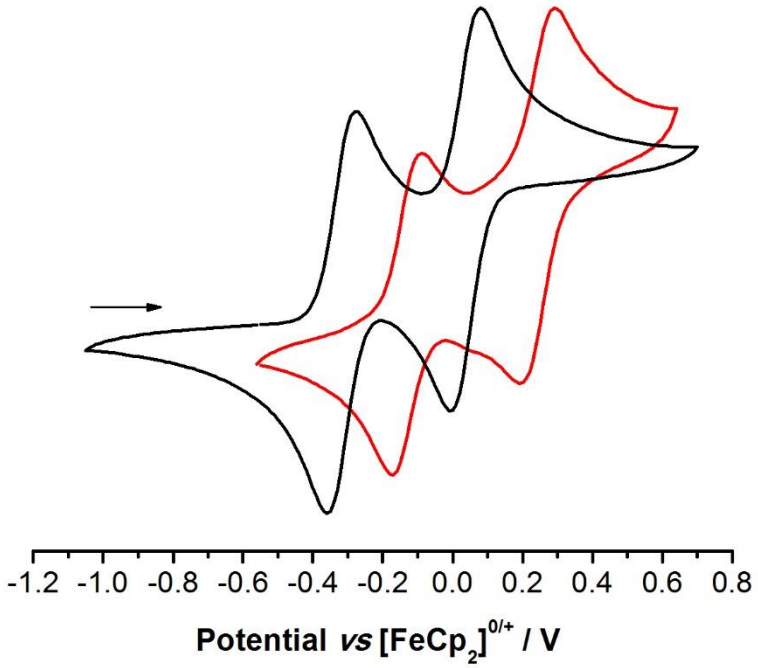

Figure 3.17: *Normalised voltammograms of **3.8** (black) and **3.12** (red) as a solution in DCM (1 mM) with [^{n}Bu$_4$N][PF$_6$] supporting electrolyte (0.1 M), 0.1 V s^{-1} scan rate*

*3.5.2 Synthesis of [{Ru(dppe)$_2$}$_2${μ-(C≡C)$_2$C$_6$F$_4$-*p*}(C≡P)$_2$]*

The synthesis of [{Ru(dppe)$_2$}$_2${μ-(C≡C)$_2$C$_6$F$_4$-*p*}(C≡P)$_2$] (**3.14**) occurred in a similar fashion to the synthesis of **3.9** and **3.10** (Scheme 3.6), though the exchange of AgOTf for TlOTf reduced the risk

of unintentional chemical oxidation of the metal centres. The formation of **3.13** was supported by NMR spectroscopic data with quintet and doublet resonances displayed at 108.0 and 42.6 ppm respectively, with a mutual coupling of 33 Hz. The $^{13}C\{^{1}H\}$ NMR spectrum of **3.13** was similar to that of **3.9**, albeit with the evolution of extra coupling arising from the presence of the spin-½ fluorine atoms on the bridging aromatic ring, which displayed as a broad doublet (J_{CF} = 251 Hz) and a quartet (J_{CF} = 322 Hz) for the fluorinated centres and *ipso* position on the ring respectively. Coordination of the phosphaalkyne was supported by the presence of an $SiMe_3$ resonance in the ^{1}H and ^{1}H-^{29}Si HMBC NMR spectra at −0.10 and −12.2 ppm, a singlet resonance in the ^{19}F spectrum at −78.9 ppm corresponding to the OTf counterion, and a singlet at −142.9 ppm arising from the fluorinated bridge. IR spectroscopic data were consistent with a coordinated phosphaalkyne ($\nu_{C\equiv P}$: 1260 cm^{-1}) and the retention of the unsaturated bridging unit ($\nu_{C\equiv C}$: 2040 cm^{-1}).

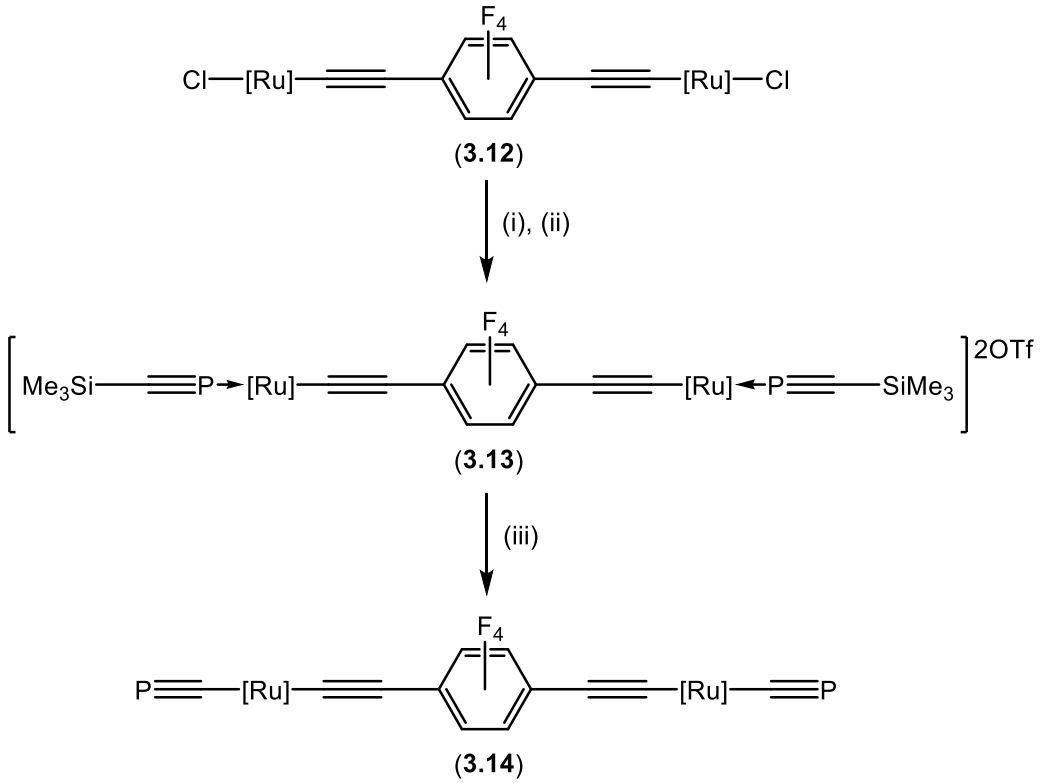

Scheme 3.6: *Synthesis of **3.13** and **3.14**, from **3.12**. Reagents and conditions: (i) 2 eq. TlOTf, DCM, 10 min; (ii) 2 eq. P≡CSiMe$_3$ in toluene, 2 h.; (iii) 2 eq. KO^{t}Bu, THF, 1 h. [Ru] = Ru(dppe)$_2$*

Treatment of **3.13** with two equivalents of KO^{t}Bu in THF afforded the expected cyaphide complex. A shift to higher frequency of both the cyaphidic and dppe $^{31}P\{^1H\}$ NMR resonances to 158.3 and 50.9 ppm is consistent with the inherent deshielding associated with conversion from η^1-coordinated phosphaalkyne to cyaphide, alongside loss of coupling between the two centres, as observed in **3.10** and *trans*-[RuH(dppe)$_2$(C≡P)]. Loss of the SiMe$_3$ and OTf resonances in the ^1H and ^{19}F NMR spectra, the increase in chemical shift of the phosphaalkyne carbon resonance to 280.1 ppm, and the decrease in the C≡P stretching frequency ($\nu_{C\equiv P}$: 1247 cm^{-1} vs 1260 cm^{-1}) further supported conversion to the cyaphide complex.

3.5.3 Electronic Structure, Electrochemical, and UV-Vis Investigations

3.5.3.1 Electronic Structure

Through-conjugation of the two cyaphide fragments *via* the unsaturated bridge was apparent in **3.14**, with the HOMO exhibiting the same out-of-phase mixing as observed in **3.10** (Figure 3.18), albeit with greater contributions from the C≡P units (20% vs 14%). The LUMO was once again primarily based on the ancillary ligand set, lying approximately 3.3 eV higher in energy than the HOMO, however, unlike **3.10** many of the unoccupied orbitals are based around only one metal centre, rather than both. Furthermore, any contributions from the $\pi^*_{C\equiv P}$ orbitals were either non-existent or negligible up until the LUMO+32, which lies 4.6 eV above the HOMO and thus remains inaccessible. The cyaphidic lone pairs of **3.14** are of comparable stability to those of **3.10**, lying approximately 2 eV lower in energy than the HOMO in the HOMO-11 and HOMO-12.

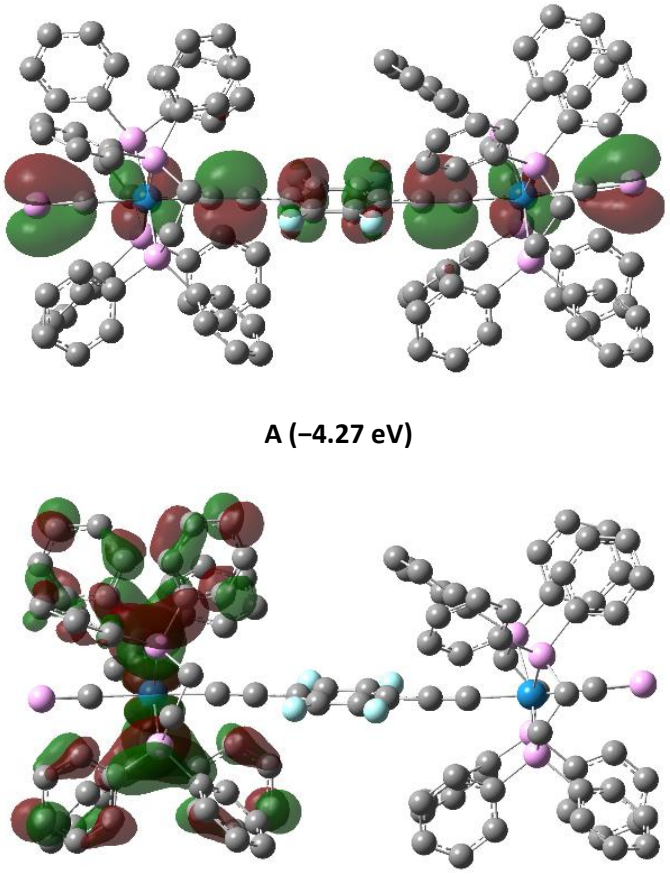

A (–4.27 eV)

B (–0.95 eV)

Figure 3.18: *Calculated frontier molecular orbitals of* ***3.14****. HOMO (A) and LUMO (B)*

3.5.3.2 Cyclic Voltammetry

In comparison to its non-fluorinated counterpart, **3.13** exhibited one quasi-reversible oxidation at 1.02 V followed by a second, irreversible oxidation wave at 1.23 V, resulting in the corresponding Ru^{III}/Ru^{III} species *via* the mixed valence complex (Figure 3.19). A significant anodic shift of both processes in the perfluorinated system when compared to the parent chloride complex likely arises due to the cationic nature of **3.13**. Further, a shift to higher potential was observed in **3.13** when compared to **3.9** for both the quasi- (1.02 V vs 0.71 V) and irreversible oxidation processes (1.23 V vs 1.00 V). It is likely that this arises from the electron-deficient 1,4-diethynyltetrafluorobenzene bridge, resulting in reduced electron density at the metal centres, thus requiring a greater potential to effect oxidation.

A smaller comproportionation constant was observed for **3.13** ($K_c = 7.9 \times 10^3$) than in **3.9** ($K_c = 0.8 \times 10^5$), alongside a 340-fold reduction when compared to the parent chloride complex. This indicated that the use of a perfluorinated bridging unit significantly reduces the stability of the transient, mono-oxidised complex **[3.13]**$^+$, in direct contrast to that observed for the generation of **[3.9]**$^+$.

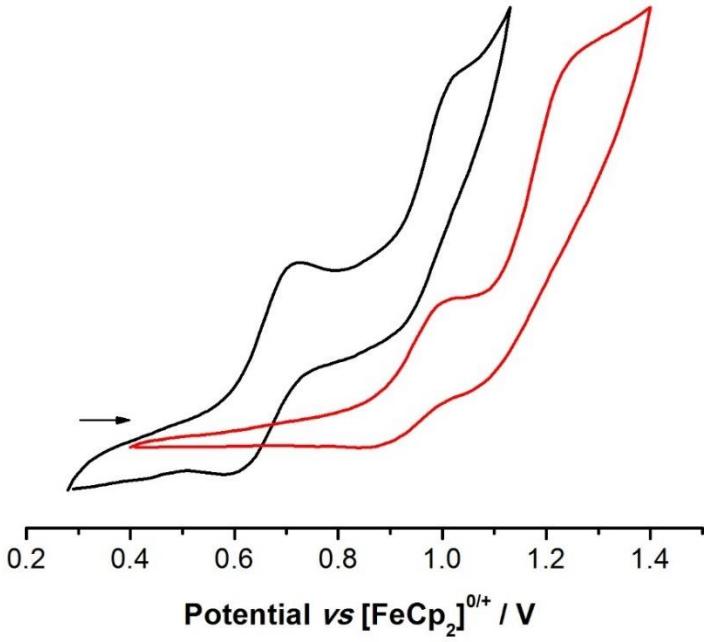

Figure 3.19: *Normalised voltammograms of **3.9** (black) and **3.13** (red) as a solution in DCM (1 mM) with [^{n}Bu$_4$N][PF$_6$] supporting electrolyte (0.1 M), 0.1 V s^{-1} scan rate*

In contrast, the redox behaviour of **3.14** was like that of **3.10** (Figure 3.20), exhibiting two sequential, irreversible oxidation waves at 0.04 and 0.18 V, albeit with an anodic shift associated with the introduction of an electron-deficient bridging alkynyl unit. However, it is noted that no well-defined corresponding reductive event (i.e. Ru^{III} → Ru^{II}) was observed in the perfluorinated system, indicative of greater irreversible behaviour than that in the non-fluorinated system. In addition, a reduction in the separation between the two events (ΔE_{pa} = 0.14 V) resulted in an almost 10-fold decrease in the comproportionation constant to 2.4×10^2. While this signifies an even further reduction in the stability of the in-situ generated mono-oxidised species, the

redox behaviour observed was still consistent with two, one-electron oxidations as opposed to one, two-electron oxidation.

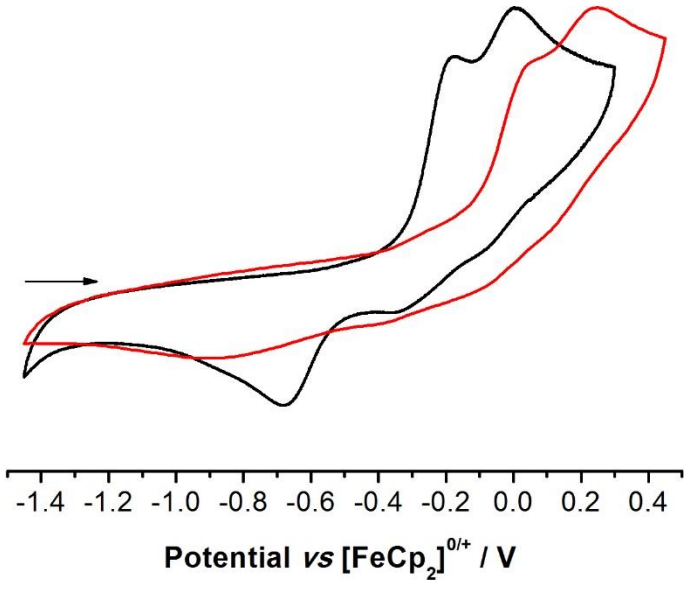

Figure 3.20: *Normalised voltammograms of* ***3.10*** *(black) and* ***3.14*** *(red) as a solution in DCM (1 mM) with* $[^{n}Bu_4N][PF_6]$ *supporting electrolyte (0.1 M), 0.1 V* s^{-1} *scan rate*

3.5.3.3 UV-Vis Spectroscopy

The experimental UV-Vis spectrum of **3.14** (Figure 3.21) was remarkably similar to that observed for **3.10**, however, a bathochromic shift of the lower energy feature by *ca.* 50 nm was observed, arising from the introduction of the fluorinated bridging unit. From TD-DFT calculations, it was apparent that all three features (248, 275, and 400 nm) were dominated by both MLCT, as well as LLCT from the C≡C and C≡P π-systems to the ancillary ligand set, with some very minor contributions arising from the bridging fluorinated arene. Similarly, virtually no contributions arising from transitions to the π* orbitals of the C≡P fragment were observed, presumably due to their high energy, as observed in **3.10**.

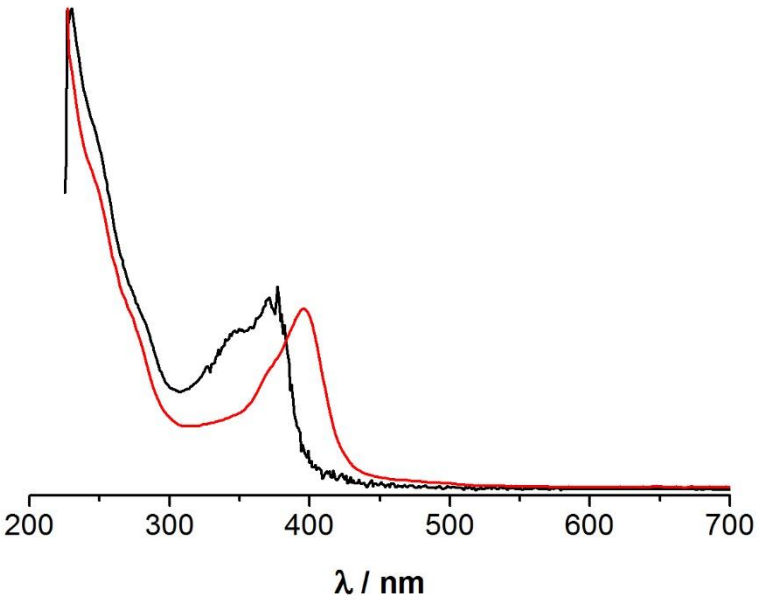

Figure 3.21: *Normalised Experimental UV-Vis Spectra of* ***3.10*** *(black, 1.0 × $\mathbf{10^{-5}}$ mol dm^{-3}) and* ***3.14*** *(red, 1.25 × $\mathbf{10^{-5}}$ mol dm^{-3}) in DCM. 1 cm path length*

3.6 Concluding Remarks

The introduction of cyaphide functionality into bimetallic transition metal complexes **3.3**, **3.10**, and **3.14** has been achieved. Complex **3.3** exhibited very similar spectroscopic data when compared to the complexes prepared in Chapter 2, exhibiting chemical shifts (δ_P: 158, δ_C: 201.2) and IR stretching frequencies ($\nu_{C\equiv P}$: 1251 cm^{-1}) consistent with cyaphide formation, with the identity ultimately supported by X-ray diffraction studies.

While attempts to furnish symmetrical bimetallic complexes featuring a 1,3-butadynye bridging fragment were unsuccessful, owing to steric constraints arising from the ancillary ligand set, the use of bridging fragments based upon 1,4-diethynylbenzene and its derivatives were successful. DFT calculations have shown that both **3.10** and **3.14** exhibit through conjugation of the two phosphaalkyne moieties, mediated by the bimetallic scaffold, and represent the first examples of complexes featuring multiple cyaphide ligands.

It was shown that unlike their monometallic counterparts, the electronic spectra of **3.10** and **3.14** have little to no contributions from $\pi_{C\equiv P} \rightarrow \pi^*_{C\equiv P}$ transitions, with the latter situated in inaccessible, high energy molecular orbitals. Lastly, through cyclic voltammetry measurements, it was shown that the incorporation of cyaphide resulted in a significant decrease in the stability of the transient mono-oxidised species, as reflected by the decrease in the calculated comproportionation constant and change from reversible to irreversible oxidative behaviour.

Chapter 4 – Modified Ligand Architectures

4.1 Introduction

Phosphaalkynes possess a variety of possible coordination modes to a transition metal centre (see Chapter 1), with the most common being the η^2 "side-on" mode, owing to the high energy of the C≡P π-system in relation to the phosphorus lone pair.[4,29,43] It is only when the ancillary ligand set is sufficiently bulky that this can be precluded, allowing end-on η^1-coordination of the phosphaalkyne *via* the lone pair. The most commonly used architecture to achieve this is that derived from $M(dppe)_2$ fragments, as dppe has a demonstrated ability to prevent side-on coordination while still leaving a pocket large enough to permit end-on coordination (Figure 4.1).[31–33,37,68]

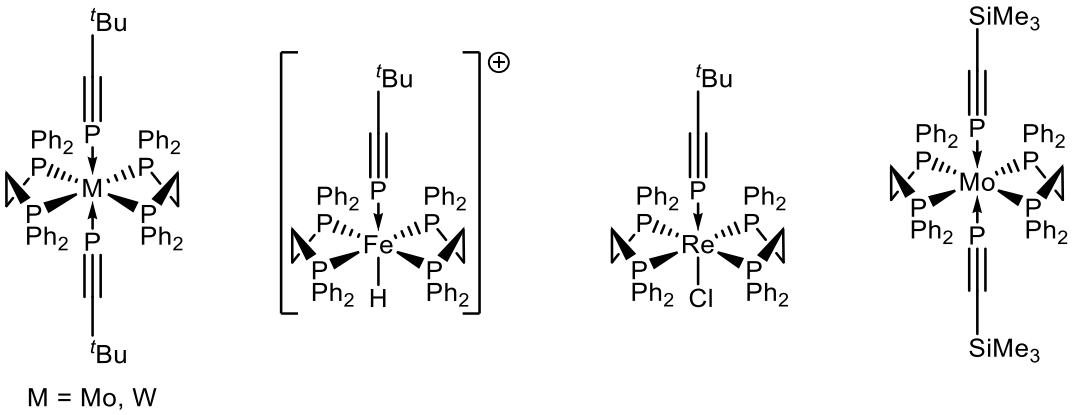

Figure 4.1: *Known examples of η^1-coordinated phosphaalkyne complexes*

By virtue of this, the development of transition metal cyaphide chemistry has become particularly reliant on the use of this bulky scaffold, as the most used methodologies require η^1-coordinated phosphaalkyne precursors, thus η^2-coordination must be precluded using sterically demanding ancillary ligand sets.[64,70] With the exception of one example based upon uranium,

synthesised *via* C-O bond cleavage of the 2-phosphaethynolate anion,[72] all isolable cyaphide complexes in the recent literature are based upon the $M(dppe)_2$ scaffold (Figure 4.2).[64,70]

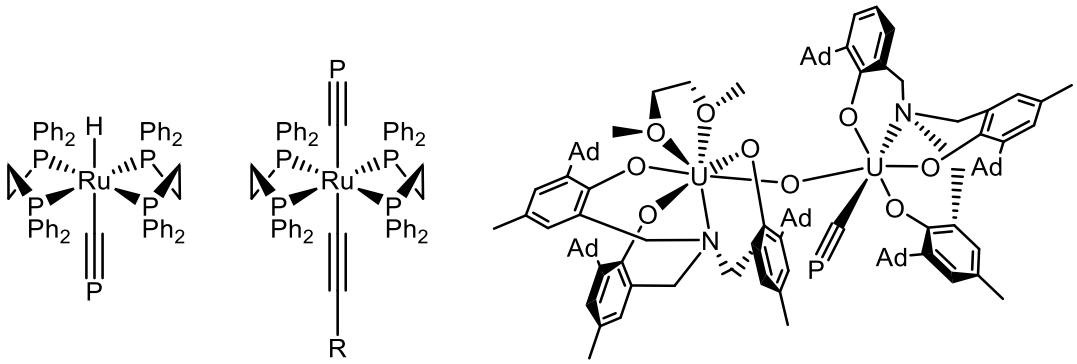

Figure 4.2: *Examples of terminal cyaphide complexes in the chemical literature*

The chemistry of organometallic-based molecular wires has shown a similar dominance of the $M(dppe)_2$ scaffold, owing to its ability to protect the long carbon chains from unwanted reactivity.[92,94] However, other less bulky architectures such as MCp^RL_2,[92–94,119,158,159,162,163] $M(dppm)_2$,[155,164,165] and $M[P(OEt)_3]_4$ have shown similar promise,[131,166–168] with the latter two allowing control of subsequent reactivity.

This work seeks to address the lack of architectural diversity in transition metal cyaphide chemistry, through the synthesis of η^1-phosphaalkyne complexes based upon MCp^R and $M(dppm)_2$ scaffolds, and address the preconceived notion that cyaphide, when ligated to a transition metal, is only stable in systems of the type *trans*-$[RuR(C{\equiv}P)(dppe)_2]$.

4.2 Synthesis of *Trans*-$[RuR(\eta^1\text{-}P{\equiv}CSiMe_3)(dppm)_2]^+$

4.2.1 Synthesis and Characterisation

The synthesis of **4.1**, the dppm-based analogue of Grützmacher's phosphaalkyne complex *trans*-$[RuH(\eta^1\text{-}P{\equiv}CSiPh_3)(dppe)_2]$,[64] was achieved in an analogous fashion to the complexes reported

in Chapter 2. Addition of silver triflate to a sample of *trans*-[RuHCl(dppm)$_2$] in DCM, followed by subsequent addition of $Me_3SiC{\equiv}P$ afforded the desired complex (**4.1**) as an orange solid upon filtration and removal of solvent (Scheme 4.1).

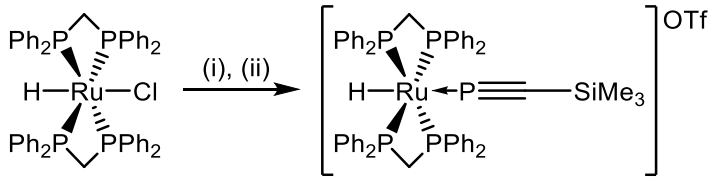

(**4.1**)

Scheme 4.1: *Synthesis of **4.1**. Reagents and conditions: (i) 1 eq. AgOTf, DCM, 10 minutes; (ii) 1 eq. P≡CSiMe$_3$ in toluene, 1 h.*

In the $^{31}P\{^1H\}$ NMR spectrum, **4.1** exhibited two resonances at 111.6 and −4.3 ppm, corresponding to the phosphaalkyne and ancillary ligand set respectively, with a splitting pattern consistent with previous reports for dppe-based systems.[70] The ^1H NMR spectrum showed a doublet of quintets at −5.35 (J = 106, 18 Hz), alongside a singlet resonance at −0.12 ppm, corresponding to the metal hydride and the $SiMe_3$ group, with the latter shown to exhibit coupling to a resonance at −14.7 ppm in the ^1H-^{29}Si HMBC spectrum. The $^{13}C\{^1H\}$ NMR spectrum displayed a doublet resonance at 190.9 ppm ($^1J_{CP}$ = 69 Hz), with correlation observed to the $SiMe_3$ proton resonance in the ^1H-^{13}C HMBC spectrum, attributable to the quaternary centre of the phosphaalkyne. IR spectroscopic data were also consistent with the retention of triple bond character, with a C≡P stretching mode observed at 1258 cm^{-1}.

Alkynyl derivatives were also sought, with samples of *trans*-[RuCl(C≡CPh)(dppm)$_2$] in DCM treated with either silver- or thallium-based halide abstracting reagents in the presence of the phosphaalkyne, which afforded a yellow-orange solid upon workup (Scheme 4.2).

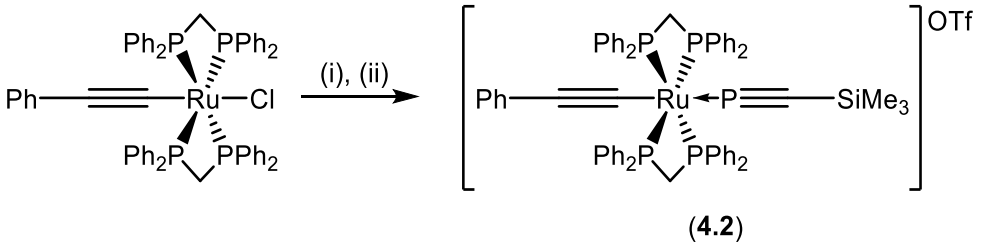

(**4.2**)

Scheme 4.2: *Attempted synthesis of* ***4.2****. Reagents and conditions: (i) 1 eq. AgOTf or TlOTf, DCM, 10 minutes; (ii) 1 eq. P≡CSiMe$_3$ in toluene, 1 h.*

The $^{31}P\{^1H\}$ NMR spectrum of **4.2** displayed quintet and doublet resonances at 105.9 and −12.8 ppm in a 1:4 ratio, with a mutual coupling of 34 Hz. Furthermore, a singlet resonance at −0.3 ppm was consistent with the retention of the $SiMe_3$ group of the phosphaalkyne, alongside the presence of a C≡P stretching mode at 1260 cm^{-1} in the IR spectrum. While these data are consistent with the formation of complex **4.2**, the reaction was never observed to go to completion, with **4.2** existing as the minor component alongside starting material and other intractable species. This precluded full characterisation due to overlapping resonances in the ^1H and $^{13}C\{^1H\}$ NMR spectra.

4.2.2 Molecular Structure Analysis

Crystals suitable for X-ray diffraction were obtained from a sample of **4.1** in DCM layered with hexane and stored at −20 °C, however, the obtained structure showed that subsequent reactivity of the phosphaalkyne had occurred, resulting in the formation of *trans*-$[RuH\{P(OH)_2CHSiMe_3\}\{dppm\}_2]$ (**4.3**; Figure 4.3).

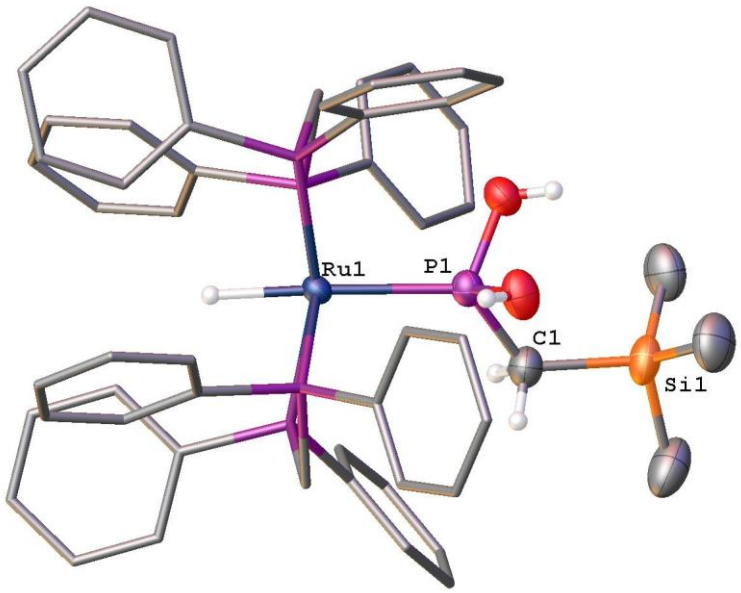

Figure 4.3: *Molecular structure of* ***4.3****; 50% thermal ellipsoids, hydrogen atoms, counter-ion, and solvent molecules omitted, and ancillary ligand set reduced for clarity.*

The structural data for **4.3** suggested addition of two equivalents of H_2O across the C≡P triple bond of **4.1**. Complex **4.3** displayed a tetrahedral geometry around the phosphorus atom, consistent with sp^3-hybridisation, with P-O distances of 1.629(2) and 1.639(2) Å consistent with single bond character.[169,170] The observed C-P distance of 1.780(3) Å is consistent with single-bond character, which is supported by similar C-P distances reported by Crossley for the complex $[Ru(P(H)ClCH_2SiMe_3)Cl_2(CO)(PPh_3)_2]$ and by Hill in the similar $[Ru(PHFCH_2{}^tBu)Cl(CO)(C{\equiv}NC_6H_3Me_2\text{-}2,6)(PPh_3)_2]$ (1.790(11) and 1.794(6) Å respectively).[36,171] It should be noted that the hydride ligand was located in the difference map and refined isotropically.

4.2.3 Attempted Formation of Cyaphide Complexes

Attempts were made to convert **4.1** into the corresponding cyaphide complex, **4.4**, using established procedures reported by Crossley and co-workers.[70] Addition of KO^{t}Bu to a sample of **4.1** in THF resulted in a dark brown solid upon filtration and removal of solvent (Scheme 4.3). The ^{1}H NMR spectrum displayed a doublet of quintets at −5.49 ppm, suggesting retention of the metal hydride, with some correlation to two differing phosphorus environments in the ^{1}H-^{31}P HMBC spectrum. Furthermore, a singlet at 0.31 ppm integrating for nine with respect to the metal hydride suggested that the $SiMe_3$ group had also been retained, alongside a second singlet of equal integration at 0.76 ppm, which was assigned as a *tert*-butyl group from incorporation of an O^{t}Bu fragment. A doublet at 4.36 ppm was also observed (J_{HP} = 6.9 Hz), which was believed to arise from a P=CH unit. These data are similar to Grützmacher's reports for the $\lambda^5\sigma^3$-phosphaketenylruthenium complex *trans*-[RuH(P(O)CHSiPh$_3$)(dppe)$_2$],[67] and are consistent with the formation of **4.5**. However, the ^{31}P{^{1}H} NMR spectrum showed a complicated mixture of additional phosphorus-containing products had formed, with several high frequency resonances observed of varying multiplicity between 280 and 320 ppm. Consequently, in the absence of full spectroscopic characterisation and X-ray diffraction data, the assignment of **4.5** remains tentative.

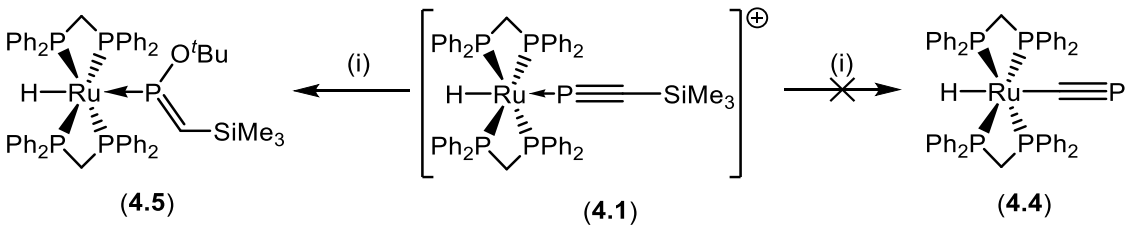

Scheme 4.3: *Attempted synthesis of **4.4**. Reagents and conditions: (i) 1 eq. KO^{t}Bu, THF, 1 h.*

4.3 Synthesis of $[M(Cp^R)(dppe)(\eta^1\text{-}P{\equiv}CSiMe_3)]^+$ (M = Ru, Fe)

4.3.1 Synthesis and Characterisation

Given the prevalence of complexes of the type $[MCp^R\{dppe\}\{(C{\equiv}C)_nR'\}]$ in molecular wire chemistry,[92–94,119,158,159,162,163] the synthesis of such complexes featuring a phosphaalkyne was attempted (**4.6**–**4.9**). Initial reactions of [FeCp*(dppe)Cl] with silver salts in the presence of $Me_3SiC{\equiv}P$ resulted in the formation of a brick-red solid. The $^{31}P\{^1H\}$ NMR spectrum revealed no resonances, consistent with the formation of a paramagnetic iron(III) species. This was ultimately confirmed by X-ray diffraction studies, which revealed the formation of [FeCp*(dppe)Cl]OTf, resulting from the chemical oxidation of the precursor by the silver salt.

Subsequently, reactions of $[FeCp^R(dppe)Cl]$ (R = Me, H) were undertaken using sodium salts to avoid unintentional oxidation, with $NaBPh_4$ chosen due to the literature precedent of iron-phosphaalkyne complexes reacting with $[BF_4]^-$ counterions.[32,33] Upon addition of phosphaalkyne and subsequent workup, **4.6** and **4.7** were isolated as red and brown solids respectively (Scheme 4.4).

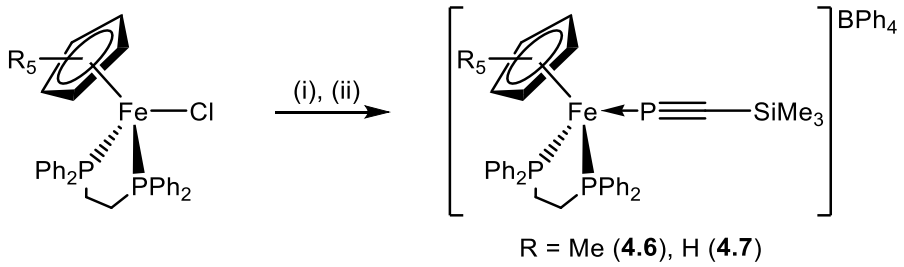

Scheme 4.4: *Synthesis of **4.6** and **4.7**. Reagents and conditions: (i) 1 eq. $NaBPh_4$, THF, 10 minutes; (ii) 1.2 eq. $P{\equiv}CSiMe_3$ in toluene, 1 h.*

In the $^{31}P\{^1H\}$ NMR spectrum, **4.6** displayed triplet and doublet resonances at 147.4 and 82.8 ppm, with a mutual coupling of 57 Hz, corresponding to the phosphaalkyne and dppe fragments respectively. In the ^1H NMR spectrum, broad resonances attributable to the ancillary ligand set

and counter-ion were observed between 7.7 and 6.8 ppm, alongside a broad doublet of multiplets at 2.50 ppm and singlet resonances at 1.49 and 0.02 ppm corresponding to the dppe backbone, Cp* and $SiMe_3$ groups respectively. The quaternary carbon centre of the phosphaalkyne was observed in the $^{13}C\{^1H\}$ NMR spectrum at 197.4 ppm, with connectivity supported by correlation in the ^1H-^{13}C HMBC spectrum to the $SiMe_3$ protons. IR spectroscopic data were consistent with the presence of an unsaturated C≡P bond ($\nu_{C\equiv P}$: 1247 cm^{-1}), which was similar to previous reports (See Chapters 2 and 3).

While these data seemed consistent with the formation of **4.6**, the possibility of a rapidly rotating η^2-phosphaalkyne could not be wholly excluded. In order to assess this prospect, variable temperature (−80 – 30 °C) $^{31}P\{^1H\}$ NMR studies were undertaken in order to assess whether any dynamic processes were present. No changes in the $^{31}P\{^1H\}$ NMR spectrum were observed at low temperatures, suggesting that either no dynamic processes were present or that they were occurring rapidly, despite the lower temperatures, when compared to the NMR timescale. Fortunately, the structure of **4.6** was ultimately confirmed by X-ray diffraction studies (See Section 4.3.2).

Complex **4.7** displayed similar spectroscopic data, with the $^{31}P\{^1H\}$ NMR spectrum exhibiting mutually coupling triplet and doublet resonances at 120.2 and 89.4 ppm ($^2J_{PP}$ = 66.1 Hz). Characteristic $SiMe_3$ resonances were observed in both the ^1H (−0.16 ppm) and $^{13}C\{^1H\}$ (1.3 ppm) NMR spectra, with the latter also displaying a broad resonance at 203.7 ppm corresponding to the C≡P fragment.

Attempts to synthesise the ruthenium analogues, **4.8** and **4.9**, were undertaken with mixed success (Scheme 4.5). Initial attempts at chloride abstraction using sodium salts at room temperature were unsuccessful, with no subsequent phosphaalkyne coordination observed by $^{31}P\{^1H\}$ NMR studies. Greater success was achieved upon reflux of samples of [RuCp*(dppe)Cl] with a slight excess of TlOTf in THF overnight, followed by addition of the phosphaalkyne upon

cooling. Subsequent workup afforded a bright yellow solid, which exhibited triplet and doublet resonances in the $^{31}P\{^{1}H\}$ NMR spectrum at 119.6 and 69.0 ppm respectively in a 1:2 ratio, with a mutual coupling of 61 Hz. The quaternary carbon centre of the phosphaalkyne was observed in the $^{13}C\{^{1}H\}$ NMR spectrum at 185.9 ppm, alongside the $SiMe_3$ protons at 0.9 ppm in the ^{1}H NMR spectrum which were shown to correlate to a resonance at −12.8 ppm in the ^{1}H-^{29}Si HMBC spectrum. IR spectroscopic data were consistent with the presence of an unsaturated C≡P unit, with a stretching mode observed at 1238 cm^{-1}. Unfortunately, the synthesis of **4.9** was unsuccessful, with attempts resulting in the formation of an intractable mixture of products.

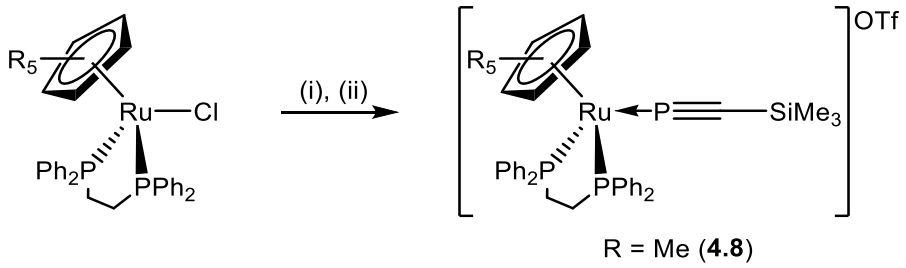

Scheme 4.5: *Synthesis of **4.8** and **4.9**. Reagents and conditions: (i) 1 eq. TlOTf, THF, reflux, 16 h.; (ii) 1.2 eq. P≡CSiMe$_3$ in toluene, 1 h.*

Interestingly, when the synthesis of **4.8** was attempted as a one-pot procedure, a pale-yellow solid was isolated upon workup (**4.10**), with subsequent synthetic attempts forming a mixture of the unknown complex **4.10** with **4.8** in varying ratios. Complex **4.10** exhibited a triplet and doublet resonance at 171.5 and 85.2 ppm respectively, with a mutual coupling of 50 Hz. The quaternary centre of the phosphaalkyne was observed as a doublet in the $^{13}C\{^{1}H\}$ NMR spectrum at 185.9 ppm (J_{CP} = 76 Hz), and retention of the $SiMe_3$ unit was supported by the presence of a singlet resonance at 0.9 ppm in the ^{1}H NMR spectrum. However, a shift in the silicon resonance from −12.8 to −0.37 ppm in the ^{1}H-^{29}Si HMBC spectrum was observed, which is inconsistent with the data observed for **4.6**–**4.8**. Distinct resonances at 1.63 and 2.67 ppm in the ^{1}H NMR spectrum supported retention of the Cp* and dppe ancillary ligands, and a stretching mode was

observed at 1238 cm^{-1} in the IR spectrum, which is consistent with the presence of a C≡P unit. Notably, upon heating of a sample of **4.8** under reflux in THF for 24 hours, conversion to **4.10** was observed. Unfortunately, in the absence of crystallographic confirmation, the identity of **4.10** remains elusive.

4.3.2 Molecular Structure Analysis

The connectivity of **4.6** was ultimately determined from X-ray diffraction data, resulting in unequivocal confirmation of the phosphaalkyne coordination mode (Figure 4.4); this represents the first example of a structurally characterised half-sandwich η^1-phosphaalkyne complex.

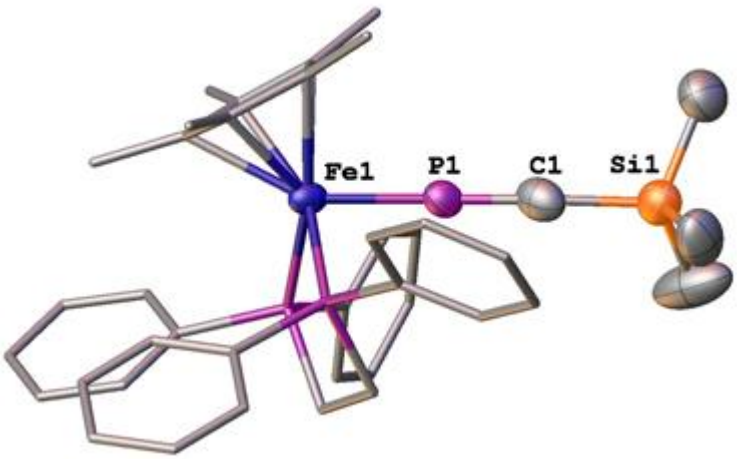

Figure 4.4: *Molecular structure of **4.6**; 50% thermal ellipsoids, hydrogen atoms and counter-ion omitted, and ancillary ligand set reduced for clarity.*

The solid-state structure of **4.6** exhibited a C-P distance of 1.539(2) Å, which is similar for the precedent η^1-phosphaalkyne complexes featuring a dppe scaffold (*ca*. 1.53–1.55 Å),[64,68,70] and thus supports triple bond character. A distortion from linearity of the M-P-C unit was observed (171.2(3) °) when compared to *trans*-[RuR(dppe)$_2$(η^1-P≡CSiR'$_3$)] (R = H, R' = Ph; R = C≡CCO_2Me, R' = Me) and Russell's *trans*-[Mo(dppe)$_2$(η^1-P≡C$SiMe_3$)$_2$] (174.9(1), 175.7(4), and 177.1 ° respectively),[64,68,70] though this is likely attributable to the greater steric shielding afforded by

Cp* when compared to dppe. Overall, the bond metrics predicted by DFT calculations (B3LYP/6-31G** for all non-metal atoms; LANL2DZ for Fe) were in good agreement with the experimental data, albeit with a greater tendency towards overall linearity. A summary of these data is presented in Table 4.1.

Table 4.1: *Selected bond lengths (Å) and angles (°) for* ***4.6*** *and comparable complexes* *trans-*$[RuR(\eta^1\text{-}P{\equiv}CSiMe_3)(dppe)_2]^+$

	4.6	**4.6$_{Calc}$**	**R = C≡CPh (2.4)**	**R = C≡CFc (3.2)**	**R = H**[64]	**R = C≡CCO$_2$Me**[70]
M-P$_1$	2.114(2)	2.187	2.2638(8)	2.246(2)	2.2486(8)	2.274(3)
P$_1$-C$_1$	1.532(9)	1.549	1.534(4)	1.522(9)	1.530(3)	1.53(1)
C$_1$-Si$_1$	1.839(9)	1.861	1.836(4)	1.846(9)	1.824(3)	1.86(1)
M-P$_1$-C$_1$	171.2(3)	170.0	176.5(2)	173.8(4)	174.9(1)	175.7(4)
P$_1$-C$_1$-Si$_1$	174.5(6)	179.1	174.9(3)	171.0(7)	165.5(2)	178.3(7)

4.3.3 Electrochemical Investigations

The electrochemical behaviours of **4.6**–**4.8** were investigated using cyclic voltammetry (Figure 4.5). Complex **4.6** displays one reversible redox process consistent with the Fe^{II}/Fe^{III} redox couple at −0.15 V, with the reversibility supported by a lack of dependence of the oxidative and reductive potentials on the experimental scan rate, alongside the I_{pa}/I_{pc} ratio approaching unity. A shift in the Fe^{II}/Fe^{III} process from 0.04 V for the parent chloride complex to more negative potential was observed, indicating more facile oxidation to the transient iron(III) species.[172] Complex **4.7** demonstrated similar redox behaviour, exhibiting one reversible redox process at −0.42 V which is 0.18 V more negative than its parent chloride complex [FeCp(dppe)Cl].[172] The large discrepancy between the half-wave potentials of **4.6** and **4.7** is most likely attributable to the greater electron-donating capacity of Cp* compared to Cp.

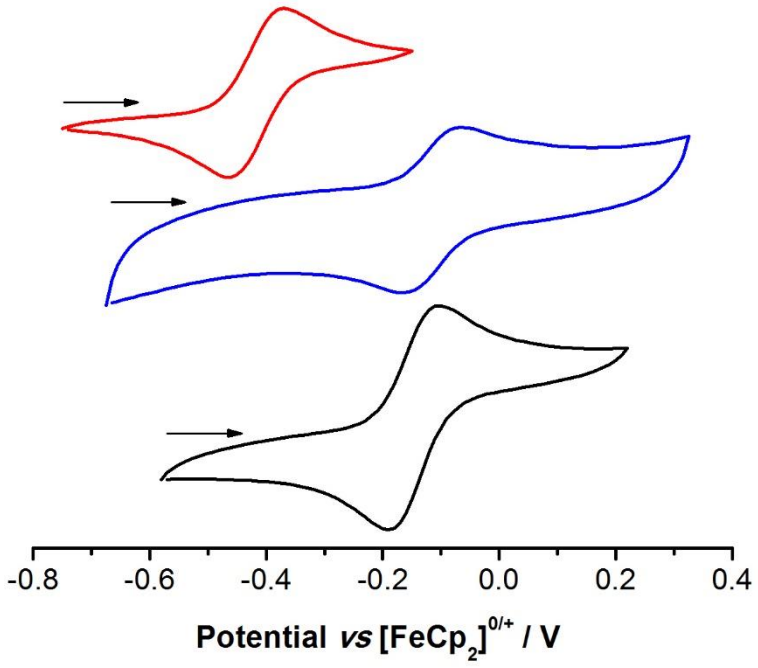

Figure 4.5: *Normalised voltammograms of* ***4.6*** *(black),* ***4.7*** *(red), and* ***4.8*** *(blue) as a solution in DCM (1 mM) with [$^{n}Bu_4N$][PF_6] supporting electrolyte (0.1 M), 0.1 V s^{-1} scan rate*

While [RuCp*(dppe)Cl] has been reported to demonstrate reversible oxidative behaviour ($E_{½}$ = 0.28 V *vs* $[FeCp_2]^{0/+}$),[172] **4.8** displays one quasi-reversible redox process at −0.11 V consistent with the Ru^{II}/Ru^{III} redox couple. The observed shifts of the half-wave potentials of **4.6**-**4.8** when compared to their parent chloride complexes suggests reduced acceptor character of the phosphaalkyne fragment when compared to chloride, resulting in these derivatives being much more easily oxidised, akin to the replacement of a Cp ring for Cp*.

4.3.4 Attempted Conversion to Cyaphide

Attempts to convert **4.8** to the corresponding cyaphide complex *via* desilylative rearrangement as previously described (see Chapters 2 and 3) were undertaken, however, addition of KO^{t}Bu resulted in the formation of the complex [RuCp*(dppe)Cl] as the sole product. Consequently, further studies were undertaken using the iron analogue **4.6** and a variety of different bases known for their ability to desilylate phosphaalkynes or phosphaalkenes (Scheme 4.6).[4,43,64,70]

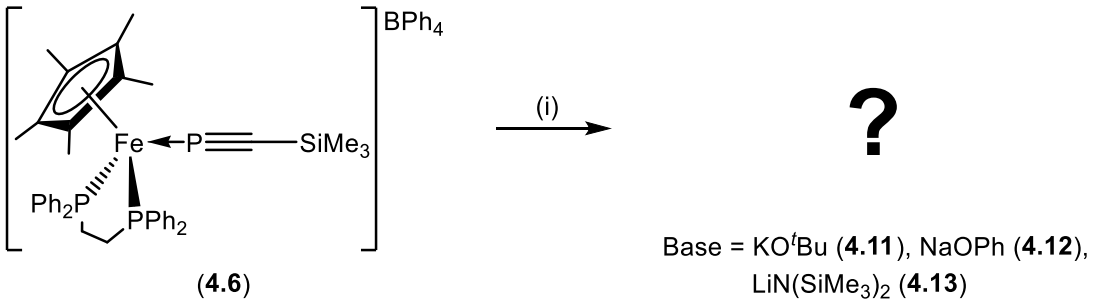

(**4.6**)

Scheme 4.6: *Attempted conversion of* ***4.6****. Reagents and conditions: (i) 1 eq. Base, THF, 16 h.*

Addition of KO^{t}Bu to a sample of **4.6** in THF resulted in the formation of a brown solid upon removal of solvent after 16 hours. The $^{31}P\{^1H\}$ NMR spectrum of **4.11** revealed a mixture of products, with four resonances observed between 170 and 85 ppm in a 1:1:1:2 ratio (Figure 4.6). Further resonances at 29.2 and 28.5 ppm were also observed, the latter as a doublet (J_{PP} = 47 Hz), alongside a singlet at −12.8 ppm, which corresponds to free dppe. The high frequency resonances were consistent with the formation of the corresponding cyaphide complex, however, due to significant contamination by dppe, further spectroscopic or X-ray characterisation was not possible.

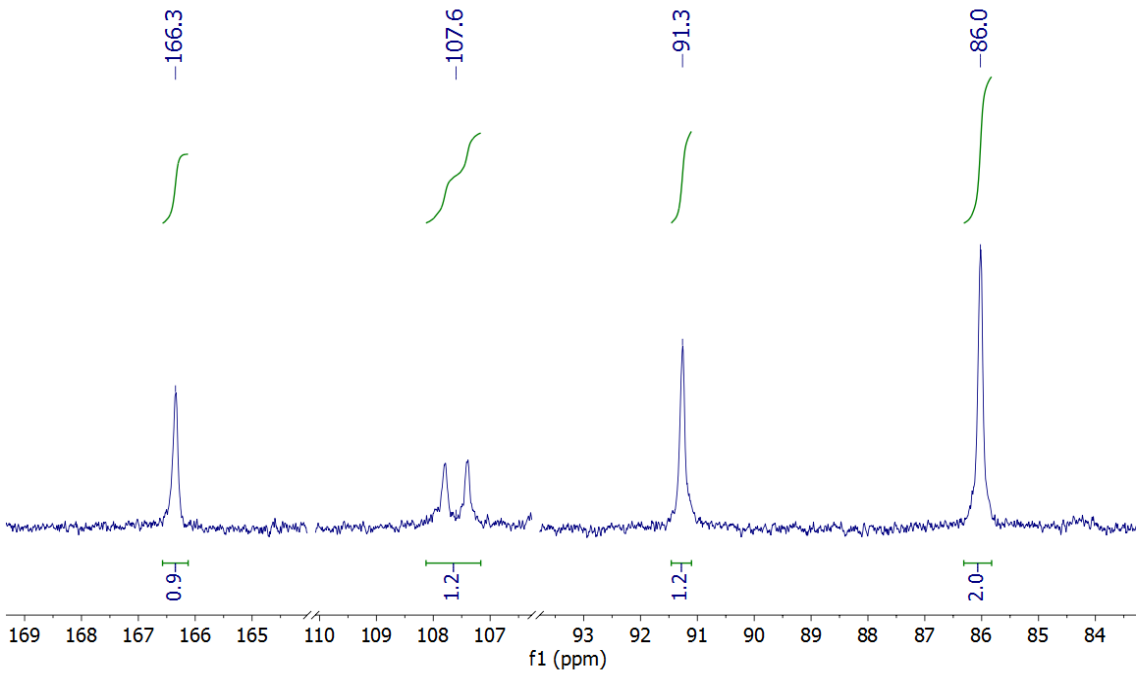

Figure 4.6: *$^{31}P\{^{1}H\}$ NMR spectrum of* ***4.11*** *(2.0 Hz line broadening)*

In light of this, an analogous reaction was undertaken using NaOPh instead of KO^{t}Bu under the same conditions. The $^{31}P\{^{1}H\}$ NMR spectrum of **4.12** revealed a complex mixture of products, with triplets at 333.3 (J_{PP} = 75 Hz) and 206.0 ppm (J_{PP} = 70 Hz), a singlet at 189.3 ppm, and doublets at 98.2 and 95.2 ppm (J_{PP} = 75 and 70 Hz respectively), in a 1:1:1:2:2 ratio (Figure 4.7). Additionally, a significant amount of contamination by free dppe was apparent, as a large singlet resonance at −12.5 ppm was observed. Furthermore, it appeared that while another complex mixture had been obtained, the components were different than those formed in **4.11**.

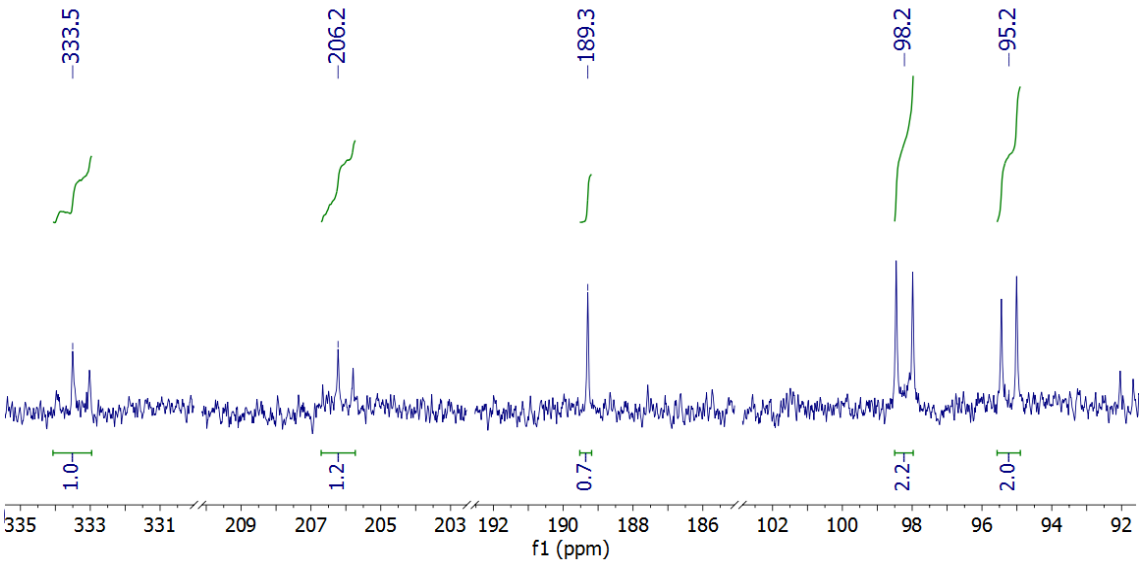

Figure 4.7: *$^{31}P\{^{1}H\}$ NMR spectrum of* ***4.12*** *(4.0 Hz line broadening)*

A final attempt at desilylation was undertaken using $LiN(SiMe_3)_2$, which formed a green solid (**4.13**) upon removal of solvent after a reaction period of 16 hours. While less complicated than the previous mixtures, the $^{31}P\{^{1}H\}$ NMR spectrum displayed four distinctive resonances: a triplet at 240.7 ppm (J_{PP} = 70 Hz), a doublet at 92.8 ppm (J_{PP} = 80 Hz), and a doublet at 87.2 ppm (J_{PP} = 70 Hz) in a 1:2:2 ratio, alongside a large singlet at −12.9 ppm corresponding to free dppe.

Further work is required in order to reduce or prevent ligand dissociation upon addition of base, in order to develop a more successful methodology for the desilylation of **4.6** to give the desired half-sandwich cyaphide complexes, if synthetically feasible.

4.4 Concluding Remarks

Attempts to introduce cyaphide functionality into systems based on the $Ru(dppm)_2$ architecture have been undertaken. While the initial coordination of the phosphaalkyne $Me_3SiC{\equiv}P$ was achieved in the hydridic system (**4.1**) limited success was had with the alkynyl system **4.2**, with the reaction failing to reach completion.

Efforts to desilylate **4.1** did not result in the formation of the corresponding cyaphide complex, and instead appeared to form the corresponding phosphaalkene complex **4.5**. This is believed to be the result of irreversible nucleophilic attack at the phosphorus centre, though further investigations are required to confirm this in the absence of crystallographic data and full spectroscopic characterisation.

Greater success was had with the initial coordination of the phosphaalkyne to systems of the type $MCp^{R}L_2$ (**4.6**–**4.8**), which possessed sufficient steric bulk to prevent side-on coordination, as supported by VT NMR spectroscopic data, alongside X-ray diffraction studies. However, desilylation to the corresponding cyaphide complexes was found to be non-trivial, with different complex mixtures formed upon the use of differing bases, and ligand loss apparent by $^{31}P\{^{1}H\}$ NMR spectroscopy. Further work is required to develop a cleaner desilylating procedure which limits loss of dppe so that the identities of the complexes formed can be determined.

Chapter 5 – Preliminary Reactivity Studies and Future Work

5.1 Introduction

While the reactivity of phosphaalkynes and their complexes is well established (see Chapter 1), that of cyaphide has received little attention, owing to a lack of examples in the literature until recent years.[64,70,72] Possible reactivity of ruthenium cyaphide complexes was first alluded to by Grützmacher in 2006 where it was reported that upon prolonged storage of samples of *trans*-[RuH(C≡P)(dppe)$_2$] in chlorinated solvents, exchange of cyaphide for chloride was observed (Scheme 5.1).[64] Indeed, similar observations were reported when samples of *trans*-[Ru(C≡P)(C≡CR)(dppe)$_2$] were dissolved in chloroform,[139] however, this was not investigated further.

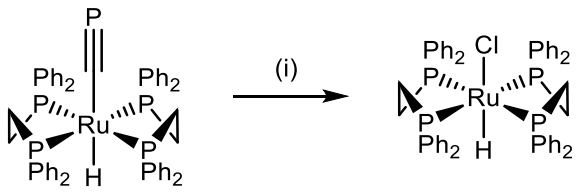

Scheme 5.1: *Cyaphide-chloride exchange of a ruthenium cyaphide complex. Conditions: (i) DCM, prolonged storage*

The possibility of reactivity at the cyaphidic lone pair was initially considered by Crossley and co-workers, whereby NBO calculations revealed that the lone pair of the cyaphide complexes *trans*-[Ru(C≡P)(C≡CR)(dppe)$_2$] (R = CO_2Me, *p*-An) is held in an orbital of 75% *s*- and 25% *p*-character,[70] with polarisation of the C≡P moiety shown to be $C^{\delta-}$–$P^{\delta+}$. These data are consistent with those of classical phosphaalkynes,[4] and thus it was rationalised that the lone pair is accessible, and that reactivity should, in fact, be possible.

Initial studies by colleagues sought to coordinate the cyaphidic phosphorus lone pair to noble metal complexes, with limited success.[139] Greater success was achieved through the addition of

$BF_3.Et_2O$ to a sample of *trans*-[Ru(C≡P)(C≡CCO_2Me)(dppe)$_2$], with two major products observed by $^{31}P\{^1H\}$ and $^{11}B\{^1H\}$ NMR spectroscopy, however, attempts to isolate these complexes as discrete species were unsuccessful.[139]

This work seeks to build upon these investigations, with attempts to engage ligated cyaphide in reactivity, either *via* the phosphorus lone pair or C≡P π-system, with a variety of substrates.

5.2 Cyaphide Reactivity

5.2.1 Group 13

Building upon previous studies,[139] attempts to engage the cyaphidic lone pair with different boranes were undertaken (Scheme 5.2). The complex *trans*-[Ru(C≡P)(C≡CPh)(dppe)$_2$] (**2.7**) was chosen for these studies due to the lack of substituents on the phenyl ring, thus reducing the likelihood of unwanted side reactions.

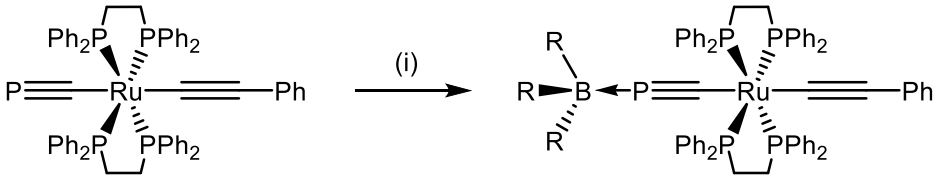

(**2.7**) R = Ph (**5.1**), C_6F_5 (**5.2**)

Scheme 5.2: *Attempted synthesis of **5.1** and **5.2**. Reagents and conditions: (i) 1 eq. BR_3, toluene-d_8, 1 h.*

Addition of BPh_3 to **2.7** was undertaken in DCM-d_2 and toluene-d_8 in an NMR tube, with the samples left to mix by repeated inversion for approximately 1 h. before the reaction was investigated by NMR spectroscopy. The $^{31}P\{^1H\}$ NMR spectrum of the reaction mixture exhibited a broad resonance at 168.1 ppm ($\nu_{½}$ = 22 Hz), alongside a somewhat broad doublet at 51.8 ppm (J_{PP} = 3.0 Hz, $\nu_{½}$ = 10 Hz). In the $^{11}B\{^1H\}$ NMR spectrum, a broad singlet at 66.5 ppm was apparent,

which is consistent with a three-coordinate boron centre. These data are consistent with a mixture of **2.7** and BPh_3 as two discrete species, with no adduct formation (**5.1**) apparent.

Later attempts focussed on the use of the more Lewis acidic $B(C_6F_5)_3$ to synthesise **5.2**, using an identical reaction setup (Scheme 5.2). The $^{31}P\{^1H\}$ NMR spectrum revealed a shift of the cyaphidic phosphorus resonance from 168.1 to 170.3 ppm, and a broadening of the dppe resonance ($\nu_{½}$ = 10.6 Hz) resulting in a loss of observable coupling. In the $^{11}B\{^1H\}$ NMR spectrum, a singlet at −15.9 ppm was observed, which is within the range of four-coordinate boron centres (−20 – 20 ppm). The ^{19}F NMR spectrum displayed a multitude of resonances of varying intensity and multiplicity between −125 and −165 ppm, suggesting either a breaking of the symmetry of the perfluorophenyl rings, presumably though loss of one or multiple fluorine atoms, or the formation of multiple species, both of which are inconsistent with the formation of **5.2**.

The alternative possibility of adduct formation between the $B(C_6F_5)_3$ and residual THF in the sample of **2.7** was investigated. The $^{11}B\{^1H\}$ NMR spectrum of a sample of $B(C_6F_5)_3$ in toluene-d_8 that had been spiked with THF exhibited a broad resonance at 7.8 ppm, which is inconsistent with that observed previously (−15.9 ppm). Similarly, the possibility of adduct formation between the borane and the C≡C π-system was assessed, through addition of $B(C_6F_5)_3$ to a sample of *trans*-$[RuCl(C{\equiv}CPh)(dppe)_2]$ in toluene-d_8. A shift in the dppe resonance to lower frequency (*ca*. 5 ppm) was observed in the $^{31}P\{^1H\}$ NMR spectrum, however, the observed resonance at 23.8 ppm in the $^{11}B\{^1H\}$ NMR spectrum was once again inconsistent with that observed previously. Further attempts to fully characterise the product of the reaction between **2.7** and $B(C_6F_5)_3$ reaction have, as of yet, been unsuccessful.

5.2.2 Group 16

Later studies sought to react the ligated cyaphide with much simpler substrates, with an initial focus on controlled oxidation of the phosphorus centre to phosphorus(V) using various chalcogens. To a sample of *trans*-[Ru(C≡P)(C≡C-*p*-An)(dppe)$_2$] (**2.8**) in DCM-d_2, an excess of elemental sulfur was added, and the suspension mixed by inversion (Scheme 5.3). The ^{1}H NMR spectrum of **5.3** was largely unremarkable, with several broad resonances observed between 7.8 and 6.8 ppm corresponding to the ancillary ligand set, alongside singlet and multiplet resonances at 3.82 and 2.84 ppm, arising from the methoxy substituent and dppe-backbone respectively. In contrast, the ^{31}P{^{1}H} NMR spectrum revealed multiple resonances between 70 and 45 ppm, alongside a doublet resonance at 41.8 ppm (J_{PP} = 29.2 Hz), though no corresponding resonance could be identified. Additionally, small quantities of dppeS$_2$ were apparent from a characteristic resonance in the ^{31}P{^{1}H} NMR spectrum at 44.1 ppm.[173]

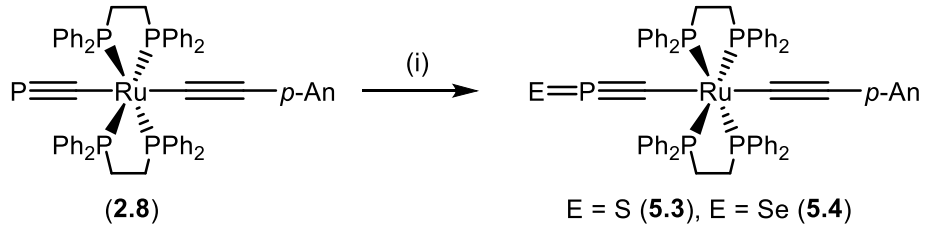

Scheme 5.3: *Addition of elemental chalcogens to* ***2.8****. Reagents and conditions: (i) excess sulfur or selenium, DCM–d_2*

Similarly, the reaction of **2.7** with selenium powder was undertaken in DCM-d_2, and the reaction monitored by ^{31}P{^{1}H} NMR spectroscopy over a period of one month (Scheme 5.3), however, it should be noted that the reaction failed to reach completion during this period. In the ^{31}P{^{1}H} NMR spectrum, a new resonance was observed at 35.6 ppm which displayed selenium satellites ($^1J_{PSe}$ = 679 Hz), however, these data are consistent with the formation of dppeSe$_2$,[174] which is supported by the observation of the associated resonances in the ^{1}H NMR spectrum. Due to the lack of desired reactivity, reactions with elemental tellurium were not undertaken. Future work

should seek to utilise single-atom chalcogen transfer reagents in order to better control the stoichiometry of these reactions in order to reduce the formation of $dppeS_2$ and $dppeSe_2$.

More promising results were obtained upon the reaction of an NMR sample of **2.7** with stoichiometric quantities of N_2O gas, with the aim of synthesising complex **5.5** (Scheme 5.4).

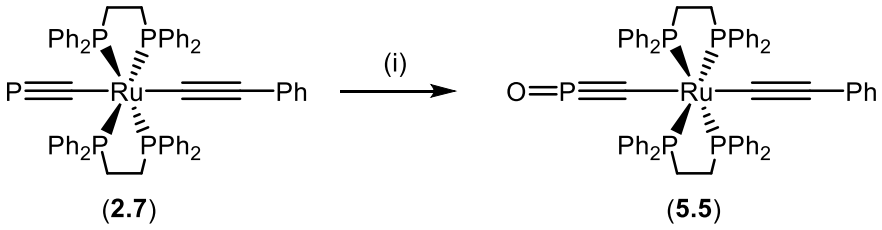

Scheme 5.4: *Attempted oxidation of* ***2.7****. Reagents and conditions: 1 eq.* N_2O*, DCM-*d_2

The reaction was monitored periodically over a period of one month by NMR spectroscopy. The $^{31}P\{^1H\}$ NMR spectrum revealed several multiplets between 45 and 32 ppm, alongside a new quintet resonance at 141.4 ppm (J = 12 Hz). Unfortunately, ^1H NMR spectroscopy revealed an intractable mixture of products, and later $^{31}P\{^1H\}$ NMR studies revealed total decomposition of **5.5**, thus further characterisation by NMR and IR spectroscopy, and mass spectrometry was not possible.

5.2.3 Group 17

Due to the propensity of phosphanes to coordinate to dihalogens in solution *via* the phosphorus lone pair,[175–177] the potential reactivity of cyaphide with halogens was investigated. Initial studies were undertaken using **2.8** and excess iodine, with the reaction monitored by $^{31}P\{^1H\}$ NMR spectroscopy (Scheme 5.5). After *ca*. 1 h., the $^{31}P\{^1H\}$ NMR spectrum of the reaction mixture displayed a singlet resonance at 173.4 ppm, which is consistent with PI_3,[178] two mutually coupling triplet resonances at 73.2 and 63.4 ppm (J_{PP} = 11.9 Hz) consistent with a five-coordinate ruthenium(II) species, and a further singlet at 29.7 ppm, the latter of which was tentatively

assigned as **5.6**. These data appeared to be consistent with the addition of I_2 across the C≡P triple bond, resulting in complete cleavage and the formation of free PI_3.[178]

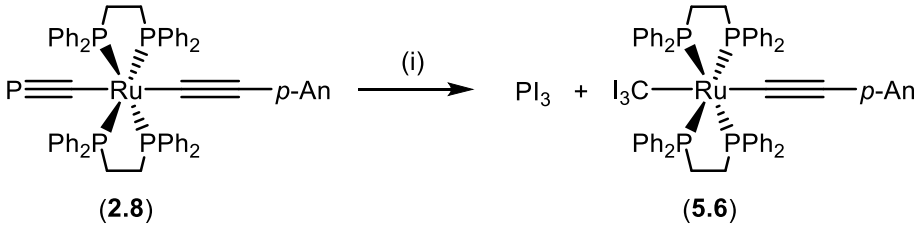

Scheme 5.5: *Proposed reactivity of **2.8** with I_2. Reagents and conditions: (i) excess I_2, DCM-d_2, 1 h.*

The reaction was repeated with **2.7** and monitored by $^{31}P\{^1H\}$ NMR spectroscopy at 10-minute intervals over a 16-hour period. An initial shift of the cyaphidic resonance in the $^{31}P\{^1H\}$ NMR spectrum from 160.4 to 101.5 ppm was observed, alongside the development of coupling, which was unobserved for the cyaphidic resonance in **2.7**, with the corresponding dppe resonance at 45.9 ppm (J_{PP} = 4 Hz). The ^1H NMR spectrum suggested retention of the ancillary ligand set, with broad resonances observed between 7.50 and 7.05 ppm, in addition to broad resonances corresponding to the phenylacetylene fragment at 7.23 and 6.63 ppm. Similar data were obtained for the reaction of **2.8**, and in both instances the reaction then proceeded to completion within two hours, as previously described, however, assignment of the ^1H NMR spectrum at completion was not possible, due to the complex mixture of products formed. These data would seem consistent with a step-wise addition of I_2 across the C≡P triple bond and consequently, efforts were undertaken to isolate the proposed intermediates (Scheme 5.6).

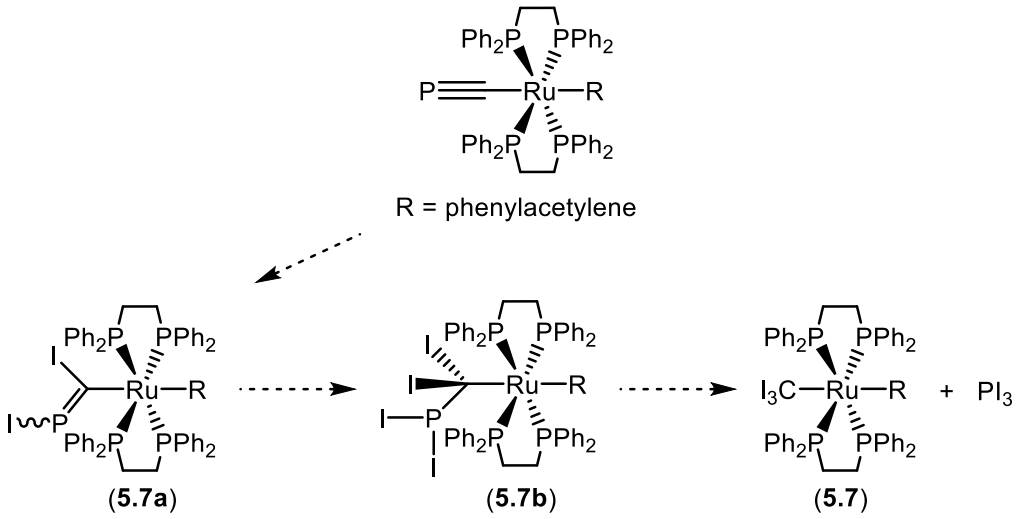

Scheme 5.6: *Proposed reaction pathway resulting in the formation of* ***5.7***

Complex **2.7** was reacted with one, two, and three equivalents of I_2 as a solution in DCM, and the reaction mixtures left to stir for 1 h. before removal of solvent and washing with pentane to remove any residual I_2. In all three cases, the $^{31}P\{^1H\}$ NMR spectrum displayed a singlet at 133 ppm, which suggests that the reaction goes to completion regardless of the quantity of iodine added. Unfortunately, in lieu of complete spectroscopic characterisation, the reaction pathway and identity of the final metal complex is currently only speculative.

Further preliminary investigations into the formation of phosphorus trihalides were undertaken as NMR scale reactions using excess bromine and $PhICl_2$. The former resulted in the rapid addition of Br_2 across the C≡P triple bond and subsequent cleavage to give PBr_3 (228.4 ppm),[178] with the reaction complete within five minutes, as determined by $^{31}P\{^1H\}$ NMR spectroscopic studies. Similar rapid reactivity was observed using $PhICl_2$, however, no PCl_3 was observed in the $^{31}P\{^1H\}$ NMR spectrum, which displayed two broad resonances at 43.9 and 33.7 ppm in a 1:4 ratio, though the latter is consistent with shifts observed upon completion of the same reaction with I_2 and Br_2.

Future work should seek to address the deficiencies in the spectroscopic characterisation of the final ruthenium containing product particularly by $^{13}C\{^{1}H\}$ NMR spectroscopy, where the shift and loss of the cyaphidic carbon resonance can be monitored. Furthermore, attempts to isolate the intermediary complexes generated *en route* to total C≡P bond cleavage should be undertaken. This could be achieved through modification of the electron density at the metal centre (as seen in Chapter 2), with significant reduction likely resulting in a slowing of the reaction rate and thus allowing more facile isolation.

However, it should also be noted that reactivity of the halogens with the C≡C triple bond of the acetylide fragment is likely. This has been determined experimentally through the addition of excess I_2 to a sample of *trans*-$[RuCl(C{\equiv}CPh)(dppe)_2]$, whereby a shift in the $^{31}P\{^{1}H\}$ resonance was observed from *ca*. 50 to 36.4 ppm, alongside significant broadening. Perhaps the most facile method of avoidance would be to synthesise transition metal cyaphide complexes with alkyl groups in the *trans*- position. Attempts to synthesise such complexes have been reported by colleagues with some success.[179]

5.3 Concluding Remarks

Initial investigations into the possible reactivity of ligated cyaphide have been undertaken. While attempts to coordinate to BPh_3 *via* the phosphorus lone pair were unsuccessful, some reactivity with the perfluorinated borane $B(C_6F_5)_3$ was observed, however, further investigations are required in order to fully characterise the resultant complex, which is not believed to be the expected classical adduct **5.2**.

Mixed success was obtained with the reaction of cyaphide complexes with chalcogens. While the reaction with selenium powder formed $dppeSe_2$ as the sole product, a mixture of phosphorus containing products was obtained upon reaction with elemental sulfur, albeit with

some contamination from $dppeS_2$. The use of N_2O as an oxygen source resulted in the formation of several products, as determined by $^{31}P\{^1H\}$ NMR studies, however, further spectroscopic characterisation was hindered by the inherent instability of these compounds, which resulted in their decomposition.

Lastly, the potential reactivity of cyaphide with various halogens was investigated. Initial attempts to form terminal dihalogen adducts instead resulted in complete cleavage of the C≡P triple bond, with the formation of free phosphorus trihalides observed by $^{31}P\{^1H\}$ NMR spectroscopy. Future work would seek to investigate the pathway of these reactions, which is believed to occur in a stepwise manner, and to isolate the proposed intermediary phosphaalkene and phosphaalkane complexes.

Chapter 6 – Concluding Remarks

6.1 Summary

6.1.1 Chapter 1

The field of low-coordinate phosphorus was introduced, with key literature regarding the synthesis, reactivity, and coordination chemistry of phosphaalkynes (R-C≡P) presented. It has been shown that phosphaalkynes possess a variety of possible coordination modes, due to the presence of both a highly reactive C≡P π-system and the phosphorus lone pair, with the steric bulk of the ancillary ligand set of the metal often dictating the coordination mode of the phosphaalkyne. The area of transition metal cyaphide chemistry was presented, and the use of silyl-substituted phosphaalkynes as a means to access transition metal cyaphide complexes *via* the intermediacy of η^1-coordinated phosphaalkyne complexes was illustrated.

The final section of this introductory chapter detailed the field of molecular electronics, specifically the use of conjugated phosphacarbons and organometallic systems. Key examples of multimetallic transition metal systems incorporating purely *sp*- and mixed *sp*/*sp*^{2}-bridging units were identified, and their possible uses as carbon σ-bonded molecular wires explored. Lastly, the amalgamation of these two areas, namely linearly conjugated phosphaorganometallics, was proposed. The likely benefits of these systems were examined, alongside possible synthetic routes for the incorporation of cyaphide into previously established mono- and multi-metallic systems.

6.1.2 Chapter 2

This work sought to examine the relationship between cyaphide, cyanide, and acetylide, by investigating how the exchange of these fragments within a complex (C≡P *vs* C≡N *vs* C≡CH) affects their electronic structure, spectroscopic properties, and electrochemical behaviour.

It was shown that the introduction of cyaphide functionality into complexes featuring an alkynyl unit in the *trans* position greatly affected their electrochemical behaviour. Compared to the parent chloride complexes *trans*-[RuCl(C≡CAr)(dppe)$_2$] (Ar = Ph (**2.1**), *p*-An (**2.2**),C_6H_3-*3,5*-CF_3 (**2.3**)) which all exhibited reversible oxidative behaviour, the cyaphidic counterparts *trans*-[Ru(C≡P)(C≡CAr)(dppe)$_2$] (Ar = Ph (**2.7**), *p*-An (**2.8**),C_6H_3-*3,5*-CF_3 (**2.9**)) each exhibit irreversible oxidative behaviour, alongside a significant shift of their respective oxidative process to more negative potential. It was rationalised that this shift was attributable to the lower σ-withdrawing capacity of cyaphide when compared to chloride.

The analogous mixed acetylide complexes *trans*-[Ru(C≡CH)(C≡CAr)(dppe)$_2$] (Ar = Ph (**2.10**), C_6H_3-*3,5*-CF_3 (**2.10**), *p*-An (**2.12**)) were synthesised. Their electrochemical behaviour was much more dependent on the nature of the trans-alkynyl than **2.7–2.9**, with the degree of reversibility of the Ru^{II}/Ru^{III} redox couple becoming greater as the electron richness of the arene was increased. The electronic structures of **2.7–2.12** were similar, all of which exhibited classic out of phase mixing of the C≡P or C≡CH, C≡C, and arene π-systems with the metal *d*-orbitals.

The hydridic systems *trans*-[RuH(C≡E)(dppe)$_2$] (E = N (**2.13**), P (**2.14**), CH (**2.15**) allowed direct comparison of ligated cyanide, cyaphide and acetylide, the associated UV-Vis spectra of which demonstrate high energy features dominated by LLCT between the C≡E π-systems and the ancillary ligand set. Cyclic voltammetry was used to show that cyaphide behaves more like its isolobal than its isoelectronic counterpart, with an increase in the oxidative potential observed upon moving from C≡CH to C≡N *via* C≡P, which arises from either the greater metal contributions

to the HOMO of **2.13** compared to **2.14** and **2.15**, the greater electronegativity of nitrogen when compared to carbon and phosphorus, or a subtle balance of the two.

Lastly, the synthesis of the first iron(II) cyaphide complex *trans*-[FeH(C≡P)$(dppe)_2$] (**2.18**) was reported, as inferred from NMR and IR spectroscopic data in lieu of crystallographic characterisation. The electrochemical behaviour of **2.18** was similar to that reported for **2.14**, exhibiting one irreversible oxidative process with no corresponding reductive process observed at moderate scan rates, however, a greater dependency of the reversibility of this redox couple upon the experimental scan rate was observed.

6.1.3 Chapter 3

Building upon work in the previous chapter, which focussed on the synthesis of monometallic cyaphide and acetylide complex, the incorporation of one or multiple C≡P fragments into conjugated hetero- and homo-bimetallic complexes was pursued, and the electrochemical behaviour of the resulting complexes investigated.

The complex *trans*-[Ru(C≡P)(C≡CFc)$(dppe)_2$] (**3.3**) exhibited similar spectroscopic data to the monometallic cyaphide complexes described in Chapter 2, with the structure ultimately elucidated by X-ray diffraction studies. Cyclic voltammetry investigations revealed similar irreversible oxidative behaviour when compared to the conjugated monometallic systems **2.7–2.9**, alongside a shift of the anodic process corresponding to the Ru^{II}/Ru^{III} redox couple to a more negative potential.

Homobimetallic complexes featuring a 1,4-diethynylbenzene bridging motif were synthesised (**3.09**, **3.10**). While the parent chloride complex exhibited two reversible, one-electron oxidations, the corresponding phosphaalkyne complex **3.09** instead displayed two quasi-reversible processes, alongside a slight reduction in the comproportionation constant (K_c), which

is consistent with reduced stability of the transient mixed-valence species. Upon conversion to the cyaphide complex **3.10**, irreversible oxidative behaviour was observed, with a 100-fold reduction of K_c. Perfluorination of the bridging arene resulted in a shift of the Ru^{II}/Ru^{III} redox couples to more positive potentials in all three analogous systems (**3.12–3.14**), alongside a reduction of the K_c values, suggesting an increase in the insulating-nature of the bridging unit.

6.1.4 Chapter 4

Attempts to address the lack of architectural diversity in transition metal cyaphide chemistry through the synthesis of η^1-phosphaalkyne complexes based upon MCp^R and $M(dppm)_2$ scaffolds were undertaken.

Efforts to coordinate the phosphaalkyne to dppm-based systems attained mixed success, with the synthesis of *trans*-[RuH(η^1-P≡CSiMe$_3$)(dppm)$_2$]OTf (**4.1**) achieved despite the synthesis of the conjugated alkynyl system *trans*-[Ru(η^1-P≡CSiMe$_3$)(C≡CPh)(dppm)$_2$]OTf (**4.2**) remaining elusive. Reactivity of the ligated phosphaalkyne was observed, with the formation of *trans*-[RuH{P(OH)$_2$CH$_2$SiMe$_3$}{dppm}$_2$]OTf (**4.3**), as determined by X-ray crystallographic studies. Attempts to form the corresponding cyaphide complex by treatment with base were unsuccessful, which instead formed the tentatively assigned complex *trans*-[RuH{P(O^{t}Bu)CHSiMe$_3$}{dppm}$_2$] (**4.5**).

Greater success was had with the coordination of the phosphaalkyne to systems based upon the MCp^R scaffold, with the synthesis of the complexes $[MCp^R(dppe)(\eta^1\text{-P}\equiv\text{CSiMe}_3)]^+$ (**4.6**–**4.8**) achieved. The iron-based systems (**4.6** & **4.7**) exhibited reversible oxidative behaviour, with a shift in the Fe^{II}/Fe^{III} redox process to more negative potentials observed. The ruthenium complex **4.8** displayed diminished reversibility when compared to the parent chloride complex, instead displaying one quasi-reversible oxidative process consistent with the Ru^{II}/Ru^{III} redox couple at a more positive potential. The observed potential shifts suggest significant electron-

donating capacity of the phosphaalkyne fragment, resulting in these derivatives being much more easily oxidised.

Unfortunately, the desilylation of these complexes to the corresponding cyaphide complexes was found to be non-trivial. While treatment of [RuCp*(dppe)(η^1-P≡CSiMe$_3$)]OTf with KO^{t}Bu resulted in the reformation of the parent chloride complex, addition of different bases to samples of [FeCp*(dppe)(η^1-P≡CSiMe$_3$)]BPh$_4$ resulted in complex mixtures of products alongside loss of ligand, the composition of which varied with the base used, as determined by $^{31}P\{^1H\}$ NMR spectroscopy.

6.1.5 Chapter 5

Attempts to engage the complexes synthesised in Chapter 2 in reactivity with a variety of substrates, either *via* the cyaphidic phosphorus lone pair or the C≡P π-system, were undertaken. While no reactivity of *trans*-[Ru(C≡P)(C≡CPh)(dppe)$_2$] (**2.7**) was observed with BPh$_3$, some reactivity with the perfluorinated borane B(C$_6$F$_5$)$_3$ was observed, however, the product did not appear to be the expected classical adduct *trans*-[Ru{C≡P-B(C$_6$F$_5$)$_3$}{C≡CPh}{dppe}$_2$] (**5.2**) and, as a result, further investigations are required.

Mixed success was obtained with the reaction of **2.7** with chalcogens. Addition of selenium powder resulted in the formation of dppeSe$_2$ as the exclusive product, while sulfur powder resulted in a mixture of phosphorus-containing products, alongside some contamination from dppeS$_2$. The use of stoichiometric N$_2$O as a source of oxygen gave rise to several phosphorus-containing species over a period of several months, as determined by $^{31}P\{^1H\}$ NMR spectroscopic studies. However, further characterisation of these species was hindered by their inherent instability, which resulted in their eventual decomposition.

Lastly, the reactivity of **2.7** and *trans*-[Ru(C≡P)(C≡C-*p*-An)(dppe)$_2$] (**2.8**) with various halogens was investigated. While initially believed to form coordination complexes akin to the coordination of phosphanes to halogens *via* the phosphorus lone pair, it was later rationalised that addition of I_2 to samples of **2.7** or **2.8** actually resulted in rapid addition across the C≡P bond, followed by complete cleavage to give the corresponding phosphorus trihalide. Arrayed $^{31}P\{^1H\}$ NMR spectra of the reaction mixture revealed the process to be step-wise and, consequently, attempts to isolate the intermediary complexes were undertaken, though little success was reported. Possible methods to both develop this chemistry and assist in the characterisation of the complexes formed were postulated.

Chapter 7 – Experimental

7.1 General Experimental Details

7.1.1 ***General Experimental Procedures***

Unless otherwise stated, all materials were prepared and handled under an inert atmosphere of dinitrogen or argon using standard Schlenk line or glove-box techniques.

Solvents were dried by being heated under reflux under a dinitrogen atmosphere over appropriate drying agents; sodium-potassium alloy (pentane, hexane, diethyl ether), potassium (THF, toluene, benzene), calcium hydride (DCM), or $Mg(OMe)_2$ (methanol). Solvents were degassed before use and stored under argon over 4 Å molecular sieves (DCM, diethyl ether, benzene, THF), 3 Å molecular sieves (methanol) or a potassium mirror (pentane, hexane, toluene). Deuterated solvents were obtained from Goss Scientific Ltd, were degassed by freeze-pump-thawing, and heated under reflux over potassium (benzene-d_6, toluene-d_8, THF-d_8), or calcium hydride (chloroform-*d*, dichloromethane-d_2) for 72 hours before being vacuum-transferred into ampoules.

The following reagents were purchased from Sigma-Aldrich, Fisher Scientific, Fluorochem, or Acros organics, and used as supplied: AgOTf, $AgPF_6$, $B(C_6F_5)_3$, CaH_2, dppe, $[FeCp_2][PF_6]$, $HC{\equiv}CC_6H_3$-*3,5*-CF_3, $HC{\equiv}CC_6H_4$-*4*-OMe, $HC{\equiv}CC_6H_5$, KOTf, $Me_3SiC{\equiv}CC{\equiv}CSiMe_3$, $NaPF_6$, ^{n}BuLi (in hexanes, 2.5 M), PPh_3, $RuCl_3.3H_2O$, $[^nBu_4N][PF_6]$ (electrochemical grade), TBAF (in THF, 1.0 M), and TlOTf. DABCO, $[FeCp_2]$, $[FeCp^*_2]$, and KO^tBu were purified by sublimation before use. PCl_3, $Me_3SiC{\equiv}CH$, and Me_3SiCH_2Cl were distilled before use. DBU was dried over KOH for 48 hours and distilled before use.

The following reagents were synthesised following literature procedures: *cis*-$[RuCl_2(dppm)_2]$,[164] $[FeCp_2][PF_6]$,[180] [FeCp(dppe)Cl],[162] [FeCp*(dppe)Cl],[162] $HC{\equiv}CC_6F_4C{\equiv}CH$,[181] LiCp*,[162] $Me_3SiC{\equiv}P$,[182]

$PhICl_2$,[183] $[RuCl(dppe)_2][OTf]$,[71] $[RuCp(dppe)Cl]$,[162] $[RuCp^*(dppe)Cl]$,[162] $[\{Ru(dppe)_2\}_2\{\mu\text{-}(C\equiv C)_2C_6H_4\text{-}p\}Cl_2]$,[71] *trans*-$[FeHCl(dppe)_2]$,[184] *trans*-$Ru(C\equiv P)(C\equiv C\text{-}p\text{-}An)(dppe)_2]$ (**2.8**),[70] *trans*-$[RuCl(C\equiv CFc)(dppe)_2]$,[155] *trans*-$[RuCl(C\equiv CH)(dppe)_2]$,[71,132] *trans*-$[RuCl(C\equiv C\text{-}p\text{-}An)(dppe)_2]$,[71] *trans*-$[RuCl(C\equiv CPh)(dppe)_2]$,[71] *trans*-$[RuCl(C\equiv CPh)(dppm)_2]$,[164] *trans*-$[RuCl_2(dppe)_2]$,[71] *trans*-$[RuHCl(dppm)_2]$.[185] The compounds BPh_3, bromine, CuI, DIPA, DIPEA, dppm, $[FeCp(PPh_3)_2Cl]$, iodine, KF, $LiN(SiMe_3)_2$, MeCN, N_2O, $NaBH_4$, $NaBPh_4$, $NaC\equiv CH$, $NaC\equiv N$, NaOCl, NaOPh, $[PdCl_2(PPh_3)_2]$, sulfur powder, and selenium powder were readily available in the lab.

7.1.2 ***Characterisation Details***

NMR spectra were obtained using a Varian VNMRS 400 MHz (^1H 399.5 MHz; ^{19}F 375.9 MHz; ^{31}P 161.7 MHz; ^{13}C 100.5 MHz; ^{29}Si 79.4 MHz; ^{11}B 128.2 MHz), 500 MHz (^1H 499.9 MHz; ^{13}C 125.7 MHz), or 600 MHz (^1H 599.7 MHz; ^{13}C 150.8 MHz) spectrometer and referenced to external $SiMe_4$, 85% H_3PO_4, $CFCl_3$, and $BF_3.Et_2O$ as appropriate. Carbon spectra were assigned with recourse to 2D (HSQC, HMBC) spectra, silicon NMR data were obtained using 2D (HMBC) experiments, and all heteronuclear NMR spectra were ^1H-decoupled and recorded at 303 K unless otherwise stated.

UV-Vis spectra were recorded on either a Thermo Spectronic UV300 or a Perkin Elmer Lambda 265 instrument. IR spectra were recorded on a Perkin Elmer Spectrum One instrument in the solid state. Mass spectra were recorded by Dr A. Abdul-Sada of the University of Sussex departmental service, and elemental analyses were obtained by Mr S. Boyer, of the London Metropolitan University Analytical Service.

Single crystal X-ray diffraction data were collected using an Agilent Technologies Excalibur diffractometer equipped with a CCD plate detector using Cu-Kα (λ = 1.514184 Å) or Mo-Kα (λ = 0.71 Å) radiation. The data were collected at 173 K using an Oxford Cryosystems Cobra low

temperature device and were processed using CrysAlisPro.[186] Solutions were determined and refined using ShelXT[187] and ShelXL[187] respectively running under Olex2.[188]

7.1.3 ***Computational Details***

Calculations were performed using Gaussian 09W, Revision C.01,[189] running on an intel i5-2500 (quad core, 3.3 GHz) equipped with 8 GB RAM, or Gaussian 09 Revision D.01,[190] running on the University of Sussex High Performance Cluster. Results were visualised using GaussView 5.0; orbital contributions and UV-Vis spectra were calculated using GaussSum.[191]

Geometries were optimised with the B3LYP hybrid density functional, using the RECP basis set LANL2DZ for Fe and Ru, and 6-31G** for all other atoms. Stationary points were characterised by frequency calculations and confirmed as minima due to the lack of imaginary frequencies.

NBO calculations were performed at the same level of theory as the optimised structures. NMR shielding tensors were calculated using the GIAO method with either the B3LYP or PBE functional at the same level of theory as the optimised structures. Excited states were calculated using TD-DFT with the B3LYP functional, using the LANL2DZ basis set for Fe and Ru, and 3-21G* for all other atoms, in the absence of a solvent model.

7.1.4 ***Electrochemical Details***

Cyclic voltammetry studies were conducted under an N_2 atmosphere using an EmStat3$^+$ Blue potentiostat under computer control at 298 K with no compensation of the internal resistance of the solvent. Sample concentrations of 1.0 mM (DCM) were used throughout, alongside 0.1 M [^{n}Bu$_4$][PF$_6$] supporting electrolyte concentrations. All experiments were conducted using a standard three-electrode setup comprising of a platinum disc (1.6 mm) working electrode, platinum wire counter electrode, and a silver wire pseudo-reference electrode. Potentials are reported relative to the [FeCp$_2$]$^{0/+}$ redox couple through the addition of an internal standard of

either ferrocene or decamethylferrocene ($FeCp^*_2$, $E_{½}$ = −0.56V *vs* ferrocene) unless otherwise stated.

7.2 Experimental Details for Chapter 2

7.2.1 ***Synthesis of Compounds Trans-[RuCl(C≡CR)(dppe)$_2$]***

Synthesis of *Trans*-[RuCl(C≡CPh)(dppe)$_2$] (2.1)

Prepared using a modified literature procedure from [RuCl(dppe)$_2$]OTf (0.96 g, 0.9 mmol), phenylacetylene (0.20 cm^3, 2 mmol), and DBU (0.18 cm^3, 1 mmol), in DCM (10 cm^3).[70] Yield: 0.44 g, 32%

^{1}H NMR (chloroform-*d*): δ_H 7.57 [8H, m (br), *o*-C_6H_5], 7.24 [8H, m (br), o-C_6H_5], 7.17 [8H, t, J_{HH} = 7.2 Hz, C_6H_5], 7.09 [2H, t, J_{HH} = 8.0 Hz, Ph], 6.98 [17H, m, C_6H_5 & Ph], 6.69 [2H, d, J_{HH} = 8.0 Hz, Ph], 2.67 [8H, m (br), C_2H_4]

^{31}P{^{1}H} NMR (chloroform-*d*): δ_P 50.0 [s]

Synthesis of *Trans*-[RuCl(C≡C-*p*-An)(dppe)$_2$] (2.2)

Prepared using a modified literature procedure from [RuCl(dppe)$_2$]OTf (1.1 g, 1 mmol), 4-methoxyphenylacetylene (0.30 cm^3, 2 mmol), and DBU (0.10 cm^3, 1 mmol), in DCM (20 cm^3).[70] Yield: 0.411 g, 38%

^{31}H NMR (chloroform-*d*): δ_H 7.58 [8H, m (br), *o*-C_6H_5], 7.26 [8H, m (br), *o*-C_6H_5], 7.18 [8H, t, J_{HH} = 7.5 Hz, C_6H_5], 6.99 [16H, m, C_6H_5], 6.64 [4H, m, C_6H_4], 3.80 [3H, s, OCH_3], 2.68 [8H, m (br), C_2H_4]

^{31}P{^{1}H} NMR (chloroform-*d*): δ_P 49.7 [s]

Synthesis of *Trans*-[RuCl(C≡CC_6H_3-*3,5*-CF_3)(dppe)$_2$] (2.3)

To a solution of [RuCl(dppe)$_2$]OTf (1.1 g, 1 mmol) in DCM (10 cm^3), 1-ethynyl-3,5-bis(trifluoromethyl)benzene (0.36 cm^3, 2 mmol) was added, and the mixture left to stir for 16 h.

Removal of solvent afforded a light brown solid. Washed with pentane (3 x 5 cm^3) and dried. Solid was isolated, but not fully characterised.

^{31}H NMR (chloroform-*d*): δ_H 7.35 [12H, m (br), C_6H_5], 7.19 (12H, m (br), C_6H_5], 7.12 [8H, t, J_{HH} = 7.2 Hz, C_6H_5], 7.01 [8H, t, J_{HH} = 7.2 Hz, C_6H_5], 6.97 [1H, s (br), C_6H_3], 6.12 [2H, s (br), C_6H_3], 5.94 [1H,quint, J_{HH} = 2.9 Hz, Ru=C=C(H)Ar], 3.00 [8H, m (br), C_2H_4]

$^{31}P\{^1H\}$ NMR (chloroform-*d*): δ_P 33.9 [s]

^{19}F NMR (chloroform-*d*): δ_F −63.0 [s, CF_3], −78.6 [s, SO_3CF_3]

To a solution of this solid (0.73 g, 0.5 mmol) in DCM (20 cm^3), DBU (0.12 cm^3, 0.8 mmol) was added, and the mixture left to stir for 3 h. Removal of solvent under reduced pressure and subsequent washing with methanol (3 x 5 cm^3) afforded a cream-coloured solid. Yield: 0.46 g, 56%

^1H NMR (Benzene-d_6): δ_H 7.63 [8H, m (br), *o*-C_6H_5], 7.39 [1H, s, *p*-Ar^F], 7.29-7.21 [16H, m, *o*/*p*-C_6H_5],7.11 [8H, t, J_{HH} = 7.25 Hz, *m*-C_6H_5], 6.98 [8H, t, J_{HH} = 7.25 Hz, *m*-C_6H_5], 6.80 [2H, s, *o*-Ar^F], 2.71 [8H, m, J_{HH} = 7.56 Hz, C_2H_4]

$^{13}C\{^1H\}$ NMR (Benzene-d_6): δ_C 137.3 [quint, J_{CP} = 15 Hz, *ipso*-Ar^F], 136.1 [quint, J_{CP} = 10 Hz, *ipso*-C_6H_5], 135.9 [quint, J_{CP} = 10 Hz, *ipso*-C_6H_5], 134.8 [m, *o*-C_6H_5], 133.9 [m, *o*-C_6H_5], 130.5 [q, J_{CF} = 32 Hz, *m*-Ar^F], 130.2 [s (br), *o*-Ar^F], 115.2 [sept, J_{CF} = 4 Hz, *p*-Ar^F], 129.3 [s, *p*-C_6H_5], 129.1 [s, *p*-C_6H_5], 127.4 [m, *m*-C_6H_5], 124.0 [q, J_{CF} = 273 Hz, CF_3], 110.8 [s, Ru-C≡C], 30.8 [quint, J_{CP} = 11 Hz, C_2H_4]

A resonance for C_α could not be identified using standard 1D or 2D experiments.

$^{31}P\{^1H\}$ NMR (Benzene-d_6): δ_P 48.7 [4P, s, dppe]

^{19}F NMR (Benzene-d_6): δ_F −62.9 [s, CF_3]

ν_{max}/cm^{-1}: 2056 (C≡C)

Anal. Calc. ($C_{62}H_{51}F_6P_4ClRu$): C; 63.60%, H; 4.39%. Found: C; 63.47%, H; 4.21%

7.2.2 Synthesis of Compounds Trans-[Ru(η¹-P≡CSiMe₃)(C≡CR)(dppe)₂]⁺

Synthesis of *Trans*-[Ru(η¹-P≡CSiMe₃)(C≡CPh)(dppe)₂]PF₆ (2.4)

To a solution of **2.1** (0.27 g, 0.3 mmol) in DCM (15 cm^3), $AgPF_6$ (0.070 g, 0.3 mmol) in DCM (5 cm^3) was added, and the brown suspension stirred for 10 minutes. $Me_3SiC{\equiv}P$ (4.5 cm^3, 0.069 M in toluene) was then added, and the reaction mixture stirred for 1 h. The suspension was filtered, and removal of solvent under reduced pressure afforded a yellow oil. Addition and removal of DCM (5 cm^3) to azeotropically remove residual toluene afforded a yellow solid. Yield: 0.17 g, 53%

^{1}H NMR (Benzene-d_6): δ_H 7.68 [8H, m (br), *o*-C_6H_5], 7.39 [4H, t, J_{HH} = 7.3 Hz, *p*-C_6H_5], 7.33 [4H, t, J_{HH} = 7.3 Hz, *p*-C_6H_5], 7.23 [3H, m, *m*/*p*-Ph], 7.17 [8H, t, J_{HH} = 7.3 Hz, *m*-C_6H_5], 7.10-7.02 [16H, m, *o*/*m*-C_6H_5], 6.82 [2H, d, J_{HH} = 7.3 Hz, *o*-Ph], 2.86 [8H, m, J_{HH} = 8.0 Hz, C_2H_4], −0.11 [9H, s, $SiMe_3$]

^{13}C{^{1}H} NMR (Benzene-d_6): δ_C 190.0 [d, J_{CP} = 88 Hz, C≡P], 134.5 [m (br), J_{CP} = 10 Hz, *ipso*-C_6H_5], 134.2 [m, *o*-C_6H_5], 132.9 [m, *o*-C_6H_5], 131.0 [s, *p*-C_6H_5], 130.1 [m, *o*-Ph], 128.5 [m (br), *m*-C_6H_5], 128.4 [m (br), *m*-C_6H_5], 126.3 [s, Ph], 116.2 [s, Ru-C≡C], 108.6 [s, Ru-C≡C], 30.8 [quint, J_{CP} = 12 Hz, C_2H_4], 0.5 [s, $SiMe_3$]

^{31}P{^{1}H} NMR (Benzene-d_6): δ_P 111.9 [1P, quint, J_{PP} = 33.8 Hz, C≡P], 42.3 [4P, d, J_{PP} = 33.8 Hz, dppe], −144.3 [sept, J_{PF} = 712.9 Hz, PF_6]

^{29}Si{^{1}H} NMR (Benzene-d_6): δ_{Si} −13.1

ν_{max}/cm^{-1}: 1245 (C≡P), 2096 (C≡C)

Anal. Calc. ($C_{64}H_{52}F_6P_6RuSi$): C; 60.98%, H; 4.96%. Found: C; 61.09%, H; 4.97%

Crystal Data: $C_{67}H_{58}Cl_4F_3O_3P_5RuSSi$, M_w = 1426.00 g mol^{-1}, monoclinic, $P2_1/c$ (No. 14), a = 12.9939(2) Å, b = 38.3986(3) Å, c = 14.8153(2) Å, α = 90, β = 115.360(2), γ = 90 °, V = 6679.12(18) $Å^3$, Z = 4. D_c = 1.418 Mg m^{-3}, μ(Cu-Kα) = 5.405 mm^{-1}, T = 173 K, 44873 independent reflections.

Full-matrix F^2 refinement. R_1 = 0.0488, wR_2 = 0.1267 on 12810 independent absorption corrected reflections [I>2σ(I); 2θmax = 142.462 °], 769 parameters.

Synthesis of *Trans*-[Ru(η^1-P≡CSiMe$_3$)(C≡C-*p*-An)(dppe)$_2$]PF$_6$ (2.5)

Prepared in a similar fashion to that described for **2.4**, from **2.2** (0.30 g, 0.3 mmol), $AgPF_6$ (0.080 g, 0.3 mmol), and $Me_3SiC{\equiv}P$ (6.0 cm^3, 0.065 M in toluene) in DCM (15 cm^3). Afforded a brown solid. Yield: 0.19 g, 54%

^{1}H NMR (Benzene-d_6): δ_H 7.68 [8H, m (br), C_6H_5], 7.36 [8H, dt, J_{HP} = 20.6 Hz, J_{HH} = 7.4 Hz, C_6H_5], 7.17 [8H, t, J_{HH} = 7.4 Hz, C_6H_5], 7.06 [16H, m, C_6H_5], 6.78 [4H, m, C_6H_4], 3.83 [3H, s, CH_3], 2.85 [8H, m, J_{HP} = 8.5 Hz, C_2H_4], −0.11 [9H, s, $SiMe_3$]

^{13}C{^{1}H} NMR (Benzene-d_6): δ_C 188.4 [d, J_{CP} = 87 Hz, C≡P], 158.2 [s, *p*-C_6H_4], 134.6 [quint, J_{CP} = 11 Hz, *ipso*-C_6H_5], 134.2 [m (br), J_{CP} = 2 Hz, C_6H_5], 132.9 [m (br), J_{CP} = 2 Hz, C_6H_5], 131.4 [m (br), *o*-C_6H_4], 131.0 [s, C_6H_5], 128.6 [m (br), J_{CP} = 2 Hz, C_6H_5], 128.4 [m (br), J_{CP} = 2 Hz, C_6H_5], 119.6 [m (br), *ipso*-C_6H_4], 115.9 [m (br), Ru-C≡C], 114.0 [s, *m*-C_6H_4], 55.5 [s, CH_3], 30.8 [quint, J_{CP} = 12 Hz, C_2H_4], 0.5 [s, $SiMe_3$]

A resonance for C_α could not be identified using standard 1D or 2D experiments.

^{31}P{^{1}H} NMR (Benzene-d_6): δ_P 112.7 [quint, J_{PP} = 32.9 Hz, CP], 42.2 [d, J_{PP} = 32.9 Hz, dppe], −144.3 [sept, J_{PF} = 711.5 Hz, PF_6]

^{29}Si NMR (Benzene-d_6): δ_{Si} −13.3

ν_{max}/cm^{-1}: 1244 (C≡P), 2102 (C≡C)

Anal. Calc. ($C_{65}H_{64}F_6P_6OSiRu$): C; 60.49%, H; 5.00%. Found: C; 60.58%, H; 5.01%

Synthesis of *Trans*-[Ru(η^1-P≡CSiMe$_3$)(C≡CC$_6$H$_3$-3,5-CF$_3$)(dppe)$_2$]PF$_6$ (2.6)

Prepared in a similar fashion to that described for **2.4**, from **2.3** (0.22 g, 0.2 mmol), $AgPF_6$ (0.062 g, 0.3 mmol), and $Me_3SiC{\equiv}P$ (6.0 cm^3, 0.042 M in toluene) in DCM (15 cm^3). Afforded a yellow solid. Yield: 0.11 g, 44%

^{1}H NMR (Benzene-d_6): δ_H 7.67 [1H, s, *p*-Ar^F], 7.47 [12H, m, *o*/*p*-C_6H_5], 7.39 [4H, t, J_{HH} = 7.4 Hz, *p*-C_6H_5], 7.24 [8H, t, J_{HH} = 7.4 Hz, *m*-C_6H_5], 7.10 [8H, t, J_{HH} = 7.4 Hz, *m*-C_6H_5], 7.19 [8H, m (br), *o*-C_6H_5], 6.99 [2H, s, *o*-Ar^F], 2.83 [8H, m (br), C_2H_4], −0.05 [9H, s, $SiMe_3$]

^{13}C{^{1}H} NMR (Benzene-d_6): δ_C 191.2 [d, J_{CP} = 89 Hz, C≡P], 134.1 [m (br), *ipso*-Ar^F], 133.7 [m, *o*-C_6H_5], 133.0 [m, *o*-C_6H_5], 132.0 [quint, J_{CP} = 11 Hz, *ipso*-C_6H_5], 131.2 [s, *p*-C_6H_5], 131.5 [q, J_{CF} = 32 Hz, *m*-Ar^F], 131.1 [s, *p*-C_6H_5], 130.2 [m (br), *o*-Ar^F], 128.7 [m, *m*-C_6H_5], 128.4 [m, *m*-C_6H_5], 123.4 [q, J_{CF} = 272 Hz, CF_3], 119.0 [m (br), *p*-Ar^F], 112.3 [dm, J_{CP} = 26 Hz, Ru-C≡C], 105.5 [m (br), Ru-C≡C], 30.2 [quint, J_{CP} = 11 Hz, C_2H_4], 0.4 [s, $SiMe_3$]

^{31}P{^{1}H} NMR (Benzene-d_6): δ_P 108.8 [quint, J_{PP} = 32.2 Hz, C≡P], 41.6 [d, J_{PP} = 32.2 Hz, dppe], −144.5 [sept, J_{PF} = 712.4 Hz, PF_6]

^{19}F NMR (Benzene-d_6): δ_F −63.3 [s, CF_3], −73.4 [d, J_{FP} = 712.4 Hz, PF_6]

^{29}Si{^{1}H} NMR (Benzene-d_6): δ_{Si} −12.5

ν_{max}/cm^{-1}: 1276 (C≡P), 2085 (C≡C)

7.2.3 Synthesis of Compounds Trans-[Ru(C≡P)(C≡CR)(dppe)$_2$]

Synthesis of *Trans*-[Ru(C≡P)(C≡CPh)(dppe)$_2$] (2.7)

To a mixture of **2.4** (0.12 g, 0.1 mmol) and KO^{t}Bu (0.011 g, 0.1 mmol), THF (10 cm^3) was added, and the mixture stirred for 1 h. Filtration followed by removal of solvent under reduced pressure afforded a pale orange solid. Yield: 0.063 g, 60%

^{1}H NMR (DCM-d_2): δ_H 7.60 [8H, m (br), *o*-C_6H_5], 7.53 [8H, m (br), *o*-C_6H_5], 7.45 [2H, m (br), *m*-Ph], 7.27 [4H, t, J_{HH} = 7.5 Hz, *p*-C_6H_5], 7.20 [4H, t, J_{HH} = 7.5 Hz, *p*-C_6H_5], 7.12 [1H, s, *p*-Ph], 7.08 [8H, t, J_{HH} = 6.9 Hz, *m*-C_6H_5], 6.97 [8H, t, J_{HH} = 6.9 Hz, *m*-C_6H_5], 6.75 [2H, d, J_{HH} = 7.5 Hz, *o*-Ph], 2.78 [8H, dm (br), J_{HP} = 94.5 Hz, C_2H_4]

^{13}C{^{1}H} NMR (DCM-d_2): δ_C 281.5 [m (br), C≡P], 137.8 [m, J_{CP} = 10 Hz, *ipso*-C_6H_5], 136.1 [m, J_{CP} = 10 Hz, *ipso*-C_6H_5], 135.4, [m, *o*-C_6H_5], 135.2 [m (br), *ipso*-Ph], 135.0 [m, *o*-C_6H_5], 134.7 [m (br), *m*-Ph], 130.4 [s (br), *o*-Ph], 129.6 [s (br), *p*-C_6H_5], 129.4 [s (br), *p*-C_6H_5], 128.1 [s (br), *p*-Ph], 127.6 [m (br), *m*-C_6H_5], 127.4 [m (br), *m*-C_6H_5], 123.9 [s, Ru-C≡C], 119.8 [s (br), Ru-C≡C], 31.7 [quint, J_{CP} = 12 Hz, C_2H_4]

^{31}P{^{1}H} NMR (DCM-d_2): δ_P 160.4 [1P, m (br), C≡P], 50.8 [4P, d (br), J_{PP} = 3.5 Hz, dppe]

ν_{max}/cm^{-1}: 1242 (C≡P), 2067 (C≡C)

Anal. Calc. ($C_{61}H_{53}P_5Ru$): C; 70.31%, H; 5.13%. Found: C; 70.19%, H; 5.06%

Crystal Data: $C_{62}H_{55}Cl_2P_5Ru$, M_w = 1134.88 g mol^{-1}, triclinic, P-1 (No. 2), *a* = 10.2592(4) Å, *b* = 13.0699(8) Å, *c* = 23.3910(9) Å, *α* = 100.095(4), *β* = 97.961(3), *γ* = 107.703(4) °, *V* = 2879.5(2) Å^3, Z = 2. D_c = 1.309 Mg m^{-3}, μ(Cu-Kα) = 4.663 mm^{-1}, *T* = 173 K, 15954 independent reflections. Full-matrix F^2 refinement. R_1 = 0.1041, wR_2 = 0.3007 on 10668 independent absorption corrected reflections [I>2σ(I); 2θmax = 142.428 °], 632 parameters.

Synthesis of *Trans*-[Ru(C≡P)(C≡CC_6H_3-3,5-CF_3)(dppe)$_2$] (2.9)

Prepared in a fashion similar to that described for **2.7**, from **2.6** (0.11 g, 0.1 mmol), and KO^{t}Bu (0.015 g, 0.1 mmol) in THF (10 cm^3). Afforded an orange solid. Yield: 0.039 g, 41%

^{1}H NMR (DCM-d_2): δ_H 7.88 [8H, m (br), *o*-C_6H_5], 7.41 [1H, s, *p*-Ar^F], 7.32 [4H, t, J_{HH} = 7.6 Hz, *p*-C_6H_5], 7.21 [8H, m (br), *o*-C_6H_5], 7.16 [12H, m, m/*p*-C_6H_5], 6.92 [8H, t, J_{HH} = 8.1 Hz, *m*-C_6H_5], 6.84 [2H, s, *o*-Ar^F], 2.85 [8H, dm (br), J_{HP} = 56.2 Hz, C_2H_4]

$^{13}C\{^{1}H\}$ NMR (DCM-d_2): δ_C 280.1 [m (br), C≡P], 137.0 [quint, J_{CP} = 10 Hz, *ipso*-C_6H_5], 136.3 [quint, J_{CP} = 10 Hz, *ipso*-C_6H_5], 135.7 [m, *o*-C_6H_5], 134.6 [m (br), *ipso*-Ar^F], 134.4 [m, *o*-C_6H_5], 130.1 [s, *p*-C_6H_5], 130.9 [quart, J_{CF} = 33 Hz, *m*-Ar^F], 130.5 [s (br) *o*-Ar^F], 129.5 [s, *p*-C_6H_5], 127.8 [m (br), *m*-C_6H_5], 127.6 [m (br), *m*-C_6H_5], 124.5 [quart, J_{CF} = 273 Hz, CF_3], 123.1 [s, Ru-C≡C], 116.3 [m (br), *p*-Ar^F], 31.6 [quint, J_{CP} = 12 Hz, C_2H_4]

A resonance for C_α could not be identified using standard 1D or 2D experiments.

$^{31}P\{^{1}H\}$ NMR (DCM-d_2): δ_P 172.9 [1P, m (br), C≡P], 50.9 [4P, d (br), J_{PP} = 4.6 Hz, dppe]

^{19}F NMR (DCM-d_2): δ_F −63.2 [s, CF_3]

ν_{max}/cm^{-1}: 1275 (C≡P), 2055 (C≡C)

*7.2.4 **Synthesis of Compounds Trans-[Ru(C≡CH)(C≡CR)(dppe)$_2$]***

Synthesis of *Trans*-[Ru(C≡CH)(C≡CPh)(dppe)$_2$] (2.10)

To a mixture of **2.1** (0.40 g, 0.4 mmol) and AgOTf (0.11 g, 0.4 mmol), DCM (10 cm^3) was added, and the forest-green suspension stirred for 10 minutes. $Me_3SiC{\equiv}CH$ (0.10 cm^3, 0.7 mmol) was added, and the mixture stirred for 2 h. before being filtered, and the solvent removed under reduced pressure to afford a copper-coloured solid. Washed with pentane (3 x 5 cm^3) and dried. Solid was isolated but not fully characterised.

^{1}H NMR (chloroform-*d*): δ_H 7.77 [8H, m (br), *o*-C_6H_5], 7.37 [4H, t, J_{HH} = 7.2 Hz, *p*-C_6H_5], 7.33 [4H, t, J_{HH} = 7.2 Hz, *p*-C_6H_5], 7.28 [1H, s, Ph], 7.16 [8H, t, J_{HH} = 7.2 Hz, *m*-C_6H_5], 7.09 [10H, t, J_{HH} = 7.2 Hz, *m*-C_6H_5 & Ph], 6.94 [8H, m (br), *o*-C_6H_5], 6.71 [2H, m (br), Ph], 2.87 [8H, m (br), C_2H_4], 2.79 [2H, m (br), $Ru{=}C{=}CH_2$]

$^{31}P\{^{1}H\}$ NMR (chloroform-*d*): δ_P 46.8 [s, dppe]

To a solution of this solid (0.22 g, 0.2 mmol) in DCM (10 cm^3), DBU (0.12 cm^3, 0.8 mmol) was added, and the brown suspension left to stir for 3 h. Removal of solvent under reduced pressure, followed by washing with methanol (3 x 5 cm^3) afforded a light brown solid. Yield: 0.11 g, 52%

^{1}H NMR (DCM-d_2): δ_H 7.67 [8H, m (br), *m*-C_6H_5], 7.38 [8H, m (br), *m*-C_6H_5], 7.29 [1H, m (br), *p*-Ph], 7.19 [4H, t, J_{HH} = 7.5 Hz, *p*-C_6H_5], 7.14 [4H, t, J_{HH} = 7.5 Hz, *p*-C_6H_5], 7.10 [2H, m, *m*-Ph], 6.98 [16H, dt, J_{HP} = 45.0 Hz, J_{HH} = 7.48 Hz, *o*-C_6H_5], 6.72 [2H, d, J_{HH} = 7.5 Hz, *o*-Ph], 2.67 [8H, m, C_2H_4], 1.63 [1H, m (br), J_{HP} = 1.7 Hz, C≡C-H]

^{13}C{^{1}H} NMR (DCM-d_2): δ_C 137.9 [m, *ipso*-C_6H_5], 135.4 [quint, J_{CP} = 3 Hz, *m*-C_6H_5],135.0 [m, *p*-Ph], 134.7 [quint, J_{CP} = 3 Hz, *m*-C_6H_5], 130.6 [m (br), *m*-Ph], 129.4 [s, *p*-C_6H_5], 129.0 [s, *p*-C_6H_5], 128.0 [s, *o*-Ph], 127.5 [quint, J_{CP} = 2 Hz, *o*-C_6H_5], 127.4 [m (br), *ipso*-Ph], 127.2 [quint, J_{CP} = 2 Hz, *o*-C_6H_5], 123.3 [s, Ru-C≡C-Ph], 121.5 [quint, J_{CP} = 15 Hz, Ru-C≡C-H], 116.1 [m (br), Ru-C≡C-Ph], 103.9 [s, Ru-C≡C-H], 32.1 [quint, J_{CP} = 12 Hz, C_2H_4]

^{31}P{^{1}H} NMR (DCM-d_2): δ_P 52.9 [s, dppe]

ν_{max}/cm^{-1}: 1925 (C≡C), 2064 (C≡C)

Crystal Data: $C_{62}H_{54}P_4Ru$, M_w = 1049.72 g mol^{-1}, triclinic, P-1 (No. 2), *a* = 10.0890(5) Å, *b* = 12.5674(7) Å, *c* = 21.5240(11) Å, *α* = 80.986(4), *β* = 80.896(4)), *γ* = 71.851(5) °, *V* = 2543.8(2) $Å^3$, Z = 2. D_c = 1.370 Mg m^{-3}, μ(Mo-Kα) = 0.502 mm^{-1}, *T* = 173 K, 22614 independent reflections. Full-matrix F^2 refinement. R_1 = 0.0435, wR_2 = 0.0939 on 11860 independent absorption corrected reflections [I>2σ(I); 2θmax = 59.068 °], 604 parameters.

Synthesis of *Trans*-[Ru(C≡CH)(C≡CC_6H_3-3,5-CF_3)(dppe)$_2$] (2.11)

Prepared in a fashion similar to that described for **2.10**, from **2.3** (0.45 g, 0.04 mmol), AgOTf (0.11 g, 0.04 mmol), Me_3SiC≡CH (70 μL, 0.5 mmol), and DBU (0.11 cm^3, 0.07 mmol) in DCM (20 cm^3). Afforded a khaki-coloured solid. Yield: 0.054 g, 30%

^{1}H NMR (DCM-d_2): δ_H 7.99 [8H, m (br), *o*-C_6H_5], 7.38 [1H, s, *p*-Ar^F], 7.16 [4H, t, J_{HH} = 6.9 Hz, *p*-C_6H_5], 7.06 [8H, m (br), *o*-C_6H_5], 6.90 [8H, t, J_{HH} = 7.5 Hz, *m*-C_6H_5], 6.85 [2H, s, *o*-Ar^F], 2.64 [8H, m (br), C_2H_4], 1.92 [1H, s, C≡CH]

^{13}C{^{1}H} NMR (DCM-d_2): δ_C 138.0 [quint, J_{CP} = 10 Hz, *ipso*-C_6H_5], 137.3 [quint, J_{CP} = 10 Hz, *ipso*-C_6H_5], 135.7 [m, J_{CP} = 3 Hz, *o*-C_6H_5], 134.6 [m (br), *ipso*-Ar^F], 134.2 [m, J_{CP} = 3 Hz, *o*-C_6H_5], 130.8 [q, J_{CF} = 32 Hz, *m*-Ar^F], 130.6 [s (br), *o*-Ar^F], 129.8 [s, *p*-C_6H_5], 129.1 [s, *p*-C_6H_5], 127.6 [m, J_{CP} = 2 Hz, *m*-C_6H_5], 127.4 [m, J_{CP} = 2 Hz, *m*-C_6H_5], 124.6 [q, J_{CF} = 272 Hz, CF_3], 120.0 [quint, J_{CP} = 17 Hz, Ru-C≡CH], 115.6 [m, J_{CF} = 4 Hz, *p*-Ar^F], 115.6 [quint, J_{CP} = 4 Hz, Ru-C≡C-Ar], 112.9 [s, Ru-C≡CH], 105.9 [s, Ru-C≡C-Ar], 32.0 [quint, J_{CP} = 13 Hz, C_2H_4]

^{31}P{^{1}H} NMR (DCM-d_2): δ_P 53.2 [s, dppe]

^{19}F NMR (DCM-d_2): δ_F −63.1

ν_{max}/cm^{-1}: 2055 (C≡C), 1923 (C≡C)

Anal. Calc. ($C_{65}H_{56}F_6P_4Ru$): C; 66.36%, H; 4.80%. Found: C; 66.29%, H; 4.73%

Crystal Data: $C_{64}H_{52}F_6P_4Ru$, M_w = 1160.00 g mol^{-1}, triclinic, P-1 (No. 2), *a* = 10.0883(5) Å, *b* = 12.6943(7) Å, *c* = 22.0130(6) Å, *α* = 85.947(3), *β* = 87.584(3), *γ* = 71.080(5) °, *V* = 2659.5(2) Å^3, Z = 2. D_c = 1.449 Mg m^{-3}, μ(Cu-Kα) = 4.085 mm^{-1}, *T* = 173 K, 16416 independent reflections. Full-matrix F^2 refinement. R_1 = 0.0529, wR_2 = 0.1480 on 10122 independent absorption corrected reflections [I>2σ(I); 2θmax = 143.744 °], 732 parameters.

Synthesis of *Trans*-[Ru(C≡CH)(C≡C-*p*-An)(dppe)$_2$] (2.12)

To a mixture of *trans*-[RuCl(C≡CH)(dppe)$_2$] (0.21 g, 0.2 mmol) and AgOTf (0.065 g, 0.2 mmol), DCM (10 cm^3) was added, and the turquoise mixture stirred for 10 minutes. To this, 4-methoxyphenylacetylene (0.10 cm^3, 0.8 mmol) was added, and the mixture stirred for 2 h. Filtration and removal of solvent under reduced pressure afforded a moss-green solid. Washed with hexane (3 x 5 cm^3) and dried. Solid was isolated but not fully characterised.

^{1}H NMR (chloroform-*d*): δ_H 7.74 [8H, m (br), *o*-C_6H_5], 7.37 [4H, t, J_{HH} = 7.2 Hz, *p*-C_6H_5], 7.32 [4H, t, J_{HH} = 7.2 Hz, *p*-C_6H_5], 7.16 [8H, t, J_{HH} = 7.2 Hz, *m*-C_6H_5], 7.08 [8H, t, J_{HH} = 7.2 Hz, *m*-C_6H_5], 6.94 [8H, m (br), *o*-C_6H_5], 6.83 [4H, m, C_6H_4], 3.85 [3H, s, OCH_3], 2.85 [8H, m (br), J_{HH} = 8.7 Hz, C_2H_4), 2.74 [2H, quint, J_{HH} = 2.7 Hz, Ru=C=CH_2].

^{31}P{^{1}H} NMR (chloroform-*d*): δ_P 46.6 [s]

To a solution of this solid (0.24 g, 0.2 mmol) in DCM (10 cm^3), DBU (0.60 cm^3, 4 mmol) was added, and the green suspension left to stir for 3 h. Removal of solvent under reduced pressure and subsequent washing with methanol (4 x 2 cm^3) afforded a pale-yellow solid. Yield: 0.11 g, 53%

^{1}H NMR (DCM-d_2): δ_H 7.68 [8H, m (br), *o*-C_6H_5], 7.39 [8H, m (br), *o*-C_6H_5], 7.19 [8H, dt, J_{HP} = 26.7 Hz, J_{HH} = 7.4 Hz, *p*-C_6H_5], 7.04 [8H, t, J_{HH} = 7.8 Hz, *m*-C_6H_5], 6.92 [8H, t, J_{HH} = 7.8 Hz, *m*-C_6H_5], 6.67 [4H, m, C_6H_4], 3.78 [3H, s, CH_3], 2.66 [8H, m (br), J_{HP} = 8.4 Hz, C_2H_4], 1.62 [1H, s, C≡CH]

^{13}C{^{1}H} NMR (DCM-d_2): δ_C 156.5 [s, *p*-C_6H_4], 138.1 [m, *ipso*-C_6H_5], 135.4 [m, J_{CP} = 3 Hz, *o*-C_6H_5], 134.8 [m, J_{CP} = 3 Hz, *o*-C_6H_5], 131.4 [s, C_6H_4], 129.3 [s, *p*-C_6H_5], 129.0 [s, *p*-C_6H_5], 127.5 [m, J_{CP} = 2 Hz, *m*-C_6H_5], 127.2 [m, J_{CP} = 2 Hz, *m*-C_6H_5], 124.3 [m (br), Ru-C≡C-Ar], 121.7 [t, J_{CP} = 15 Hz, Ru-C≡CH], 115.1 [s, Ru-C≡C-Ar], 113.6 [s, C_6H_4], 103.7 [s, Ru-C≡CH], 55.7 [s, CH_3], 32.1 [quint, J_{CP} = 12 Hz, C_2H_4]

A resonance for the *ipso* carbon of the *p*-anisole ring could not be identified by standard 1D or 2D experiments.

^{31}P{^{1}H} NMR (DCM-d_2): δ_P 53.0 [s, dppe]

ν_{max}/cm^{-1}: 2072 (C≡C), 1923 (C≡C)

Crystal Data: $C_{64}H_{56}Cl_2OP_4Ru$, M_w = 1136.93 g mol^{-1}, triclinic, P-1 (No. 2), *a* = 9.2584(4) Å, *b* = 12.9223(4) Å, *c* = 24.2666(13) Å, *α* = 92.921(3), *β* = 96.145(4), *γ* = 99.128(3) °, *V* = 2843.2(2) $Å^3$, Z = 2. D_c = 1.328 Mg m^{-3}, μ(Cu-Kα) = 4.473 mm^{-1}, *T* = 173 K, 11927 independent reflections. Full-

matrix F^2 refinement. R_1 = 0.1000, wR_2 = 0.3097 on 8555 independent absorption corrected reflections [I>2σ(I); 2θmax = 142.67 °], 651 parameters.

7.2.5 Attempted Synthesis of Trans-[Ru(C≡N)(C≡CPh)(dppe)$_2$]

Attempted Synthesis of *Trans*-[Ru(C≡N)(C≡CPh)(dppe)$_2$]

Method A: To a mixture of **2.1** (0.10 g, 0.1 mmol) and sodium cyanide (0.011 g, 0.2 mmol), methanol (10 cm^3) was added, and the suspension left to stir for 16 h. Filtration and washing with methanol (3 x 2 cm^3) afforded a pale-yellow solid.

Method B: Prepared in a similar fashion to that reported for **Method A**, from **2.1** (0.076 g, 0.07 mmol), and sodium cyanide (0.012 g, 0.2 mmol) in THF (10 cm^3) and DCM (5 cm^3). A pale-yellow solid was afforded.

NMR spectroscopic data showed no change from the starting material, 2.1.

7.2.6 Synthesis of Compounds Trans-[RuH(R')(dppe)$_2$]

Synthesis of *Trans*-[RuH(C≡CH)(dppe)$_2$] (2.15)

To a mixture of *trans*-[RuHCl(dppe)$_2$] (0.14 g, 0.2 mmol) and sodium acetylide (0.075 g, 2 mmol), methanol (10 cm^3) was added, and the mixture left to stir for one month. Filtration and subsequent washing with methanol (3 x 2 cm^3) afforded a pale-yellow solid.

^{1}H NMR (THF-d_8): δ_H 7.57 [8H, m (br), *o*-C_6H_5], 7.40 [8H, m (br), *o*-C_6H_5], 7.08 [8H, m, *p*-C_6H_5], 6.96 [16H, m, *m*-C_6H_5], 2.58 [4H, m (br), C_2H_4], 2.06 [4H, m (br), C_2H_4], 1.75 [1H, s, C≡CH], −10.77 [1H, quint, J_{HP} = 19.8 Hz, Ru-H]

^{13}C{^{1}H} NMR (THF-d_8): δ_C 140.7 [quint, J_{CP} = 14 Hz, *ipso*-C_6H_5], 139.1 [quint, J_{CP} = 14 Hz, *ipso*-C_6H_5], 135.2 [m, J_{CP} = 3 Hz, *o*-C_6H_5], 134.5 [m, J_{CP} = 3 Hz, *o*-C_6H_5], 129.1 [s, *p*-C_6H_5], 128.9 [s, *p*-C_6H_5], 127.7 [m, J_{CP} = 2 Hz, *m*-C_6H_5], 127.3 [m, J_{CP} = 2 Hz, *m*-C_6H_5], 122.9 [quint, J_{CP} = 14 Hz, Ru-C≡C], 101.4 [s, Ru-C≡C], 33.8 [quint, J_{CP} = 12 Hz, C_2H_4]

$^{31}P\{^{1}H\}$ NMR (THF-d_8): δ_P 69.4 [d (br), J_{PH} = 3.0 Hz dppe]

ν_{max}/cm^{-1}: 2070 (C≡C)

Synthesis of *Trans*-[RuH(C≡CCH$_2$Cl)(dppe)$_2$] (2.16)

To a solution of *trans*-[RuCl(C≡CH)(dppe)$_2$] (0.097 g, 0.1 mmol) in DCM (10 cm^3), KO^{t}Bu (0.013 g, 0.1 mmol) in methanol (5 cm^3) was added, and the yellow suspension left to stir for 1h. Removal of the DCM under reduced pressure afforded a yellow precipitate, which was collected by filtration, and washed with methanol (3 x 2 cm^3).

^{1}H NMR (DCM-d_2): δ_H 7.46 [8H, m (br), C_6H_5], 7.33 [8H, m (br), C_6H_5], 7.17 [4H, m, *p*-C_6H_5], 7.14 [4H, m, *p*-C_6H_5], 7.03 [16H, m, C_6H_5], 4.15 [2H, d (br), J_{HH} = 5.2 Hz, CH_2Cl], 2.55 [4H, m (br), C_2H_4], 1.99 [4H, m (br), C_2H_4], −10.46 [1H, quint, J_{HH} = 19.5 Hz, Ru-H]

$^{13}C\{^{1}H\}$ NMR (Benzene-d_6): δ_C 139.8 [quint, J_{CP} = 10 Hz, *ipso*-C_6H_5], 138.3 [quint, J_{CP} = 10 Hz, *ipso*-C_6H_5], 134.5 [m, J_{CP} = 3 Hz, *o*-C_6H_5], 134.2 [m, J_{CP} = 3 Hz, *o*-C_6H_5], 128.8 [s, *p*-C_6H_5], 127.4 [s, *p*-C_6H_5], 127.4 [m, *m*-C_6H_5], 127.1 [m, *m*-C_6H_5], 123.0 [quint, J_{CP} = 13 Hz, Ru-C≡C], 112.8 [s, Ru-C≡C], 55.2 [s, CH_2Cl], 33.2 [quint, J_{CP} = 13 Hz, C_2H_4]

$^{31}P\{^{1}H\}$ NMR (DCM-d_2): δ_P 68.4 [s, dppe]

ν_{max}/cm^{-1}: 2072 (C≡C)

7.2.7 Synthesis of Trans-[FeH(η^1-P≡CSiMe$_3$)(dppe)$_2$]OTf

Synthesis of *Trans*-[FeH(η^1-P≡CSiMe$_3$)(dppe)$_2$]OTf (2.17)

Method A: To a mixture of *trans*-[FeHCl(dppe)$_2$] (0.10 g, 0.1 mmol) and KOTf (0.026 g, 0.1 mmol), DCM (10 cm^3) was added, and the mixture stirred for 15 minutes. $Me_3SiC{\equiv}P$ (4.0 cm^3, 0.054 M in toluene) was added, and the mixture left to stir for 16 h. The solvent was removed under reduced pressure, and the product extracted with DCM (3 x 5 cm^3). Removal of solvent afforded an orange solid.

Method B: Synthesised in a similar fashion to that described for **Method A**, from *trans*-[FeHCl(dppe)$_2$] (0.22 g, 0.2 mmol), TlOTf (0.089 g, 0.2 mmol), and $Me_3SiC{\equiv}P$ (4.5 cm^3, 0.099 M in toluene) in DCM (15 cm^3). Afforded a yellow solid. Yield: 0.071 g, 30%

^{1}H NMR (THF-d_8): δ_H 7.80 [4H, m (br), *p*-C_6H_5], 7.58 [8H, br, *o*-C_6H_5], 7.35 [4H, m (br), *p*-C_6H_5], 7.30 [8H, br, *o*-C_6H_5], 7.17 [8H, m (br), *m*-C_6H_5], 7.13 [8H, m (br), *m*-C_6H_5], 2.73 [4H, m (br), C_2H_4], 2.38 [4H, m (br), C_2H_4], 0.10 [9H, s, $SiMe_3$], −10.45 [1H, dquint, J_{HP} = 52.4 Hz, Ru-H]

^{13}C{^{1}H} NMR (THF-d_8): δ_C 189.9 [d, J_{CP} = 80 Hz, C≡P], 137.2 [quint, J_{CP} = 10 Hz, *ipso*-C_6H_5], 135.0 [m, *o*-C_6H_5], 134.4 [m, *o*-C_6H_5], 131.3 [s, *p*-C_6H_5], 131.1 [s, *p*-C_6H_5], 129.5 [m (br), *m*-C_6H_5], 128.8 [m (br), *m*-C_6H_5], 34.6 [quint, J_{CP} = 12 Hz, C_2H_4], 1.1 [s (br), $SiMe_3$]

^{31}P{^{1}H} NMR (THF-d_8): δ_P 158.7 [1P, quint, J_{PP} = 34.5 Hz, C≡P], 80.0 [4P, d, J_{PP} = 34.5 Hz, dppe]

^{29}Si{^{1}H} NMR (THF-d_8): δ_{Si} −15.9

ν_{max}/cm^{-1}: 1262 (C≡P)

Crystal Data: $C_{57}H_{57}F_3FeO_3P_4S_2Si$, M_w = 1118.96 g mol^{-1}, monoclinic, $P2_1$ (No. 4), a = 11.0277(4) Å, b = 17.3205(6) Å, c = 14.4468(5) Å, α = 90, β = 97.063(3), γ = 90 °, V = 2738.47(17) Å^3, Z = 2. D_c = 1.357 Mg m^{-3}, μ(Cu-Kα) = 4.674 mm^{-1}, T = 173 K, 24555 independent reflections. Full-matrix F^2 refinement. R_1 = 0.0655, wR_2 = 0.1190 on 9713 independent absorption corrected reflections [I>2σ(I); 2θmax = 136.522 °], 647 parameters.

7.2.8 Synthesis of Trans-[FeH(C≡P)(dppe)$_2$] (2.18)

Synthesis of *Trans*-[FeH(C≡P)(dppe)$_2$] (2.18)

Method A: To a mixture of **2.17** (0.071 g, 0.06 mmol) and KO^{t}Bu (0.013 g, 0.1 mmol), THF (10 cm^3) was added, and the mixture stirred for 1 h. Removal of solvent afforded a brick-red solid. NMR spectroscopic data were unassignable, due to the formation of an intractable mixture of products, which contained paramagnetic complexes.

Method B: To a mixture of **2.17** (0.086 g, 0.08 mmol) and NaOPh (0.011 g, 0.1 mmol), THF (10 cm^3) was added, and the mixture left to stir for 24 h. Removal of solvent under reduced pressure afforded an orange solid. Washed with acetonitrile (2 x 3 cm^3) and dried.

^{1}H NMR (THF-d_8): δ_H 7.57 [8H, m (br), C_6H_5], 7.42 [8H, m (br), C_6H_5], 7.12 [12H, m (br), C_6H_5], 6.93 [8H, m (br), C_6H_5], 6.81 [4H, m (br), *p*-C_6H_5], 2.84 [4H, m, C_2H_4], 2.05 [4H, m, C_2H_4], −14.46 [1H, m, Ru-H]

^{13}C{^{1}H} NMR (THF-d_8): δ_C 140.7 [quint, J_{CP} = 7 Hz, *ipso*-C_6H_5], 138.7 [quint, J_{CP} = 7 Hz, *ipso*-C_6H_5], 135.6 [s (br), *o*-C_6H_5], 134.8 [s (br), *o*-C_6H_5], 129.2 [m, *p*-C_6H_5], 127.7 [m (br), *m*-C_6H_5], 127.2 [m (br), *m*-C_6H_5], 33.8 [quint, J_{CP} = 11 Hz, C_2H_4]

A cyaphidic carbon resonance could not be assigned using standard 1D or 2D experiments.

^{31}P{^{1}H} NMR (THF-d_8): δ_P 201.6 [1P, m, C≡P], 85.3 [4P, s (br), dppe]

ν_{max}/cm^{-1}: 1246 (C≡P)

*7.2.9 **Synthesis of Trans-[RuH(η^1-P≡CSiMe$_3$)(dppe)$_2$]PF$_6$***

Synthesis of *Trans*-[RuH(η^1-P≡CSiMe$_3$)(dppe)$_2$]PF$_6$ (2.19)

To a solution of *trans*-[RuHCl(dppe)$_2$] (0.19 g, 0.2 mmol) in DCM (10 cm^3), $AgPF_6$ (0.055 g, 0.2 mmol) in DCM (5 cm^3) was added, and the red suspension left to stir for 10 minutes. $Me_3SiC{\equiv}P$ (3.0 cm^3, 0.069 M in toluene) was then added, and the mixture left to stir for 90 minutes. Filtration and subsequent removal of solvent afforded an orange oil. Addition and removal of DCM (5 cm^3) to azeotropically remove residual toluene afforded a pale orange solid. Washed with pentane and dried. Yield: 0.13 g, 53%

^{1}H NMR (DCM-d_2): δ_H 7.41 [4H, t, J_{HH} = 7.48 Hz, *p*-C_6H_5], 7.33 [4H, t, J_{HH} = 7.48 Hz, *p*-C_6H_5], 7.30 [8H, m (br), *o*-C_6H_5], 7.20 [16H, t, J_{HH} = 7.38 Hz, *m*-C_6H_5], 7.07 [8H, m (br), *o*-C_6H_5], 2.62 [4H, m

(br) C_2H_4], 2.22 [4H, m (br), C_2H_4], 0.08 [9H, s, $Si(CH_3)_3$], −9.03 [1H, dquint, J_{HP} = 114.9 Hz, J_{HH} = 16.5 Hz, Ru−H]

$^{13}C\{^1H\}$ NMR (DCM-d_2): δ_C 188.5 [d, J_{CP} = 68.0 Hz, C≡P], 134.2 [quint, J_{CP} = 11.2 Hz, *ipso*-C_6H_5], 133.5 [quint, J_{CP} = 11.2 Hz, *ipso*-C_6H_5], 132.9 [m, J_{CP} = 2.9 Hz, *o*-C_6H_5], 132.7 [m, J_{CP} = 2.9 Hz, *o*-C_6H_5], 130.7 [s, *p*-C_6H_5], 128.2 [m, J_{CP} = 2.4 Hz, *m*-C_6H_5], 32.4 [quint, J_{CP} = 11.0 Hz, C_2H_4], 0.2 [d, J_{CP} = 5.4 Hz, $Si(CH_3)_3$]

$^{31}P\{^1H\}$ NMR (DCM-d_2): δ_P 111.8 [1P, m (br), C≡P], 60.6 [4P, d, J_{PP} = 28.1 Hz, dppe]

$^{29}Si\{^1H\}$ NMR (DCM-d_2): δ_{Si} −15.2

ν_{max}/cm^{-1}: 1262 (C≡P)

*7.2.10 **Synthesis of Trans-[FeH{P(O)=CHSiMe$_3$}{dppe}$_2$]***

Synthesis of *Trans*-[FeH{P(O)=CHSiMe$_3$}{dppe}$_2$] (2.20)

To a mixture of **2.17** (0.095 g, 0.08 mmol) and NaOPh (0.011 g, 0.1 mmol), THF (15 cm^3) was added, and the mixture left to stir for 24 h. Filtration and subsequent removal of solvent under reduced pressure afforded a brown solid.

^1H NMR (DCM-d_2): δ_H 7.66 [8H, m (br), C_6H_5], 7.46 [8H, t (br), J_{HH} = 7.1 Hz, C_6H_5], 7.40 [4H, t (br), C_6H_5], 7.19 [12H, m, C_6H_5], 6.90 [8H, m (br), C_6H_5], 6.12 [1H, d (br), J_{HP} = 6.4 Hz, P=CH], 2.11 [8H, m, C_2H_4], −0.50 [9H, s, $SiMe_3$], −9.87 [1H, dquint, J_{HP} = 50.4 Hz, Ru-H]

$^{13}C\{^1H\}$ NMR (DCM-d_2): δ_C 134.2 [m (br), C_6H_5], 133.6 [m (br), C_6H_5], 131.2 [s, C_6H_5], 129.2 [s, C_6H_5], 120.8 [d, J_{CP} = 3 Hz, P=C], 31.2 [quint, J_{CP} = 12 Hz, C_2H_4], 1.0 [d, J_{CP} = 4 Hz, $SiMe_3$]

$^{31}P\{^1H\}$ NMR (DCM-d_2): δ_P 328.1 [1P, quint, J_{PP} = 36.6 Hz, C=P], 80.1 [4P, d, J_{PP} = 36.6 Hz, dppe]

$^{29}Si\{^1H\}$ NMR (DCM-d_2): δ_{Si} −10.1

7.3 Experimental Details for Chapter 3

7.3.1 ***Synthesis of Trans-[Ru(η^1-P≡CSiMe$_3$)(C≡CFc)(dppe)$_2$]***

Synthesis of *Trans*-[Ru(η^1-P≡CSiMe$_3$)(C≡CFc)(dppe)$_2$]OTf (3.2)

To a mixture of *trans*-[RuCl(C≡CFc)(dppe)$_2$] (0.068 g, 0.06 mmol) and AgOTf (0.017g, 0.06 mmol), DCM (10 cm^3) was added, and the blue-black suspension left to stir for 15 minutes. $Me_3SiC{\equiv}P$ (2.0 cm^3, 0.071 M in toluene) was then added, and the mixture stirred for 1 h. Filtration, removal of solvent, and addition and removal of DCM (5 cm^3) to azeotropically remove residual toluene afforded a dark brown solid.

^{1}H NMR (Benzene-d_6): δ_H 7.77 [8H, m (br), *o*-C_6H_5], 7.39 [8H, m, J_{HH} = 8.0 Hz, *p*-C_6H_5], 7.17 [16H, m, J_{HH} = 7.6 Hz, *m*-C_6H_5], 6.99 [8H, m (br), *o*-C_6H_5], 4.17 [2H, t, J_{HH} = 1.7 Hz, $C_{3\,\&\,4}$ - C_5H_4], 4.06 [2H, t, J_{HH} = 1.6 Hz, $C_{2\,\&\,5}$ – C_5H_4], 3.94 [5H, s, C_5H_5], 2.86 [8H, m, J_{HH} = 8.0 Hz, C_2H_4], −0.15 [9H, s, $SiMe_3$],

^{13}C{^{1}H} NMR (Benzene-d_6): δ_C 187.8 [d, J_{CP} = 89 Hz, C≡P], 134.7 [quint, J_{CP} = 11 Hz, *ipso*-C_6H_5], 134.4 [m, J_{CP} = 2 Hz, *o*-C_6H_5], 133.2 [quint, J_{CP} = 11 Hz, *ipso*-C_6H_5], 132.9 [m, J_{CP} = 2 Hz, *o*-C_6H_5], 131.1 [s, *p*-C_6H_5], 130.9 [s, *p*-C_6H_5], 128.5 [m, J_{CP} = 2 Hz, *m*-C_6H_5], 128.4 [m, J_{CP} = 2 Hz, *m*-C_6H_5], 119.7 [s (br), Ru-C≡C], 113.3 [m, Ru-C≡C], 71.7 [s, ipso-C_5H_4], 69.2 [s, $C_{2\,\&\,5}$ - C_5H_4], 68.8 [s,C_5H_5], 67.7 [s, $C_{3\,\&\,4}$ - C_5H_4], 31.1 [quint, J_{CP} = 12 Hz, C_2H_4], 0.5 [s, $SiMe_3$]

^{31}P{^{1}H} NMR (Benzene-d_6): δ_P 112.9 [1P, quint, J_{PP} = 33.8 Hz, C≡P], 42.6 [4P, d, J_{PP} = 33.8 Hz, dppe]

^{29}Si{^{1}H} NMR (Benzene-d_6): δ_{Si} −13.3

ν_{max}/cm^{-1}: 1262 (C≡P), 1991 (C≡C)

Anal. Calc. ($Ru_1Fe_1P_5C_{69}H_{66}F_3O_3S_1Si_1$): C; 60.41%, H; 4.85%. Found: C; 60.28%, H; 4.76%

Crystal Data: $C_{69}H_{66}F_3FeO_3RuSSi$, M_w = 1372.13 g mol^{-1}, monoclinic, Cc (No. 9), *a* = 25.2154(6) Å, *b* = 12.0619(2) Å, *c* = 23.3482(6) Å, *α* = 90, *β* = 116.822(3), *γ* = 90 °, *V* = 6337.2(3) Å^3, Z = 4. D_c = 1.438 Mg m^{-3}, μ(Cu-Kα) = 5.901 mm^{-1}, *T* = 173 K, 10195 independent reflections. Full-matrix F^2

refinement. R_1 = 0.0542, wR_2 = 0.1395 on 6979 independent absorption corrected reflections [I>2σ(I); 2θmax = 142.306 °], 706 parameters.

*7.3.2 **Synthesis of Trans-[Ru(C≡P)(C≡CFc)(dppe)$_2$]***

Synthesis of *Trans*-[Ru(C≡P)(C≡CFc)(dppe)$_2$] (3.3)

To a mixture of **3.2** (0.082 g, 0.06 mmol) and KO^{t}Bu (0.010 g, 0.09 mmol), THF (10 cm^3) was added, and the dark orange solution left to stir for 1 h. Filtration and removal of solvent afforded an orange solid. Residual ^{t}BuOH was removed azeotropically by addition and subsequent evaporation of benzene (3 x 5 cm^3). The sample was re-dissolved in benzene (5 cm^3) and lyophilised to afford a free-flowing orange powder. Yield: 0.048 g, 70%

^{1}H NMR (DCM-d_2): δ_H 7.70-7.65 [8H, m (br), C_6H_5], 7.53-7.48 [8H, m (br), C_6H_5], 7.26 [8H, dt (br), J_{HH} = 8.3 Hz, C_6H_5], 7.08 [16H, dt (br), J_{HH} = 6.7 Hz, C_6H_5], 4.22 [2H, s, Cp ring], 4.02 [5H, s, Cp ring], 3.98 [2H, t (br), Cp ring], 3.91 [2H, t (br), Cp ring], 2.80 [8H, dm (br), C_2H_4]

^{13}C{^{1}H} NMR (DCM-d_2): δ_C 201.2 [s, C≡P], 137.4 [quint, J_{CP} = 11 Hz, *ipso*-C_6H_5], 135.4 [quint, J_{CP} = 11 Hz, *ipso*-C_6H_5], 134.7 [quint (br), C_6H_5], 134.6 [quint (br), J_{CP} = 3 Hz, C_6H_5], 128.9 [s, C_6H_5], 128.8 [s, C_6H_5], 127.0 [quint (br), J_{CP} = 2 Hz, C_6H_5], 126.7 [quint (br), J_{CP} = 2 Hz, C_6H_5], 119.5 [quint, J_{CP} = 14 Hz, Ru-C≡C], 114.0 [s, Ru-C≡C], 75.8 [s, ipso-C_5H_4], 68.7 [s, C_5H_5], 68.3 [s, C_5H_4], 66.0 [s, C_5H_4], 31.2 [quint, J_{CP} = 12 Hz, C_2H_4]

^{31}P{^{1}H} NMR (DCM-d_2): δ_P 158.1 [1P, m (br), C≡P], 50.7 [4P, d (br) J_{PP} = 4.4 Hz, dppe]

ν_{max}/cm^{-1}: 1251 (C≡P), 2067 (C≡C)

Crystal Data: $C_{65}H_{57}FeP_5Ru$, M_w = 1092.67 g mol^{-1}, monoclinic, $P2_1/n$ (No. 14), a = 19.7444(3) Å, b = 21.9969(4) Å, c = 25.7743(5) Å, α = 90, β = 109.419(2), γ = 90 °, V = 10557.4(3) Å^3, Z = 4. D_c = 0.687 Mg m^{-3}, μ(Cu-Kα) = 3.135 mm^{-1}, T = 173 K, 55461 independent reflections. Full-matrix F^2 refinement. R_1 = 0.0638, wR_2 = 0.1563 on 20131 independent absorption corrected reflections [I>2σ(I); 2θmax = 142.524 °], 1297 parameters.

7.3.3 ***Attempted Synthesis of [{Ru(dppe)$_2$}$_2${μ-(C≡C-C≡C)}Cl$_2$]***

Attempted Synthesis of [{Ru(dppe)$_2$}$_2${μ-(C≡C-C≡C)}Cl$_2$] (3.4)

Method A: [RuCl(dppe)$_2$]OTf (0.22 g, 0.2 mmol), 1,4-bis(trimethylsilyl)butadiyne (0.022g, 0.1 mmol), and KF (0.019 g, 0.03 mmol) were combined in a round-bottomed flask and dissolved in methanol (40 mL), forming an orange suspension. DIPA (0.10 cm^3, 0.07 mmol) was added, and the yellow suspension heated under reflux for 16 h. After cooling to ambient temperature, the mixture was filtered, and the solvent removed under reduced pressure to afford a yellow solid.

Method B: Prepared in a similar fashion to that described for **Method A** from [RuCl(dppe)$_2$]OTf (0.22 g, 0.20 mmol), 1,4-bis(trimethylsilyl)butadiyne (0.029 g, 0.1 mmol), KF (0.019 g, 0.03 mmol), and DIPEA (0.10 cm^3, 0.05 mmol) in methanol (40 mL). Afforded a pale green solid.

Method C: Prepared in a similar fashion to that described for **Method A** from [RuCl(dppe)$_2$]OTf (0.22 g, 0.2 mmol), 1,4-bis(trimethylsilyl)butadiyne (0.026 g, 0.1 mmol), and TBAF (0.23 cm^3, 0.10 M in THF) in THF (40 mL). Afforded a yellow solid.

$^{31}P\{^1H\}$ NMR (Benzene-d_6): δ_P 62.9 [d, J_{PP} = 17.42 Hz, dppe]

1H NMR (Benzene-d_6): δ_H 7.71 [8H, m (br), C_6H_5], 7.40 [8H, m (br), C_6H_5], 7.04−6.85 [24H, m, C_6H_5], 2.67 [4H, m (br), C_2H_4], 2.05 [4H, m (br), C_2H_4], −18.53 [19.5 Hz]

Method D: Prepared in a similar fashion to that described for **Method A** from [RuCl(dppe)$_2$]OTf (0.22 g, 0.2 mmol), 1,4-bis(trimethylsilyl)butadiyne (0.026 g, 0.1 mmol), KF (0.019 g, 0.03 mmol), and DIPEA (0.10 cm^3, 0.05 mmol) in THF (40 mL). Afforded a brick red solid. No reaction observed by $^{31}P\{^1H\}$ NMR spectroscopy.

Attempted Synthesis of [{Ru(dppe)$_2$}$_2${μ-(C≡C-C≡C)}Cl$_2$], resulting in the synthesis of *Trans*-[RuCl(=C=CH$_2$)(dppe)$_2$]PF$_6$ (3.5)

To a J Young NMR tube charged with $FcPF_6$ (4.0×10^{-3} g, 0.01 mmol, synthesised by the author), *trans*-[RuCl(C≡CH)(dppe)$_2$] (0.023 g, 0.02 mmol) and DCM-d_2 were added. The tube was inverted repeatedly, resulting in the formation of a dark green solution. Observed NMR spectroscopic data were in agreement with literature reports for **3.5**.[132] Conversion was quantitative by $^{31}P\{^1H\}$ NMR.

Attempted Synthesis of [{Ru(dppe)$_2$}$_2${μ-(C≡C-C≡C)}Cl$_2$], resulting in the synthesis of *Trans*-[RuCl(C≡CH)(dppe)$_2$]PF$_6$ (3.6)

To a J Young NMR tube charged with $FcPF_6$ (4.0×10^{-3} g, 0.01 mmol), *trans*-[RuCl(C≡CH)(dppe)$_2$] (0.021 g, 0.02 mmol) and DCM-d_2 were added. The tube was inverted repeatedly, resulting in the formation of a dark green solution. Conversion was quantitative by $^{31}P\{^1H\}$ NMR.

^{1}H NMR (DCM-d_2): δ_H 7.53 [8H, m (br), C_6H_5], 7.29 [8H, m (br), C_6H_5], 7.22 [8H, m (br), C_6H_5], 7.02 [8H, m, J_{HH} = 7.6 Hz, C_6H_5], 6.88 [8H, m, J_{HH} = 7.3 Hz, C_6H_5], 2.83 [4H, m (br), C_2H_4], 1.98 [4H, m (br), C_2H_4], 1.34 [1H, s (br), C≡CH]

$^{31}P\{^1H\}$ NMR (DCM-d_2): δ_P 48.9 [s, dppe], −144.5 [sept, J_{PF} = 706.9 Hz, PF_6]

7.3.4 Synthesis of [{Ru(dppe)$_2$}$_2${μ-(C≡C)$_2$C$_6$H$_4$-p}R$_2$]

Synthesis of [{Ru(dppe)$_2$}$_2${μ-(C≡C)$_2$C$_6$H$_4$-*p*}(η^1-P≡CSiMe$_3$)$_2$].2OTf (3.9)

[{RuCl(dppe)$_2$}$_2$(C≡C-C$_6$H$_4$-C≡C)] (0.23 g, 0.1 mmol) was combined with AgOTf (0.061 g, 0.2 mmol) in dichloromethane (15 cm^3) and the resulting suspension stirred for 10 min. Me$_3$SiC≡P (6.5 cm^3, 0.030 M in toluene) was added, and the mixture stirred for 2 h. Filtration and removal of solvent under reduced pressure afforded a yellow oil. The residue was dissolved in DCM, filtered through Celite® and the resulting solution taken to dryness, affording a yellow solid. Yield: 0.12 g, 50%.

^{1}H NMR (Benzene-d_6): δ_H 7.76-7.69 [16H, m (br), C_6H_5], 7.42 [16H, m, C_6H_5], 7.17 [32H, dt, J_{HP} = 31.8 Hz, J_{HH} = 7.6 Hz, C_6H_5], 7.10-7.04 [16H, m (br), C_6H_5], 6.73 [4H, s, C_6H_4], 2.90 [16H, m (br), dppe], −0.08 [18H, s, $SiMe_3$]

^{13}C{^{1}H} NMR (DCM-d_2): δ_C 189.8 [d, J_{CP} = 88 Hz, C≡P], 134.7 [quint (br), J_{CP} = 2 Hz, C_6H_5], 133.4 [quint (br), J_{CP} = 2 Hz, C_6H_5], 131.5 [s, C_6H_5], 131.3 [s, C_6H_5], 130.4 [m (br), C_6H_4], 129.0 [quint (br), J_{CP} = 2.3 Hz, C_6H_5], 128.8 [quint (br), J_{CP} = 2 Hz, C_6H_5], 125.2 [m (br), *ipso*-C_6H_4], 116.9 [m (br), Ru-C≡C], 31.2 [quint, J_{CP} = 11 Hz, C_2H_4], 0.64 [s, $SiMe_3$]

Resonances for *ipso*-C_6H_5 and C_α could not be identified using standard 1D or 2D experiments.

^{31}P{^{1}H} NMR (Benzene-d_6): δ_P 111.4 [2P, quint, J_{PP} = 33.8 Hz, C≡P], 42.2 [8P, d, J_{PP} = 33.8 Hz, dppe]

^{29}Si{^{1}H} NMR (Benzene-d_6): δ_{Si} −12.9 [$SiMe_3$]

^{19}F{^{1}H} NMR (DCM-d_2): δ_F −78.9 [s, OTf]

ν_{max}/cm^{-1}: 1262 (C≡P), 2054 (C≡C)

Anal. Calc. ($C_{124}H_{118}P_{10}Ru_2Si_2S_2O_6F_6$): C; 60.79%, H; 4.85%. Found: C; 60.55%, H; 5.00%

Crystal Data: $C_{122}H_{118}P_{10}Ru_2Si_2$, M_w = 2152.18 g mol^{-1}, triclinic, P-1 (No. 2), a = 14.3964(4) Å, b = 19.4639(5) Å, c = 23.3880(5) Å, α = 95.011(2), β = 90.319(2), γ = 91.956(2) °, V = 6524.4(3) Å^3, Z = 2. D_c = 1.096 Mg m^{-3}, μ(Cu-Kα) = 3.519 mm^{-1}, T = 173 K, 41580 independent reflections. Full-matrix F^2 refinement. R_1 = 0.0611, wR_2 = 0.1701 on 23612 independent absorption corrected reflections [I>2σ(I); 2θmax = 136.502 °], 1369 parameters.

Synthesis of [{Ru(dppe)$_2$}$_2${μ-(C≡C)$_2$C$_6$H$_4$-*p*}(C≡P)$_2$] (3.10)

To a mixture of **3.9** (0.16 g, 0.06 mmol) and KO^{t}Bu (0.017 g, 0.2 mmol), THF (15 cm^3) was added, and the mixture stirred for 1 h. The solvent volume was reduced to 50%, and the resulting suspension filtered. Removal of solvent afforded a yellow solid. Residual ^{t}BuOH was removed

azeotropically by sequential addition and evaporation of benzene (3 x 5 cm^3). Yield: 0.080 g, 62%

^{1}H NMR (DCM-d_2): 7.66-7.61 [16H, m (br), C_6H_5], 7.55-7.50 [16H, m (br), C_6H_5], 7.04 [48H, dt, J_{HP} = 31.6 Hz, J_{HH} = 7.6 Hz, C_6H_5], 6.57 [4H, s, C_6H_4], 2.80 [16H, dm (br), C_2H_4]

$^{13}C\{^1H\}$ NMR (DCM-d_2): δ_C 281.8 [m (br), C≡P], 138.0 [quint, J_{CP} = 10 Hz, *ipso*-C_6H_5], 136.1 [quint, J_{CP} = 10 Hz, *ipso*-C_6H_5], 135.4 [quint (br), J_{CP} = 2 Hz, C_6H_5], 135.1 [quint (br), J_{CP} = 2 Hz, C_6H_5], 129.4 [s, C_6H_5], 129.6 [s, C_6H_5], 127.4 [quint (br), J_{CP} = 2 Hz, C_6H_5], 127.7 [quint (br), J_{CP} = 2 Hz, C_6H_5], 129.7 [s, C_6H_4], 127.8 [s, *ipso*-C_6H_4], 126.0 [s, Ru-C≡C], 120.8 [s, Ru-C≡C], 31.8 [quint, J_{CP} = 12 Hz, C_2H_4]

$^{31}P\{^1H\}$ NMR (DCM-d_2): δ_P 159.7 [2P, m, C≡P], 50.7 [8P, s, dppe]

ν_{max}/cm^{-1}: 1247 (C≡P), 2057 (C≡C)

ESI MS (*m/z*): Calc. for $C_{116}H_{100}P_{10}Ru_2$; 2006.3337 ($[M^+]$), found; 2007.4279 $([MH]^+)$

Attempted Synthesis of [{Ru(dppe)$_2$}$_2${μ-(C≡C)$_2$C$_6$H$_4$-*p*}(η^1-P≡CSiMe$_3$)(C≡P)]OTf (3.11)

To a mixture of **3.9** (0.039 g, 0.02 mmol) and KO^{t}Bu (2 x 10^{-3} g, 0.02 mmol) THF (10 cm^3) was added, and the golden solution left to stir for 1 h. Subsequent removal of solvent under reduced pressure afforded a yellow solid.

$^{31}P\{^1H\}$ NMR (DCM-d_2): δ_P 159.7 [1P, s (br), C≡P], 111.5 [1P, m (br), Me_3SiC≡P], 50.7 [4P, s, dppe], 42.2 [4P, d, J_{PP} = 31.8 Hz, dppe]

*7.3.5 Synthesis of [{Ru(dppe)$_2$}$_2${μ-(C≡C)$_2$C$_6$F$_4$-*p*}R$_2$]*

Synthesis of [{Ru(dppe)$_2$}$_2${μ-(C≡C)$_2$C$_6$F$_4$-*p*}Cl$_2$] (3.12)

To a solution of [RuCl(dppe)$_2$]OTf (1.1 g, 1.0 mmol) in DCM (10 cm^3), 1,4-diethynyltetrafluorobenzene (0.10 g, 0.5 mmol) was added, and the mixture left to stir for 16 h.

Removal of solvent afforded a brick-red solid. Washed with pentane (3 x 10 cm^3) and dried. Compound was isolated, but not fully characterised.

^{1}H NMR (DCM-d_2): δ_H 7.44 – 7.06 [80H, C_6H_5], 3.82 [1H, quint, J_{HH} = 2.7 Hz, Ru=C=C(H)Ar], 3.70 1H, quint, J_{HH} = 2.7 Hz, Ru=C=C(H)Ar], 3.01 [8H, m (br), C_2H_4], 2.85 [8H, m (br), C_2H_4]

^{31}P{^{1}H} NMR (DCM-d_2): δ_P 35.6 [s]

^{19}F NMR (DCM-d_2]: δ_F −78.8 [s, SO_3CF_3], −153.3 [s, C_6F_4]

To a suspension of this solid (0.73 g, 0.3 mmol) in DCM (15 cm^3), DBU (0.14 cm^3, 0.9 mmol) was added, and the red solution left to stir for 3 h. Removal of solvent afforded a brown solid. Washed with methanol (4 x 5 cm^3) and dried. Yield: 0.37 g, 18%

^{1}H NMR (Benzene-d_6): δ_H 7.65 [16H, m (br), *o*-C_6H_5], 7.22 [16H, m, C_6H_5], 7.17 [16H, m (br), *o*-C_6H_5], 7.02 [32H, q, J_{HH} = 7.0 Hz, C_6H_5], 2.77 [16H, m (br), C_2H_4]

^{13}C{^{1}H} NMR (DCM-d_2): δ_C 147.7 [dm (br), J_{CF} = 239 Hz, C_6F_4], 136.9 [quint, J_{CP} = 10 Hz, *ipso*-C_6H_5], 135.0 [quint, J_{CP} = 10 Hz, *ipso*-C_6H_5], 134.9 [m, *o*-C_6H_5], 134.3 [m, *o*-C_6H_5], 129.3 [s, *p*-C_6H_5], 128.7 [s, *p*-C_6H_5], 127.3 [m (br), *m*-C_6H_5], 127.0 [m (br), *m*-C_6H_5], 101.1 [s (br), Ru-C≡C], 30.9 [quint, J_{CP} = 12 Hz, C_2H_4]

Resonances for the *ipso* carbons of the C_6F_4 group and C_β could not be identified using standard 1D or 2D experiments.

^{31}P{^{1}H} NMR (Benzene-d_6): δ_P 48.6 [s, dppe]

^{19}F NMR (Benzene-d_6): −146.4 [s, C_6F_4]

ν_{max}/cm^{-1}: 2025 (C≡C)

Anal. Calc. ($C_{114}H_{96}P_8F_4Cl_2Ru_2$): C; 66.36%, H; 4.69%. Found: C; 66.27%, H; 4.34%

Synthesis of [{Ru(dppe)$_2$}$_2${μ-(C≡C)$_2$C$_6$F$_4$-*p*}(η^1-P≡CSiMe$_3$)$_2$].2OTf (3.13)

To a solution of **3.12** (0.18 g, 0.09 mmol) in DCM (10 cm^3), $AgPF_6$ (0.052 g, 0.2 mmol) in DCM (5 cm^3) was added, and the green suspension stirred for 10 minutes. $Me_3SiC{\equiv}P$ (2.6 cm^3, 0.086 M in toluene) was added, and the light brown suspension stirred for 1 h. Subsequent filtration and removal of solvent under reduced pressure afforded a brown solid.

^{1}H NMR (Benzene-d_6): δ_H 7.75 [16H, m (br), *o*-C_6H_5], 7.43 [16H, m, J_{HH} = 8.1 Hz, *p*-C_6H_5], 7.21 [16H, m, *m*-C_6H_5], 7.16 [16H, m, *m*-C_6H_5], 7.01 [16H, m (br), *o*-C_6H_5], 2.92 [16H, m (br), J_{HH} = 8.3 Hz, C_2H_4], −0.10 [18H, s, $SiMe_3$]

^{13}C{^{1}H} NMR (DCM-d_2): δ_C 192.5 [d, J_{CP} = 87 Hz, C≡P], 147.8 [d (br), J_{CF} = 251 Hz, C_6F_4] 134.8 [m, J_{CP} = 3 Hz, *o*-C_6H_5],134.6 [quint, J_{CP} = 11 Hz, *ipso*-C_6H_5], 133.3 [m, J_{CP} = 3 Hz, *o*-C_6H_5], 133.1 [quint, J_{CP} = 11 Hz, *ipso*-C_6H_5], 131.6 [s, *p*-C_6H_5], 131.5 [s, *p*-C_6H_5], 129.1 [m, J_{CP} = 3 Hz, *m*-C_6H_5], 128.7 [m, J_{CP} = 3 Hz, *m*-C_6H_5], 121.7 [q, J_{CF} = 322 Hz, ipso-C_6F_4] 104.1 [m (br), Ru-<u>C</u>≡C], 31.2 [quint, J_{CP} = 11 Hz, C_2H_4], 0.6 [s, $SiMe_3$]

A resonance for C_β could not be identified using standard 1D or 2D experiments.

^{31}P{^{1}H} NMR (DCM-d_2): δ_P 108.0 [2P, quint, J_{PP} = 33.4 Hz, C≡P], 42.6 [8P, d, J_{PP} = 33.4 Hz, dppe]

^{19}F{^{1}H} NMR (DCM-d_2): δ_F −78.88 [s, SO_3CF_3], −142.90 [s, C_6F_4]

^{29}Si{^{1}H} NMR (DCM-d_2): δ_{Si} −12.2

ν_{max}/cm^{-1}: 1260 (C≡P), 2040 (C≡C)

Synthesis of [{Ru(dppe)$_2$}$_2${μ-(C≡C)$_2$C$_6$F$_4$-*p*}(C≡P)$_2$] (3.14)

To a mixture of **3.13** (0.12 g, 0.06 mmol) and KO^{t}Bu (0.014 g, 0.1 mmol), THF (15 cm^3) was added, and the dark red suspension stirred for 2 h. The mixture was then filtered, and the solvent removed under reduced pressure to afford a dark orange solid.

^{1}H NMR (Benzene-d_6): δ_H 7.81 [16H, m (br), *o*-C_6H_5], 7.30 [16H, m (br), *o*-C_6H_5], 7.24 [16H, m, *p*-C_6H_5], 7.04 [32H, t, J_{HH} = 7.4 Hz, *m*-C_6H_5], 2.98 [8H, m (br), C_2H_4], 2.68 [8H, m (br), C_2H_4]

^{13}C{^{1}H} NMR (DCM-d_2): δ_C 280.1 [d (br), J_{CP} = 237 Hz, C≡P], 137.8 [quint, J_{CP} = 10 Hz, *ipso*-C_6H_5], 135.6 [quint, J_{CP} = 10 Hz, *ipso*-C_6H_5], 135.3 [m (br), *o*-C_6H_5], 135.1 [m (br), *o*-C_6H_5], 129.7 [s, *p*-C_6H_5], 129.5 [s, *p*-C_6H_5], 127.6 [m (br), *m*-C_6H_5], 127.4 [*m*-C_6H_5], 147.9 [d (br), J_{CF} = 252 Hz, C_6F_4], 117.4 [q, J_{CF} = 295 Hz, *ipso*-C_6F_4], 104.4 [m (br), Ru-C≡C], 31.7 [quint, J_{CP} = 12 Hz, C_2H_4]

A resonance for C_β could not be identified using standard 1D or 2D experiments.

^{31}P{^{1}H} NMR (DCM-d_2): δ_P 158.3 [2P, m (br), C≡P], 50.9 [8P, s, dppe]

^{19}F{^{1}H} NMR (DCM-d_2): δ_F −145.77 [s, C_6F_4]

ν_{max}/cm^{-1}: 1247 (C≡P), 2055 (C≡C)

7.4 Experimental Details for Chapter 4

7.4.1 ***Synthesis of Trans-[RuR(η^1-P≡CSiMe$_3$)(dppm)$_2$]***

Synthesis of *Trans*-[RuH(η^1-P≡CSiMe$_3$)(dppm)$_2$]OTf (4.1)

To a mixture of *trans*-[RuHCl(dppm)$_2$] (0.092 g, 0.1 mmol) and AgOTf (0.026 g, 0.1 mmol), DCM (10 cm^3) was added, forming an orange solution with a white precipitate, which was left to stir for 10 minutes. $Me_3SiC{\equiv}P$ (3.0 cm^3, 0.030 M in toluene) was added, and the yellow suspension left to stir for 1 h. Filtration and removal of solvent under reduced pressure afforded a yellow oil. Addition and removal of DCM (5 mL) to azeotropically remove residual toluene afforded a yellow solid.

^{1}H NMR (DCM-d_2): δ_H 7.50 [4H, t, J_{HH} = 7.5 Hz, *p*-C_6H_5], 7.44 [4H, t (br), *p*-C_6H_5], 7.35 [8H, t, J_{HH} = 7.5 Hz, *m*-C_6H_5], 7.31 [8H, m (br), *o*-C_6H_5], 7.22 [16H, m (br), o & *m*-C_6H_5], 4.83 [4H, dm (br), CH_2], −0.12 [9H, s, $SiMe_3$], −5.35 [1H, dquint, J_{HP} = 105.8, 18.2 Hz, Ru-H]

^{13}C{^{1}H} (DCM-d_2, 298K): δ_C 190.9 [d, J_{CP} = 69 Hz, C≡P], 135.4 [quint, J_{CP} = 10 Hz, *ipso*-C_6H_5], 135.1 [quint, J_{CP} = 10 Hz, *ipso*-C_6H_5], 132.9 [m, J_{CP} = 4 Hz, *o*-C_6H_5], 132.6 [m, J_{CP} = 4 Hz, *o*-C_6H_5], 131.6 [s, *p*-C_6H_5], 131.5 [s, *p*-C_6H_5], 129.5 [m, J_{CP} = 3 Hz, *m*-C_6H_5], 129.2 [m, J_{CP} = 3 Hz, *m*-C_6H_5], 55.1 [quint, J_{CP} = 13 Hz, CH_2], 0.7 [d, J_{CP} = 5 Hz, $SiMe_3$]

^{31}P NMR (DCM-d_2): δ_P 111.6 [1P, m (br), C≡P], −4.3 [4P, d, J_{PP} = 29.9 Hz, dppm]

^{29}Si NMR (DCM-d_2): δ_{Si} −14.7

ν_{max}/cm^{-1}: 1258 (C≡P)

A sample of **4.1** was dissolved in DCM (5 cm^3), layered with pentane (20 cm^3) and stored at −20 °C indefinitely, resulting in crystals of **4.3** after *ca*. 2 years.

Crystal Data: $C_{56}H_{59}Cl_2F_3O_5P_5RuSSi$, M_w = 1256.00 g mol^{-1}, monoclinic, $P2_1/c$ (No. 14), a = 13.9159(2) Å, b = 22.6473(2) Å, c = 18.6531(2) Å, β = 95.3490(10)°, V = 5853.07(12) Å^3, Z = 4. D_c = 1.425 Mg m^{-3}, μ(Cu-Kα) = 5.290 mm^{-1}, T = 173 K, 21825 independent reflections. Full-matrix F^2 refinement. R_1 = 0.0389, wR_2 = 0.1014 on 11113 independent absorption corrected reflections [I>2σ(I); 2θmax = 142.55 °], 676 parameters.

Attempted Synthesis of *Trans*-[Ru(C≡CPh)(η^1-P≡CSiMe$_3$)(dppm)$_2$] (4.2)

To a mixture of *trans*-[RuCl(C≡CPh)(dppm)$_2$] (0.072 g, 0.07 mmol) and AgOTf (0.017 g, 0.07 mmol), DCM (10 cm^3) was added, forming an orange solution with a white precipitate, which was left to stir for 10 minutes. $Me_3SiC{\equiv}P$ (3.0 cm^3, 0.056 M in toluene) was added, and the orange suspension left to stir for 1 h. Filtration and removal of solvent under reduced pressure afforded an orange oil. Addition and removal of DCM (5 mL) to azeotropically remove residual toluene afforded an orange-yellow solid.

^{31}P NMR (Benzene-d_6): δ_P 105.9 [1P, quint, J_{PP} = 33.9 Hz, C≡P], −12.8 [4P, d, J_{PP} = 33.9 Hz, dppm]

*7.4.2 **Addition of KO^{t}Bu to 4.1***

Attempted Synthesis of *Trans*-[RuH(C≡P)(dppm)$_2$], resulting in the synthesis of Trans-[RuH{P(O^{t}Bu)CHSiMe$_3$}{dppm}$_2$] (4.5)

To a mixture of **4.1** (0.022 g, 0.02 mmol) and KO^{t}Bu (5.0×10^{-3} g, 0.05 mmol), THF (5 cm^3) was added, and the brown solution left to stir for 1 h. Removal of solvent under reduced pressure afforded a brown solid.

^{1}H NMR (DCM-d_2): δ_H 7.62 [8H, m (br), C_6H_5], 7.49 [4H, m (br), C_6H_5], 7.41 [8H, m (br), C_6H_5], 7.34 [8H, m (br), C_6H_5], 7.19 [16H, m (br), C_6H_5], 6.97 [8H, m (br), C_6H_5], 4.84 [4H, m, dppm], 4.36 [1H, d (br), J_{HP} = 6.9 Hz, P=CH], 0.76 [9H, s, C(CH3)3], −0.31 [9H, s, $SiMe_3$], −5.49 [1H, dquint, J = 125.6, 20.7 Hz, Ru-H]

^{31}P NMR (DCM-d_2): δ_P 320.4 [t, J_{PP} = 27.2 Hz], 287.7 [quint, J_{PP} = 27.2 Hz], 280.4 [quint, J_{PP} = 27.2 Hz], 166.0 [s], 164.7 [s], 5.7 [d, J_{PP} = 30.7 Hz], 4.33 [dd, J_{PP} = 30.7, 12.0 Hz], −1.7 [s], −2.7 [[d, J_{PP} = 30.7 Hz], −8.0 [s], −9.9 [d, J_{PP} = 30.7 Hz], −11.2 [d, J_{PP} = 30.7 Hz]

*7.4.3 **Synthesis of [FeCp^R(dppe)(η^1-P≡CSiMe$_3$)]$^+$***

Synthesis of [FeCp*(dppe)(η^1-P≡CSiMe$_3$)]BPh$_4$ (4.6)

To a mixture of [FeCp*(dppe)Cl] (0.19 g, 0.3 mmol) and $NaBPh_4$ (0.11 g, 0.03 mmol), THF (15 cm^3) was added, and the dark brown solution left to stir for 10 minutes. $Me_3SiC{\equiv}P$ (6.5 cm^3, 0.063 M in toluene) was added, and the mixture left to stir for 1 h. Removal of solvent under reduced pressure afforded a wine-red oil. Extraction with DCM (3 x 5 cm^3) and removal of solvent afforded a cherry-red solid. Washed with pentane (3 x 5 cm^3) and dried. Yield: 0.15 g, 50%

^{1}H NMR (THF-d_8): δ_H 7.63 [8H, m, C_6H_5], 7.52[8H, m, C_6H_5], 7.35 [8H, m (br), C_6H_5], 7.30 [4H, m (br), C_6H_5], 7.03 [8H, t, J_{HH} = 6.8 Hz, C_6H_5], 6.88 [4H, t, J_{HH} = 6.8 Hz, C_6H_5], 2.50 [4H, dm (br), C_2H_4], 1.49 [15H, s, $C_5(CH_3)_5$], 0.02 [9H, s, $SiMe_3$]

^{13}C{^{1}H} (THF-d_8, 298K): δ_C 197.4 [d, J_{CP} = 76 Hz, C≡P], 165.4 [q, J_{CB} = 49 Hz, *ipso*-C_6H_5], 137.4 [s, *o*-C_6H_5], 134.5 [t, J_{CP} = 5 Hz, C_6H_5], 134.1 [t, J_{CP} = 5 Hz, C_6H_5], 132.5 [s, C_6H_5], 134.1 [s, C_6H_5], 129.8 [t, J_{CP} = 5 Hz, C_6H_5], 129.5 [t, J_{CP} = 5 Hz, C_6H_5], 125.8 [m, *m*-C_6H_5], 121.9 [s, *p*-C_6H_5], 93.9 [s, C_5Me_5], 32.0 [m, C_2H_4], 10.6 [s, $C_5(\underline{C}H_3)_5$], 1.1 [d (br), J_{CP} = 5 Hz, $SiMe_3$]

^{31}P NMR (THF-d_8): δ_P 147.4 [1P, t, J_{PP} = 57.0 Hz, C≡P], 82.8 [2P, d, J_{PP} = 57.0 Hz, dppe]

^{29}Si NMR (THF-d_8): δ_{Si} −12.5

^{11}B{^{1}H} NMR (THF-d_8): δ_B −4.7

ν_{max}/cm^{-1}: 1247 (C≡P)

Anal. Calc. ($C_{64}H_{68}P_3SiBFe$): C; 75.00%, H; 6.69%. Found: C; 74.87%, H; 6.79%

Crystal Data: $C_{64}H_{68}BFeP_3Si$, M_w = 1024.84 g mol^{-1}, monoclinic, $P2_1/n$ (No. 14), a = 16.2438(9) Å, b = 18.4835(10) Å, c = 18.3779(10) Å, α = 90, β = 99.171(5), γ = 90 °, V = 5447.3(5) Å^3, Z = 4. D_c = 1.250 Mg m^{-3}, μ(Cu-Kα) = 3.558 mm^{-1}, T = 173 K, 17741 independent reflections. Full-matrix F^2 refinement. R_1 = 0.0891, wR_2 = 0.2618 on 10364 independent absorption corrected reflections [I>2σ(I); 2θmax = 148.1 °], 671 parameters.

Synthesis of [FeCp(dppe)(η^1-P≡CSiMe$_3$)]BPh$_4$ (4.7)

Prepared in a similar fashion to that described for **4.6** from [FeCp(dppe)Cl] (0.27 g, 0.5 mmol), $NaBPh_4$ (0.16 g, 0.5 mmol), and $Me_3SiC{\equiv}P$ (12 cm^3, 0.048 M in toluene) in THF (10 cm^3). Brown solid afforded.

^{1}H NMR (THF-d_8): δ_H 7.67 [4H, m (br), C_6H_5], 7.55 [4H, m, C_6H_5], 7.47 [4H, t, J_{HH} = 7.1 Hz, C_6H_5], 7.33 [8H, m (br), C_6H_5], 7.24 [8H, m, C_6H_5], 7.01 [8H, t, J_{HH} = 7.1 Hz, C_6H_5], 6.85 [4H, t, J_{HH} = 6.9 Hz, *p*-C_6H_5], 4.63 [5H, s, C_5H_5], 2.66 [4H, m (br), C_2H_4], −0.16 [9H, s, $SiMe_3$]

^{13}C{^{1}H} (, 298K): δ_C 203.7 [C≡P], 165.3 [q, J_{CB} = 51 Hz, *ipso*-C_6H_5], 137.2 [s, C_6H_5], 135.8 – 128.1 [C_6H_5], 125.7 [s, C_6H_5], 121.8 [s, C_6H_5], 81.4 [s, C_5H_5], 23.1 [s (br), C_2H_4], 1.3 [s, $SiMe_3$]

^{31}P NMR (THF-d_8): δ_P 120.2 [1P, t, J_{PP} = 66.1 Hz, C≡P], 89.4 [2P, d, J_{PP} = 66.1 Hz, dppe]

^{29}Si NMR (THF-d_8): δ_{Si} −13.7

^{11}B{^{1}H} NMR (THF-d_8): δ_B −4.7

ν_{max}/cm^{-1}: 1247 (C≡P)

Synthesis of [RuCp*(dppe)(η^{1}-P≡CSiMe$_3$)]OTf (4.8)

To a mixture of [RuCp*(dppe)Cl] (0.10 g, 0.2 mmol) and TlOTf (0.074 g, 0.2 mmol) in an ampoule, THF (15 cm^3) was added. The solution was freeze-thaw degassed, before being heated under reflux for 16 h. After cooling to room temperature, $Me_3SiC{\equiv}P$ (2.4 cm^3, 0.082 M in toluene) was added, and the orange suspension left to stir for 1 h. Filtration and removal of solvent afforded an orange solid. Washed with pentane (3 x 5 cm^3) and dried.

^{1}H NMR (DCM-d_2): δ_H 7.63-7.58 [4H, m (br), *p*-C_6H_5], 7.55-7.48 [8H, m (br), *o*-C_6H_5], 7.26-7.16 [8H, m, *m*-C_6H_5], 2.67 [4H, m, C_2H_4], 1.63 [15H, s, $C_5(CH_3)_5$], −0.11 [9H, s, $SiMe_3$]

^{13}C{^{1}H} (DCM-d_2, 298K): δ_C 185.9 [d, J_{CP} = 76 Hz, C≡P], 133.2 [m, J_{CP} = 5 Hz, *o*-C_6H_5], 132.9 [m, J_{CP} = 5 Hz, *o*-C_6H_5], 132.1 [s, *p*-C_6H_5], 132.0 [s, *p*-C_6H_5], 129.5 [m, J_{CP} = 5 Hz, *m*-C_6H_5], 129.3 [m, J_{CP} = 5 Hz, *m*-C_6H_5], 98.5 [s, C_5Me_5], 30.8 [m, C_2H_4], 10.5 [s, $C_5(CH_3)_5$], 0.9 [d, J_{CP} = 6 Hz, $SiMe_3$]

^{31}P NMR (DCM-d_2): δ_P 119.6 [1P, t, J_{PP} = 61.0 Hz, C≡P], 69.0 [2P, d, J_{PP} = 61.0 Hz, dppe]

^{29}Si NMR (DCM-d_2): δ_{Si} −12.8

ν_{max}/cm^{-1}: 1238 (C≡P)

Attempted Synthesis of [RuCp(dppe)(η^1-P≡CSiMe$_3$)]OTf (4.9)

Prepared in a similar fashion to that described for **4.8**, from [RuCp(dppe)Cl) (0.090 g, 0.2 mmol), TlOTf (0.086 g, 0.2 mmol), and $Me_3SiC{\equiv}P$ (5.0 cm^3, 0.057 M in toluene) in THF (30 cm^3). Orange solid afforded.

Unable to assign $^{31}P\{^1H\}$ or ^1H NMR spectral data due to an intractable mixture of products formed.

Synthesis of Compound 4.10

Method A: To a mixture of [RuCp*(dppe)Cl (0.10 g, 0.2 mmol) and TlOTf (0.070 g, 0.2 mmol), THF (35 cm^3) and $Me_3SiC{\equiv}P$ (5.0 cm^3, 0.048 M in toluene) were added, and the mixture heated under reflux for 16 h. After cooling to room temperature, filtration and subsequent removal of solvent under reduced pressure afforded a pale-yellow solid.

Method B: A sample of **4.8** (0.050 g, 0.06 mmol) was dissolved in THF (20 mL) in an ampoule, freeze-thaw degassed, and heated under reflux for 48 h. Removal of solvent under reduced pressure after cooling afforded a yellow-orange solid.

^1H NMR (DCM-d_2): δ_H 7.66 [4H, m, J_{HH} = 7.5 Hz, C_6H_5], 7.55 [4H, m (br), C_6H_5], 7.39 [8H, m, C_6H_5], 7.17 [4H, m, J_{HH} = 8.6 Hz, C_6H_5], 3.14 [2H, m (br), C_2H_4], 2.29 [2H, m (br), C_2H_4], 1.54 [15H, s, C_5Me_5], −0.17 [9H, s, $SiMe_3$]

$^{13}C\{^1H\}$ (DCM-d_2, 298K): δ_C 230.2, 199.7, 138.2 [dm (br), *ipso*-C_6H_5], 136.4 [dm (br), *ipso*-C_6H_5], 132.8 [m, J_{CP} = 5 Hz, C_6H_5], 131.2 [s, C_6H_5], 130.6 [s, C_6H_5], 129.6 [m, J_{CP} = 5 Hz, C_6H_5], 128.7 [m, J_{CP} = 5 Hz, C_6H_5], 97.1 [m (br), J_{CP} = 2 Hz, C_5Me_5], 29.5 [m, C_2H_4], 27.2 [s, $C_5(CH_3)_5$], 0.04 [d, J_{CP} = 4 Hz, $SiMe_3$]

$^{31}P\{^1H\}$ NMR (DCM-d_2): δ_P 171.5 [1P, t, J_{PP} = 50.4 Hz, C≡P], 85.2 [2P, d, J_{PP} = 50.4 Hz, dppe]

^{29}Si NMR (DCM-d_2): δ_{Si} −0.37

ν_{max}/cm^{-1}: 1238 (C≡P)

7.4.4 ***Reactivity Studies with Compounds 4.6 and 4.8***

Addition of KO^{t}Bu to 4.8

To a mixture of **4.8** (0.047 g, 0.05 mmol) and KO^{t}Bu (7.0 x 10^{-3} g, 0.06 mmol), THF (10 cm^3) was added, and the orange solution stirred for 1 h., before removal of solvent under reduced pressure afforded an orange solid.

NMR spectroscopic data matched those of [RuCp*(dppe)Cl].[162]

Addition of KO^{t}Bu to 4.6

To a mixture of **4.6** (0.046 g, 0.05 mmol) and KO^{t}Bu (6.0 x 10^{-3} g, 0.05 mmol), THF (10 cm^3) was added, forming a dark green solution and the precipitation of a white solid. After stirring for 16 h., the reaction mixture was filtered, and the solvent removed under reduced pressure to afford a light-orange solid.

^{31}P{^{1}H} NMR (Benzene-d_6): δ_P 166.3 [1P, s], 107.6 [1P, d, J_{PP} = 63.1 Hz], 91.3[2P, s], 86.0 [2P, s (br)], 29.2 [2P, s (br)], 28.5 [2P, d, J_{PP} = 47.1 Hz], −12.8 [s, free dppe]

Addition of NaOPh to 4.6

To a mixture of **4.6** (0.056 g, 0.05 mmol) and NaOPh (0.060 g, 0.5 mmol), THF (15 cm^3) was added, forming a brown solution. After stirring for 16 h., the reaction mixture was filtered, and the solvent removed under reduced pressure to afford a brown solid.

^{31}P{^{1}H} NMR (DCM-d_2): δ_P 333.3 [1P, t, J_{PP} = 75 Hz], 206.0 [1P, t, J_{PP} = 70 Hz], 189.3 [1P, s], 98.2 [2P, d, J_{PP} = 75 Hz], 95.2 [2P, d, J_{PP} = 70 Hz], 84.2 [2P, s], 39.1 [2P, s], −12.5 [s (br), free dppe]

Addition of $LiN(SiMe_3)_2$ to 4.6

To a mixture of **4.6** (0.051 g, 0.05 mmol) and $LiN(SiMe_3)_2$ (0.010 g, 0.06 mmol), THF (10 cm^3) was added, forming an olive-green solution. After stirring for 16 h., the reaction mixture was filtered, and the solvent removed under reduced pressure to afford an olive-brown solid.

$^{31}P\{^1H\}$ NMR (DCM-d_2): δ_P 240.7 [1P, t (br), J_{PP} = 70 Hz],92.8 [2P, d, J_{PP} = 80 Hz], 87.2 [2P, d, J_{PP} = 70 Hz], −12.9 [s (br), free dppe]

7.5 Experimental Details for Chapter 5

7.5.1 ***Reactivity Studies with Compounds 2.7 and 2.8***

Addition of BPh_3 to 2.7

To a J Young NMR tube charged with **2.7** (0.012 g, 0.02 mmol) in toluene-d_8, BPh_3 (5.0 x 10^{-3} g, 0.02 mmol) was added, and the tube mixed by continuous inversion for 1 h., affording a pale-yellow solution.

$^{31}P\{^1H\}$ NMR (toluene-d_8): δ_P 168.1 [1P, m (br), C≡P], 51.8 [4P, d (br), J_{PP} = 3.0 Hz, dppe]

$^{11}B\{^1H\}$ NMR (toluene-d_8): δ_B 66.5 [s (br)]

Addition of $B(C_6F_5)_3$ to 2.7

To a J Young NMR tube charged with **2.7** (0.015 g, 0.01 mmol) in toluene-d_8, $B(C_6F_5)_3$ (0.010 g, 0.02 mmol) was added, and the tube mixed by continuous inversion for 1 h., affording a pale-orange solution.

$^{31}P\{^1H\}$ NMR (toluene-d_8): δ_P 170.3 [1P, m (br), C≡P], 50.8 [4P, s (br), dppe]

^{1}H NMR (toluene-d_8): δ_H 7.70 [8H, m (br), C_6H_5], 7.60 [8H, m (br), C_6H_5], 7.18 [3H, t, J_{HH} = 8.0 Hz, Ph], 7.09 [2H, m (br), Ph], 6.98 [16H, m, C_6H_5], 6.87 [8H, t, J_{HH} = 7.4 Hz, C_6H_5], 2.77 [4H, m, C_2H_4], 2.54 [4H, m, C_2H_4]

^{11}B{^{1}H} NMR (toluene-d_8): δ_B −15.9 [s]

^{19}F NMR (toluene−d_8): δ_F −126.6 [m (br)], −126.9 [m (br)], −127.6 [m], −128.3 [m], −145.4 [tt, J_{FF} = 20.7, 3.2 Hz], −152.2 [t, J_{FF} = 21.2 Hz], −153.6 [t, J_{FF} = 19.9 Hz], −156.3 [m], −157.2 [s (br)], −157.8 [t, J_{FF} = 20.5 Hz], −159.6 [m], −161.5 [m]

Addition of Sulfur Powder to 2.8

To a J Young NMR tube charged with **2.8** (0.011 g, 0.01 mmol) in DCM-d_2, sulfur powder (0.010 g, 0.04 mmol) was added, and the tube mixed by continuous inversion for 1 h., affording a pale-yellow solution.

^{1}H NMR (DCM-d_2): δ_H 7.76 [8H, m (br), C_6H_5], 7.43 [8H, t, J_{HH} = 8.0 Hz, C_6H_5], 7.37 [8H, t, J_{HH} = 8.0 Hz, C_6H_5], 7.20 [8H, t, J_{HH} = 7.8 Hz, C_6H_5], 7.12 [8H, t, J_{HH} = 7.8 Hz, C_6H_5], 7.03 [8H, m (br), C_6H_5], 6.89 [2H, m, C_6H_4], 6.83 [2H, m, C_6H_4], 3.82 [3H, s, OCH_3], 2.84 [8H, m, J_{HH} = 7.7 Hz, C_2H_4]

^{31}P{^{1}H} NMR (DCM-d_2): δ_P 66.4 [1P, s], 51.0 [1P, s], 48.9 [2P, s], 45.9 [28P, s], 44.1 [1P, s, dppeS_2], 41.8 [4P, d, J_{PP} = 29.2 Hz]

Addition of Selenium Powder to 2.8

To a J Young NMR tube charged with **2.8** (0.010 g, 0.01 mmol) in DCM-d_2, selenium powder (0.010 g, 0.02 mmol) was added, and the tube mixed by continuous inversion for one month, affording a pale-yellow solution.

^{1}H NMR (DCM-d_2): δ_H 7.80 [8H, m, C_6H_5], 7.47 [12H, m, C_6H_5], 2.82 [4H, d (br), J_{HH} = 2.3 Hz, C_2H_4]

^{31}P{^{1}H} NMR (DCM-d_2): δ_P 35.6 [s, J_{PSe} = 679 Hz, dppeSe_2]

Addition of N_2O to 2.7

To a J Young NMR tube charged with **2.7** (0.041 g, 0.02 mmol) in DCM-d_2, N_2O gas (6.0 mmHg, 0.02 mmol) was added *via* toepler pump, and the tube mixed by continuous inversion for one month, affording a pale-orange solution.

$^{31}P\{^1H\}$ NMR (DCM-d_2, 303K) δ_P 159.6 [1P, m (br), C≡P], 141.4 [1P, quint, J_{PP} = 12.3 Hz], 50.8 [4P, d (br), J_{PP} = 3.7 Hz, dppe], 45.2 [1P, m], 41.8 [1P, m], 40.1 [1P, m], 37.6 [1P, m], 32.0 [1P, m]

Addition of Excess I_2 to 2.7

To a J Young NMR tube charged with **2.7** (*ca*. 0.015 g, 0.01 mmol) in DCM-d_2, three crystal of I_2 were added, and the tube mixed by inversion, affording a dark brown suspension.

$^{31}P\{^1H\}$ NMR (DCM-d_2): δ_P 101.5 [1P, quint, J_{PP} = 4.9 Hz], 45.9 [4P, d, J_{PP} = 4.9 Hz]

^1H NMR (DCM-d_2): δ_H 7.50 [4H, t, J_{HH} = 7.4 Hz, C_6H_5], 7.43−7.30 [28H, m, C_6H_5], 7.23 [3H, d (br), Ph], 7.05 [8H, t, J_{HH} = 7.4 Hz, C_6H_5], 6.63 [2H, dm (br), Ph], 2.95 [4H, m (br), C_2H_4], 2.81 [4H, m (br), C_2H_4]

Addition of Excess I_2 to 2.8

To a J Young NMR tube charged with **2.8** (*ca*. 0.015 g, 0.01 mmol) in DCM-d_2, three crystal of I_2 were added, and the tube mixed by inversion, affording a dark brown suspension.

$^{31}P\{^1H\}$ NMR (DCM-d_2): δ_P 103.0 [1P, quint, J_{PP} = 4.3 Hz], 45.9 [4P, d, J_{PP} = 4.3 Hz]

^1H NMR (DCM-d_2): δ_H 7.50 [4H, t, J_{HH} = 6.8 Hz, C_6H_5], 7.45−7.30 [28H, m, C_6H_5], 7.05 [8H, t, J_{HH} = 6.8 Hz, C_6H_5], 6.78 [2H, m, C_6H_4], 6.59 [2H, m, C_6H_4], 3.83 [3H, s, OCH_3], 2.94 [4H, m (br), C_2H_4], 2.79 [4H, m (br), C_2H_4].

After *ca.* 1 h., a dark orange solution was afforded.

$^{31}P\{^{1}H\}$ NMR (DCM-d_2): δ_P 173.4 [1P, s, PI_3], 73.2 [8P, t, J_{PP} = 11.9 Hz], 63.4 [8P, t, J_{PP} = 11.9 Hz], 29.7 [12P, s]

Addition of 1 eq. I_2 to 2.7

To a J Young NMR tube charged with **2.7** (9.0 x 10^{-3} g, 6 x 10^{-3} mmol) in DCM-d_2, I_2 (0.20 cm^3, 0.04 M in DCM-d_2) was added, and the tube mixed by inversion, forming a deep orange/red solution and the precipitation of a dark brown solid.

$^{31}P\{^{1}H\}$ NMR (DCM-d_2): δ_P 132.8 [1P, s], 81.2 [1P, quint, J_{PP} = 5.3 Hz], 44.2 [12P, s (br)], 42.8 [4P, d, J_{PP} = 5.3 Hz], 31.2 [1P, s]

^{1}H NMR (DCM-d_2): δ_H 7.70 [8H, m (br), C_6H_5], 7.27 [2H, d (br), Ph], 7.20 [9H, m, C_6H_5], 7.12 [8H, m (br), C_6H_5], 7.03 [8H, m, C_6H_5], 6.96 [8H, t, J_{HH} = 7.7 Hz, C_6H_5], 6.60 [2H, d, J_{HH} = 7.5 Hz, Ph], 3.01 [4H, m (br), C_2H_4], 2.72 [4H, m (br), C_2H_4]

Addition of 2 eq. I_2 to 2.7

To a J Young NMR tube charged with **2.7** (5.0 x 10^{-3} g, 4 x 10^{-3} mmol) in DCM-d_2, I_2 (0.22 cm^3, 0.04 M in DCM-d_2) was added, and the tube mixed by inversion, forming a deep orange/red solution.

$^{31}P\{^{1}H\}$ NMR (DCM-d_2): δ_P 132.8 [1P, s], 44.2 [4P, s], 39.3 [1P, s], 31.1 [8P, s]

Addition of 3 eq. I_2 to 2.7

To a J Young NMR tube charged with **2.7** (8.0 x 10^{-3} g, 8 x 10^{-3} mmol) in DCM-d_2, I_2 (0.60 cm^3, 0.04 M in DCM-d_2) was added, and the tube mixed by inversion, forming a deep orange/red solution.

$^{31}P\{^{1}H\}$ NMR (DCM-d_2): δ_P 132.9 [1P, s], 49.9 [2P, s], 40.1 [1P, s], 31.3 [8P, s]

^{1}H NMR (DCM-d_2): δ_H 7.39 [8H, t, J_{HH} = 7.1 Hz, C_6H_5], 7.31 [8H, m (br), C_6H_5], 7.25 [8H, m (br), C_6H_5], 7.14 [16H, m, C_6H_5], 6.98 [2H, m (br), Ph], 6.89 [2H, t, J_{HH} = 7.1 Hz, Ph], 5.87 [1H, d, J_{HH} = 8.0 Hz, Ph], 3.18 [4H, m (br), C_2H_4], 2.80 [4H, m (br), C_2H_4]

Addition of 1, 2, and 3 eq. I_2 to 2.8

To a solution of **2.8** (0.010 g, 9 x 10^{-3} mmol) in DCM (1 cm^3), I_2 solution (0.37 cm^3,0.024 M in DCM) was added, and the light brown solution left to stir for 1 h. Removal of solvent under reduced pressure and subsequent washing with pentane (5 x 5 cm^3) afforded a light brown solid.

Two and Three equivalents reactions were similarly undertaken using **2.8** (6 x 10^{-3} g, 6 x 10^{-3} mmol; 6.0 x 10^{-3} g, 6 x 10^{-3} mmol) and I_2 (0.46 cm^3, 0.024 M; 0.66 cm^3, 0.024 M) respectively.

^{31}P{^{1}H} NMR (DCM-d_2): δ_P 31.3 [4P, s, dppe]

^{1}H NMR (DCM-d_2): δ_H 7.38 [8H, m, C_6H_5], 7.32 [8H, m (br), C_6H_5], 7.25 [8H, m (br), C_6H_5], 7.13 [16H, m, C_6H_5], 6.38 [2H, d, J_{HH} = 8.4 Hz, C_6H_4], 5.81 [2H, d, J_{HH} = 8.4 Hz, C_6H_4], 3.71 [3H, s, OCH_3], 3.18 [4H, m (br), C_2H_4], 2.82 [4H, m (br), C_2H_4]

Addition of Excess Br_2 to 2.7

To a J Young NMR tube charged with **2.7** (6.0 x 10^{-3} g, 0.01 mmol) in DCM-d_2, Br_2 solution (0.15 cm^3, 0.25 M in DCM-d_2) was added, forming a dark brown solution.

^{31}P{^{1}H} NMR (DCM-d_2): δ_P 228.4 [1P, s, PBr_3] 44.2 [4P, s (br)] 30.5 [1P, s]

Addition of Excess $PhICl_2$ to 2.7

To a J Young NMR tube charged with **2.7** (*ca*. 0.010 g, 5 x 10^{-3} mmol) in DCM-d_2, $PhICl_2$ (*ca*. 0.010 g, 0.04 mmol) was added, forming a murky green suspension.

^{31}P{^{1}H} NMR (DCM-d_2): δ_P 43.9 [4P, m (br)], 33.7 [1P, s]

7.5.2 ***Additional Reactivity Studies***

Addition of THF to $B(C_6F_5)_3$

To a J Young NMR tube charged with $B(C_6F_5)_3$ (0.010 g, 0.02 mmol) in toluene-d_8, THF (25 µL, 0.3 mmol) was added, and the tube inverted continuously for 1 h., affording a colourless solution.

$^{11}B\{^1H\}$ NMR (toluene-d_8): δ_B 7.8 [s (br)]

^{19}F NMR (toluene-d_8): δ_F −128.0 [2F, d, J_{FF} = 20.6 Hz, C_6F_5], −150.3 [1F, t, J_{FF} = 20.6 Hz, p-C_6F_5], −158.0 [2F, m, C_6F_5]

Addition of $B(C_6F_5)_3$ to 2.1

To a J Young NMR tube charged with **2.1** (0.023 g, 0.02 mmol) in toluene-d_8, $B(C_6F_5)_3$ (0.012 g, 0.02 mmol) was added, and the tube inverted continuously for 1 h., affording a pale-yellow solution.

$^{31}P\{^1H\}$ NMR (toluene-d_8): δ_P 45.4 [s (br)]

$^{11}B\{^1H\}$ NMR (toluene-d_8): δ_B 23.8 [br]

^{19}F NMR (toluene-d_8): δ_F −77.4 [s], −130.0 [d (br), J = 13.5 Hz], −152.8 [s (br)], −163.6 [s (br)]

Addition of Excess I_2 to 2.1

To a J Young NMR tube charged with **2.1** (*ca*. 0.010 g, 6 x 10^{-3} mmol) in DCM-d_2, two crystals of iodine were added, and the tube mixed by vigorous shaking, affording a dark brown solution.

$^{31}P\{^1H\}$ NMR (Benzene-d_6): δ_P 36.4 [4P, s]

^1H NMR (Benzene-d_6): δ_H 7.47 [8H, m (br), C_6H_5], 7.31 [8H, m, C_6H_5], 7.17 [8H, t, J_{HH} = 7.7 Hz, C_6H_5], 7.05 [16H, m (br), C_6H_5], 6.55 [1H, t, J_{HH} = 7.3 Hz, *p*-Ph], 6.41 [2H, t, J_{HH} = 7.2 Hz, m−Ph], 5.89 [2H, d, J_{HH} = 7.8 Hz, o−C_6H_5], 3.00 [8H, dm (br), C_2H_4]

Chapter 8 – References

1 J. I. Bates, J. Dugal-Tessier, D. P. Gates, *Dalton Trans.*, 2010, **39**, 3151–3159.

2 N. N. Greenwood, A. Earnshaw, *Chemistry of the Elements*, Butterworth-Heinemann, London, 2nd Edition., 1997.

3 M. Elian, M. M. L. Chen, D. M. P. Mingos, R. Hoffmann, *Inorg. Chem.,* 1976, **15**, 1148–1155.

4 K. B. Dillon, F. F. Mathey, J. F. Nixon, *Phosphorus: The Carbon Copy: From Organophosphorus to Phospha-organic Chemistry*, John Wiley and Sons, Chichester, 1998.

5 T. E. Gier, *J. Am. Chem. Soc.*, 1961, **83**, 1769–1770.

6 H. Albers, *Angew. Chem.*, 1950, **62**, 443–467.

7 J. K. Tyler, *J. Chem. Phys.*, 1964, **40**, 1170.

8 N. P. C. Westwood, H. W. Kroto, J. F. Nixon, N. P. C. Simmons, *J. Chem. Soc., Dalton Trans.*, 1979, 1405–1409.

9 H. W. Kroto, J. F. Nixon, N. P. C. Simmons, N. P. C. Westwood, *J. Am. Chem. Soc.*, 1978, **100**, 446–448.

10 H. W. Kroto, J. F. Nixon, N. P. C. Simmons, *J. Mol. Spec.*, 1980, **82**, 185–192.

11 H. W. Kroto, J. F. Nixon, N. P. C. Simmons, *J. Mol. Spec.*, 1979, **77**, 270–285.

12 M. J. Hopkinson, H. W. Kroto, J. F. Nixon, N. P. C. Simmons, *Chem. Phys. Lett.*, 1976, **42**, 460–461.

13 M. J. Hopkinson, H. W. Kroto, J. F. Nixon, N. P. C. Simmons, *J. Chem. Soc., Chem. Commun.*, 1976, 513–515.

14 R. Appel, G. Maier, H. P. Reisenauer, A. Westerhaus, *Angew. Chem. Int. Ed. Engl.*, 1981, **20**, 197.

15 G. Becker, G. Gresser, W. Uhl, *Zeitschrift für Naturforsch. B*, 1981, **36**, 16–19.

16 A. N. Chernega, M. Y. Antipin, Y. T. Struchkov, M. F. Meidine, J. F. Nixon, *Heteroatom Chem.*, 1991, **2**, 665–667.

17 M. Y. Antipin, A. N. Chernega, K. A. Lysenko, Y. T. Struchkov, J. F. Nixon, *J. Chem. Soc., Chem. Commun.*, 1995, **5**, 505–506.

18 J. C. T R Burckett-St Laurent, M. A. King, H. W. Kroto, J. F. Nixon, R. J. Suffolk, *J. Chem. Soc., Dalton Trans.,* 1983, 755–759.

19 K. K. Laali, B. Geissler, M. Regitz, J. J. Houser, *J. Org. Chem.*, 1995, **60**, 6362–6367.

20 A. M. Arif, A. R. Barron, A. H. Cowley, S. W. Hall, *J. Chem. Soc., Chem. Commun.*, 1988, 171–172.

21 G. Markl, H. Sejpka, *Tetrahedron Lett.*, 1986, **27**, 1771–1774.

22 F. Tabellion, A. Nachbauer, S. Leininger, C. Peters, F. Preuss, M. Regitz, *Angew. Chem. Int. Ed.*, 1998, **37**, 1233–1235.

23 P. Binger, S. Leininger, J. Stannek, R. Mynott, J. Bruckmann, C. Kruger, B. J. Dipl-Chem Stannek, R. J. Mynott Ilipl-Min Bruckmann C Kruger, *Angew. Chem. Int. Ed. Engl.*, 1995, **34**, 2227–2230.

24 T. Wettling, J. Schneider, O. Wagner, C. G. Kreiter, M. Regitz, *Angew. Chem. Int. Ed. Engl.*, 1982, **86**, 1013–1014.

25 J. C. T. R. Burckett-St. Laurent, P. B. Hitchcock, H. W. Kroto, J. F. Nixon, *J. Chem. Soc., Chem. Commun.*, 1981, 1141–1143.

26 S. I. Al-Resayes, P. B. Hitchcock, M. F. Meidine, J. F. Nixon, *J. Chem. Soc., Chem. Commun.*, 1984, 1080–1082.

27 H. W. Kroto, J. F. Nixon, *ACS Symposium Series*, 1981, **171**, 383.

28 G. Brauers, M. Green, C. Jones, J. F. Nixon, *J. Chem. Soc., Chem. Commun.*, 1995, 1125–1126.

29 R. A. Sanguramath, N. S. Townsend, J. M. Lynam, C. A. Russell, *Eur. J. Inorg. Chem.*,

2014, **2014**, 1783–1787.

30 T. N. Hooper, M. Green, C. A. Russell, *Chem. Commun.*, 2010, **46**, 2313–2315.

31 P. B. Hitchcock, M. J. Maah, J. F. Nixon, J. A. Zora, G. J. Leigh, M. A. Bakar, *Angew. Chem. Int. Ed. Engl.*, 1987, **26**, 474–475.

32 P. B. Hitchcock, M. A. N. D. A. Lemos, M. F. Meidine, J. F. Nixon, A. J. L. Pombeiro, *J. Organomet. Chem.*, 1991, **402**, C23–C26.

33 M. F. Meidine, M. A. N. D. A. Lemos, A. J. L. Pombeiro, J. F. Nixon, P. B. Hitchcock, *J. Chem. Soc., Dalton Trans.*, 1998, 3319–3323.

34 T. A. Van Der Knaap, T. C. Klebach, F. Visser, F. Bickelhaupt, P. Ros, E. J. Baerends, C. H. Stam, M. Konun, *Tetrahedron*, 1984, **40**, 765–776.

35 R. B. Bedford, A. F. Hill, C. Jones, *Angew. Chem. Int. Ed.*, 1996, **35**, 547–549.

36 R. B. Bedford, D. E. Hibbs, A. F. Hill, M. B. Hursthouse, K. M. Abdul Malik, C. Jones, *Chem. Commun.*, 1996, 1895–1896.

37 P. B. Hitchcock, J. A. Johnson, M. A. N. D. A. Lemos, M. F. Meidine, J. F. Nixon, A. J. L. Pombeiro, *J. Chem. Soc., Chem. Commun.*, 1992, 645–646.

38 M. Brönstrup, J. Gottfriedsen, I. Kretzschmar, S. J. Blanksby, H. Schwarz, H. Schumann, *Phys. Chem. Chem. Phys.*, 2000, **2**, 2245–2250.

39 M. Brym, C. Jones, *Dalton Trans.*, 2003, 3665–3667.

40 F. Brodkorb, M. Brym, C. Jones, C. Schulten, *J. Organomet. Chem.*, 2006, **691**, 1025–1029.

41 L. A. Jones, E. P. F. Lee, P. Soldan, T. G. Wright, *Phys. Chem. Chem. Phys.*, 1999, **1**, 391–395.

42 F. M. Bickelhaupt, F. Bickelhaupt, *Chem. Eur. J.*, 1999, **5**, 162–174.

43 M. Regitz, P. Binger, *Angew. Chem. Int. Ed. Engl.*, 1988, **27**, 1484–1508.

44 Z.-J. Quan, X.-C. Wang, *Org. Chem. Front.*, 2014, **1**, 1128–1131.

45 G. Becker, W. Schwarz, N. Seidler, M. Westerhausen, *Z. Anorg. Allg. Chem.*, 1992, **612**,

72–82.

46 M. Westerhausen, S. Schneiderbauer, H. Piotrowski, M. Suter, H. Nö, H. Nöth, *J. Organomet. Chem.*, 2002, **643–644**, 189–193.

47 F. F. Puschmann, D. Stein, D. Heift, C. Hendriksen, Z. A. Gal, H.-F. H. F. Grützmacher, H.-F. H. F. Grützmacher, *Angew. Chem. Int. Ed.*, 2011, **50**, 8420–8423.

48 M. Podewitz, J. D. Van Beek, M. Wörle, T. Ott, D. Stein, H. Rüegger, B. H. Meier, M. Reiher, H. Grützmacher, *Angew. Chem. Int. Ed.*, 2010, **49**, 7465–7469.

49 I. Krummenacher, C. C. Cummins, *Polyhedron*, 2012, **32**, 10–13.

50 A. R. Jupp, J. M. Goicoechea, *Angew. Chem. Int. Ed.*, 2013, **52**, 10064–10067.

51 T. P. Robinson, M. J. Cowley, D. Scheschkewitz, J. M. Goicoechea, *Angew. Chem. Int. Ed.*, 2015, **54**, 683–686.

52 K. M. Szkop, A. R. Jupp, R. Suter, H. Grützmacher, D. W. Stephan, *Angew. Chem. Int. Ed.*, 2017, **56**, 14174–14177.

53 L. E. Longobardi, T. C. Johnstone, R. F. Alconer, C. A. Russell, D. W. Stephan, *Chem. Eur. J.*, 2016, **22**, 12665–12669.

54 L. N. Grant, B. Pinter, B. C. Manor, H. Grützmacher, D. J. Mindiola, *Angew. Chem. Int. Ed.*, 2017, 1–5.

55 L. N. Grant, B. Pinter, B. C. Manor, R. Suter, H. Grützmacher, *Chem. Eur. J.*, 2017, **23**, 6272–6276.

56 M. G. Fickes, A. L. Odom, C. C. Cummins, *Chem. Commun.*, 1997, 1993–1994.

57 F. F. Puschmann, D. Stein, D. Heift, C. Hendriksen, Z. A. Gal, H. Grützmacher, *Angew. Chem. Int. Ed.*, 2011, **50**, 8420–8423.

58 A. R. Jupp, J. M. Goicoechea, *Angew. Chem. Int. Ed.*, 2013, **52**, 10064–10067.

59 L. Liu, D. A. Ruiz, F. Dahcheh, G. Bertrand, R. Suter, A. M. Tondreau, H. Grützmacher, *Chem. Sci.*, 2016, **7**, 2335–2341.

60 S. Alidori, D. Heift, G. Santiso-Quinones, Z. Benkå, H. Grützmacher, M. Caporali, L.

Gonsalvi, A. Rossin, M. Peruzzini, *Chem. Eur. J.*, 2012, **18**, 14805–14811.

61 G. Pascoli, H. Lavendy, *J. Phys. Chem. A*, 1999, **103**, 3518–3524.

62 O. Mo, M. Yáñez, J.-C. Guillemin, E. Hassan Riague, J.-F. Gal, P.-C. Maria, C. D. Poliart, *Chem. Eur. J.*, 2002, **8**, 4919–4924.

63 H. Jun, V. G. Young, R. J. Angelici, *J. Am. Chem. Soc.*, 1992, **114**, 10064–10065.

64 J. G. Cordaro, D. Stein, H. Rüegger, H. Grützmacher, *Angew. Chem. Int. Ed.*, 2006, **45**, 6159–6162.

65 J. G. Cordaro, D. Stein, H. Grützmacher, *J. Am. Chem. Soc.*, 2006, **128**, 14962–14971.

66 M. Y. Antipin, A. N. Chernega, K. A. Lysenko, Y. T. Struchkova, J. F. Nixonc, Y. T. Struchkov, J. F. Nixon, *J. Chem. Soc., Chem. Commun.*, 1995, 505–506.

67 A. Ehlers, J. G. Cordaro, D. Stein, H. Grützmacher, *Angew. Chem. Int. Ed.*, 2007, **46**, 7878–7881.

68 S. M. Mansell, M. Green, C. A. Russell, *Dalton Trans.*, 2012, **41**, 14360.

69 P. B. Hitchcock, M. J. Maah, J. F. Nixon, J. A. Zora, G. J. Leigh, M. A. Bakar, *Angew. Chem. Int. Ed. Engl.*, 1987, **26**, 474–475.

70 N. Trathen, M. C. Leech, I. R. Crossley, V. K. Greenacre, S. M. Roe, *Dalton Trans.*, 2014, **43**, 8961–9364.

71 M. A. Fox, J. E. Harris, S. Heider, V. Pérez-Gregorio, M. E. Zakrzewska, J. D. Farmer, D. S. Yufit, J. A. K. Howard, P. J. Low, *J. Organomet. Chem.*, 2009, **694**, 2350–2358.

72 C. J. Hoerger, F. W. Heinemann, E. Louyriac, L. Maron, H. Grützmacher, K. Meyer, *Organometallics*, 2017, **36**, 4351–4354.

73 H. S. La Pierre, K. Meyer, *Progress in Inorganic Chemistry Volume 58*, John Wiley and Sons, New Jersey, 2014.

74 T. Baumgartner, *Acc. Chem. Res.*, 2014, **47**, 1613–1622.

75 T. Baumgartner, R. Réau, *Chem. Rev.*, 2006, **106**, 4681–4127.

76 X. He, T. Baumgartner, *RSC Adv.*, 2013, **3**, 11334.

77 J. H. Burroughes, D. D. C. Bradley, A. R. Brown, R. N. Marks, K. Mackay, R. H. Friend, P. L. Burns, A. B. Holmes, *Nature*, 1990, **347**, 539–541.

78 T. Yamamoto, *Bull. Chem. Soc. Jpn.*, 1999, **72**, 621–638.

79 A. Kraft, A. C. Grimsdale, A. B. Holmes, *Angew. Chem. Int. Ed.*, 1998, **37**, 402–428.

80 U. H. F. Bunz, *Chem. Rev.*, 2000, **100**, 1605–1644.

81 A. Saito, T. Miyajima, M. Nakashima, T. Fukushima, H. Kaji, Y. Matano, H. Imahori, *Chem. Eur. J.*, 2009, **15**, 10000–10004.

82 V. A. Wright, B. O. Patrick, C. Schneider, D. P. Gates, *J. Am. Chem. Soc.*, 2006, **128**, 8836–8844.

83 O. Gaudin, R. B. Jackman, T.-P. Nguyen, P. Le Rendu, *J. Appl. Phys.*, 2001, **90**, 4196–4204.

84 M. A. Shameem, A. Orthaber, *Chem. Eur. J.*, 2016, **22**, 10718–10735.

85 M. Hissler, P. W. Dyer, R. Réau, *Coord. Chem. Rev.*, 2003, **244**, 1–44.

86 A. Saito, T. Miyajima, M. Nakashima, T. Fukushima, H. Kaji, Y. Matano, H. Imahori, *Chem. Eur. J.*, 2009, **15**, 10000–10004.

87 E. Deschamps, L. Ricard, F. Mathey, *Angew. Chem. Int. Ed. Engl.*, 1994, **33**, 1158–1161.

88 V. A. Wright, D. P. Gates, *Angew. Chem. Int. Ed.*, 2002, **41**, 2389–2392.

89 S. Shah, J. D. Protasiewicz, *Chem. Commun.*, 1998, **3**, 1585–1586.

90 S. Shah, T. Concolino, A. L. Rheingold, J. D. Protasiewicz, *Inorg. Chem.*, 2000, **39**, 3860–3867.

91 M. Yoshifuji, K. Toyota, N. Inamoto, *Tetrahedron Lett.*, 1985, **26**, 1727–1730.

92 P. Aguirre-Etcheverry, D. O'Hare, *Chem. Rev.*, 2010, **110**, 4839–4864.

93 F. Paul, C. Lapinte, *Coord. Chem. Rev.*, 1998, **178–180**, 431–509.

94 A. Ceccon, S. Santi, L. Orian, A. Bisello, *Coord. Chem. Rev.*, 2004, **248**.

95 B. Kim, J. M. Beebe, C. Olivier, S. Rigaut, D. Touchard, J. G. Kushmerick, X.-Y. Zhu, C. D. Frisbie, *J. Phys. Chem. C*, 2007, **111**, 7521–7526.

96 R. Dembinski, T. Bartik, B. Bartik, M. Jaeger, J. A. Gladysz, *J. Am. Chem. Soc.*, 2000, **122**, 810–822.

97 K. A. Goldsby, T. J. Meyer, *Inorg. Chem.*, 1984, **23**, 3002–3010.

98 M. Akita, M. Terada, S. Oyama, S. Sugimoto, Y. Moro-oka, *Organometallics*, 1991, **10**, 1561–1568.

99 K. G. Caulton, R. H. Cayton, M. H. Chisholm, J. C. Huffman, E. B. Lobkovsky, Z. Xue, *Organometallics*, 1992, **11**, 321–326.

100 M.-C. Chen, Y.-J. Tsai, C.-T. Chen, Y.-C. Lin, T.-W. Tseng, G.-H. Lee, Y. Wang, *Organometallics*, 1991, **10**, 378–380.

101 J. Heidrich, M. Steimann, M. Appel, W. Beck, *Organometallics*, 1990, **9**, 1296–1300

102 P. Belanzoni, N. Re, A. Sgamellotti, C. Floriani, *J. Chem. Soc., Dalton Trans.*, 1998, 1825–1835.

103 M. I. Bruce, *Chem. Rev.*, 1998, **98**, 2797–2858.

104 M. I. Bruce, *Coord. Chem. Rev.*, 1997, **166**, 91–119.

105 F. Coat, F. Paul, C. Lapinte, L. Toupet, K. Costuas, J.-F. Halet, *J. Organomet. Chem.*, 2003, **683**, 368–378.

106 W. Mohr, J. Stahl, F. Hampel, J. A. Gladysz, *Chem. Eur. J.*, 2003, **9**, 3324–3340.

107 W. Weng, T. Bartik, M. Brady, B. Bartik, J. A. Ramsden, A. M. Arif, J. A. Gladysz, *J. Am. Chem. Soc.*, 1995, **117**, 11922–11931.

108 X. Zhang, C. Zhang, H. Guo, W. Huang, T. Polenova, L. C. Francesconi, D. L. Akins, *J. Phys. Chem. B*, 2005, **109**, 19156–19160.

109 M. I. Bruce, K. Costuas, B. G. Ellis, J.-F. Halet, P. J. Low, B. Moubaraki, K. S. Murray, N. Oudda, G. J. Perkins, B. W. Skelton, A. H. White, *Organometallics*, 2007, **26**, 3735–3745.

110 M. I. Bruce, B. G. Ellis, M. Gaudio, C. Lapinte, G. Melino, F. Paul, B. W. Skelton, M. E. Smith, L. Toupet, A. H. White, *Dalton Trans.*, 2004, 1601–1609.

111 L.-B. Gao, S.-H. Liu, L.-Y. Zhang, L.-X. Shi, Z.-N. Chen, *Organometallics*, 2006, **25**, 506–

512.

112 M. Akita, Y. Tanaka, C. Naitoh, T. Ozawa, N. Hayashi, M. Takeshita, A. Inagaki, M.-C. Chung, *Organometallics*, 2006, **25**, 5261–5275.

113 Y. Matsuura, Y. Tanaka, M. Akita, *J. Organomet. Chem.*, 2009, **694**, 1840–1847.

114 C. Olivier, B. Kim, D. Touchard, S. Rigaut, *Organometallics*, 2008, **27**, 509–518.

115 L. D. Field, A. M. Magill, T. K. Shearer, S. B. Colbran, S. T. Lee, S. J. Dalgarno, M. M. Bhadbhade, *Organometallics*, 2010, **29**, 957–965.

116 A. Klein, O. Lavastre, J. Fiedler, *Organometallics*, 2006, **25**, 635–643.

117 L. Medei, L. Orian, O. V Semeikin, M. G. Peterleitner, N. A. Ustynyuk, S. Santi, C. Durante, A. Ricci, C. Lo Sterzo, *Eur. J. Inorg. Chem.*, 2006, 2582–2597.

118 F. De Montigny, G. Argouarch, K. Costuas, J.-F. Halet, T. Roisnel, L. Toupet, C. Lapinte, *Organometallics*, 2005, **24**, 4558–4572.

119 F. de Montigny, G. Argouarch, T. Roisnel, L. Toupet, C. Lapinte, S. Chan-Fung Lam, C.-H. Tao, V. Wing-Wah Yam, *Organometallics*, 2008, **27**, 1912–1923.

120 F. Justaud, G. Argouarch, S. I. Ghazala, L. Toupet, F. Paul, C. Lapinte, *Organometallics*, 2008, **27**, 4260–4264.

121 S. I. Ghazala, F. Dé, R. Paul, L. Toupet, T. Roisnel, P. Hapiot, C. Lapinte, *J. Am. Chem. Soc.*, 2006, **128**, 2463–2476.

122 F. Paul, S. Goeb, F. Justaud, G. Argouarch, L. Toupet, R. F. Ziessel, C. Lapinte, *Inorg. Chem.*, 2007, **46**, 9036–9038.

123 Y. Tanaka, J. A. Shaw-Taberlet, F. Justaud, O. Cador, T. Roisnel, M. Akita, J. R. Hamon, C. Lapinte, *Organometallics*, 2009, **28**, 4656–4669.

124 C. Lapinte, *J. Organomet. Chem.*, 2008, **2008**, 793–801.

125 P. J. Low, M. I. Bruce, *Adv. Organomet. Chem.*, 2001, **48**, 71–288.

126 M. I. Bruce, P. J. Low, *Adv. Organomet. Chem.*, 2004, **50**, 179–444.

127 P. J. Low, R. L. Roberts, R. L. Cordiner, F. Hartl, *J. Solid State Electrochem.*, 2005, **9**, 717–

731.

128 M. Brady, W. Weng, Y. Zhou, J. W. Seyler, A. J. Amoroso, A. M. Arif, M. Bohme, G. Frenking, J. A. Gladysz, *J. Am. Chem. Soc.*, 1997, **119**, 775–788.

129 A. Wong, P. C. W Kang, C. D. Tagge, D. R. Leon, *Organometallics*, 1990, **9**, 1992–1994.

130 C. W. Faulkner, S. L. Ingham, M. S. Khan, J. Lewis, N. J. Long, P. R. Raithby, *J. Organomet. Chem.*, 1994, **482**, 139–145.

131 G. Albertin, S. Antoniutti, E. Bordignon, F. Cazzaro, S. Ianelli, G. Pelizzi, *Organometallics*, 1995, **14**, 4114–4125.

132 D. Touchard, P. Haquette, S. Guesmi, L. Le Pichon, A. Daridor, L. Toupet, P. H. Dixneuf, *Organometallics*, 1997, **16**, 3640–3648.

133 N. Gauthier, N. Tehouar, F. Justaud, G. Argouarch, M. P. Cifuentes, L. Toupet, D. Touchard, J. F. Halet, S. Rigaut, M. G. Humphrey, K. Costuas, F. Paul, *Organometallics*, 2009, **28**, 2253–2266.

134 C. Jones, C. Schulten, A. Stasch, *Eur. J. Inorg. Chem.*, 2008, 1555–1558.

135 T. P. Fong, C. E. Forde, A. J. Lough, R. H. Morris, P. Rigo, E. Rocchini, T. Stephan, *J. Chem. Soc., Dalton Trans.*, 1999, 4475–4486.

136 E. Rocchini, P. Rigo, A. Mezzetti, T. Stephan, R. H. Morris, A. J. Lough, C. E. Forde, T. P. Fong, S. D. Drouin, *J. Chem. Soc., Dalton Trans.*, 2000, 3591–3602.

137 M. Liu, J. Hu, Y. Wang, *Polyhedron*, 2018, **149**, 79–83.

138 M. C. Leech, Masters Dissertation, University of Sussex, 2014.

139 N. Trathen, PhD Thesis, University of Sussex, 2014.

140 C. Creutz, H. Taube, *J. Am. Chem. Soc.*, 1969, **91**, 3988–3989.

141 U. Fürholz, S. Joss, H. Beat Bürgi, A. Ludi, *Inorg. Chem.*, 1985, **24**, 943–948.

142 L.-T. Zhang, J. Ko, M. J. Ondrechen, *J. Am. Chem. Soc.*, 1987, **109**, 1666–1671.

143 W. Kaim, B. Sarkar, *Coord. Chem. Rev.*, 2007, **251**, 584–594.

144 H. Adams, P. J. Costa, M. Newell, S. J. Vickers, M. D. Ward, V. Félix, J. A. Thomas, *Inorg.*

Chem., 2008, **47**, 11633–11643.

145 R. J. Crutchley, *Adv. Inorg. Chem.*, 1994, **41**, 273–325.

146 S. S. Chavan, S. R. Lolage, S. B. Pawal, *J. Organomet. Chem.*, 2016, **815**–**816**, 65–73.

147 M. I. Bruce, M. L. Cole, K. Costuas, B. G. Ellis, K. A. Kramarczuk, C. Lapinte, B. K. Nicholson, G. J. Perkins, B. W. Skelton, A. H. White, N. N. Zaitseva, *Z. Anorg. Allg. Chem.*, 2013, **639**, 2216–2223.

148 C. Lebreton, D. Touchard, L. Le Pichon, A. Daridor, L. Toupet, P. H. Dixneuf, *Inorg. Chim. Acta*, 1998, **272**, 188–196.

149 O. Lavastre, J. Plass, P. Bachmann, S. Guesmi, C. Moinet, P. H. Dixneuf, *Organometallics*, 1997, **16**, 184–189.

150 G. A. Koutsantonis, G. I. Jenkins, P. A. Schauer, B. Szczepaniak, B. W. Skelton, C. Tan, A. H. White, *Organometallics*, 2009, **28**, 2195–2205.

151 C. F. R. Mackenzie, S. Bock, C. Y. Lim, B. W. Skelton, C. Nervi, D. A. Wild, P. J. Low, G. A. Koutsantonis, *Organometallics*, 2017, **36**, 1946–1961.

152 P. A. Schauer, B. W. Skelton, G. A. Koutsantonis, *Organometallics*, 2015, **34**, 4975–4988.

153 L.-B. Gao, J. Kan, Y. Fan, L.-Y. Zhang, S.-H. Liu, Z.-N. Chen, *Inorg. Chem.*, 2007, **46**, 5651–5664.

154 S. Clément, L. Guyard, M. Knorr, F. Villafañe, C. Strohmann, M. M. Kubicki, *Eur. J. Inorg. Chem.*, 2007, 5052–5061.

155 C. Lebreton, D. Touchard, L. Le Pichon, A. Daridor, L. Toupet, P. H. Dixneuf, L. Le, A. Daridor, P. H. Dixneuf, *Inorg. Chim. Acta*, 1998, **272**, 188–196.

156 J.-L. L. Fillaut, N. N. Dua, F. Geneste, L. L. Toupet, S. Sinbandhit, *J. Organomet. Chem.*, 2006, **691**, 5622–5630.

157 F. Coat, P. Thominot, C. Lapinte, *J. Organomet. Chem.*, 2001, **629**, 39–43.

158 N. Narvor Le, L. Toupet, C. Lapinte, *J. Am. Chem. Soc.*, 1995, **117**, 7129–7138.

159 M. I. Bruce, B. G. Ellis, P. J. Low, B. W. Skelton, A. H. White, *Organometallics*, 2003, **22**,

3184–3198.

160 L. D. Field, A. M. Magill, T. K. Shearer, S. B. Colbran, S. T. Lee, S. J. Dalgarno, M. M. Bhadbhad, *Organometallics*, 2010, **29**, 957–965.

161 T. Gröer, G. Baum, M. Scheer, *Organometallics*, 1998, **17**, 5916–5919.

162 J. B. G. Gluyas, N. J. Brown, J. D. Farmer, P. J. Low, *Aust. J. Chem.*, 2016, **91**, 509.

163 W. E. Geiger, *Coord. Chem. Rev.*, 2013, **257**, 1459–1471.

164 S. G. Eaves, D. S. Yufit, B. W. Skelton, J. M. Lynam, P. J. Low, *Dalton Trans.*, 2015, **44**, 21016–21024.

165 Y. Tanaka, M. Kiguchi, M. Akita, *Chem. Eur. J.*, 2017, **23**, 4741–4749.

166 S. Bock, O. A. Al-Owaedi, S. G. Eaves, D. C. Milan, M. Lemmer, B. W. Skelton, H. M. Osorio, R. J. Nichols, S. J. Higgins, P. Cea, N. J. Long, T. Albrecht, S. Martin, C. J. Lambert, P. J. Low, *Chem. Eur. J.*, 2017, **23**, 2133–2143.

167 S. G. Eaves, B. W. Skelton, P. J. Low, *J. Organomet. Chem.*, 2017, **847**, 242–250.

168 K. Sugimoto, Y. Tanaka, S. Fujii, T. Tada, M. Kiguchi, M. Akita, *Chem. Commun.*, 2016, **52**, 5796–5799.

169 B. deB. Darwent, *National Standard Reference Data Series*, National Bureau of Standards, Washington, 1970.

170 T. L. Cottrell, *The Strengths of Chemical Bonds*, Butterworths, London, 2nd edition., 1958.

171 V. K. Greenacre, I. J. Day, I. R. Crossley, *Organometallics*, 2017, **36**, 435–442.

172 G. J. Perkins, M. I. Bruce, B. W. Skelton, A. H. White, *Inorg. Chim. Acta*, 2006, **359**, 2644–2649.

173 J. Uziel, C. Darcel, D. Moulin, C. Bauduin, S. Jugé, *Tetrahedron Asymmetry*, 2001, **12**, 1441–1449.

174 C. G. Hrib, P. G. Jones, W. W. Du Mont, V. Lippolis, F. A. Devillanova, *Eur. J. Inorg. Chem.*, 2006, 1294–1302.

175 N. Bricklebank, S. M. Godfrey, A. G. Mackie, C. A. McAuliffe, R. G. Pritchard, *J. Chem. Soc., Chem. Commun.*, 1992, 355–356.

176 S. M. Godfrey, D. G. Kelly, C. A. McAuliffe, A. G. Mackie, R. G. Pritchard, S. M. Watson, *J. Chem. Soc., Chem. Commun.*, 1991, 1163–1164.

177 W.-W. du Mont, M. Batcher, S. Pohl, W. Saak, *Angew. Chem. Int. Ed. Engl.*, 1987, **26**, 912–913.

178 O. Kühl, *Phosphorus-31 NMR Spectroscopy: A Concise Introduction for the Synthetic Organic and Organometallic Chemist*, Springer, Berlin, 2008.

179 P. Winrow, Masters Dissertation, University of Sussex, 2015.

180 M. A. Bazhenova, S. S. Bogush, A. G. Herbst, T. V Demeshchik, Y. G. Komarovskaya, V. S. Kurova, M. D. Reshetova, A. D. Ryabov, E. S. Ryabova, Y. N. Frrsova, *Russ. Chem. Bull.*, 1996, **45**, 2445–2451.

181 M. Charlot, L. Porrès, C. D. Entwistle, A. Beeby, T. B. Marder, M. Blanchard-Desce, *Phys. Chem. Chem. Phys.*, 2005, **7**, 600–606.

182 N. Trathen, V. K. Greenacre, I. R. Crossley, S. M. Roe, *Organometallics*, 2013, **32**, 2501–2504.

183 X.-F. Zhao, C. Zhang, *Synthesis (Stuttg).*, 2007, **4**, 551–557.

184 P. Giannoccaro, A. Sacco, *Inorg. Synth.*, 1997, **17**, 69–70.

185 B. Chaudfet, G. Commenges, R. Poilblanc, L. De Chimie, D. Coordination, P. Sabatier, *J. Chem. Soc., Dalton Trans.*, 1984, 1635–1639.

186 Agilent Technologies, *Crysalis Pro 1.171.36.32*, 2011.

187 G. M. Sheldrick, *Acta Cryst.*, 2008, **A64**, 112–122.

188 O. V. Dolomanov, L. J. Bourhis, R. J. Gildea, J. A. K. Howard, H. Puschmann, *J. Appl. Cryst.*, 2009, **42**, 339–341.

189 M. J. Frisch, G. W. Trucks, H. B. Schlegel, G. E. Scuseria, M. A. Robb, J. R. Cheeseman, G. Scalmani, V. Barone, B. Mennucci, G. A. Petersson, H. Nakatsuji, M. Caricato, X. Li, H. P.

Hratchian, A. F. Izmaylov, J. Bloino, G. Zheng, J. L. Sonnenberg, M. Hada, M. Ehara, K. Toyota, R. Fukuda, J. Hasegawa, M. Ishida, T. Nakajima, Y. Honda, O. Kitao, H. Nakai, T. Vreven, J. Montgomery, J. A., J. E. Peralta, F. Ogliaro, M. Bearpark, J. J. Heyd, E. Brothers, K. N. Kudin, V. N. Staroverov, R. Kobayashi, J. Normand, K. Raghavachari, A. Rendell, J. C. Burant, S. S. Iyengar, J. Tomasi, M. Cossi, N. Rega, J. M. Millam, M. Klene, J. E. Knox, J. B. Cross, V. Bakken, C. Adamo, J. Jaramillo, R. Gomperts, R. E. Stratmann, O. Yazyev, A. J. Austin, R. Cammi, C. Pomelli, J. W. Ochterski, R. L. Martin, K. Morokuma, V. G. Zakrzewski, G. A. Voth, P. Salvador, J. J. Dannenberg, S. Dapprich, A. D. Daniels, Ö. Farkas, J. B. Foresman, J. V. Ortiz, J. Cioslowski, D. J. Fox, *Gaussian 09, Revision C.01*, Gaussian, Inc., Wallingford CT, 2010.

190 M. J. Frisch, G. W. Trucks, H. B. Schlegel, G. E. Scuseria, M. A. Robb, J. R. Cheeseman, G. Scalmani, V. Barone, B. Mennucci, G. A. Petersson, H. Nakatsuji, M. Caricato, X. Li, H. P. Hratchian, A. F. Izmaylov, J. Bloino, G. Zheng, J. L. Sonnenberg, M. Hada, M. Ehara, K. Toyota, R. Fukuda, J. Hasegawa, M. Ishida, T. Nakajima, Y. Honda, O. Kitao, H. Nakai, T. Vreven, J. Montgomery, J. A., J. E. Peralta, F. Ogliaro, M. Bearpark, J. J. Heyd, E. Brothers, K. N. Kudin, V. N. Staroverov, R. Kobayashi, J. Normand, K. Raghavachari, A. Rendell, J. C. Burant, S. S. Iyengar, J. Tomasi, M. Cossi, N. Rega, J. M. Millam, M. Klene, J. E. Knox, J. B. Cross, V. Bakken, C. Adamo, J. Jaramillo, R. Gomperts, R. E. Stratmann, O. Yazyev, A. J. Austin, R. Cammi, C. Pomelli, J. W. Ochterski, R. L. Martin, K. Morokuma, V. G. Zakrzewski, G. A. Voth, P. Salvador, J. J. Dannenberg, S. Dapprich, A. D. Daniels, Ö. Farkas, J. B. Foresman, J. V. Ortiz, J. Cioslowski, D. J. Fox, *Gaussian 09, Revision D.01*, Gaussian, Inc., Wallingford CT, 2013.

191 N. M. O'Boyle, A. L. Tenderholt, K. M. Langner, *J. Comp. Chem.*, 2008, **29**, 839–845.

192 W. Kaim, G. K. Lahiri, W. Kaim, G. K. Lahiri, *Angew. Chem. Int. Ed.*, 1915, **46**, 1778–1796.

Chapter 9 – Appendices

9.1 Additional Structural Characterisation

9.1.1 Structural Characterisation of [FeCp(dppe)Cl]OTf*

Crystal was grown by M. C. Leech by layering a saturated DCM solution of [FeCp*(dppe)Cl]OTf with pentane at room temperature.

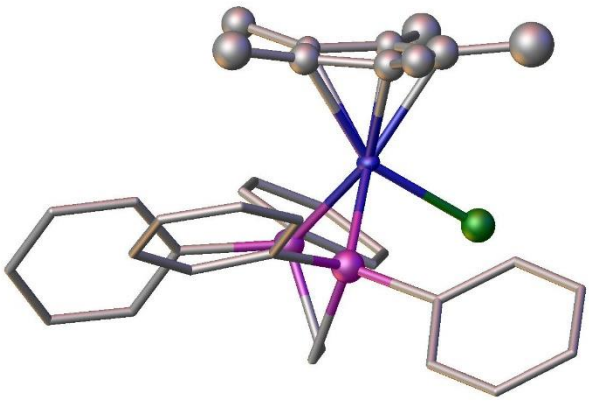

Figure 9.1: *Molecular structure of [FeCp*(dppe)Cl]OTf. The data were refined isotropically, with hydrogen atoms omitted and the ancillary ligand set reduced for clarity.*

Crystal Data: $C_{37}H_{39}ClF_3FeO_3P_2S$, M_w = 773.98 g mol^{-1}, orthorhombic, $P2_12_12_1$ (No. 19), a = 12.8182(8) Å, b = 16.7455(3) Å, c = 16.9540(8) Å, α = 90, β = 90, γ = 90 °, V = 3639.1(3) Å^3, Z = 4. D_c = 1.413 Mg m^{-3}, μ(Cu-Kα) = 5.796 mm^{-1}, T = 173 K, 1424 independent reflections. Full-matrix F^2 refinement. R_1 = 0.0368, wR_2 = 0.0792 on 1075 independent absorption corrected reflections [I>2σ(I); 2θmax = 88.914 °], 203 parameters.

9.1.2 Structural Characterisation of Trans-[Ru(=C=CH$_2$)(C≡CPh)(dppe)$_2$]OTf

Crystal was grown by M. C. Leech by layering a saturated DCM solution of *trans*-[Ru(=C=CH$_2$)(C≡CPh)(dppe)$_2$]OTf with hexane at room temperature.

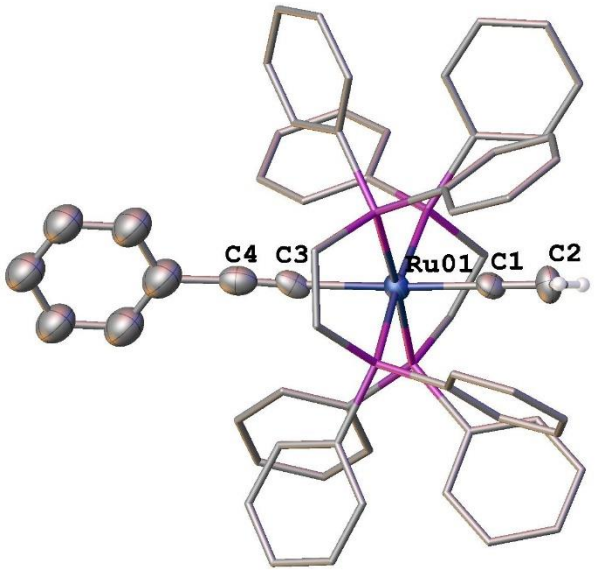

Figure 9.2: *Molecular structure of trans-[Ru(=C=CH$_2$)(C≡CPh)(dppe)$_2$]OTf, 50% thermal ellipsoids, hydrogen atoms, counter-ion, and solvent molecules omitted, and ancillary ligand set reduced for clarity.*

Crystal Data: $C_{127}H_{110}Cl_2F_6O_6P_8Ru_2S_2$, M_w = 2431.06 g mol^{-1}, monoclinic, Cc (No. 9), a = 26.5185(6) Å, b = 12.8518(2) Å, c = 33.8435(8) Å, α = 90, β = 95.313(2), γ = 90 °, V = 11484.7(4) Å^3, Z = 4. D_c = 1.406 Mg m^{-3}, μ(Cu-Kα) = 4.485 mm^{-1}, T = 173 K, 34000 independent reflections. Full-matrix F^2 refinement. R_1 = 0.0639, wR_2 = 0.1677 on 17516 independent absorption corrected reflections [I>2σ(I); 2θmax = 143.048 °], 1300 parameters.

9.1.3 Structural Characterisation of Trans-[RuH(η¹-P≡CSiMe₃)(dppe)₂]PF₆

Crystal was grown by M. C. Leech by layering a saturated DCM solution of *trans*-[RuH(η¹-P≡CSiMe$_3$)(dppe)$_2$]PF$_6$ with Et$_2$O at room temperature.

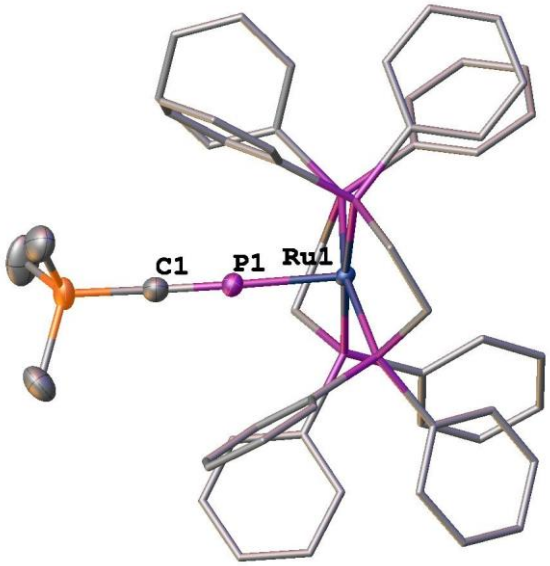

Figure 9.3: *Molecular structure of trans-[RuH(η¹-P≡CSiMe$_3$)(dppe)$_2$]PF$_6$, 50% thermal ellipsoids, hydrogen atoms and counter-ion omitted, and ancillary ligand set reduced for clarity.*

Crystal Data: $C_{56}H_{58}F_6SiP_6Ru$, M_w = 1160.00 g mol^{-1}, monoclinic, $P2_1$ (No. 4), a = 10.8821(2) Å, b = 17.5578(4) Å, c = 14.4037(3) Å, α = 90, β = 96.395(2), γ = 90 °, V = 2734.93(10) Å^3, Z = 2. D_c = 1.409 Mg m^{-3}, μ(Mo-Kα) = 0.541 mm^{-1}, T = 173 K, 14907 independent reflections. Full-matrix F^2 refinement. R_1 = 0.0471, wR_2 = 0.1075 on 10560 independent absorption corrected reflections [I>2σ(I); 2θmax = 59.044 °], 604 parameters.

9.1.4 Structural Characterisation of Trans-[Ru(η^1-P≡CSiMe$_3$)(C≡CH)(dppe)$_2$]PF$_6$

Crystal was grown by M. C. Leech by layering a saturated DCM solution of *trans*-[Ru(η^1-P≡CSiMe$_3$)(C≡CH)(dppe)$_2$]PF$_6$ with Et$_2$O at room temperature.

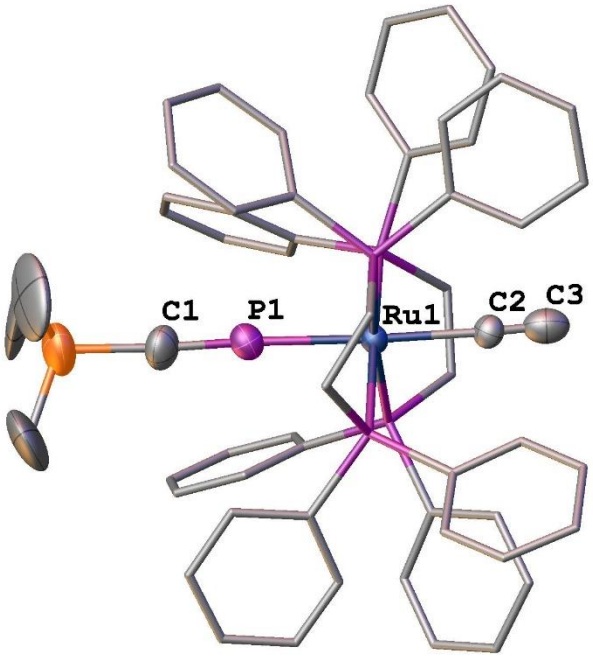

Figure 9.4: *Molecular structure of trans-[Ru(η^1-P≡CSiMe$_3$)(C≡CH)(dppe)$_2$]PF$_6$, 50% thermal ellipsoids, hydrogen atoms, counter-ion, and solvent molecules omitted, and ancillary ligand set reduced for clarity.*

Crystal Data: $C_{58}H_{58}F_6SiP_6Ru$, M_w = 1184.02 g mol^{-1}, monoclinic, Cc (No. 9), a = 19.8066(7) Å, b = 14.7411(5) Å, c = 19.2089(7) Å, α = 90, β = 93.236(3), γ = 90 °, V = 5599.5(3) Å^3, Z = 4. D_c = 1.404 Mg m^{-3}, μ(Cu-Kα) = 4.571 mm^{-1}, T = 173 K, 16086 independent reflections. Full-matrix F^2 refinement. R_1 = 0.0485, wR_2 = 0.1464 on 7520 independent absorption corrected reflections [I>2σ(I); 2θmax = 142.91 °], 652 parameters.

9.1.5 Structural Characterisation of Trans-[RuCl(C≡CC$_6$H$_3$-3,5-CF$_3$)(dppe)$_2$]

Crystal was grown by M. C. Leech by layering a saturated DCM solution of *trans*-[RuCl(C≡CC$_6$H$_3$-3,5-CF$_3$)(dppe)$_2$] with Et$_2$O at room temperature.

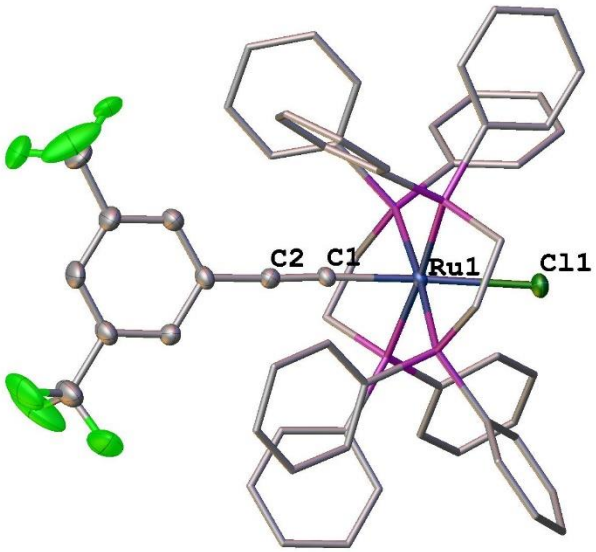

Figure 9.5: *Molecular structure of trans-[RuCl(C≡CC$_6$H$_3$-3,5-CF$_3$)(dppe)$_2$] (**2.3**), 50% thermal ellipsoids, hydrogen atoms and solvent molecules omitted, and ancillary ligand set reduced for clarity.*

Crystal Data: $C_{62}H_{51}F_6P_4Cl_3Ru$, M_w = 1241.32 g mol^{-1}, triclinic, P-1 (No. 2), a = 10.9558(5) Å, b = 11.6589(5) Å, c = 24.0385(9) Å, α = 77.417(4), β = 82.926(4), γ = 70.766(4) °, V = 2825.1(2) Å^3, Z = 2. D_c = 1.459 Mg m^{-3}, μ(Cu-Kα) = 5.121 mm^{-1}, T = 173 K, 17806 independent reflections. Full-matrix F^2 refinement. R_1 = 0.0573, wR_2 = 0.1947 on 17806 independent absorption corrected reflections [I>2σ(I); 2θmax = 142.764 °], 722 parameters.

9.2 Additional DFT Calculations

The following gas-phase optimisations were run at the B3LYP/6-31G** level of theory for all non-metal atoms; LANL2DZ for all metal atoms. All hydrogen atoms have been omitted for clarity. Additional calculations pertaining to each complex can be found in the supporting CD.

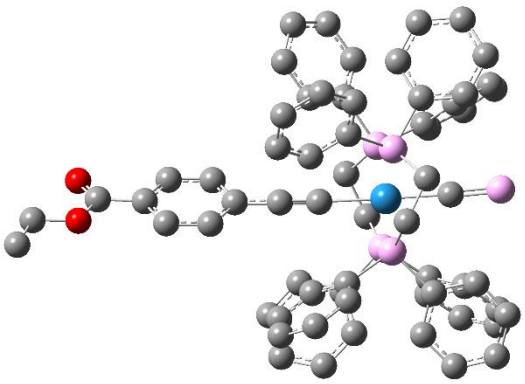

Trans-[Ru(C≡P)(C≡C$C_6H_4CO_2Et$)(dppe)$_2$]

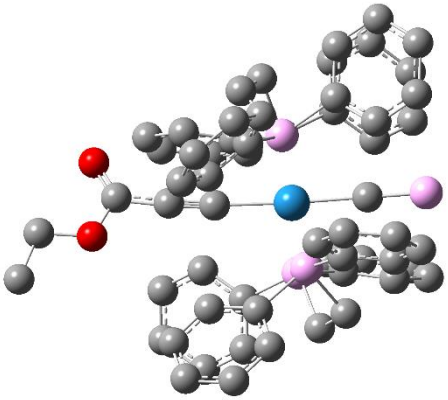

Trans-[Ru(C≡P)(C≡CCCO_2Et)(dppe)$_2$]

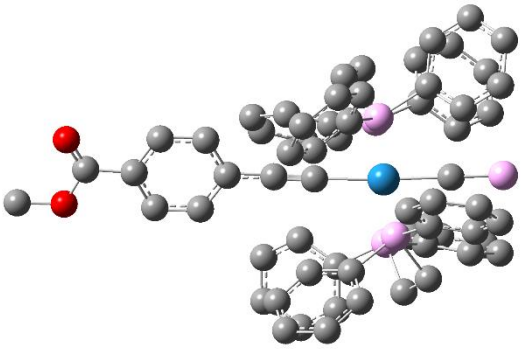

Trans-[Ru(C≡P)(C≡C$C_6H_4CO_2Me$)(dppe)$_2$]

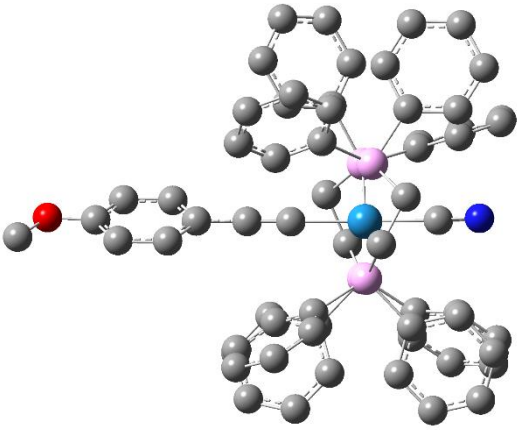

Trans-[Ru(C≡N)(C≡CC_6H_4OMe)(dppe)$_2$]

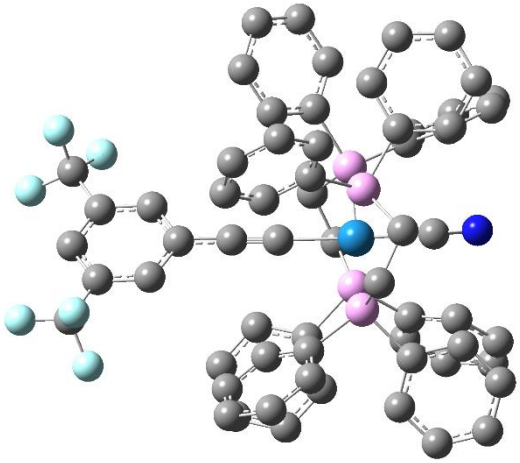

Trans-[Ru(C≡N)(C≡CC_6H_3-*3,5*-CF_3)(dppe)$_2$]

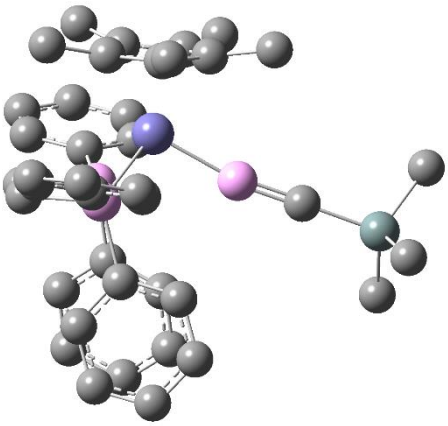

[FeCp*(dppe)(η^1-P≡C$SiMe_3$)]$^+$

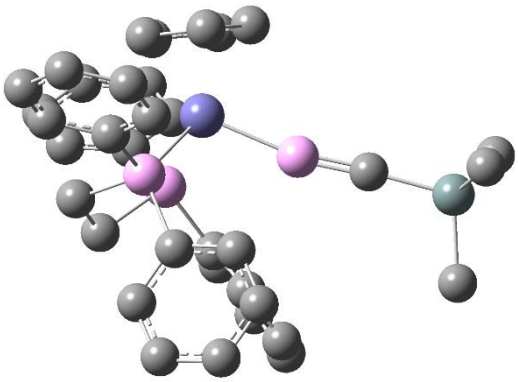

[FeCp(dppe)(η^1-P≡CSiMe$_3$)]$^+$

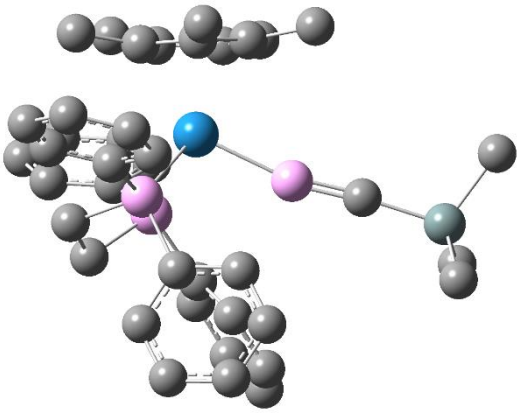

[RuCp*(dppe)(η^1-P≡CSiMe$_3$)]$^+$

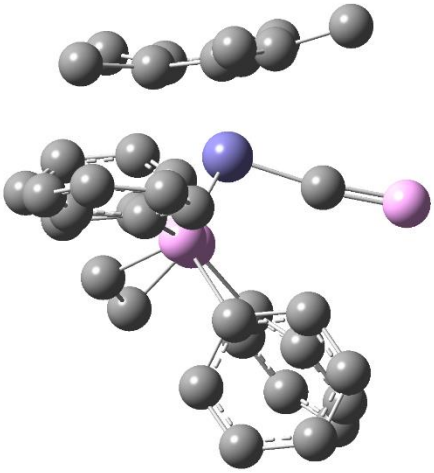

[FeCp*(dppe)(C≡P)]

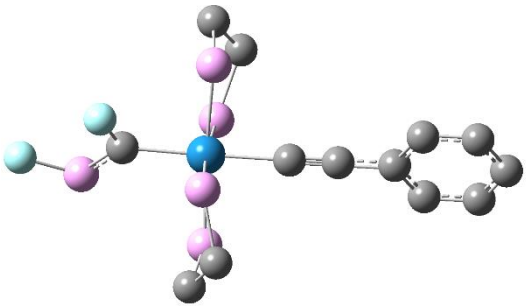

Trans-[Ru(PF=CF)(C≡CPh)(H$_2$PC$_2$H$_4$PH$_2$)$_2$]

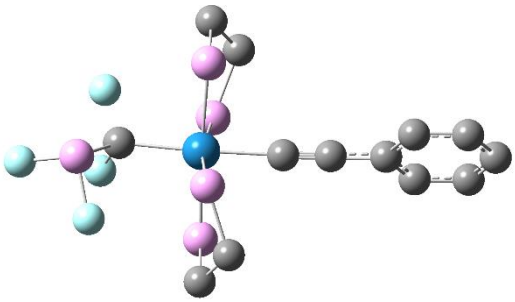

Trans-[Ru(PF$_2$CF$_2$)(C≡CPh)(H$_2$PC$_2$H$_4$PH$_2$)$_2$]

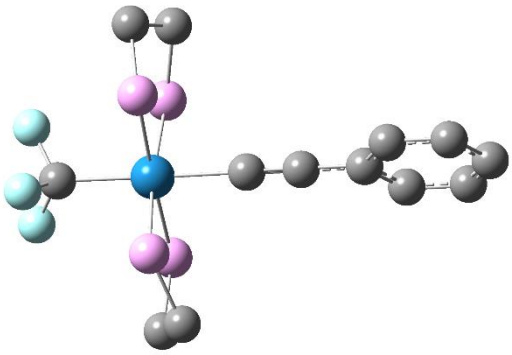

Trans-[Ru(CF$_3$)(C≡CPh)(H$_2$PC$_2$H$_4$PH$_2$)$_2$]

9.3 Academic Papers Published

Leech, Matthew C., and Crossley, Ian R.

***Dalton Transactions*, 2018, 47, 4428-4432**

"*Through-Conjugation of Two Phosphaalkyne ('C≡P') Moieties Mediated by a Bimetallic Scaffold*"

9.4 Conference Attendances

Leech, Matthew C.; Trathen, N.; Crossley, Ian R.; Greenacre, Victoria K.; "*π-Conjugated Transition Metal Cyaphides*"; Poster Presentation at RSC Southern Dalton Meeting, 20-21 April 2015, University of Sussex, UK

Leech, Matthew C.; Crossley, Ian R.; "*π-Conjugated Cyaphide Complexes*"; Poster Presentation at RSC Dalton Younger Members Event, 9-10 September 2015, University of Leeds, UK

Leech, Matthew C.; Crossley, Ian R.; "*Towards Multi-Metallic Cyaphide Complexes*"; Poster Presentation at RSC Dalton Meeting, 29-31 March 2016, University of Warwick, UK

Leech, Matthew C.; Crossley, Ian R.; "*Cyaphide and Acetylide – The Effects of Isolobal Fragment Exchange*"; Poster Presentation at EUCheMS International Organometallic Conference XXII, 9-13 July 2017, Amsterdam

Leech, Matthew C.; Crossley, Ian R.; "*Cyaphide and Acetylide – The Effects of Isolobal Fragment Exchange*"; Oral Presentation at RSC Dalton Younger Members Event, 7-8 September 2017, University of Bath, UK

Leech, Matthew C.; Crossley, Ian R.; "*Escaping Obscurity – Transition Metal Cyaphide Complexes*"; Oral Presentation at RSC Dalton Meeting, 3-5 April 2018, University of Warwick, UK